Geology, geochemistry and alteration of the Eagle River Au-deposit near Wawa, Ontario

Paul Wawrzonkowski

A thesis presented to Lakehead University

In partial fulfillment of the requirement for the

degree of Master of Science in Geology

Department of Geology

Thunder Bay, Ontario, Canada, 2023

Abstract

The Eagle River mine is a mesothermal orogenic gold deposit hosted within the Archean Mishibishu Lake greenstone belt, approximately 50 km west of Wawa, Ontario. The underground mine has been in constant production since 1995, mining multiple steeply dipping quartz-bearing, shear-hosted gold horizons that dip to the north. As of the end of 2021 the Eagle River Mine has produced a total of 7.4 Mt of ore averaging 9.86 g/t Au yielding 1.5 M oz of refined Au (SRK, 2022). The majority of the gold mineralization is hosted within an ellipsoidal quartz diorite, with the remainder hosted within the surrounding calc-alkaline to tholeiitic volcanic rocks. The Mishibishu Lake greenstone belt is surrounded by granitic units which include the Bowman Lake batholith to the north-east, the Floating Heart batholith to the south and the Central pluton to the northwest. The objective of the study was to correlate veining in the chaotic unit to mineralization, investigate alteration geochemistry, and to compare Eagle River to other Archean Au deposits. This was undertaken using a combination of geochronology, petrography, and whole rock lithogeochemistry. The thesis focused on four zones within the deposit, the 8, Falcon, Newt Lake, and Peek-a-Boo zones.

For the thesis, drill core within the four zones has been reexamined (154 drillholes) to have consistent logs between drillholes, and to focus on the chaotic and Laminated units. This constrained the extent of the units and how they are related to one another. Within the Falcon zone part of the mineralization is hosted within the Laminated unit that cuts the chaotic unit. Due to the association with the mineralization a vein paragenesis of the chaotic unit has been developed to determine how the veins are related to one another, and if there is any association with mineralization. To assess the tectonic history of the Eagle River area, geochronological, geochemical, and petrographical samples were collected to determine the ages of the surrounding batholiths and the diorite, to determine the geodynamic setting of the area, as well as to see how the rocks are geochemically related.

A total of 95 samples (geochronology=4, geochemistry=57, and thin sections=34) were selected from the four zones. The new U-Pb zircon ages from this study include the Central pluton (2656.38 ± 0.41 Ma), the Bowman Lake batholith (2658.35 ± 0.41 Ma), the Floating Heart batholith (2687.26 ± 0.42 Ma), and the mine diorite (2716.22 ± 0.41 Ma). The new age of the Bowman Lake batholith provides a tighter constraint on plutonism whereas the mine diorite age constrains the lower limit of mineralization.

Whole rock geochemistry was completed on the volcanic rocks, gabbro, feldspar porphyry, granite, and diorite, as well as the chaotic and Laminated units from the four zones. The Laminated unit has been subdivided into two subgroups (A and B) based on the volcanic classification of Pearce (1996). The volcanic rocks, gabbro, and Laminated Group B unit are characterized by La/Sm_{pm} ratios of 0.8-1.4, variable Ti anomalies (Ti/Ti* of 0.5-1.2), and negative Nb anomalies (Nb/Nb* of 0.5-0.9), consistent with a magmatic arc affinity and melts derived by slab dehydration. The feldspar porphyry, chaotic, and Laminated Group A units are characterized by enriched La/Sm_{pm} ratios of 2.1-6.1, variable Ti anomalies (Ti/Ti* of 0.3-1.0), and Zr anomalies (Zr/Zr* of 0.7-2.3), as well as negative Nb anomalies (Nb/Nb* of 0.3-0.6) consistent with a magmatic arc origin with a higher degree of crustal contamination. The granites are characterized by La/Sm_{pm} ratios of 2.8-7.1, generally negative Ti anomalies (Ti/Ti* of 0.1-0.6), and negative Nb anomalies (Nb/Nb* of 0.1-0.3), consistent with an arc origin possibly related to melting of the downgoing slab. The diorite is characterized by La/Sm_{pm} ratios of 1.7-3.5, variable Ti anomalies (Ti/Ti* of 0.6-1.8), and negative Nb anomalies (Nb/Nb* of 0.3-0.5), consistent with an arc origin with magmas derived from either a mix of slab melts and slab-dehydration or garnet-bearing source rocks. Based on the geochemical differences, the rocks from Eagle River area suggest a switch between slab melting and slab-dehydration in the arc source, but further geochronological dating is required to constrain the timing.

Eight different vein types were identified within the chaotic unit, as well as five different generations of quartz veining. The chaotic unit veins are similar between the zones, suggesting that the chaotic unit is

continuous between the zones. The chaotic unit veins are variably striking, have variable infill and alteration halos, and the sequence of younging is dominantly unidirectional (with exception of Q3 which has multiple cross-cutting relationships, and Q4 which has poor constraints) based on cross-cutting relationships. From the vein types there were a total of six occurrences of gold found within the 8 and the Falcon zones, all of which are hosted within quartz veins (Q2 and Q5 veins) that are parallel to the bands within the Laminated unit. The gold can either be found as inclusions within pyrite, or along grain boundaries that include pyrite-pyrite, quartz-clinochlore, or quartz-pyrite. The alteration within the Eagle River complex is dominated by albitization, K-feldspar, chloritization and carbonatization. The potassic and hematite alteration commonly increases towards the quartz veining within the mine, but not consistently. Potassic and hematite alteration are associated with faulting and generally increases towards the fault. The sericite alteration is commonly associated with the Laminated unit, and can be categorized based on thickness, alteration intensity and associated minerals to point towards the center of the deformation zone, as well as potentially used as markers when cut by younger units or faults. The albite alteration is dominantly associated with the chaotic unit and the variable striking veining. In general, the alteration types and intensity are variable, but the alteration intensities do not consistently increase towards mineralization and consequently do not serve as reliable vectors towards it.

Acknowledgments

This work would not have been possible without the financial support of an NSERC Alliance grant and Wesdome Gold Mines. I would like to express my deepest appreciation to Dr. Peter Hollings who has been supportive of my career goals and having the patience and knowledge to provide me with guidance and feedback throughout this project.

I am grateful to all of those with whom I have had the pleasure to work on this project. I would like to thank Kristi Tavener and Dr. Jonas Valiunas for the technical support making sure that the thin sections are to the highest standards. Lakehead University for providing facilities for classes and petrographic analysis. The Wesdome staff, especially the exploration crew, for help with collecting and preparing the samples. Laurentian University staff for allowing me to use their petrographic microscope, Raman microscope and SEM to help further my research.

I would like to thank my friends, family and loved ones for their continuous support throughout the project and for being there when needed.

Table of Contents

List of Figures

List of Tables

1. Introduction

1.1 Objective

Metamorphic belts have complex histories of formation, involving accretion to collisions that have thickened the continental crust (Groves et al., 2003). Due to gold deposits forming at all stages of orogen evolution, the metamorphic belts contain diverse gold deposits that can either be juxtaposed or overprinted (Groves et al., 2003). Additionally, there is ongoing debate about the source of the mineralizing fluids, which can range from hydrothermal, magmatic and metamorphic fluids as well as about methods of metal concentration (Groves et al., 2003; Goldfarb & Groves, 2015). Due to the complexity of the gold mineralization different models have been proposed to explain their origin and formation, but there exists controversies and overlap between them (Groves et al., 1998; Sillitoe, 2020).

The Eagle River gold deposit has been the subject of little research. Some of the uncertainties include the origin of the deposit, source of mineralizing fluids and how are they controlled, and whether there is any link between alteration and mineralization.

The purpose of the study was to achieve a better understanding of the alteration and geochemistry within the Eagle River Complex which hosts the Eagle River gold mine. The geochemistry will provide a better constraint on the tectonic setting of the region, as well differences and similarities between the units. Logging of the drillholes focused on the chaotic and Laminated units to provide a better understanding of the spatial distribution and occurrence of the two units. These units are associated with mineralization and the quartz veining within the Laminated unit is the dominant host to mineralization. Specific objectives included: (1) investigating the occurrence of the Laminated and the chaotic unit; (2) evaluating the paragenesis of the different vein types found within the

Laminated and chaotic units; (3) geochemical classification of different zones with focus on the 8, Falcon, Newt Lake and Peek-a-Boo zones; (4) classification of alteration within the zones to determine if there is any consistency between them; and (5) determining the ages of the surrounding batholiths and the mine diorite. These objectives were investigated using a combination of geochronology, logging, petrology, and geochemistry.

1.2 Orogenic gold deposits

Gold deposits have a wide range of characteristics and can occur in a wide range of tectonic settings, and ages with a range of methods for concentrating metals (i.e., hydrothermally, magmatically, and mechanically; Goldfarb & Groves, 2015; Sillitoe, 2020). Many attempts have been made to classify the deposits by various authors, with the major styles summarized in Figure 1.1 (Sillitoe, 2020) and Figure 1.2 A and B (Groves et al., 1998). Although these deposits are the most accepted models, there exists controversies and overlap between the gold deposit models, which include tectonic environment, sources of fluids and metals, and depositional mechanism of gold (Sillitoe, 2020; Goldfarb & Groves, 2015). This thesis focused on orogenic gold deposits, the characteristics of which are summarized below.

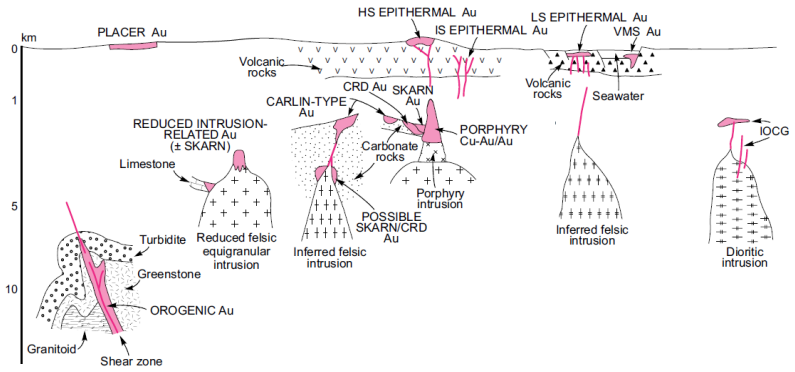

Figure 1.1: Schematic diagram displaying various types of gold deposits. Modified from Sillitoe (2020).

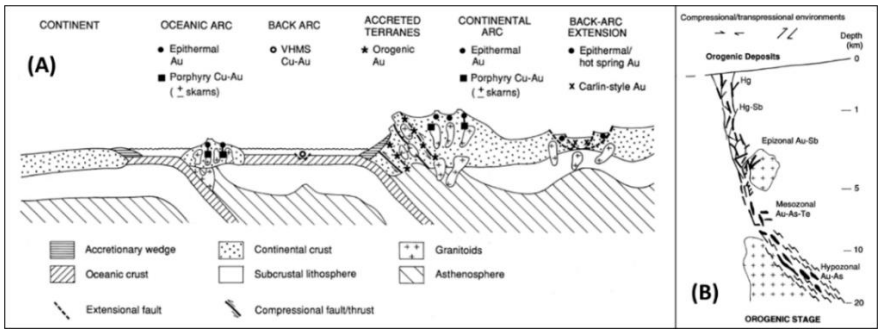

Figure 1.2: Schematic diagram classifying the setting and nature of the orogenic gold deposits (a) and tectonic environment of the gold deposits (b). Modified from Groves et al. (1998).

Orogenic gold deposits form in metamorphic terranes during the late-stages of regional-scale orogeny (Sillitoe, 2020) associated with hydrothermal alteration, and are structurally controlled by 2nd to 3rd order fault splays from major structures or from terrane boundaries (Groves et al., 1998). Gold deposits that have formed in metamorphic environments have a wide range of characteristics including their age, geometry, structural controls, host rocks, metamorphic grade, temperature and pressure of formation, wall-rock alteration assemblages and metal associations (Groves et al., 2003). Orogenic gold deposits are thought to have formed in accretionary or collisional orogens at paleodepths of ~5 to 15 km from low-salinity, gold- and/or arsenic-bearing aqueous carbonic fluids generated by devolatilization reactions associated with regional greenschist- to amphibolite-facies metamorphism (Sillitoe, 2020).

The mineralizing fluids that form orogenic gold deposits are interpreted to be low in salinity (H_2O, CO_2, $H_2S \pm CH_4 \pm N_2$) and formed from devolatilization of hydrated minerals (Goldfarb et al., 2005; Dubé & Gosselin, 2007). The fluids transport the gold as a bisulfide complex in near-neutral pH and relatively reduced fluids (Goldfarb et al., 2005). The $Au(HS)_2$ is considered the most significant complex in mesozonal environments, with AuHS species being dominant below 300°C (Goldfarb et al., 2005). At temperatures above 500°C and 500 bar gold-hydroxide and gold-chloride complexes becomes more important for transporting ligands (Stefansson & Seward, 2004). Other potential

gold-transporting ligands include As-, Sb-, Bi-, and Te-bearing species (Groves et al., 2003). These fluids are transported upward through series of shear zones and major structures, particularly during seismic events (Fig. 1.3; Goldfarb et al., 2005; Dubé & Gosselin, 2007). The gold will remain in solution until changing conditions cause it to be precipitated, in either a structural or a chemical trap. Structural traps include fold hinges, dilational jogs along faults or shear zones (Dubé & Gosselin, 2007) and/or zones of competency contrast (Groves et al., 2003). Chemical traps include rocks with higher Fe/Fe + Mg (± Ca) ratios (i.e., tholeiitic dolerites or basalts, and banded iron formation (BIF)), or anomalously high carbon contents (Groves et al., 2003). Other proposed traps include an association with porphyry stocks and dykes, margins of intrusive complexes, or clastic sedimentary rocks (Dubé & Gosselin, 2007). Additional factors that influence precipitation of gold include temperature and pressure, fluid mixing or back mixing, H_2O-CO_2 phase separation, fluid/rock ratios, salinity (Groves et al., 2003), pH and other physio-chemical variations (Groves et al., 2003, Dubé & Gosselin, 2007).

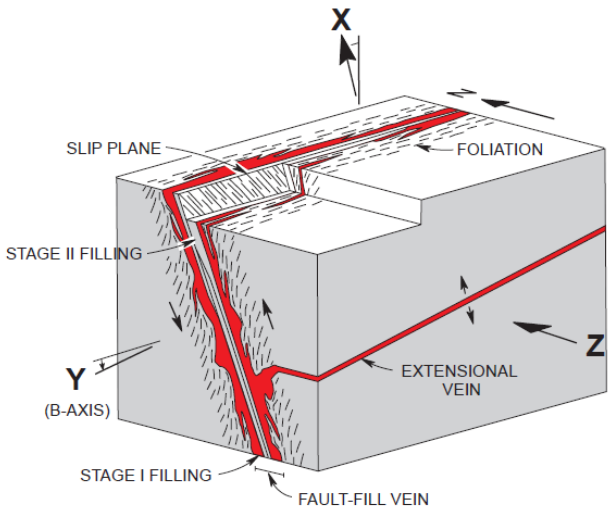

Figure 1.3: Schematic diagram showing the relationships between shear zone and veins. Modified from Dubé & Gosselin (2007).

Orogenic gold deposits form a diverse range of mineralization and alteration styles which are summarized in Table 1.1. These include (a) Quartz-carbonate veins; (b) sulfidic replacement in BIF;

(c) sulfidic replacement and crustiform veins; (d) disseminated-stockwork zones; (e) sulfide-rich veins and veinlet zones; and (f) semi-massive to massive sulfide lenses (Robert et al., 2005). Within extensional quartz-carbonate veins the quartz and carbonate fibers are at a high angle to the vein walls, whereas in laminated veins they are composed of massive to fine-grained quartz subparallel to the vein walls (Dubé & Gosselin, 2007). The crystallization of quartz-carbonate veins can provide insight into the geodynamic environment of formation. Greenstone-hosted quartz-carbonate vein orebodies are characterized by elevated Au, Ag, As, W, B, Sb, Te and Mo with slightly anomalous Cu, Pb, Zn, and Au/Ag ratio typically between 5 to 10 (Groves et al., 2003). In general, the alteration assemblages vary from sericite-carbonate-pyrite at shallower depths, to biotite-carbonate-pyrite to biotite-amphibole-pyrrhotite-arsenopyrite and biotite/phlogopite-diopside-pyrrhotite at greater depths (amphibole-facies rocks; Groves et al., 2003). Sulfide poor quartz-carbonate veins are commonly associated with white mica (sericite)/biotite-carbonate-pyrite alteration and anomalous As-Sb-W±Te (Sillitoe, 2020). Within syngenetic to diagenetic sedimentary rocks gold is sourced and released from pre-existing pyrite during prograde desulfidation to form pyrrhotite (Saunders et al., 2014).

The sulfide replacements in BIF deposits are hosted within iron-rich layers in chert-magnetite, or magnetite-rich graywacke-mudstone, that are commonly associated with cross-cutting quartz-carbonate veins (Robert et al., 2005). The sulfides include pyrite, arsenopyrite, or pyrrhotite. These deposits occur along fold hinges, folds, or along the intersections with cross-cutting structures. Examples of these deposits include Mount Magnet and Musselwhite (Robert et al., 2005).

Sulfidic replacement and crustiform veins consist of lodes that have varying proportions of crustiform-colloform-texture carbonate-quartz vein or breccias and sulfidic replacement of host rock or carbonate vein (Robert et al., 2005). These deposits are dominantly hosted within mafic rocks,

and associated with pyrite, and less commonly arsenopyrite, stibnite or tellurides. Examples of these deposits include Golden Mile, Jundee, Mount Charlotte, and Campbell-Red Lake deposits.

Disseminated-stockwork deposits consist of zones of sulfides (5-20%) that can be either found as disseminated sulfides along foliation planes in highly strained rocks or as a stockwork of sulfide-rich fractures within quartz veinlets (Robert et al., 2005). The sulfides include pyrite or arsenopyrite with less commonly molybdenite. These deposits can be associated with intermediate to felsic porphyry intrusions that were emplaced in clastic sedimentary rocks, or confined within mafic rock units that are strata bound and commonly in contact with ultramafic units. Examples of these deposits include Madsen, Beattie, Kanowna Belle, Wallaby or Plutonic deposits.

Sulfide-rich veins are similar to quartz-carbonate veins but have a higher abundance of sulfides (>25% sulfides) within the veins and a higher association with base metal sulfides (Robert et al., 2005). The sulfides include pyrite, sphalerite, chalcopyrite and galena. Examples of these deposits include Boyon, Sleeping Giant, Daigneault and Mount Gibson.

Semi-massive to massive sulfide lenses (>50% sulfides) occur near the top of the felsic volcanic rock sequences, are highly strained, and associated with alteration zones (Robert et al., 2005). These can have barren quartz-carbonate veins cutting the deposit. The sulfides include pyrite, chalcopyrite, sphalerite, galena, and magnetite. Examples of these deposits include Horne, Bousquet 2-Dumagami, and LaRonde-Penna.

Ore-forming fluids in orogenic deposits typically have 1.5 ± 0.5 kb, 350 ± 50°C, low-salinity H_2O-CO_2 ± CH_4 ± N_2 transported as a reduced sulphur complex (Groves et al., 2003), but the source of fluids is controversial. Potential fluid sources include metamorphic derived, magmatic derived or deeply circulating meteoric water (Dubé & Gosselin, 2007). Based on isotopic and fluid inclusion studies, gold mineralizing fluids have been characterized as an aqueous-carbonic fluid with low salinity (<3

Table 1.1: Characteristics of gold mineralization gold deposits from the Superior and Yilgarn Gold cratons. Modified from Robert et al. (2005).

Style of mineralization	Characteristics	Associated alteration assemblages	Metal association	Selected examples where mineralization type is dominant or important (>5 Moz examples in bold character)
Quartz-carbonate veins	Quartz veins with <25% carbonate, <10% sulfide, ±albite, tourmaline, scheelite Vein types include laminated fault-fill and extensional veins. Sulfides are mainly pyrite, with arsenopyrite and pyrrhotite.	Carbonate-sericite-(albite)-pyrite (arsenopyrite), at greenschist grade Biotite-actinolite-pyrite ± carbonate, at lower amphibolite grade Biotite-calc-silicate-pyrrhotite ± pyrite at mid amphibolite grade	Au > Ag As, W ± Te, Mo, B	Superior: **Hollinger-McIntyre, Kirkland Lake, Sigma-Lamaque**, San Antonio Yilgarn: **Mount Charlotte, Victory-Defiance, Norseman**, Centenary, Bayleys, Westonia
Sulfidic replacements in BIF	Strata-bound replacements of Fe-rich layers by mainly pyrite, arsenopyrite, or pyrrhotite. Associated with quartz veins or zones of veinlets or silica flooding.	Pyrite (arsenopyrite)-sericite-chlorite-carbonate at greenschist grade Pyrrhotite (loellingite) grunerite-garnet at amphibolite grade	Au > Ag As ± Cu	Superior: Musselwhite, Cockshutt-McLeod, Pickle Crow Yilgarn: Mount Magnet, Mount Morgans, Sunrise Dam (in part), Nevoria
Sulfidic replacements and crustiform veins	Crustiform-colloform carbonate-quartz veins and breccias, with various proportions of sulfidic replacements of wall rocks or vein carbonates. Sulfides are pyrite or arsenopyrite; stibnite and tellurides abundant in some deposits.	Sericite-carbonate-(albite)-pyrite at greenschist grade Biotite-carbonate-silica ± alumino-silicate at amphibolite grade	Au > Ag, As, Te, ± Sb, Hg, W, Zn	Superior: **Campbell-Red Lake** (in part), Cochenour Yilgarn: Golden Mile, Jundee, Wiluna, Racetrack
Disseminated-stockwork zones	Zones of 5 to 20% sulfides, as uniform disseminations or along foliation-parallel bands, with variably developed stockworks of sulfidic fractures or quartz veinlets, and crackle-type breccias. Sulfides are pyrite or arsenopyrite, with molybdenite abundant at Hemlo.	Albite-carbonate-sericite-pyrite at greenschist grade Biotite-calc-silicate-pyrrhotite ± pyrite at amphibolite grade K feldspar-muscovite ± calc-silicates at Hemlo	Au > Ag, As, Te, ± W, Hg, Cu, Mo, Sb	Superior: **Malartic, Hemlo, Kerr Addison (Flow ore), Ross, Beattie, Madsen Yilgarn: Wallaby, Plutonic, Sons of Gwalia, Kanowna Belle, Binduli**
Sulfide-rich veins and veinlet zones	Sulfide-rich (25–100% sulfide) veins and veinlet zones with intervening disseminated sulfides. Sulfides include pyrite, sphalerite, chalcopyrite, and galena.	Sericite-chlorite ± chloritoid at greenschist grade Biotite-garnet-cordierite at amphibolite grade	Ag > Au, Cu, Zn, Pb ± As, Te	Superior: **Doyon**, Mouska, Copper Rand, Sleeping Giant Yilgarn: Mount Gibson, Bellevue
Semimassive to massive sulfide lenses	Semimassive to massive sulfide lenses of pyrite, chalcopyrite, sphalerite, and galena, with pyrrhotite and magnetite in some cases.	Sericite-quartz ± chlorite or garnet-biotite Quartz-andalusite-kyanite-pyrophyllite	Ag > Au, Cu, Zn, Pb, As ± Te, Sb	Superior: **Horne, LaRonde-Penna**, Bousquet 2-Dumagami, Bousquet 1 Yilgarn: none

Table 1.2: Models for the orogenic gold deposits of the Superior Province and Yilgarn Cratons. Modified from Kerrich and Cassidy (1994).

Hypothesis	Terrane/time connotation	Process, or evidence	Sources	Comments
TTG	Abttibi Subprovince ~2695 to 2685 Ma	- Gold from abundant TTG magmas in mid-crust	Burrows & Spooner, 1987	- Gold related in time to late accretion and shoshonites at -2680-2670 Ma - Pb, Sr, 0, C isotopes of deposits are inconsistent with TTG source alone
"Early gold" models				
Granulization	Superior Province ~2710 to 2670 Ma	- Granulization of mid-crust by mantle CO_2 - Gold, LILE driven to mid-crust	Cameron, 1988 Colvine et al., 1988 Card et al., 1989	- Pb, Sr isotopes of deposits unlike Kapuskasing, C isotopes dissimilar to mantle C alone, LILE of deposits not complementary to LILE-depleted granulites
Cratonization	Superior Province ~2710 to 2670 Ma	- Empirical evidence for deposits forming in equilibirium with ambient metamorphic and rhelogoical environment	Colvine, 1989	- Corroborative evidence from Archean Yilgam and Zimbabwe deposits, and lode gold deposits of all ages
Gold-shoshonite (A)	Superior Province ~2710-2670 Ma	- Association of gold and shoshonites in space and time with terrane boundary structures marking accretionary tectonics - robust -2680 Ma vein zircon ages in Abitibi Subprovince - Young ages reflect disturbance	Wyman & Kerrich, 1988 Kerrich & Wyman, 1993 Claoue-Long et al., 1990	- Gold mineralization "flare-up" over 1,500,000 sq. km during restricted interval of 2710-2670 Ma based on roboust ages - Explains sparsity of Au in early Archean; abundant Au in Cordillerao-type tectonicsat -2680 Ma, and in Mesozoic Cordillera - Deposits in metamorphic and rheological equilibrium with host terrane - Stable and radiogenic isotope and field evidence for secondary resetting, abberant young ages equilibrium with host terrane
Gold-shoshonite (B)	Superior Province ~2710 to 2670 Ma	- Relationships as in (A) - Shoshonites intrinsically Au-rich	Rock et al., 1989	- Consistent with accretionary tectonic models of Superior Province and Yilgam Craton - Shoshonites have average crustal Au
Crustal continuum	Yilgam Craton 2630 ± 10 Ma	-related to accretionary processes	Groves et al., 1992, 1994 and references therein	- Gold mineralization occurred over 1,000,000 sq. km in restricted interval of 2630±10 Ma - Deposits in metamorphic and rheological equilibrium with host terrane
"Late gold" models				
Delayed thermal rebound	Abitibi Subprovince ~2630 to 2580 Ma	- Based on variably young ages in Val d'Or area - Thermal rebound ~50-100 m.y.	Hodgson et al., 1989	- Young ages likely record isotopic resetting - Stable isotopes variably reset - Time constants of thermal rebound are <10 to 40 m.y., not 100 m.y.
Late metamorphism	Abitibi Subprovince ~2630 to 2580 Ma	- Gold related to young zircon metamorphic ages in Kapuskasing - Unrelated to greenstone belt metamorphic or magmatic evolution - Magmatic underplating provides late heat for young ages, and CO2 for ore fluids	Jemielita et al., 1990 Wong et al., 1991 Hanes et al., 1992 Zweng et al., 1993	- Young ages likely record isotopic resetting - Sr, Pb, C isotopes of deposits unlike Kapuskasing (Kerrich, 1991) - No evidence for magmatic underplating of Kapuskasing at ca. 2600 Ma - Inconsistent with province-wide accretion

wt.% NaCl equiv.) containing $CO_2 \pm CH_4 \pm N_2 \pm H_2S$ (Kerrich et al., 2000). Detailed fluid inclusion work has aided in modeling of fluids derived from metamorphic devolatilization, which is gaining increased acceptance (Bodnar et al., 2014). Evidence for metamorphic devolatilization includes (1) the common $H_2O–CO_2–CH_4–N_2–H_2S$, low salinity fluids; (2) the isotopically heavy $\delta^{18}O$ and δ D values for hydrothermal minerals; (3) variable $\delta^{34}S$ values; and (4) the general lack of ores in high-grade metamorphic rocks (Saunders et al., 2014).

Although a metamorphic fluid source is currently the favored model, no single model can account for all the different types of gold occurrences. The range of models are summarized in Table 1.2. The models include (1) tonalite-trondhjemite-granodiorite (TTG) where orogenic gold deposits are linked to the voluminous TTG magmas that are exposed in the Kapuskasing Structural Zone; (2) granulitization of mid- and lower-crustal rocks drives gold and lithophile elements into structural traps within the upper crustal rocks; (3) cratonization where orogenic gold deposits are closely related to the thermal and rheological characteristics of their environment, as well as to a late-kinematic timing throughout the late Archean terranes; (4) a gold-shoshonite association where the spatial association between gold, shoshonites, and terrane boundary structures is interpreted to have a common geodynamic setting; (5) a second gold-shoshonite association where gold-rich shoshonites with a source near the core-mantle boundary, contribute gold to metamorphic fluid reservoirs in shear zones; (6) crustal continuum model where orogenic gold deposits in greenschist facies have counterparts in subgreenschist, amphibolite and granulite facies; (7) delayed dehydration where a thickened greenstone belt undergoing dehydration during thermal rebound, leads to mineralization occurring 100 m.y. post collision; and (8) late deep metamorphic activity with late gold mineralization in the supercrustal sequences related to deep fluid and metamorphic activity.

1.3 Location and Access

The Eagle River complex is situated in the Algoma Highlands, near the headwaters of the Eagle River in northern Ontario. The study area is located 50 km west of Wawa, Ontario. From Wawa, following the TransCanada Highway (No. 17) northward for roughly 50 km until the intersection with the Paint Lake Road (Fig. 1.4). Follow the Paint Lake Road southwestward for roughly 50 km until the Mishi mill area. The road continues for another 20 km southwest to reach the Eagle River complex.

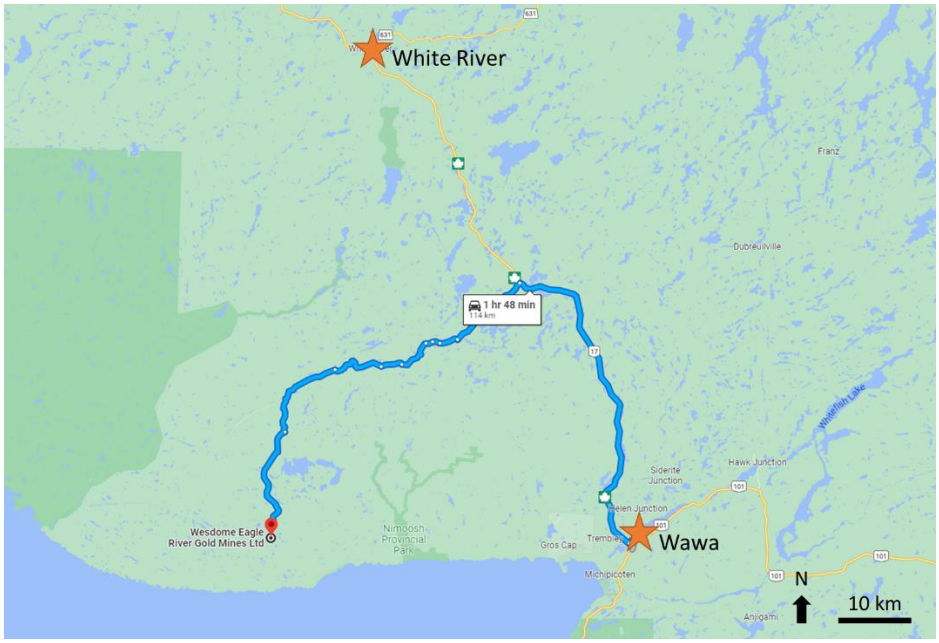

Figure 1.4: Location map from Wawa, Ontario to Wesdome Eagle River Complex (Map courtesy of Wesdome Gold Ltd.).

2. Geological setting

2.1 Regional Geology

2.1.1 Superior Province

The Eagle River deposit is located within the Superior Province within the Wawa Terrane, which will be discussed in detail below. The Superior Province (Fig. 2.1) is one of the largest preserved Archean cratons, covering $1.4x10^6$ km^2 (Percival et al., 2012), and forms the core of the Canadian shield. The Superior Province consists of Archean plutonic and supracrustal rocks. The province has been subdivided into superterranes, terranes, domains and tectonostratigraphic assemblages based on similar metamorphism, deformation, lithology, or age (Stott et al., 2010), with the terranes being generally fault bounded. The greenstone belts are generally greenschist grade, but smaller areas can reach amphibolite-granulite grade (Thurston, 2015).

The Superior Province was formed by a series of accretionary events occurring around 2.6 Ga, with different accretionary sequences occurring roughly 10 m.y. apart. The Northern Superior superterrane formed between 3.9 and 2.81 Ga and acted as the core for further accretion from the south to south-east. Percival et al. (2006) summarized the events that occurred during the formation of the Superior craton as follows: (1) the 3.7 to 2.75 Ga Northern Superior superterrane collided with 3.0 Ga North Caribou superterrane around 2.72 Ga (2) rifting occurring at 2.98 Ga of the Uchi terrane; (3) the 3.4 to 2.8 Ga Winnipeg River terrane collided at 2.72 to 2.7 Ga, which in turn trapped the English River turbidities; (4) accretion of the juvenile western Wabigoon terrane during the central Superior orogeny; (5) synorogenic Quetico turbidities were trapped by the Wawa-Abitibi terrane at 2.695 Ga during the Shebandownian collision; (6) the final accretion of the Minnesota

River Valley terrane occurred at ~2.68 Ga which includes deposition and metamorphism of synorogenic turbidites of the Pontiac terrane.

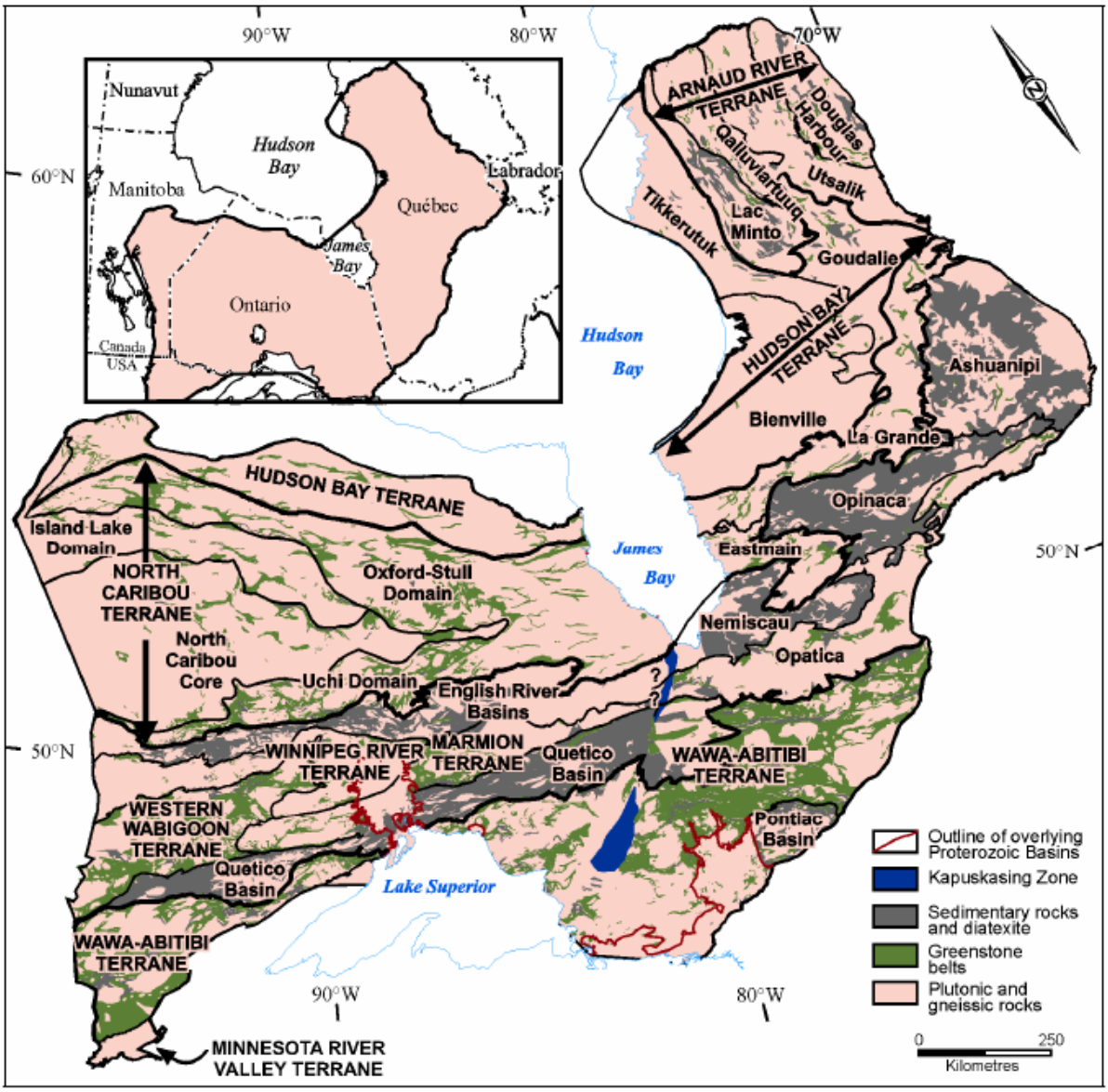

Figure 2.1: Terrane map of the Archean Superior Province. Modified from Stott et al. (2010).

2.1.2 Wawa-Abitibi terrane

The general consensus is that there is a correlation between the Wawa and Abitibi terrane across the Kapuskasing uplift structure (Percival et al., 2006; Fig. 2.1). The Wawa-Abitibi terrane is host to a number of greenstone belts (Figs. 2.2, 2.3), many of which are host to mineralization including gold

deposits, porphyries and base metal deposits (Card & Poulsen, 1998). The Abitibi greenstone belt (Fig. 2.1) is dominated by komatiitic to tholeiitic basalt to calc-alkaline mafic to felsic lavas, that formed between 2750 to 2697 Ma (Ayer et al., 2002). The volcanism consists of six stratigraphic episodes, many of which are capped by a "sedimentary interface zone" dominated by chemical sedimentary rocks (Thurston et al., 1991). There are three major fault systems within the belt that host the majority of the gold deposits namely the Porcupine-Destor fault, Cadillac-Larder Lake Fault, and the Pipestone Fault (Fig. 2.3). The base metal deposits are located between the major fault systems.

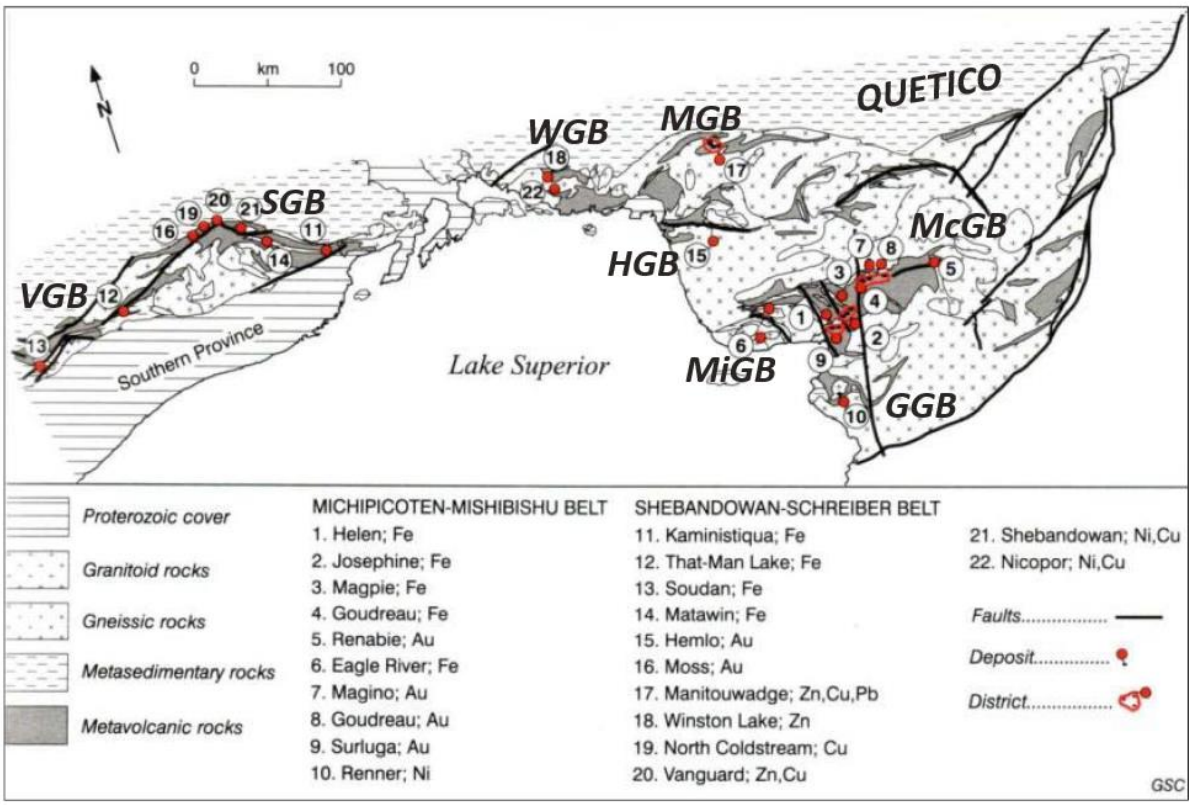

Figure 2.2: Location of different greenstone belts within the western and central Wawa-Abitibi terrane. Modified from Card and Poulsen (1998). Abbreviations: MGB - Manitouwadge greenstone belt; SGB - Shebandowan greenstone belt; VGB - Vermilion greenstone belt; WGB - Winston Lake greenstone belt; McGB – Michipicoten Greenstone belt; MiGB – Mishibishu Lake greenstone belt; HGB – Hemlo greenstone belt; GGB – Gamitagama greenstone belt.

Within the Wawa terrane volcanism began at 2.89-2.88 Ga Hawk assemblage (Fig. 2.4; Turek et al., 1992; Percival et al., 2006). The Greenwater assemblage has been dated at 2.7 Ma and is dominated by mafic to felsic metavolcanic rocks, unconformably overlain by clastic metasedimentary rocks of the Shebandowan assemblage (Lodge et al., 2015). The 2.72 Ma Mantiouwadge greenstone belt is located on the northern margin of the Wawa-Abitibi terrane adjacent to the Quetico terrane (Fig. 2.2). In the southern part of the Wawa-Abitibi terrane, the terrane evolved in a dominantly oceanic setting until the Shebandowanian collision at 2.695 Ga (Percival et al., 2006). The volcanism at ~2.695 Ga occurred during D_1 thrusting, followed by ~2.689 Ga calc-alkalic to alkalic magmatism, <2.689 Ga Timiskaming-type sedimentation, 2.685 to 2.680 Ga sanukitoid magmatism, dextral transpressive D_2 deformation, and <2.682 Ga conglomerates concurrent with D_2 deformation (Turek et al., 1992).

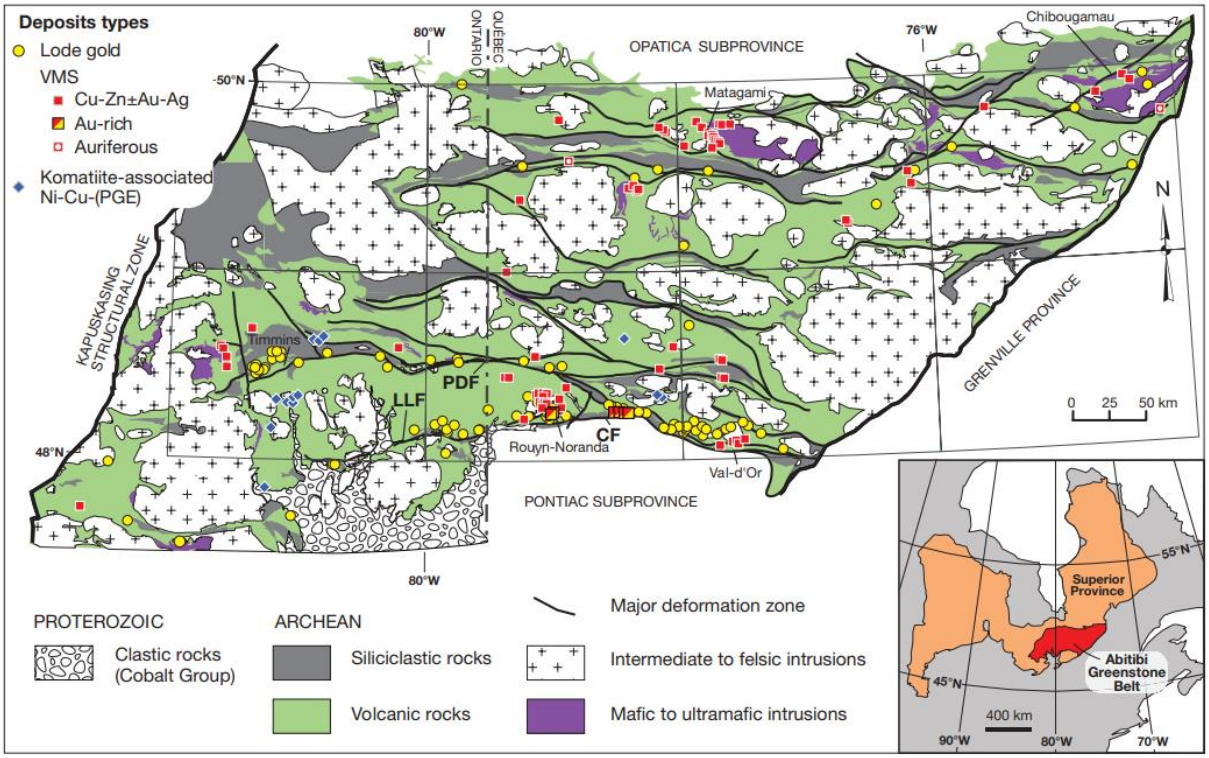

Figure 2.3: Location and distribution of massive sulphide and gold deposits within the eastern Wawa-Abitibi terrane. Modified from Mercier-Langevin et al. (2013). Abbreviations: LLF – Larder Lake fault, CF – Cadillac fault, PDF – Porcupine-Destor fault.

The Abitibi greenstone belt (Fig. 2.3) is one of the largest Neoarchean greenstone belts. The geology of the Abitibi greenstone belt is summarized by Ludden et al. (1986). The belt is divided into the southern volcanic zone (SVZ) and the northern volcanic zone (NVZ). The SVZ is dominated by komatiitic to tholeiitic volcanic plateaus and 2710 to 2700 Ma bimodal volcanics centers, which

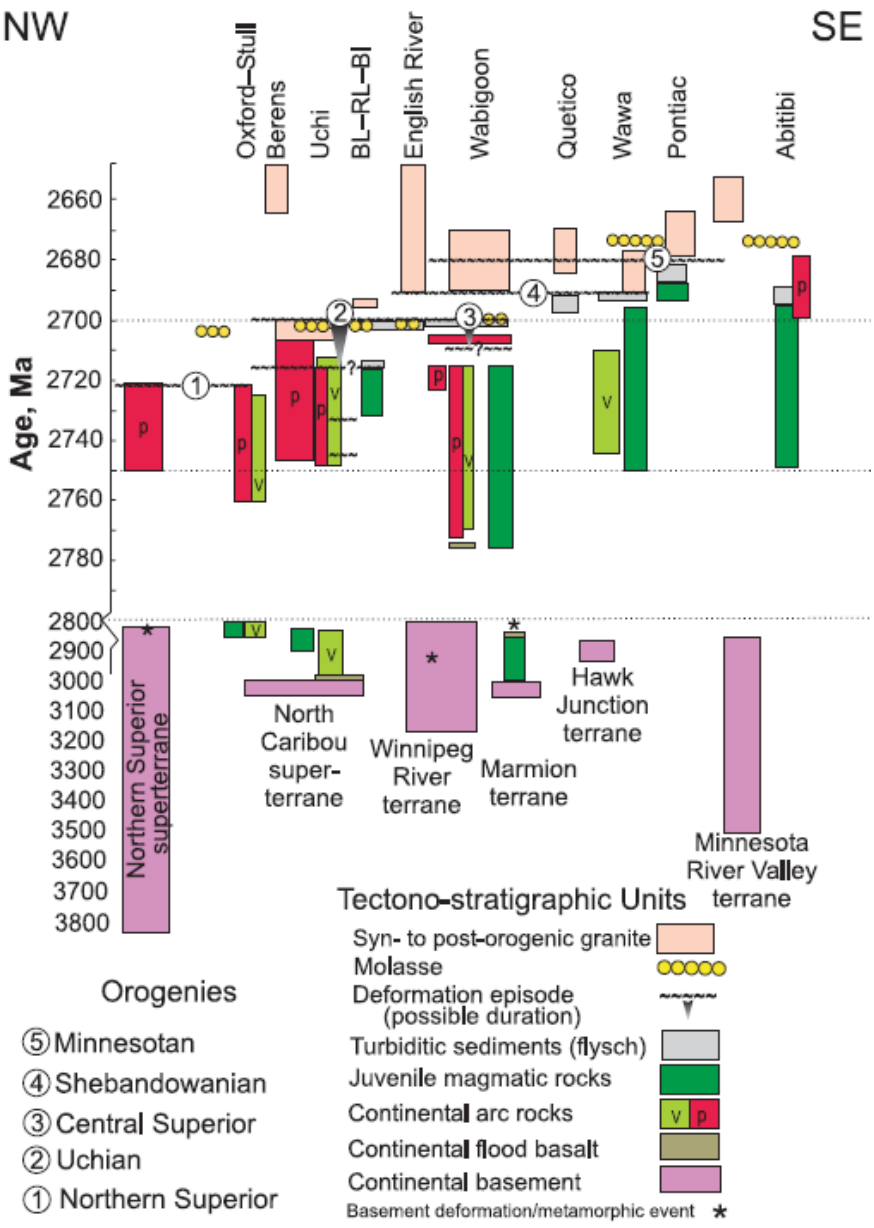

Figure 2.4: Time-space correlation diagram showing the assembly of the western Superior Province. Modified from Percival et al. (2006).

formed in rift basins. The SVZ is superimposed on older 2720 Ma NVZ and consists of basaltic to andesitic and dacitic volcanic rocks which are intruded by a layered mafic-anorthositic plutonic complex. The volcanic rocks are overlain by felsic pyroclastic rocks that are coeval with tonalitic plutons at 2717 ± 2 Ma (Ludden et al. 1986). Six volcanic assemblages have been defined, which formed between 2795 and 2695 Ma. The belt is host to multiple VMS and gold deposits, most of which lie along or between the major faults (Mercier-Langevin et al., 2013). These faults are east-west trending and include the Larder Lake-Cadillac fault and the Porcupine-Destor fault.

The Manitouwadge greenstone belt is composed of bimodal volcanic rocks, layered gabbro-anorthosite intrusions and sedimentary rocks that have been metamorphosed to amphibolite grade, with granulite grade towards the Quetico boundary (Fig. 2.2; Lodge, 2012). D_1 deformation is expressed through mylonitic faults and D_2 through sheath folding. The Greenwater and Manitouwadge assemblages are interpreted to have formed in an arc to back-arc system (Percival et al., 2006), which is consistent with presence of a massive sulphide deposit in the Shebandowan, Winston Lake, and Manitouwadge areas.

The 2.72 to 2.67 Ma Hemlo greenstone belt is bounded on the north, east and south by Archean granitoid batholiths (Fig. 2.2; Beakhouse & Davis, 2005). The eastern part of the belt is dominated by massive to pillowed tholeiitic basalt flows and felsic to intermediate calc-alkaline pyroclastic rocks with minor sedimentary rocks, whereas the western part of the belt is dominated by turbiditc wacke-mudstone and minor conglomerates (Muir, 2003). The rocks are metamorphosed to greenschist facies in the west and amphibolite in the east (Beakhouse & Davis, 2005). There are at least six stages of deformation (D_1-D_6) recorded within the area, with the gold being emplaced during mid-D_2 deformation defined by rock foliation (S_2), large folds (F_2) and high-strain zones (Muir, 2003). The gold mineralization is thought to have occurred between 2693 Ma and 2680 to 2690 Ma

(Jackson et al., 1998). The later date marks the termination of magmatic arc stage (~2720-2688 Ma) and onset of uplift, erosion and deposition of late sedimentary rocks (Jackson et al., 1998).

2.1.3 Michipicoten greenstone belt

The Michipicoten greenstone belt is located near the center of the Wawa-Abitibi terrane trending roughly northeast and is the largest greenstone belt in the Wawa region measuring 140 km long and 45 km wide (Fig. 2.2; Williams et al., 1991; Jackson, 2000). The belt consists of three mafic to felsic volcanic cycles namely the 2.9 Ga Hawk assemblage, the 2.75 Ga Wawa assemblage and the 2.7 Ga Catfish assemblage (Fig. 2.5; Sage, 1994; Jackson, 2000). The Hawk assemblage consists of massive to pillowed basaltic to peridotitic komatiites overlain by pyroclastic rocks and capped by chert-magnetite-sulphide iron formation. The Wawa assemblage comprises of high Mg- and Fe-rich tholeiites overlain by intermediate to felsic volcanic and pyroclastic rocks (Sage, 1994). The assemblage is capped by a sequence of carbonate and sulphide facies iron formation (Jackson, 2000). The Catfish assemblage is like the Wawa assemblage but also contains a thin sequence of chert-magnetite iron formation and is capped by metasedimentary rocks. The youngest unit is a metasedimentary sequence containing conglomerate horizons with trondhjemite clasts and boulders which increase in size and number towards Lake Superior. Based on clast size and pressure indicators it is interpreted that different aged volcanic cycles developed in different water horizons, with 2.9 Ga cycle 1 being in deeper water, the 2.75 Ga cycle 2 in transition from deep to shallow water, and the 2.7 Ga cycle 3 in shallow water (Sage, 1994).

Granitic stocks in the belt are generally younger than the supracrustal rocks and consist of potassium feldspar-rich granitic intrusions, ranging from tonalite to nepheline syenite in composition. The granitic stocks range in age from 2670 to 2700 Ma (Williams et al., 1991). The belt contains multiple sets of mafic dykes with variable strike orientations ranging from east-southeast to

northwest. Due to similar textures the age relations are not well constrained but older dykes show metamorphic textures (Sage, 1994). The belt is interpreted to represent a north-facing monoclinal sequence of supracrustal rocks younging to the north, that developed within an island arc or convergent plate margin environment with early crustal contamination (Sage, 1994). The alteration

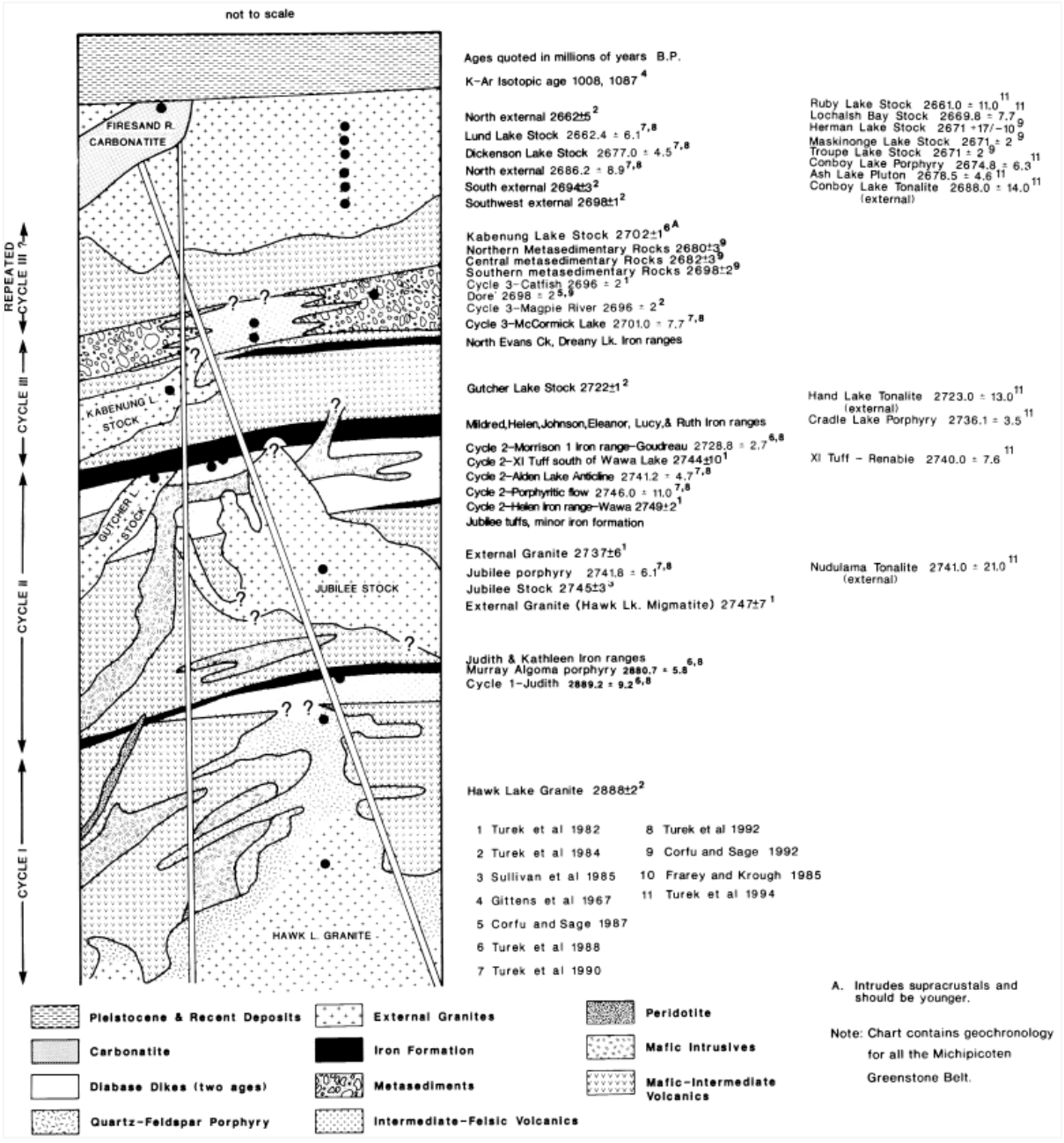

Figure 2.5: Schematic stratigraphic column of the Michipicoten greenstone belt (from Sage, 1994).

styles found within the belt include carbonatization, tourmalinization, chloritoid porphyroblasts and Ca-Na metasomatism (Sage, 1994).

The gold mineralization within the belt occurs in different environments with at least three ages of mineralization (Sage, 1994; Jackson, 2000). The gold mineralization is associated with various rock assemblages which include the 2900 Ma Hawk Lake granitic complex, the 2750 Ma Jubilee Lake Stock, and at least one event post-supracrustral rock potentially related to hydrothermal stage of regional metamorphism (Sage, 1994). Gold is hosted by plutonic rocks within shear zones, hosted by quartz veining with minor sulphides and CO_2, K and S metasomatism (Jackson, 2000). The alteration minerals include ankerite, calcite, pyrite, pyrrhotite, potassium feldspar, sericite, biotite, and hydrous mineral assemblage. The most favorable place for gold mineralization is the older, saccharoidal textured, folded quartz with minor sulphide mineralization (Sage, 1994) or mechanical and chemical traps along a jog in a major sinistral Hemlo shear zone, most likely during early deformation of second generation structures (Davis & Lin, 2003).

2.1.4 Mishibishu Lake Greenstone belt

The Mishibishu Lake greenstone belt (Figs. 2.2 and 2.6) extends from Dog Harbour in the east, northwest through Mishibishu Lake and west to the Pukaskwa River (Fig. 2.6; Evans, 1942; Bennet & Thurston, 1977). The belt consists of similar geology to the Michipicoten greenstone belt to the northeast, and potentially the Gamitagama belt to the south (Mordaunt, 1986; Keller, 1989; Turek et al., 1990). The correlation between the greenstone belts is based on the zircon ages of volcanic and plutonic rocks as well as correlation between four Michipicoten-type iron facies (Turek et al., 1990). The Mishibishu Lake greenstone belt formed between >2721 Ma and 2671 Ma, the Gamitagama greenstone belt formed between > 2713 and 2668 Ma, and the Michipicoten greenstone belt formed between > 2889 and 2668 Ma (Turek et al., 1990). The iron facies include (1) the oxide facies

of magnetite-hematite-chert, (2) carbonate as siderite stained with limonite, (3) sulphide as pyrite lenses in the carbonate facies, and (4) the silicate phase composed of chlorite, biotite and actinolite (Keller, 1989; Turek et al., 1990).

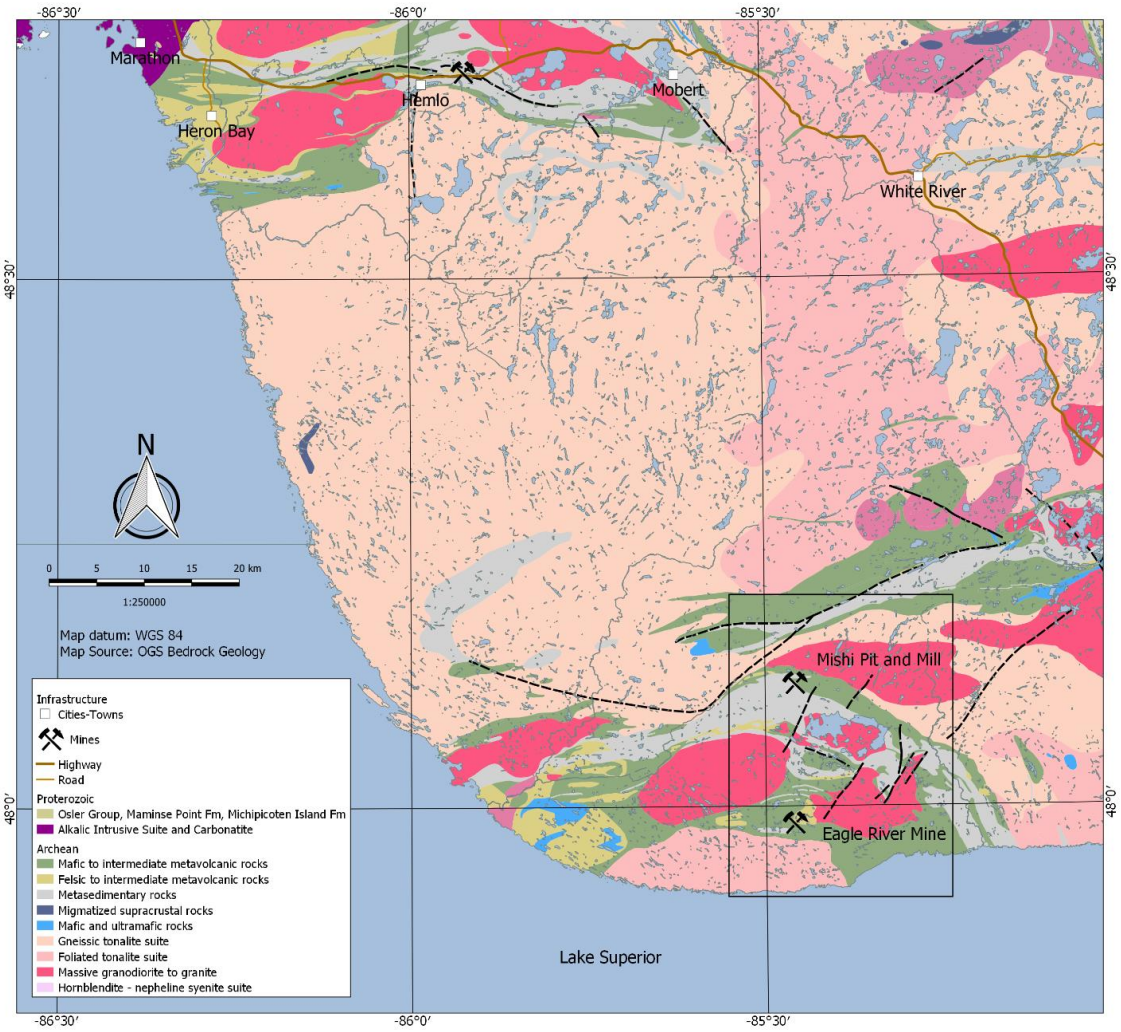

Figure 2.6: Geology of the Wawa terrane showing the location of the Eagle River mine and the Mishi Pit hosted within the Mishibishu Lake greenstone belt. The Eagle River complex is located 51.5 km west of Wawa, Ontario (Map courtesy of Wesdome Gold Ltd.).

The Mishibishu Lake greenstone belt is dominated by greenschist facies mafic to intermediate volcanic rocks of tholeiitic to calc-alkaline affinity with sedimentary sequence ranging from conglomerate to argillite, and felsic volcanic rocks, quartz-feldspar porphyry, and iron formation (Keller, 1989; Turek et al., 1990). The rocks generally strike 90-120° and dip to the north. The belt is

surrounded by three Archean granitic units which include the Bowman Lake batholith (~2639 ± 25 Ma) to the north-east, the Floating Heart batholith (2693.2 ± 6.9 Ma) to the south and the Central pluton to the northwest (Fig. 2.7; Keller, 1989; Turek et al., 1990; Sage, 1994; Kilbourne, 2020).

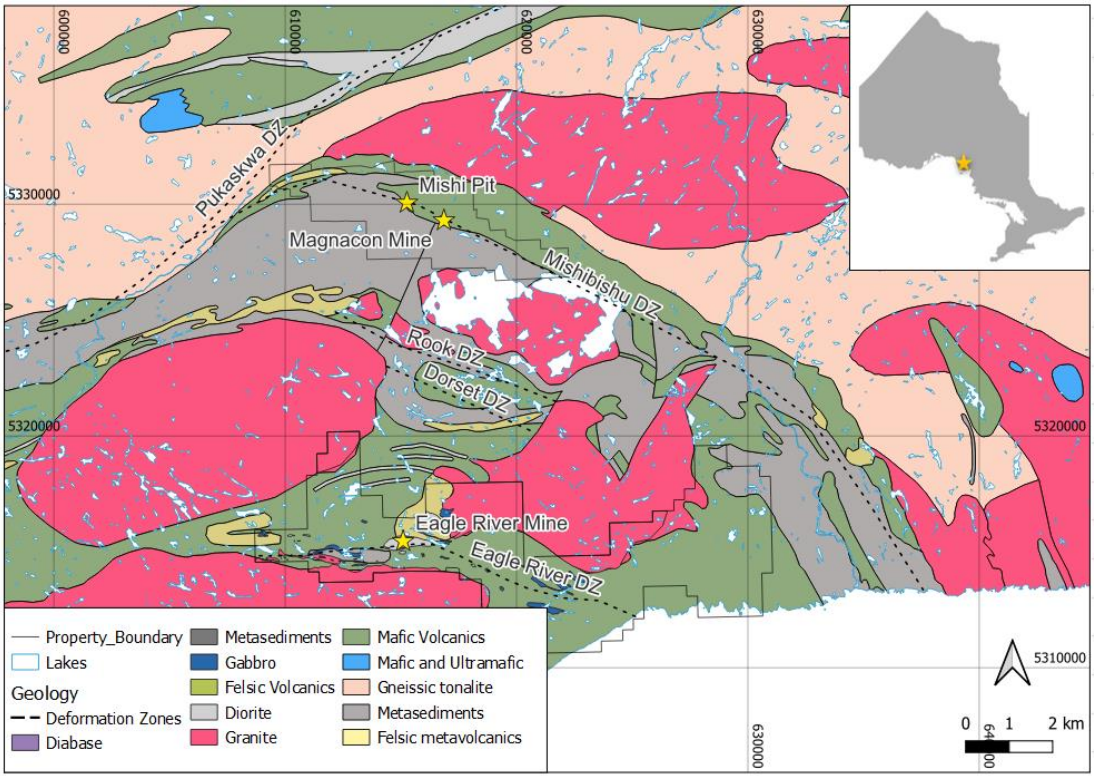

Figure 2.7: Local geology of Eagle River mine (Map courtesy of Wesdome Gold Ltd.).

The belt is bound on the north side by the Pukaskwa deformation zone which is oriented generally north-east. There are numerous topographic lineaments visible on maps and air topography of the region which are interpreted as faults and shear zones (Bennet and Thurston, 1977). The main structures are dominantly northeast striking with lesser northwest striking faults and fractures, which offset the greenstone stratigraphy, and are commonly infilled by the Proterozoic diabase dikes (Brousseau et al., 2011). There are three major faults found within the area in the vicinity of the Mishibishu Lake and Katzenbach Lakes, which have a displacement from 600 to as much as 3000 m, that post date the major period of granitic intrusions (Bennet and Thurston, 1977). Several persistent lineaments parallel to the strike of the rocks are interpreted to represent strike-slip faults

or early thrust faults which have been rotated into a near vertical dip by later folding (Bennet and Thurston, 1977).

The Mishibishu Lake greenstone belt was metamorphosed under greenschist facies conditions indicated by the common occurrence of albite with the calcium-bearing minerals clinozoisite and epidote (Bennet and Thurston, 1977). The presence of biotite within metasediments and metavolcanics indicates that conditions for lower greenschist facies had been reached locally. The western part of the Mishibishu Lake greenstone belt contains oligoclase or sodic andesine indicating a higher grade of metamorphism than greenschist facies, or contact metamorphism under hornblende-hornfels facies caused by intrusion of numerous northwest-trending diabase dikes (Bennet and Thurston, 1977).

The Mishibishu deformation zone varies in width from 200 to 500 m and is composed of several shear zones, which may have developed due to emplacement of the large Pukaskwa Gneiss Complex (Gneiss tonalite) to the north (Fig. 2.7; Heather, 1986). The deformation zone is defined by rock textures that are partially or totally destroyed by hydrothermal alteration and/or deformation, and hosts several gold showings within large zones of intense hydrothermal alteration (Heather, 1986). The mafic rocks to the north of the shear are generally massive and consist of gabbros and quartz porphyry. The quartz-feldspar and feldspar porphyry dykes are cut by and cut the mineralization (Heather, 1986). The felsic-intermediate lapilli tuff makes up the footwall portion of the gold deposit. South of the felsic-intermediate lapilli tuff consists of a package of heterogenous conglomerates, arkoses and wackes. The gold mineralization is an orogenic gold occurrence related to a longitudinal shear zone hosted within quartz-carbonate veining (Brousseau et al., 2011). The style of veining ranges from mafic-hosted, iron-rich schists and quartz veins to felsic-hosted veins of the quartz feldspar porphyry unit (Brousseau et al., 2011). Gold is dominantly contained in fine-

grained euhedral to subhedral pyrite, or present as free gold in quartz-carbonate veining (Brousseau et al., 2011).

The Mishi pit (Figs. 2.7, 2.8) is described in detail in a 2011 technical report and pre-feasibility study by Brousseau et al. (2011) and is only summarized here. The Mishi open pit is a low-grade disseminated gold deposit located along the contact of the Mishibishu deformation zone, oriented roughly east-south-east and is hosted in clastic sedimentary rocks, felsic tuffs, and mafic flows (Fig. 2.8). The Mishi Pit was first staked in 1982 by MacMillan Energy Corp. In 2002 the Mishi Pit started producing its first ore, and since then has been mined intermittently producing a total of 9,580 ounces from 423,019 tonnes at grade of 2.71 g/t. At the end of 2003 resource and reserves were calculated with a proven reserve of 44,000 tonnes at a grade of 3.8 g/t (Brousseau et al., 2011). Wesdome Gold Mines Ltd purchased the property in 2006 and has been its current owner since

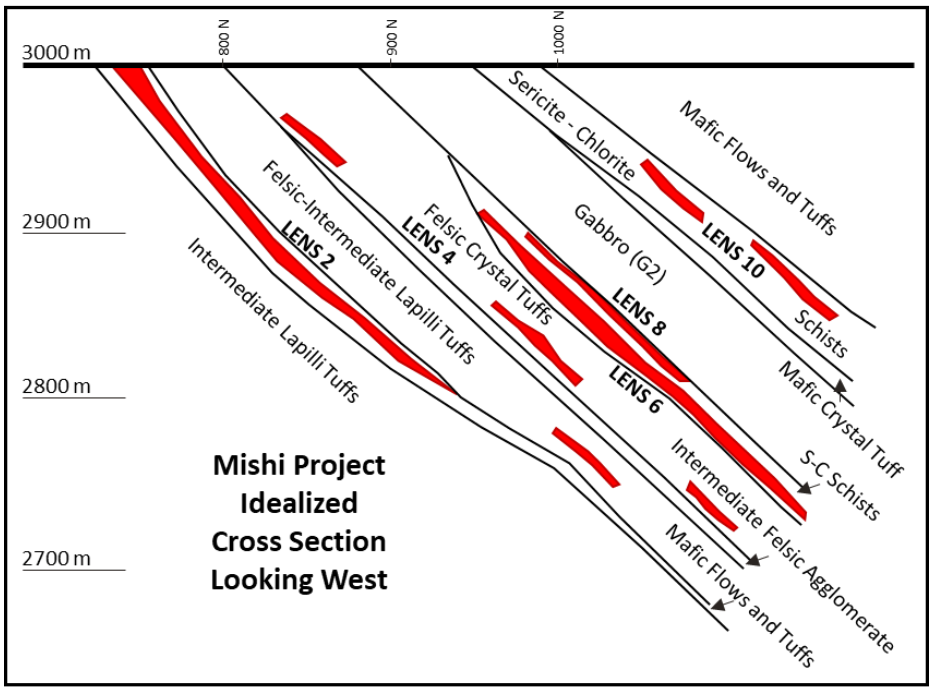

Figure 2.8: Idealized cross section of the Mishi Main Zone. Modified from Bates and Miree (1991).

then. The proven and probable reserves as of 2015 include 131,000 ounces from 1.885 million tonnes at a grade of 2.2 g/t Au (Kilbourne, 2020). At the current time the Mishi open pit is not being mined and is under care and maintenance. The Magnacon underground deposit is hosted in the same structure as the Mishi Pit located approximately 2 km southeast of the Mishi Pit. The mineralization is hosted within white quartz veins containing galena, chalcopyrite, sphalerite, pyrite, and tourmaline. The mine was in operation from 1989 to 1990 producing a total of 43,275 ounces of Au from 241,000 tonnes at 5.6 g/t Au (Mannard & Ng, 2016; SRK, 2022). Currently the Magnacon deposit is under care and maintenance.

South of the Mishibishu deformation zone is the Rook and Dorset Deformation Zone, striking generally at 110° and dipping steeply to the southwest, oriented sub parallel to the Mishibishu deformation zone (Fig. 2.7). The most prospective area within the Dorset Deformation Zone is termed the Dorset zone with grades reporting up to 6.0 g/t Au (Kilbourne, 2020). The Dorset zone (Fig. 2.9) is summarized from a technical report by Kilbourne (2020). The Dorset zone is hosted in mafic metavolcanic rocks dominated by greenschist massive to pillowed flows. The flows are calcite and ankerite altered, often associated with mineralization. The metasedimentary rocks vary from greywacke to siltstone to argillite, which exhibit lamination and well-developed foliation with local kink bands. The volcanic rocks and sedimentary units are intruded by quartz-feldspar and feldspar porphyry units which display moderate to strong silicification and sericitic alteration. The porphyry unit is locally mineralized with fine-grained pyrite and low gold values (Kilbourne, 2020). The gold mineralization is associated with strongly albitized and carbonate altered sections, with silicification and associated with sulphides consisting of pyrite and arsenopyrite with trace amounts of pyrrhotite and chalcopyrite (Kilbourne, 2020). Increased gold values are commonly associated with increased sulphide concentrations and higher pyrite:arsenopyrite ratios. Drilling of the Dorset Zone includes the 1.5 g/t Au ranging in length from 1.0 to 19.1m, with higher values of 2.01 g/t Au over 12.1 m and

2.77 g/t Au over 16.2m (Kilbourne, 2020). The indicated resource consists of 780,000 tonnes at 1.42 g/t Au and inferred resource of 4,760,000 tonnes at 1.19 g/t Au (Kilbourne, 2020).

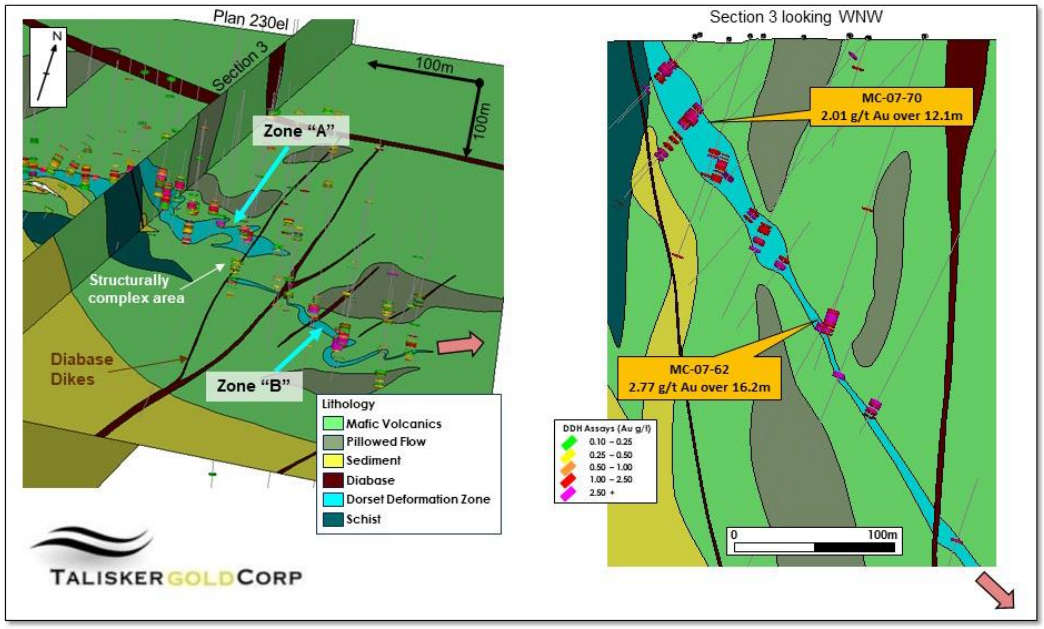

Figure 2.9: Geological Interpretation of the Dorset zone. Modified from Kilbourne (2020).

South of the Dorset Deformation Zone there is a thick package of banded iron formation exhibiting signs of folding, sub-parallel to the Eagle River deformation zone located further south (Fig. 2.7). The Eagle River deformation zone is a 16-km long shear zone oriented generally east to east-south-east (Kilbourne, 2020). The zone is dominated by tholeiitic basalts and calc-alkaline andesites with minor clastic sedimentary rocks, chert-magnetite iron formation and diabase intrusions. The supracrustal rocks are steeply north dipping and north facing, plunging moderately to steeply to the east.

2.2 Eagle River mine geology

The Eagle River property is made up of three mining leases that span a total of 882 hectares and an additional 426 contiguous single cell mining claims that make up 9205 hectares (Fig. 2.7; Forslund, 2020). The Eagle River Mine is located along the hinge of the Eagle River Deformation Zone, with the majority of the mineralization hosted in a stockwork diorite intrusion, with additional mineralization

in the surrounding volcanic rocks (Fig. 2.10). The mine is hosted within an ellipsoidal quartz diorite body 2.4 km long and 0.5 km wide. The diorite dips roughly 70° to the north and has a slight bend northward along the middle (Fig. 2.11). The diorite ranges from medium- to coarse-grained with weak to strong potassic alteration, and weak to moderate epidote alteration. The alteration tends to increase towards the mineralization (Jennifer Moscalli, personal communication, 2022). Several mineralized zones have been identified within the deposit including the No. 8, 7, 6 and 300 zone hosted in quartz diorite, and No. 2 and 3, No Name Lake and HP zone hosted in sheared mafic volcanics (Figs. 2.11 and 2.12). The mineralization is hosted in sheared quartz-carbonate veining that are sub-parallel to the deformation and consist of pods that are spaced 400 m apart. Previous work

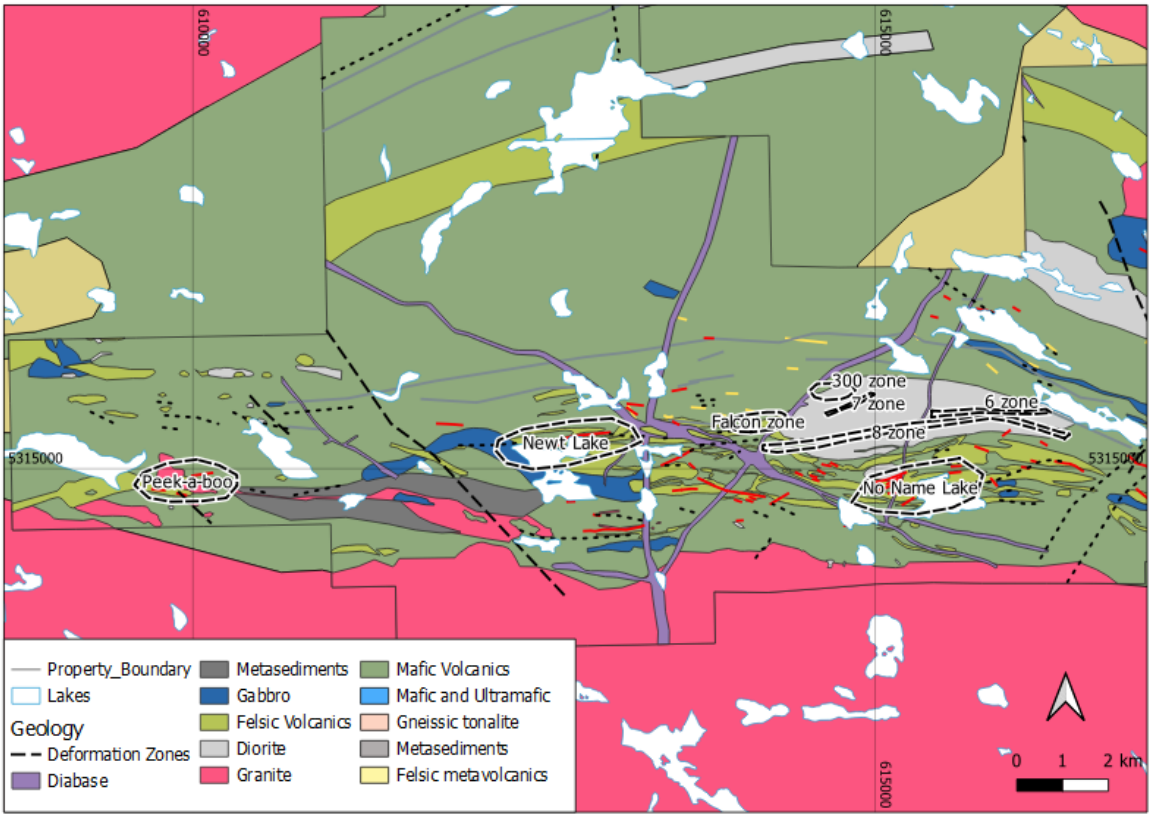

Figure 2.10: Mine geology and the location of the different zones within the property (Map courtesy of Wesdome Gold Ltd.).

by Clemson (1989) showed that gold occurs dominantly along the quartz-sericite grain contact, less so along the sulphide-gangue contacts, and trace amounts within sulphide grains. The following zone descriptions are a compilation of historical and current drill logs.

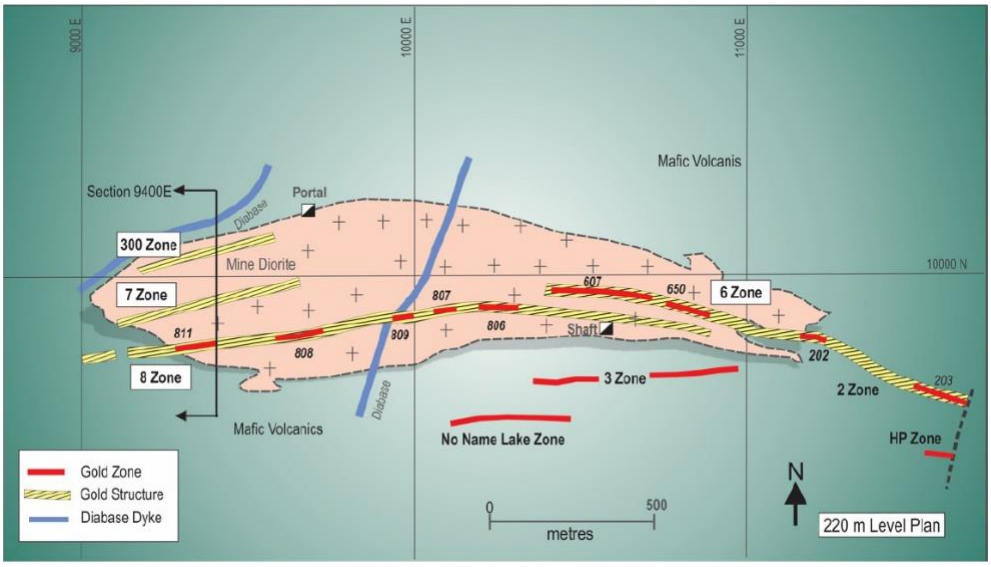

Figure 2.11: Location of different zones within the Eagle River mine(modified from Mannard & Ng, 2016).

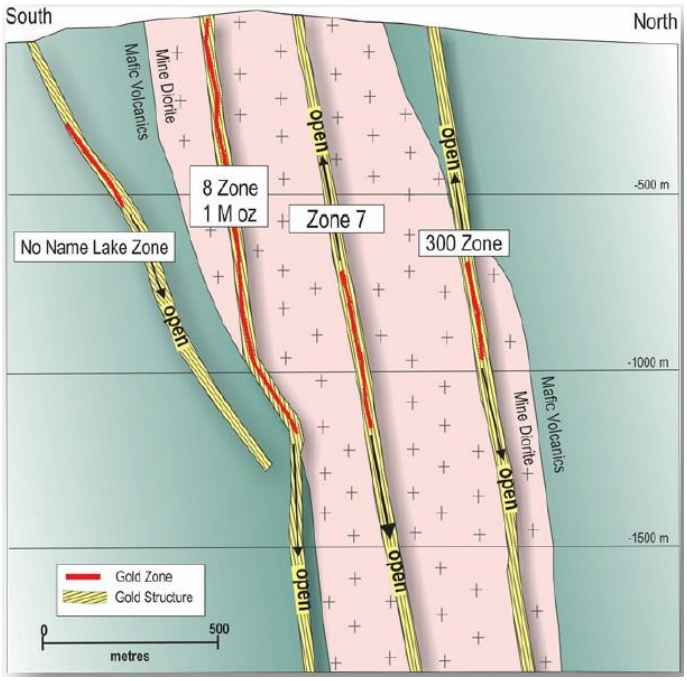

Figure 2.12: Cross section of the Eagle River mine along 9400E (modified from Mannard & Ng, 2016).

The mine has been in constant production since 1995 focusing on mining multiple quartz-bearing, shear-hosted gold horizons (Fig. 2.11). As of 2021 the Eagle River Mine had produced a total of 7.4 Mt of ore averaging 9.86 g/t Au yielding 1.5 M oz of Au (SRK, 2022). The bulk of mining took place in the west portion of the 8 zone, with two new parallel zones (7 and 300) being discovered in 2013 (Forslund, 2022).

2.2.1 8 zone

The majority of the ore at Eagle River is found in the 8 zone which is entirely hosted in dark grey to beige diorite (Figs. 2.11 and 2.12). Strong pervasive chlorite-biotite alteration is present with localized sections of strong hematite-potassic-albite. Generally, the intensity of potassic alteration increases towards the deformation zone. Trace patchy pyrite-pyrrhotite is commonly associated with minor shearing or deformation. The diorite is bound by a diabase intrusion on the northern, southern, and western sides. The diabase is dominantly fine- to medium-grained dark grey to black with chill margins, exhibiting both magnetic highs and lows, with local hematite fracture infill throughout the unit. Rare Matachewan diabase dykes cut the diorite on the west and north side of the zone distal to mineralization. Mafic intrusive rocks are dark green, very fine- to fine-grained with chlorite-biotite alteration. Trace amounts of disseminated pyrite-pyrrhotite are associated with the unit.

The mineralization is hosted within a series of steeply north dipping, laminated quartz vein shoots. The veins tend to vary in thickness from one meter to fifteen meters, with an average thickness of two and a half meters. The veins have a spatial relationship with mafic dykes, which are sub-parallel to oblique, and pre-date the mineralization (Michaud, 2019). The gold is structurally controlled within highly strained smoky quartz with sericite-chlorite and sulfides consisting of pyrite-pyrrhotite-galena-sphalerite-chalcopyrite.

2.2.2 Falcon zone

The Falcon zone (Figs. 2.10 and 2.13) was discovered in 2018 during surface exploration (Forslund, 2022). The zone is hosted in tholeiitic mafic volcanic rocks underlain by calc-alkaline volcaniclastic rocks of intermediate to felsic composition. The gold mineralization is situated along two distinct structural trends within the calc-alkaline pyroclastic rocks.

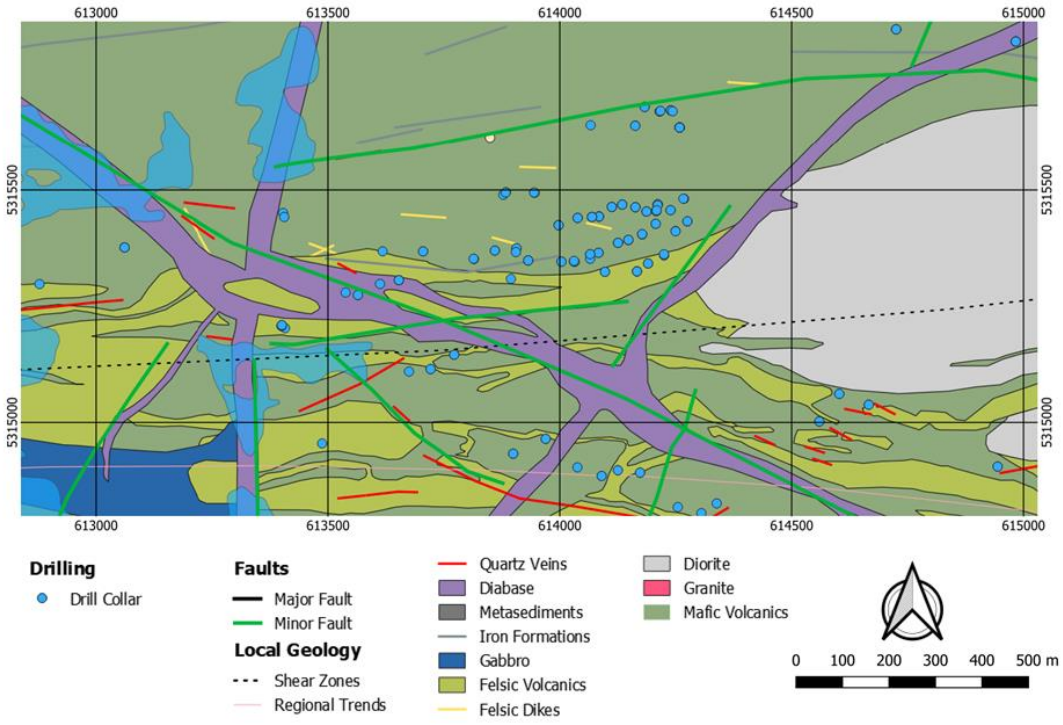

Figure 2.13: Local map showing the Falcon zone and the associated drilling locations (Map courtesy of Wesdome Gold Ltd.).

The Falcon zone is dominated by mafic volcanic rocks to the north and south, and felsic volcanic rocks in the center with minor felsic intrusive rocks (Fig. 2.13). A northeast trending diabase dyke cross cuts the unit on the east side, and a porphyritic unit cutting the zone at various intervals (Fig. 2.15). The feldspar porphyritic unit is massive to very fine-grained grey to dark grey with anhedral to subhedral feldspar phenocrysts. The unit has sharp, straight contacts with the surrounding volcanic rocks.

Mafic volcanic rocks are fine- to medium-grained greyish green basaltic flows and tuffs with pervasive veinlets infilled with quartz. The unit is locally potassic-chlorite-sericite-albite altered. Trace disseminated pyrite locally occurs throughout the unit. Felsic volcanic rocks are variable in appearance and range from massive to fine-grained to moderately to strongly laminated. The unit is very fine- to fine-grained grey to dark grey with variable alteration including silica-albite, chlorite, quartz-carbonate. The laminated section varies from moderate to strong, with white to dark grey banding ranging from 0.1 cm to 2 cm in width with sharp contacts (Fig. 2.14). Some of the banded unit has variably striking veinlets of quartz-carbonate with variable weak to strong alteration including potassic, albite and epidote. The felsic intrusive rocks are green-gray, fine- to medium-grained tuffs with patchy epidote-potassic-biotite alteration. Weak to moderate foliation is

Figure 2.14: Variability within the Laminated unit of the felsic volcanic rocks in the Falcon zone. The diagram is a compilation of multiple different drillholes.

developed throughout the unit. Sulphides consist of disseminated to blebby pyrite-pyrrhotite-sphalerite. The diabase unit is a fine- to medium-grained gray green to black rock with pronounced chill margins. The unit has hematite fracture filling throughout, some of which contains minor gouge. Minor quartz-carbonate variably oriented fracture infills locally throughout the unit. Variable styles of alteration halos are noted around the quartz veining, which vary in intensity. The alteration styles include albite-sericite, chlorite-quartz-carbonate, and potassic alteration with minor hematite. Alteration is dominantly found in the calc-alkaline volcaniclastic unit and extends between 10 to 50m into the host rock.

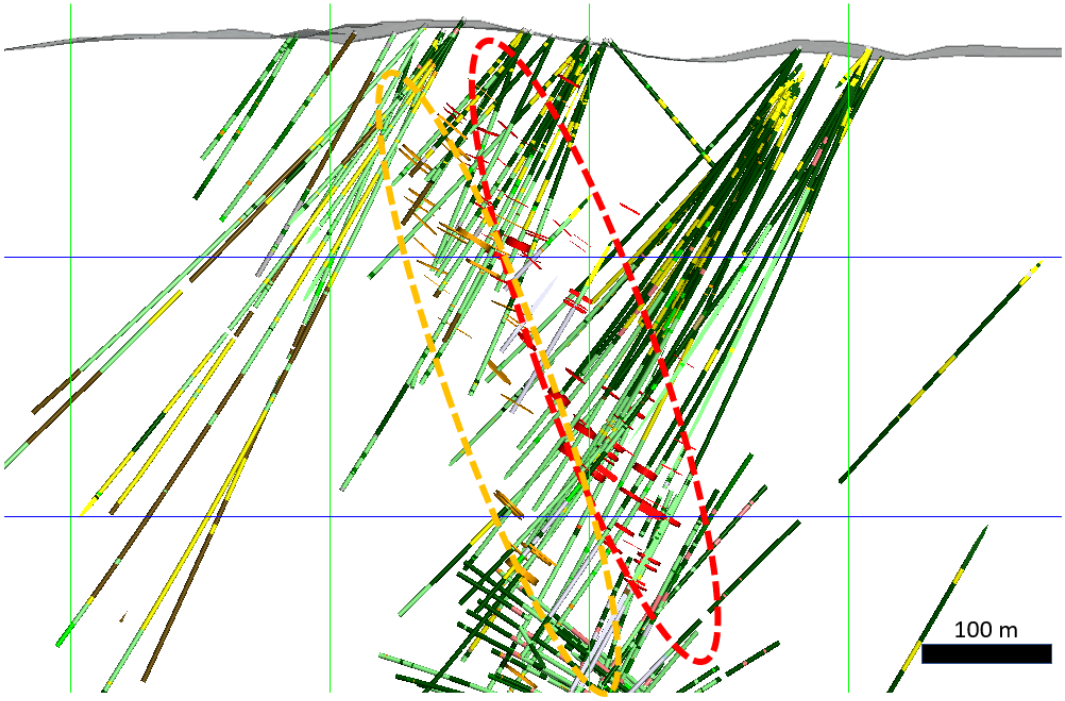

Figure 2.15: Geological section showing the zone 5 (red) and zone 7 (orange) in Falcon Zone. Dark green = mafic volcanics, light green = felsic volcanics, yellow = intrusive unit, grey = diorite, pink = feldspar porphyry.

Gold mineralization is concentrated along two horizons within the calc-alkaline pyroclastic rocks, occurring as laminated quartz-carbonate veining, termed zones 5 and 7 (Fig. 2.15; Forslund, 2022). The gold occurs dominantly as free gold, locally associated with galena, sphalerite, and chalcopyrite. The highest grades reported includes a 36.28 g/t over 1m interval, and some of the additional

intervals include 15.52 g/t Au over 5.4 m, 12.33 g/t Au over 7.5m, 7.67 g/t Au over 6.5 m, and others (Forslund, 2022). Lower grade gold occurrences are also found in thin quartz-carbonate veining in the hanging wall, but they lack continuity. The lower grades samples include 1.23 g/t Au over 9 m, 1.83 g/t Au over 9.1 m, 1.08 g/t Au over 10m, and others (Forslund, 2022).

2.2.3 Newt Lake zone

The Newt Lake zone is located 2.3 km east of the Eagle River Mine (Figs. 2.10 and 2.16). The area is dominated by felsic to mafic volcanic rocks, and felsic intrusive rocks, with a gabbro unit to the south and diabase intrusions to the east.

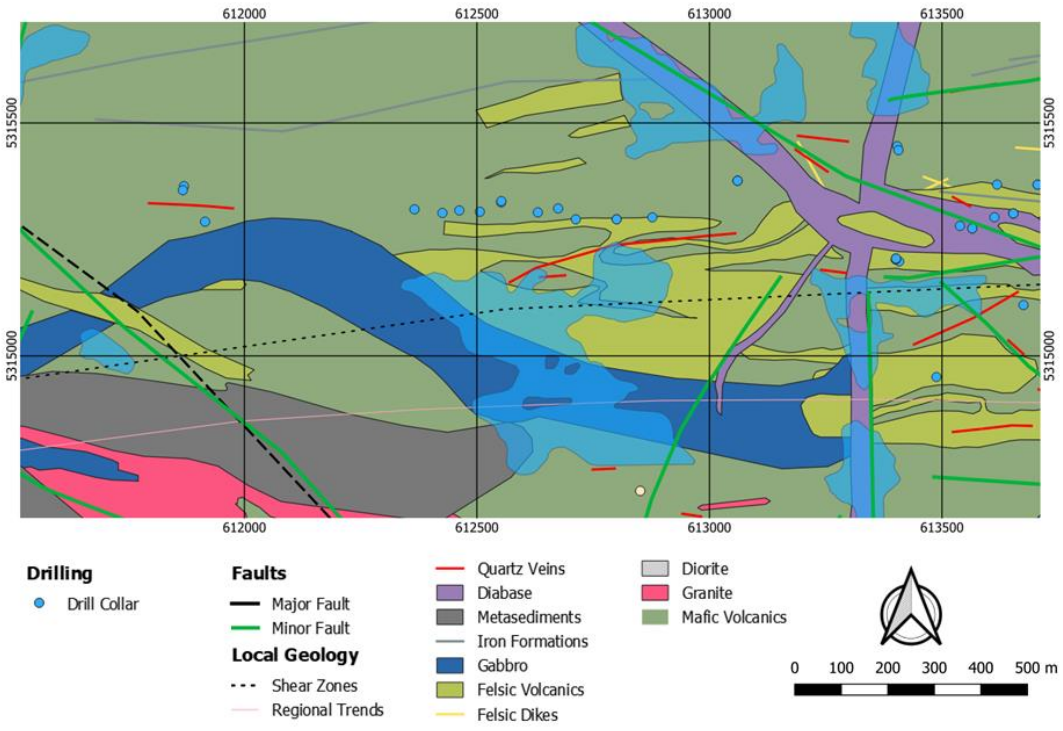

Figure 2.16: Local map showing the Newt Lake zone and the associated drilling locations (Map courtesy of Wesdome Gold Ltd.).

The felsic volcanic rocks are variable in appearance and range from very fine-grained to fine-grained grey to dark grey with variable alteration including silica-albite, chlorite, quartz-carbonate, which are moderately to strongly laminated. The laminated section comprises moderate to strong bands of

white to dark grey ranging from 0.1 to 2 cm in width with sharp contacts. Some of the banded units have variably striking veinlets of quartz-carbonate with potassic, albite and epidote alteration. The mafic volcanic rocks are characterized by green-grey very fine- to fine-grained volcanic flows. Alteration includes chlorite-sericite-biotite, calcite-chlorite. The sulphides consist of disseminated to blebby pyrite-pyrrhotite to chalcopyrite.

The felsic intrusive unit is a fine- to medium-grained dark to light grey to green rhyolite with strong foliation and shearing. The fractures are commonly infilled with quartz-carbonate with limited alteration. Locally the unit is interbedded with Al-rich metasedimentary zones containing up to 0.2 cm subhedral garnets. The feldspar porphyritic unit is a massive to very fine-grained grey to dark grey rock with anhedral to subhedral feldspar phenocrysts. The unit has a sharp, straight contact with the surrounding volcanic rocks. Alteration intensity is variable from weak to moderate-strong albite-potassic-sericite alteration. The unit is cut by variably oriented fractures with alteration halos that alter both the feldspar porphyritic unit and the volcanic rock.

Quartz veining occurs as boudinaged milky quartz ranging from 0.3 to 2.3 m thick with sharp undulating contacts. Weak to moderate shearing is sometimes seen along the contacts. The veining shows crack and seal texture and is locally epidote-sericite-potassic altered. The veining contains minor disseminated pyrite, dominantly along the contacts.

2.2.4 Peek-a-Boo zone

The Peek-a-Boo zone, formerly known as Oneida Lake, is located 4.5 km west of the Eagle River Mine and is the most distal mineralized area identified to date east of the mine (Figs. 2.10 and 2.17). The area was discovered based on high grade grab samples from quartz veins hosted within mafic and felsic volcanic rocks from a surface trenching program (Forslund, 2022). The area consists of mafic to felsic volcanic rocks, and granitic intrusions with minor intrusive rhyolite.

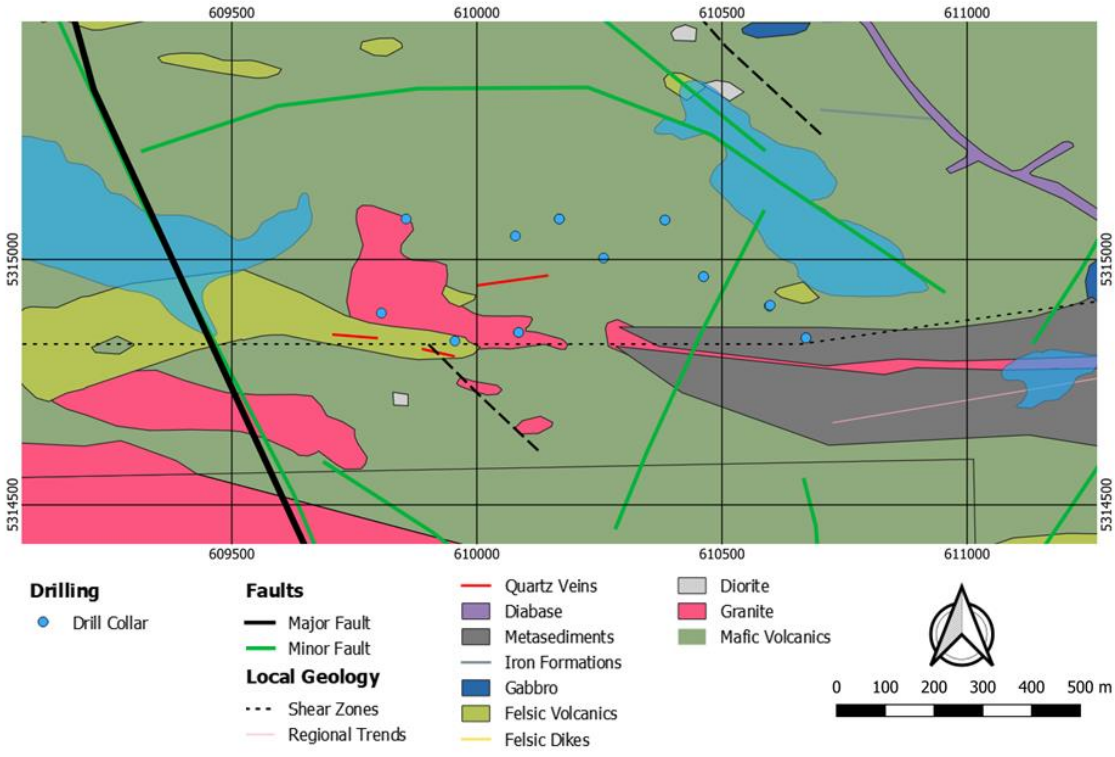

Figure 2.17: Local map showing the Peek-a-Boo zone and the associated drilling locations (Map courtesy of Wesdome Gold Ltd.).

The mafic volcanic rock is very fine- to fine-grained, green-gray to dark-gray with weak patchy-fracture controlled hematite alteration, sericite-chlorite, and biotite alteration. Quartz-carbonate veins cut the volcanic unit and are associated with disseminated to blebby pyrite, pyrrhotite and chalcopyrite. Weak to moderate foliation is developed in the unit defined by actinolite. Local subhedral 1 to 3 mm garnets are found within the unit, sometimes associated with weak foliation. Felsic volcanic rocks are green, fine- to medium-grained to moderately foliated tuffs associated with disseminated to blebby pyrite and pyrrhotite, and locally stretched lapilli fragments. Alteration varies from biotite-chlorite to sericite. Subhedral 1-3 mm garnets are found within the unit. A minor medium- to coarse-grained diabase intrusion occurs on the east side of the area. It is black to dark-grey with moderate pervasive magnetism associated with chill margins. The felsic intrusive is a green and white, fine- to coarse-grained rhyolite, cut by quartz-carbonate stringers, dominantly

found on the north side of the area. Minor intrusions of a very fine-grained porphyritic unit with 1 to 2 mm feldspathic clasts, are present and have been cut by variably striking fractures with alteration halos of potassic-albite-epidote-carbonate. The intrusions are generally <0.5 m in width, but locally can be up to 3 m, and are found throughout the area as a discontinuous unit hosted within the volcanic rocks or along contacts.

A north dipping medium- to coarse-grained light to light gray to gray granite cross cuts the volcanic unit, varying in thickness from 20 to 40m. Alteration varies from weak to moderate patchy potassic and sericite alteration to fracture controlled hematite alteration. Epidote veinlets 1 to 2 cm wide crosscut the granite. Occasional anhedral to subhedral tourmaline occurs associated with quartz-carbonate veining. The contacts with volcanic rocks are dominantly sharp and straight, and commonly contacts exhibit signs of shearing. Thinner granitic intrusions (<10 m but locally can be up to 20 m in width) with similar characteristic are found throughout the area with higher concentrations in the south.

The veining is hosted in either the contact between the felsic volcanic rock and the intermediate lapilli tuff or within the intermediate tuff. The quartz vein is discontinuous from 0.4 to 1.5 m in width with sharp straight to undulating contacts. The veins are locally associated with hematite fracture filling, and local potassic alteration exhibiting weak to moderate crack and seal texture. Au-bearing veins are hosted in mafic volcanic rocks and gabbro that have been metamorphosed up to garnet-amphibolite facies. The sulphides generally are located along sheared laminated sections or along contacts of units and are dominated by pyrite-pyrrhotite-chalcopyrite.

3. Analytical Methods

3.1 Sampling

For this study, a total of 95 samples were selected from the four regions of interest (8 zone, Falcon zone, Newt Lake zone, and Peek-a-Boo zone). The samples dominantly focused on the alteration, but least altered samples were collected to understand the host rocks and cross-cutting relationships. The chaotic and Laminated units are heterogenous so in order to get a more representative sample a bigger section of the unit was sampled.

3.2 Light Microscopy

A total of 74 thin (~30 micrometers) polished section (PTS) were prepared and examined under transmitted and reflected light on an Olympus BX41 microscope. Sample distribution varies based on locality which includes 38 samples from the 8 zone, 20 samples from Falcon zone, six samples from Newt Zone, and nine samples from Peek-a-Boo. The samples were selected based on mineralogy, alteration, and cross cutting relationships. Each sample was examined for modal abundances, grain textures, sizes, twinning planes, exsolution, and cross-cutting relationships.

3.3 U-Pb Geochronology

A total of four samples were collected for age dating. The samples included the Bowman Lake batholith to the north-east, the Floating Heart batholith (Pilot Harbour granite) to the south, the Central pluton to the northwest, and the mine diorite central to the batholiths (Fig. 3.1).

The analyses were completed at the Pacific Centre of Isotopic and Geochemical Research of University of British Columbia. The zircons were separated using conventional density and magnetic methods, and subsequently placed in a muffle furnace. The grains underwent additional chemical

abrasion using the modified method of Wall et al. (2018) with HF, HNO_3, and HCl. The single grains were dissolved in Parr vessels with 29 M HF, 3.5 M HNO_3 and re-dissolved in 6 M HCl. The U and Pb were separated from the zircon matrix using an HCl-based anion-exchange chromatographic procedure (Krogh, 1973).

U-Pb dates and uncertainties were calculated using the algorithms of Schmitz and Schoene (2007), calibration of ET535 tracer solution (Condon et al., 2015) of $^{235}U/^{205}Pb$ = 100.233, $^{233}U/^{235}U$ = 0.99506, and $^{205}Pb/^{204}Pb$ = 11268, U decay constants recommended by Jaffey et al. (1971), and $^{238}U/^{235}U$ of 137.818 (Hiess et al., 2012). $^{206}Pb/^{238}U$ ratios and dates were corrected for initial ^{230}Th disequilibrium using $D_{Th/U}$ = 0.20 ± 0.05 (1σ) and the algorithms of Crowley et al. (2007), resulting in an increase in the $^{206}Pb/^{238}U$ dates of ~0.09 Ma.

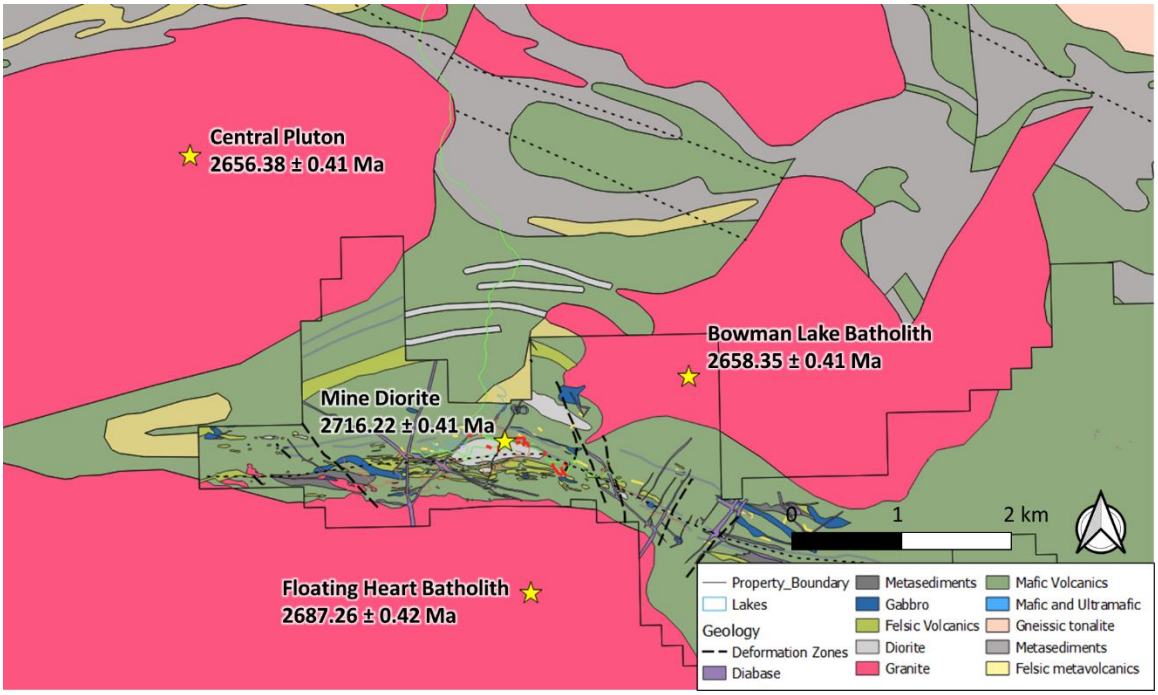

Figure 3.1: Location of geochronological sample and the results. (Modified after Wesdome Gold Ltd. map).

3.4 Lithogeochemistry

A total of 57 samples were collected to investigate the alteration and evolution of the greenstone belt, which are summarized in Appendix A. Representative least altered samples were chosen from each zone to assess the variability of the units between the zones. Additionally, altered samples were chosen from units of interest (i.e., Laminated and chaotic units) to assess the elemental gains and losses associated with alteration. To account for the heterogenity of the Laminated unit, longer sections (up to 1m) of the unit were sampled to homogenize the sample. All samples had weathered surfaces and vein material cut from the samples and were submitted to ALS Geochemistry in Thunder Bay for analysis.

Major elements were determined using the ME-ICP06 service code by fused bead, acid digestion and ICP-AES. Carbon and sulfur were measured using the ME-IR08 service code by induction furnace/infrared. Trace elements were analyzed by various techniques which include the ME-MS81 technique by Lithium Borate fusion prior to acid dissolution and ICP-MS analysis. Loss on ignition (LOI) were determined using the ME-MS42 service code by aqua regia digestion followed by ICP-MS measurement. Base metals were measured using the ME-4ACD81 service code by lithium borate fusion followed by acid dissolution and ICP-AES measurement. For elements present in concentrations below that of analytical detection, the elements were reported at values of one half the detection limit.

3.5 SEM-EDS Analyses

Qualitative analyses were conducted to investigate the mineral chemistry of selected samples, and to identify the opaque and non-opaque phases. X-ray thin section maps were generated to investigate elemental zonation (core-rim, homogenous vs. heterogeneous distribution), and distributions of minor and major elements within the grains.

Qualitative analyses were performed on a JEOL JSM-6400 scanning electron microscope (SEM) with an Oxford INCA energy-dispersive spectrometer (EDS) at the Central Analytical Facility (CAF) of Laurentian University. Oxford AZtec suite version 4.1 was used to process the data from the SEM-EDS analyses. Analyses were collected for 6 s using an operating voltage of 20 kV and an estimated beam current of 1.005 nA. Aztec SmartMap spectral mapping was used to collect full thin section maps.

3.6 Raman Microscope

Raman spectroscopy was conducted to help identify finer grained minerals. Spectra were collected at Laurentian University using a XploRA (Horiba Jobin Yvon) microscope. LabSepc version 5.26.11 was calibrated to a piece of pure Si which provides a strong spectrum at 521 nm. The acquisition was completed using a 532 nm laser for 5 seconds. CrystalSleuth version May 19, 2008 was used to process the spectrum data for comparison. Each spectrum had the 'remove background' function performed for increased comparison.

4. Results

4.1 Petrography of rock units

Thin section descriptions are provided in Appendix B, and full thin section maps in Appendix C. SEM-EDS data is provided as a digital appendix.

4.1.1 Chaotic Unit

The chaotic unit is an altered unit that consists of vein types that vary in strike, dip, and alteration. The dips can vary from shallow to steeply dipping, and the alteration around the veins can consist of either albite, potassic or hematite. The veins are discussed in detail in section 5.1. The altered matrix by the vein alteration halos is texture destructive, which are described in Chapter 5. The unaltered matrix is found distal to the vein alteration halo which consists of very fine- to fine-grained minerals that consists of plagioclase-quartz-biotite-clinozoisite with minor titanite-muscovite-prehnite-pumpellyite (Fig. 4.1).

The quartz and plagioclase (An_{36-44}) are anhedral to subhedral up to 15 Hs across, commonly less than 10 micrometers. The biotite grains are anhedral up to 30 micrometers across, commonly less than 10 micrometers and make up the fabric of the rock. Anhedral clinozoisite grains up to 10 micrometers are elongated parallel to the fabric. Locally they form clusters that are distributed throughout the rock. Locally anhedral muscovite grains up to 40 micrometers across, commonly less than 20 micrometers are found parallel to the fabric. The titanite grains are anhedral up to 10 micrometers across.

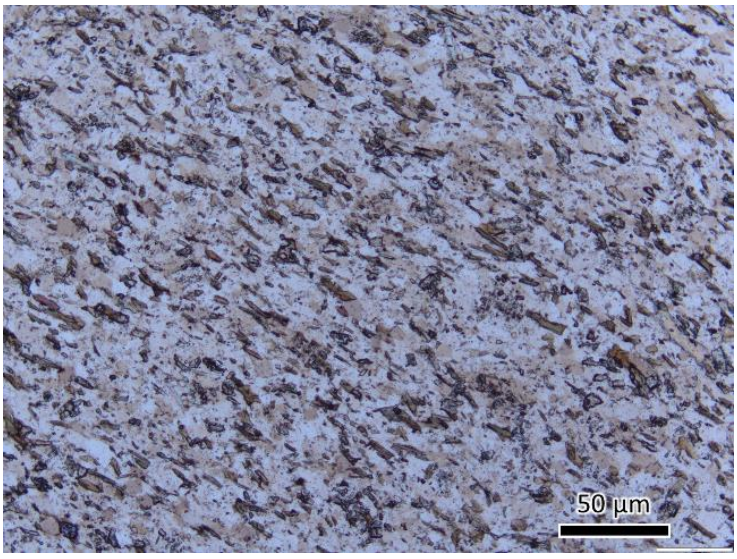

Figure 4.1: Photomicrograph of the chaotic unit matrix in plane polarized light from ER-2021-WP-8Z-17B.

4.1.2 Laminated Unit

The Laminated unit is an altered unit that is highly variable with different proportions of biotite, muscovite, clinozoisite, chlorite, quartz, plagioclase, and sulphides (Fig. 4.2 A-D). The layers can be either muscovite-, biotite-, clinozoisite-, or quartz-plagioclase-rich layers. The layers are broken out based on the change in the dominant mineralogy, which is also usually reflected a change in coloration on a macro scale (i.e., darker colors for biotite-rich, and lighter layers for muscovite-rich layers). A total of 10 samples were collected from the Laminated unit between the four zones (three from 8 zone, one from Falcon zone, three from Newt Lake zone, and three from Peek-a-Boo zone). All the zones have the same minerology and show similar characteristics (Appendix B).

In layers that are quartz-plagioclase-rich the phyllosilicates tend to be finer-grained and less abundant. The quartz and plagioclase are subhedral up to 10 micrometers across, but commonly less than 5 micrometers. The quartz occurs as discontinuous boudins with grains up to 20 micrometers across, with phyllosilicates and clinozoisite wrapping around the quartz-plagioclase boudins (Fig. 4.2 D). In areas where quartz veining is parallel to the fabric the quartz grains can be up to 50 micrometers, and associated with coarse clinozoisite, phyllosilicates, and sulphides. The

muscovite and biotite grains are subhedral and tend to be less than 10 micrometers across. Anhedral clinozoisite up to 5 micrometers across can be associated with the layers, which are elongated parallel to the fabric.

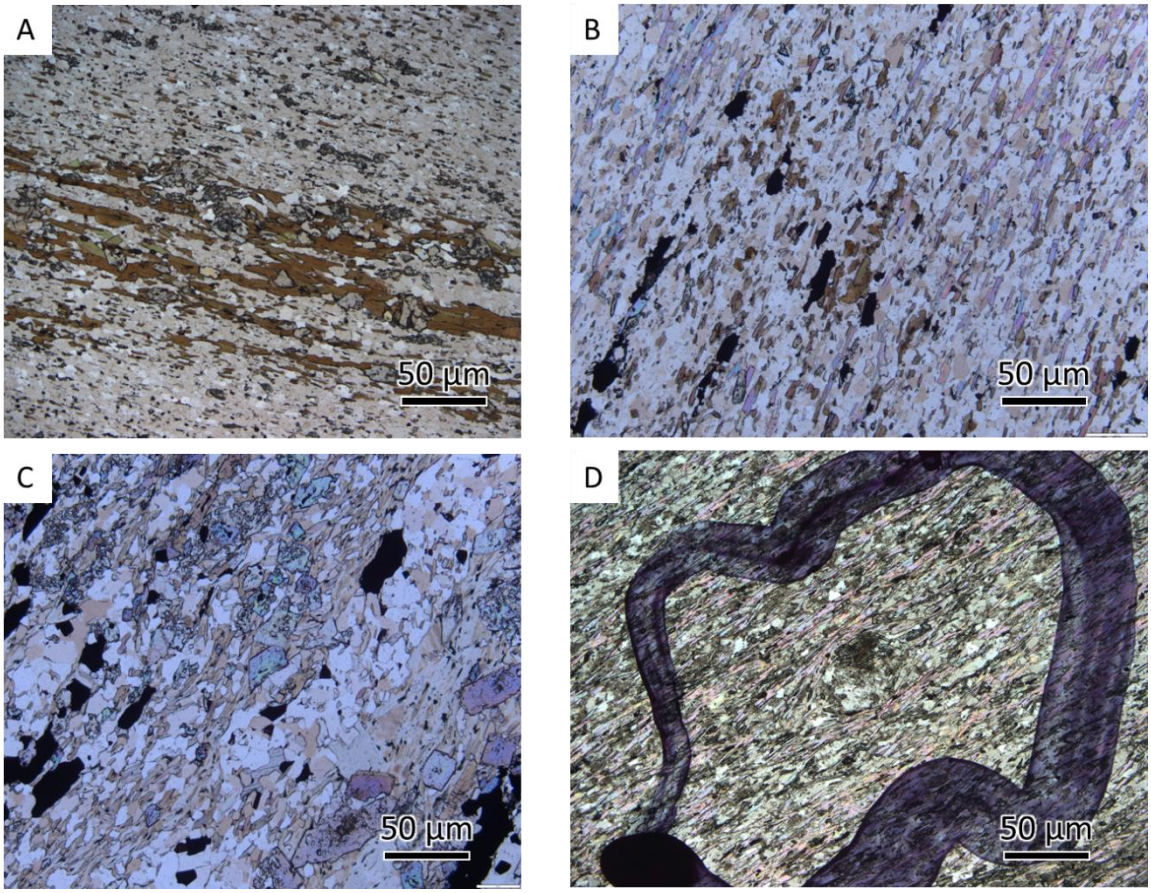

Figure 4.2: Photomicrographs of the variations within the Laminated unit in plane polarized light. The layers range from biotite-rich layers (ER-2021-WP-8z-50) (a); to muscovite-rich layers (ER-2021-WP-8z-29) (b); clinozoisite-rich layers (ER-2021-WP-F-11) (c); and clasts within the layers (ER-2022-WP-8z-62) (d).

Within the biotite- or muscovite-rich layers the phyllosilicates are coarser grained and have higher abundance. The quartz and plagioclase grains are similar in size to those in the quartz-plagioclase-rich layers. The phyllosilicates can be up to 60 micrometers across, commonly ranging between 15 and 30 micrometers. Chlorite grains are only found within phyllosilicate-rich layers and are dominantly associated with biotite grains. The chlorite Fe# (Fe # = Fe / [Fe + Mg]) ranges from 51 to 77. With coarser phyllosilicates the clinozoisite also increases in size and can be up to 50

micrometers across, commonly ranging between 10 and 20 micrometers, with phyllosilicates wrapping around the clinozoisite.

The sulphides are inclusion-poor which are dominated by pyrite with minor pyrrhotite and chalcopyrite. The sulfides are interpreted to be dominantly secondary based on the elongated and anhedral morphology. They occur either as coarser grains associated with the quartz veining or as finer disseminated grains within the layering. The coarser grained sulphides are dominated by pyrite with minor chalcopyrite-pyrrhotite. The pyrite grains are subhedral to euhedral up to 70 micrometers across and are inclusion-poor that are zoned with finer grained pyrite. The finer grained sulphides are dominated by pyrrhotite with minor pyrite and chalcopyrite, as anhedral to subhedral grains up to 20 micrometers.

Locally the laminate unit wraps around coarse boudins, which can be either dominated by coarse clinozoisite or amphibole with clinozoisite (Fig. 4.2 D). In both instances the boudins are surrounded by a quartz-plagioclase rich matrix. The clinozoisite has a bimodal distribution with coarser grained crystals up to 80 micrometers across, but commonly less than 40 micrometers, and finer grains less than 15 micrometers. The coarser clinozoisite tends to be in the core of the boudin and finer grained around the edges. Where clinozoisite is in association with the amphiboles, the clinozoisite tends to be finer grained up to 30 micrometers. The amphiboles are subhedral up to 50 micrometers across, commonly less than 20 micrometers, oriented sub parallel to the contact with the host rock. The amphiboles contain inclusions of quartz and pyrrhotite.

4.1.3 Diorite

The diorite is an unaltered unit within the 8 zone varies from fine- to coarse-grained (Figs. 2.11, 2.12, and 4.3). The samples from the Falcon zone are medium-grained diorite. The plagioclase grains are up to 150 micrometers across exhibiting simple to polysynthetic twinning with patchy sericite

alteration. They contain inclusions of clinozoisite, chlorite, amphibole, sulphide and titanite. The quartz grains have bimodal distribution with coarser grains being subhedral up to 100 micrometers across exhibiting undulatory extinction. The finer grains are less than 10 micrometers across commonly found along the quartz grain boundaries. The amphibole grains are anhedral up to 150 micrometers across but are commonly between 60-80 micrometers containing inclusions of sulphides and titanite, with weak to moderate chlorite alteration along the edges. The biotite grains are subhedral up to 100 micrometers across with minor chlorite alteration and containing inclusions of sulphides. The clinozoisite grains are anhedral to subhedral up to 10 micrometers across as inclusions within plagioclase. The chlorite grains are anhedral to subhedral up to 25 micrometers across, but are commonly less than 15 micrometers, with inclusions of titanite. The chlorite Fe# ranges between 59 to 67. The ilmenite grains are anhedral up to 30 micrometers across, found along grain boundaries of quartz, amphiboles, chlorite, and plagioclase. The titanite grains occur as subhedral to euhedral grains up to 15 micrometers across as inclusions in chlorite and amphiboles, or around edges of the ilmenite grains. The sulphides are disseminated and consist of pyrite with minor chalcopyrite. The pyrite is anhedral to subhedral up to 20 micrometers across, and is dominantly inclusion-poor, but less commonly inclusion-rich pyrite is also noted. The grains are

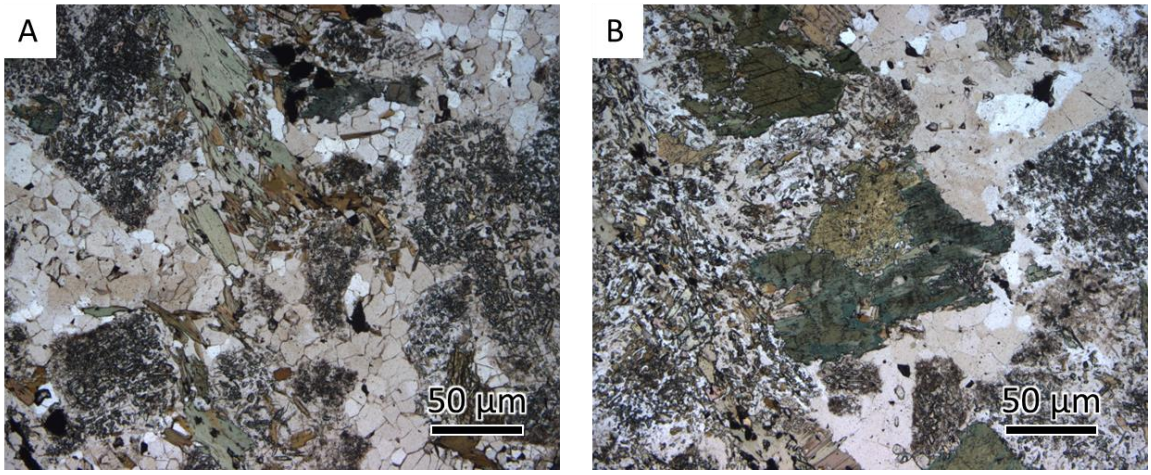

Figure 4.3: Photomicrographs of the variations within the fine- to medium-grained diorite unit in plane polarized light ER-2022-WP-8z-49.

dominantly found associated with amphiboles and chlorite. The sulphides are zoned with the outer zone consisting of finer grained sulphides with the same composition as the inner zone (see Section 4.1.8 for further details).

4.1.4 Gabbro

The gabbro is an unaltered unit that is found in all the zones except for the Peek-a-Boo zone. The gabbro consists of amphibole, quartz, and clinozoisite with minor titanite (Fig. 4.4). The amphibole grains have a bimodal distribution with coarser grains ranging between 40 and 80 micrometers across, and finer grains commonly less than 5 micrometers. The amphiboles make up the fabric of the rock and are elongated parallel to it. They contain inclusions of clinozoisite, quartz, pyrite, and chalcopyrite. The amphiboles are locally weakly altered by chlorite. The chlorite Fe# ranges from 51-56. The matrix is composed of fine-grained amphibole, clinozoisite, quartz and plagioclase. The clinozoisite grains are subhedral up to 10 micrometers across but are commonly less than 5

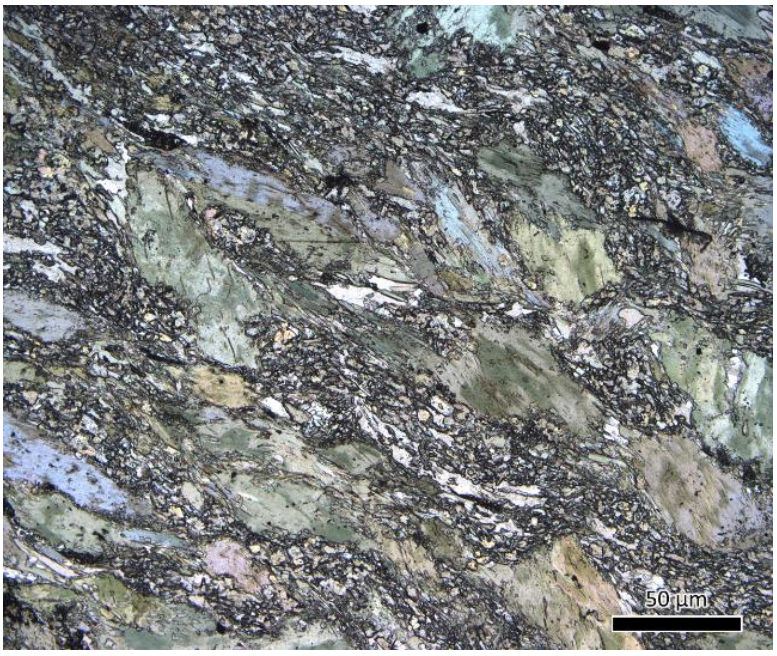

Figure 4.4: Photomicrograph of the gabbro unit in plane polarized light ER-2022-WP-8z-51.

micrometers. The quartz and plagioclase grains are subhedral up to 10 micrometers across, with coarser grains along the boundary of the amphiboles. The titanites grains are subhedral up to 5 micrometers across elongated sub-parallel to the fabric of the rock. They are found as inclusions within amphiboles or along grain boundaries. The sulphides grains consist of disseminated pyrite and minor pyrrhotite and chalcopyrite. The pyrite grains are subhedral up to 5 micrometers across, commonly less than 2 micrometers and are inclusion-poor. The chalcopyrite and pyrrhotite are both anhedral up to 2 micrometers across.

4.1.5 Granite

The granite unit is only found within the Peek-a-Boo zone and consists of two different zones. The upper zone is a thicker package of granite up to 30 m thick, whereas the lower zone is a thinner package ranging from 5 to 10 m in width.

The upper granite unit is composed of plagioclase, orthoclase, quartz, biotite, and muscovite. The plagioclase grains are subhedral to euhedral up to 90 micrometers across, exhibiting simple to polysynthetic twinning, locally exhibiting oscillatory zonation. The grains have moderate patchy sericite alteration which can be either patchy or concentrated within the core of the grains. The orthoclase grains are anhedral up to 90 micrometers across with weak sericite alteration. The quartz grains are anhedral up to 30 micrometers across with micro inclusions and weak undulatory extinction. Finer grained quartz up to 10 micrometers across are found along grain boundaries. The granite exhibits wavy fabric that is defined by biotite, muscovite, clinozoisite, and minor chlorite that wrap around the plagioclase-orthoclase grains (Fig. 4.5 A). The biotite grains are subhedral up to 20 micrometers across with inclusions of titanite. The muscovite grains are coarser grained relative to biotite, up to 50 micrometers across with micro inclusions of titanite. The clinozoisite grains are anhedral up to 30 micrometers across with irregular grain boundaries, containing inclusions of

titanite, dominantly found along the edges of the biotite grains. The chlorite grains are either anhedral grains up to 20 micrometers across, or as an alteration of muscovite and biotite. The titanite grains are subhedral up to 5 micrometers across.

The lower granite is composed of plagioclase, orthoclase, and quartz with minor amounts of muscovite, prehnite and pumpellyite (Fig. 4.5 B). Trace amounts of zircon, titanite, sphalerite and apatite were noted. Unlike the upper granite the lower granite does not exhibit any fabric or strain. The plagioclase (An_{3-27}), orthoclase and quartz are finer grained, with plagioclase and orthoclase up to 60 micrometers across and quartz up to 20 micrometers across. The plagioclase and orthoclase grains contain inclusions of biotite, muscovite and prehnite-pumpellyite with patchy moderate sericite alteration. The muscovite grains are anhedral up to 40 micrometers across but are commonly 20 to 30 micrometers with inclusions of plagioclase and prehnite-pumpellyite. The prehnite-pumpellyite grains are subhedral to euhedral up to 70 micrometers across with irregular grain boundaries. They contain inclusions of biotite, titanite and plagioclase. The chlorite grains resemble the chlorite from the upper granite. The chlorite Fe# ranges from 47 to 52. Carbonate

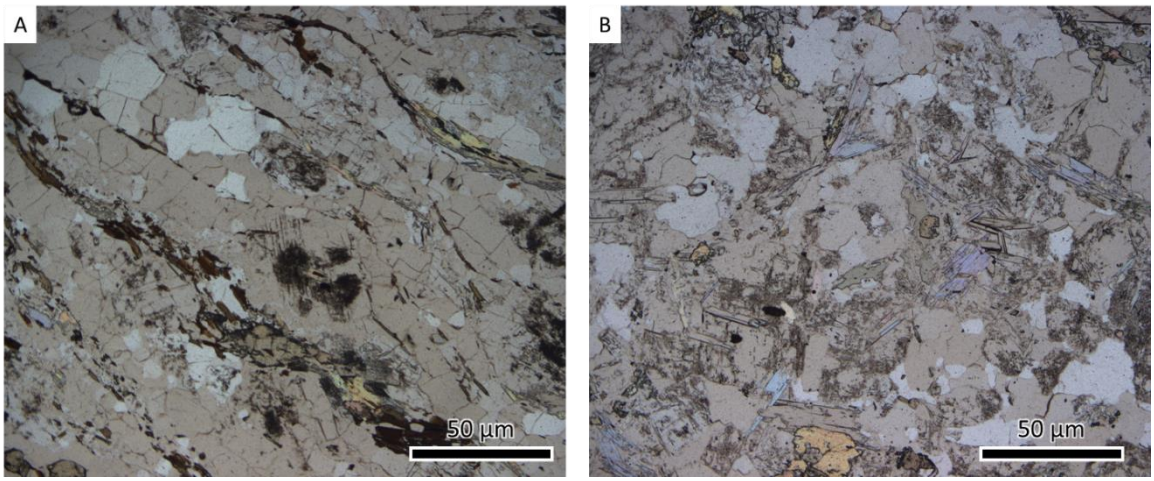

Figure 4.5: Photomicrographs showing the upper granite (ER-2022-P-34) (a) and the lower granite (ER-2022-P-33) (b) within the Peek-a-Boo zone in plane polarized light.

alteration is associated with the muscovite and clinozoisite. The titanite grains are anhedral up to 20 micrometers across and are found either associated with the amphiboles or chlorite. Trace amounts of subhedral disseminated pyrite and chalcopyrite are found throughout the rock, with pyrite being inclusion-poor.

4.1.6 Feldspar porphyry

The feldspar porphyry is an unaltered unit that consists of coarser plagioclase phenocrysts within a matrix of quartz, plagioclase, amphibole with minor orthoclase, biotite, titanite, ilmenite, chlorite, clinozoisite and pyrite (Fig. 4.6). The plagioclase phenocrysts can be up to 300 micrometers across exhibiting simple and polysynthetic twinning with moderate to strong sericite alteration. They contain inclusions of biotite and amphibole. The amphibole grains are subhedral to euhedral up to 70 micrometers across, commonly ranging between 30 and 50 micrometers. They are randomly oriented throughout the rock and wrap around the plagioclase phenocrysts (Fig. 4.6 B). The ilmenite, pyrite and sphalerite grains occur as inclusions within the amphiboles. The biotite grains are anhedral up to 15 micrometers across, occurring as inclusions within amphiboles or randomly

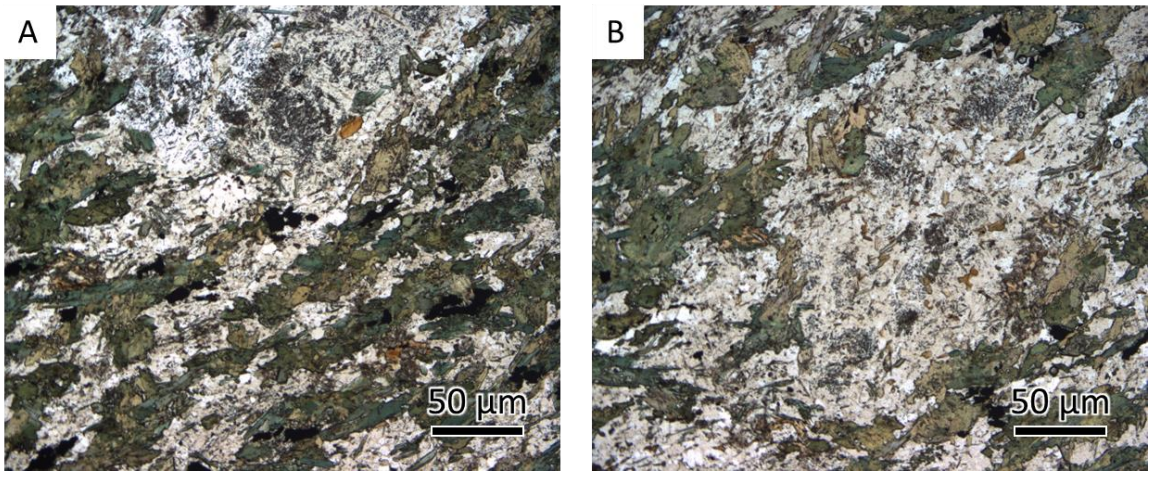

Figure 4.6: Photomicrographs of the variations within the feldspar porphyry unit showing more altered clasts (a) and less altered clasts (b) within the unit in plane polarized light ER-2022-WP-F-47.

oriented within the rock. The matrix is made up of quartz and plagioclase up to 10 micrometers across, commonly less than 5 micrometers. Coarser plagioclase with simple twinning is noted up to 20 micrometers across. The ilmenite grains are anhedral up to 20 micrometers across and can be found as inclusions within amphibole grains. Trace amounts of anhedral pyrite and chalcopyrite are found throughout the rock. The chlorite grains are anhedral up to 30 micrometers commonly associated with amphiboles. The chlorite Fe# ranges from 60 to 66.

4.1.7 Volcanic Rocks

The mafic volcanic rocks are variably altered that vary from those with a strong fabric defined by amphiboles with weak alteration, to strongly altered with weak to no fabric (Fig. 4.7 A and B). The volcanic rock with strong fabric is from the Peek-a-Boo zone and the altered volcanic is from the Falcon zone.

The sample from the Peek-a-Boo zone consists of amphibole, quartz, plagioclase, ilmenite, and titanite with minor magnetite, pyrite and chalcopyrite (Fig. 4.7 A). The amphiboles have a bimodal distribution with coarser grains up to 120 micrometers across, commonly less than 40 micrometers, and finer grains up to 20 micrometers commonly less than 10 micrometers. They contain inclusions of ilmenite, quartz, ilmenite, pyrite, and chalcopyrite. The amphiboles have a strong fabric that wraps around the plagioclase phenocrysts. The plagioclase grains are subhedral up to 40 micrometers across with strong sericite alteration, some displaying polysynthetic twinning. They contain inclusions of pyrite and chalcopyrite. The quartz grains are anhedral up to 10 micrometers across, commonly less than 5 micrometers. Magnetite grains are anhedral up to 5 micrometers across distributed throughout the rock. The ilmenite grains are anhedral up to 10 micrometers across, commonly less than 5 micrometers elongated parallel to the fabric of the host rock. The ilmenite grains have titanite rims. The pyrite grains are subhedral up to 10 micrometers across and

can either be inclusion-rich or inclusion-poor. The chlorite grains are anhedral up to 20 micrometers commonly associated with amphiboles. The chlorite Fe# ranges from 70 to 75.

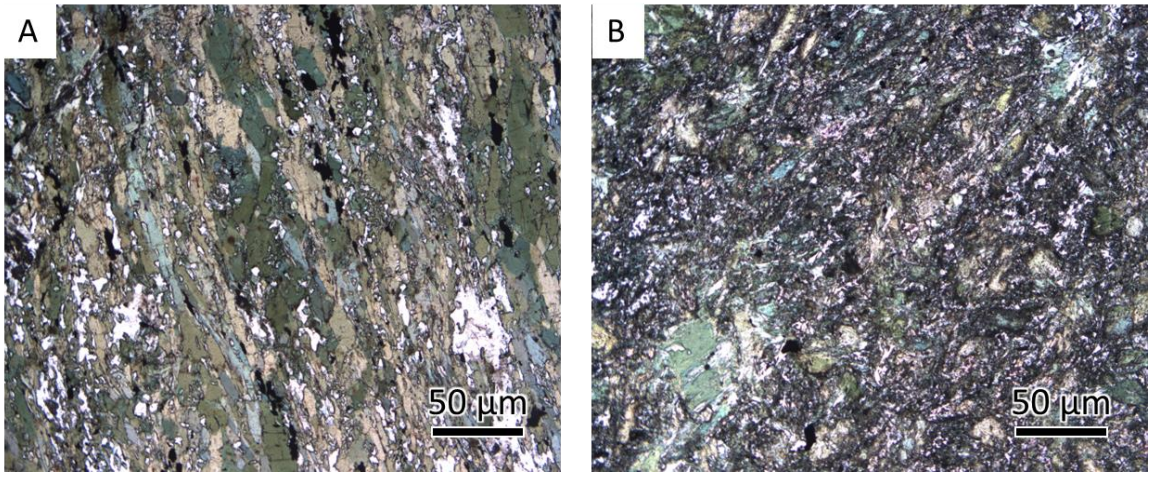

Figure 4.7: Photomicrographs of the variations within the volcanic rock showing less altered (ER-2022-P-37) (a) and more altered (ER-2022-F-48) (b) volcanic rock in plane polarized light.

The sample from the Falcon zone consists of amphiboles, plagioclase, quartz with minor magnetite, prehnite-pumpellyite, titanite, and sulphides (Fig. 4.7 B). The amphibole grains have a bimodal distribution with coarser grains up to 60 micrometers, commonly less than 40 micrometers across, and the finer grained are less than 10 micrometers. The amphiboles contain inclusions of quartz, pyrite, pyrrhotite and chalcopyrite. The chlorite grains are up to 10 micrometers across and can be found as elongated grains or altering the amphiboles. The chlorite Fe# ranges from 49 to 59. The quartz and plagioclase grains are anhedral up to 10 micrometers across, commonly less than 5 micrometers, both containing micro inclusions. The magnetite grains are anhedral up to 5 micrometers across distributed throughout the rock. The sulphide grains consist of pyrrhotite, pyrite and chalcopyrite. The pyrite grains are anhedral to subhedral up to 10 micrometers across, commonly less than 5 micrometers, and are inclusion-poor. The pyrrhotite and chalcopyrite grains are both anhedral up to 5 micrometers across. Both volcanic rocks contain zoned sulphides with the outer zone consisting of finer grained sulphides with the same composition as the inner zone.

4.1.8 Sulphides

Between the four zones there are similarities between the units, which include sulphides (pyrite, pyrrhotite, and sphalerite) inclusions, and the alteration of ilmenite with minor rutile by titanite. The pyrite, pyrrhotite and chalcopyrite can be either inclusion-rich or inclusion-poor varieties (Fig. 4.8).

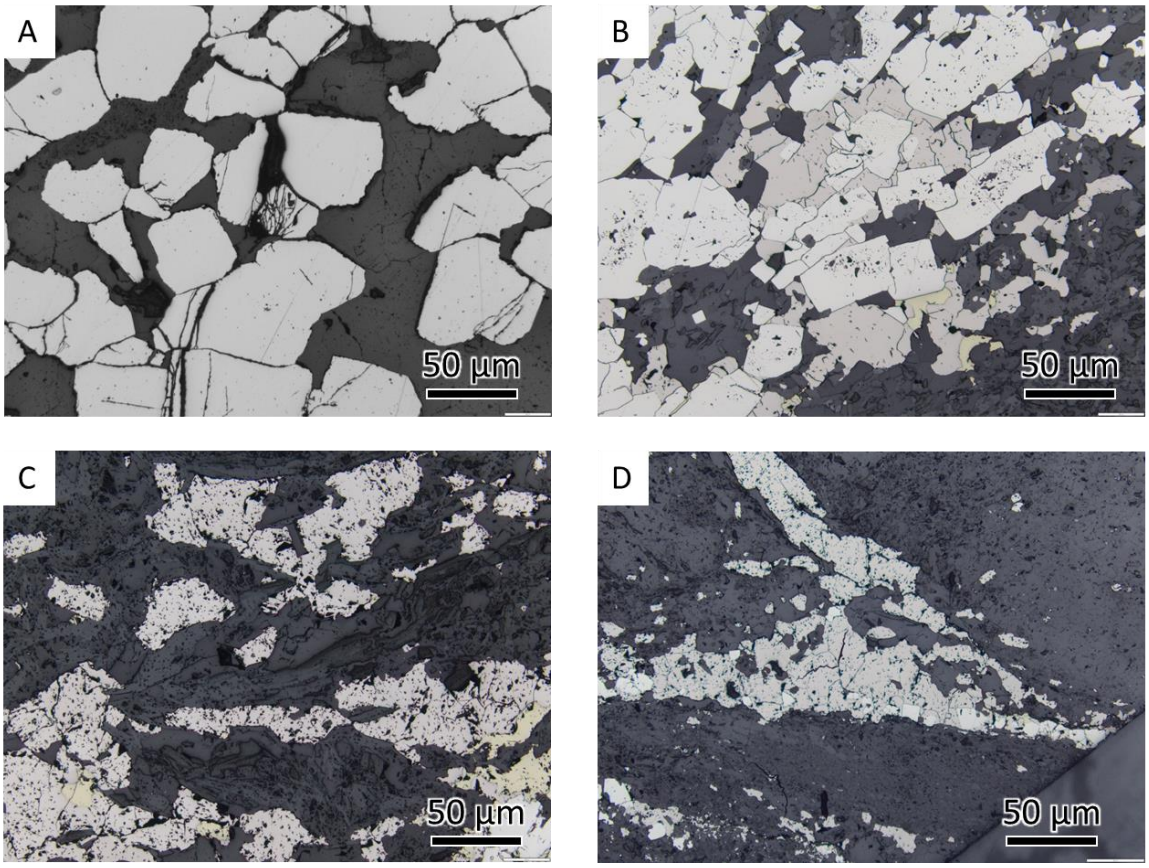

Figure 4.8: Photomicrographs of sulphides within the zones in reflected light. Inclusion-poor pyrite grains (ER-2021-WP-8z-01) (a); inclusion-rich pyrite and inclusion-poor pyrrhotite grains (ER-2021-WP-F-11) (b); and inclusion-rich pyrrhotite and chalcopyrite grains (c) (ER-2021-WP-F-03); and inclusions-poor pyrite within inclusions-rich pyrrhotite (ER-2021-WP-F-03) (d).

Commonly the sulphides are disseminated throughout the units as anhedral to euhedral grains up to 30 micrometers that are dominantly inclusion-poor. In higher concentrations of sulphides there is a variety of inclusion-rich and inclusion-poor grains that are either dominated by pyrite or pyrrhotite. The inclusion-rich pyrite grains tend to be coarser up to 150 micrometers and more anhedral, whereas the inclusion-poor grains tend to be finer grained up to 50 micrometers and more

euhedral. Locally inclusion-rich pyrite is rimmed by inclusion-poor pyrite (Fig. 4.8B). Within inclusion-rich pyrrhotite grains there are inclusions of inclusion-poor subhedral to euhedral pyrite (Fig. 4.8 D). The pyrrhotite grains are anhedral and like the pyrite grains tend to be inclusion-poor in smaller concentrations and inclusion-rich in higher concentrations. Commonly, chalcopyrite is associated with both pyrite and pyrrhotite, but inclusion-rich chalcopyrite is dominantly associated with inclusion-rich pyrrhotite. The sulphides contain inclusions of Bi-Te, either tetradymite or bismuthinite. The Bi-Te grains are anhedral up to 2 micrometers. The sulphides found within the four zones commonly have an medium to dark grey border alteration zone around them when viewed under reflected light (Fig. 4.9). The medium to dark grey alteration zone consist of quartz, which suggests a dissolution of the sulfides and replacement by massive to very fine grained quartz.

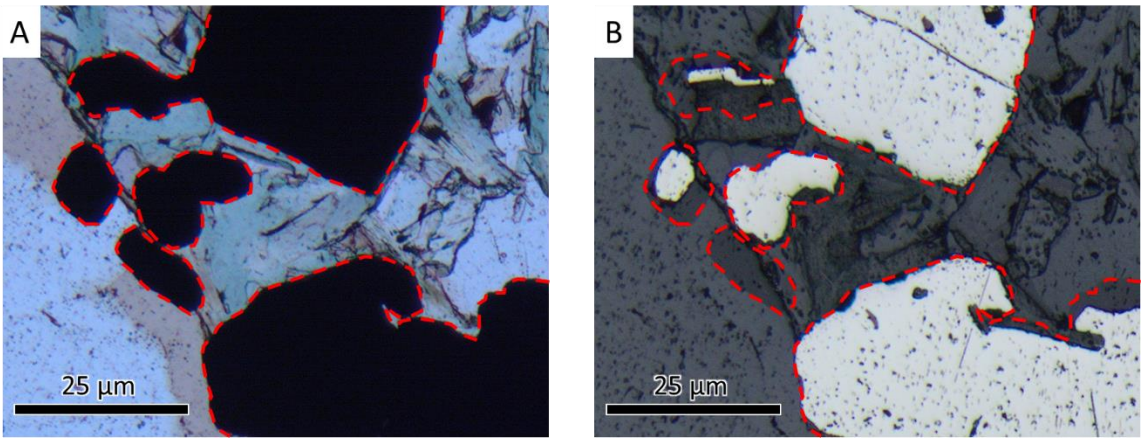

Figure 4.9: Photomicrographs of the alteration halo of the sulphides in plane polarized light (a); and reflected light (b) from sample ER-2021-WP-F-04. Red circles show the grains that have alteration halos.

4.2 U-Pb Geochronology

4.2.1 ER-2021-WP-G1: Central pluton

Sample ER-2021-WP-G1 is from the Central pluton located on the northwest side of the study area, which is elongated striking at ~50° (Figs. 2.6 and 2.7). The pluton has not been previously dated. The

sample is a fine-grained granite with coarse grained plagioclase phenocrysts up 3 cm in length (Fig. 4.10 A). The groundmass consists of K-feldspar, plagioclase, quartz, amphibole and albite with minor biotite. Very weak patchy potassic alteration is present dominantly within the plagioclase phenocrysts.

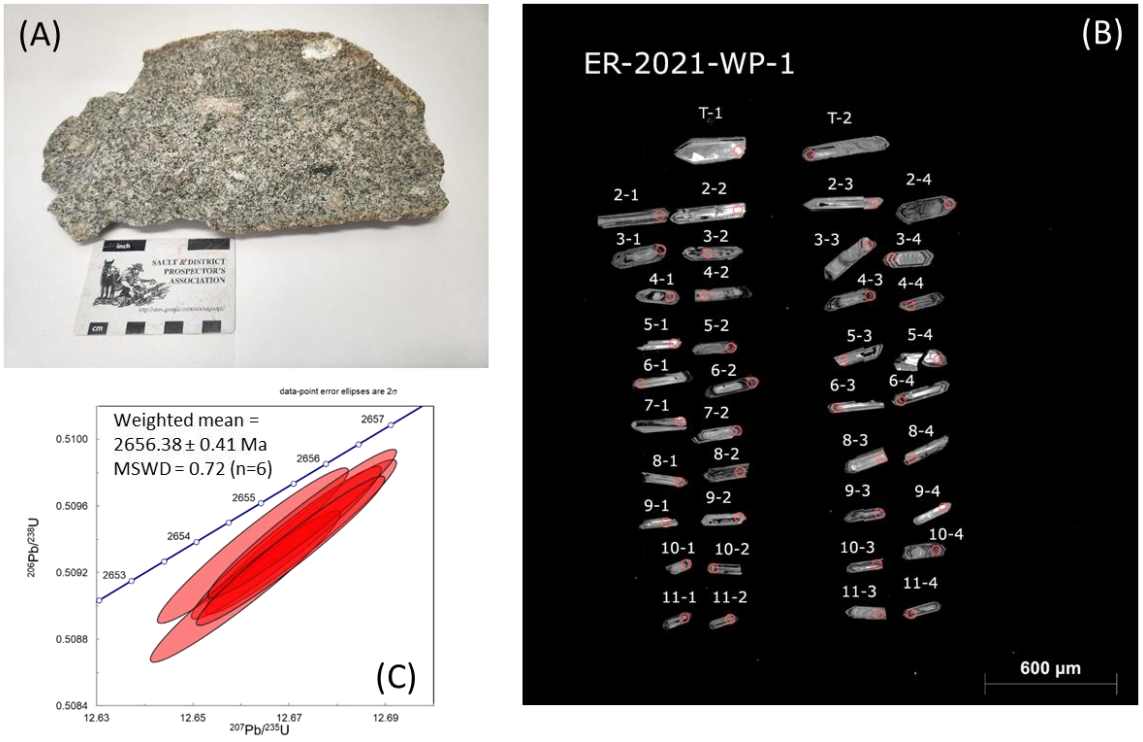

Figure 4.10: Representative sample of the Central pluton (a) extracted zircons (b) and the concordia diagram with the elipses denoting 2σ errors (c).

A total of 40 zircons were extracted from the granite, six of which were selected for CA-TIMS based on LA-ICP-MS (laser ablation inductively coupled plasma mass spectrometry) geochemistry, morphology, absence of inclusions and minimal rounded edges (Fig. 4.10 B). The methodology for choosing zircons was the same for all samples. All six zircons were concordant and equivalent, yielding a weighted mean $^{207}Pb/^{206}Pb$ date of 2656.38 ± 0.41 Ma (Fig. 4.10 C). This date is interpreted as the crystallization age of the sample and is a new age for the unit.

4.2.2 ER-2021-WP-G2: Bowman Lake batholith

Sample ER-2021-WP-G2 is from the previously dated 2639.0 ± 25 Ma (Turek et al., 1990) Bowman Lake batholith located on the northeast side of the study area (Figs. 2.6 and 2.7). The sample is a granite, composed of fine- to medium-grained quartz, K-feldspar, plagioclase, albite, amphiboles and biotite, with patchy weak-moderate potassic alteration that dominantly affects the felsic minerals (Fig. 4.11 A).

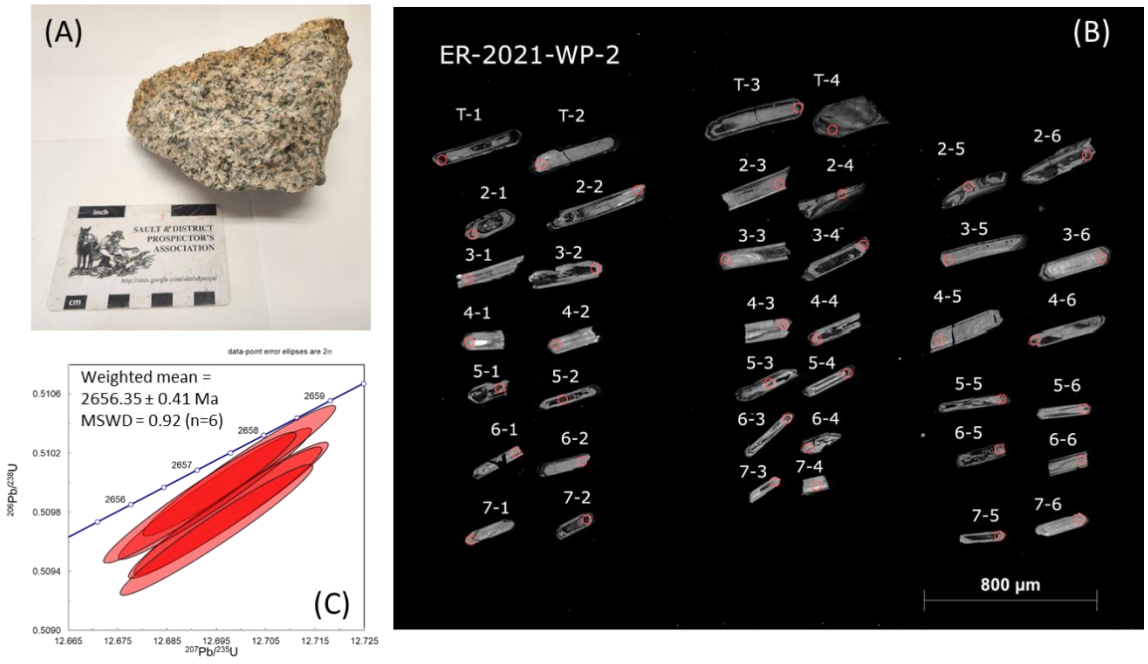

Figure 4.11: Representative sample of the Bowman Lake batholith (a) extracted zircons (b) and the concordia diagram with the ellipses denoting 2σ errors (c).

A total of 40 zircons were extracted from the granite, six of which were selected for CA-TIMS analysis (Fig. 4.11 B). All six zircons were concordant and equivalent, yielding a weighted mean $^{207}Pb/^{206}Pb$ date of 2658.35 ± 0.41 Ma (Fig. 4.11 C). This is interpreted as the crystallization age of the sample.

4.2.3 ER-2021-WP-G3: Floating Heart batholith

Sample ER-2021-WP-G3 is from the previously dated 2693.2 ± 6.9 Ma (Turek et al., 1990) Floating Heart batholith located on the south side of the study area (Figs. 2.6 and 2.7). The sample is a quartz monzonite with medium- to coarse-grained quartz, K-feldspar, plagioclase, albite, amphibole and minor biotite, with a strong pervasive potassic alteration throughout (Fig. 4.12 A). Minor pyrite was noted in the vicinity of the sample.

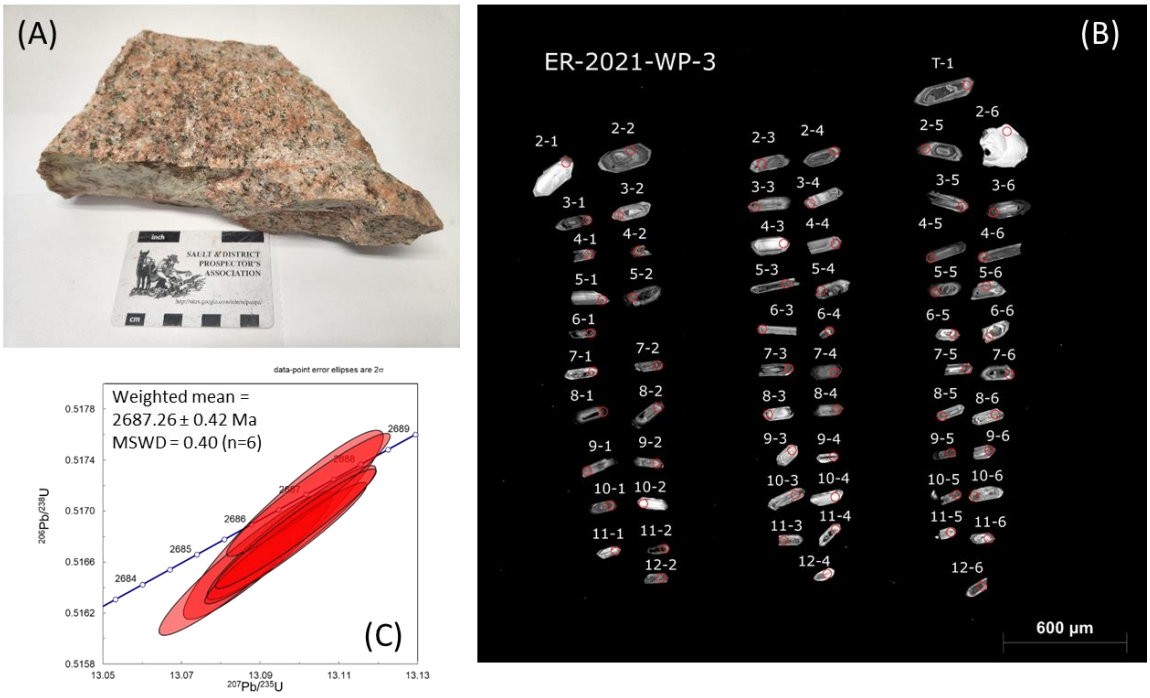

Figure 4.12: Representative sample of the Floating Heart batholith (a) extracted zircons (b) and the concordia diagram with the ellipses denoting 2σ errors (c).

A total of 63 zircons were extracted from the granite, six of which were selected for CA-TIMS analysis (Fig. 4.12 B). All six samples were concordant and equivalent, yielding a weighted mean $^{207}Pb/^{206}Pb$ date of 2687.26 ± 0.42 Ma (Fig. 4.12 C). This date is interpreted as the crystallization age of the sample.

4.2.4 ER-2021-WP-G4: Mine diorite

Sample ER-2021-WP-G4 is from the mine diorite located in the center of the study area (Figs. 2.6 and 2.7). The sample is medium- to coarse-grained diorite composed of amphibole, plagioclase, albite, quartz, and biotite (Fig. 4.13 A). Locally the diorite varies from medium- to coarse-grained, exhibiting alteration (i.e., potassic, hematite, albite, sericite, biotite, etc.) of variable intensities. The sample chosen for analysis was a medium-grained diorite with minimal alteration and is representative of the majority of the mine diorite.

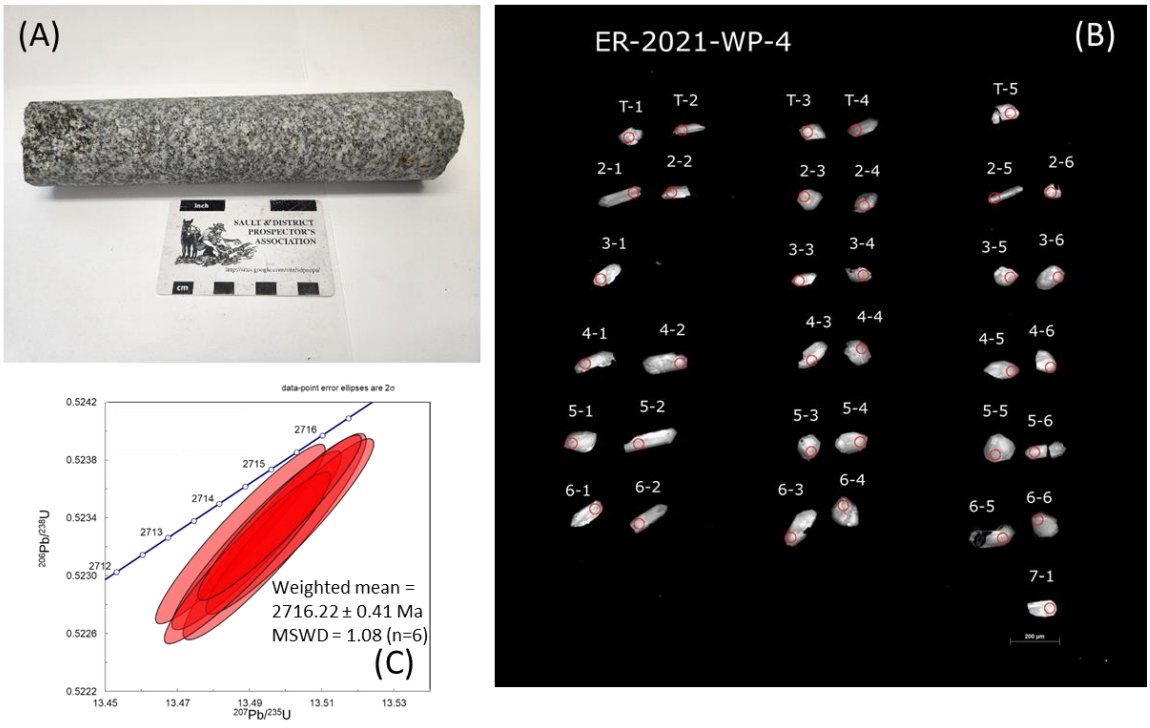

Figure 4.13: Representative sample of the mine diorite (a) extracted zircons (b) and the concordia diagram with the ellipses denoting 2σ errors (c).

A total of 35 zircons were extracted from the diorite, six of which were selected for CA-TIMS analysis (Fig. 4.13 B). All six samples were concordant and equivalent, yielding a weighted mean $^{207}Pb/^{206}Pb$ date of 2716.22 ± 0.41 Ma (Fig. 4.13 C). This is interpreted as the crystallization age of the sample.

4.3 Lithogeochemistry

The TAS classification diagrams that are widely used to discriminate between different volcanic rocks cannot be used in this study due to the mobility of the major elements as a result of alteration and metamorphism (Pearce, 1996; Ross & Bedard, 2009). The mobility of major elements is shown in Figure 4.14, which shows poor correlation due to alteration and metamorphism within the region. Polat (2009) suggested that volcanic rocks with Ce anomalies (Ce/Ce* 1.1 or Ce/Ce* < 0.9) should be considered strongly altered, whereas samples with Ce/Ce* ratios between 1.0 and 1.1 indicates that REE were immobile during post-magmatic alteration. All the volcanic rocks samples have Ce/Ce* between 1.0 and 1.09, except for five samples which have ratios between 0.96 and 0.99. This would suggest that the REE in the majority of the samples were immobile during post-magmatic alteration, with only some samples exhibiting some mobility. For this study, trace elements have been used to plot data with a full list of geochemical results displayed in Appendix A.

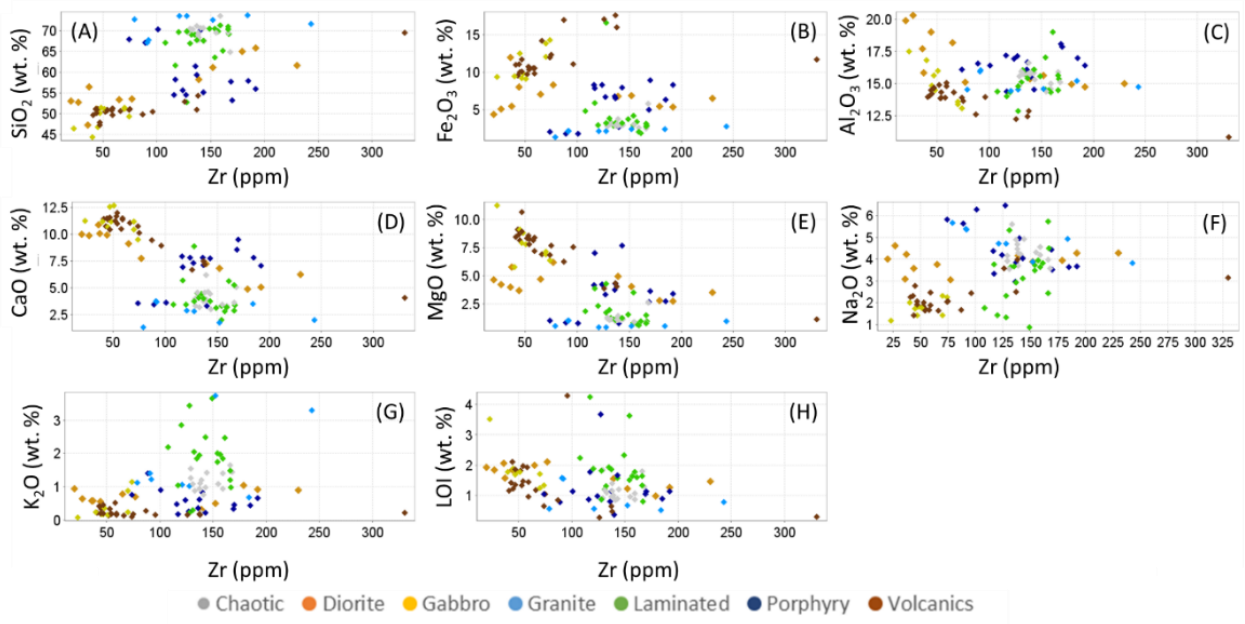

Figure 4.14: Major element scatter plots all the unit showing the mobility of major elements plotted against Zr.

4.3.1 Chaotic Unit

Based on the volcanic classification of Pearce (1996), the chaotic unit plots within the trachy-andesite to trachyte field, except for one of the samples from the Peek-a-Boo area that plots in the andesite basaltic field, and are all calc-alkaline (Fig. 4.15). The chaotic unit is characterized by 64.9 to 73.9 wt.% SiO_2, 0.6 to 2.6 wt.% MgO, and 0.3 to 0.6 wt.% TiO_2, Ni contents range from 0.5 to 36 ppm and the Ti/Zr ratio from 9.7 to 20.2.

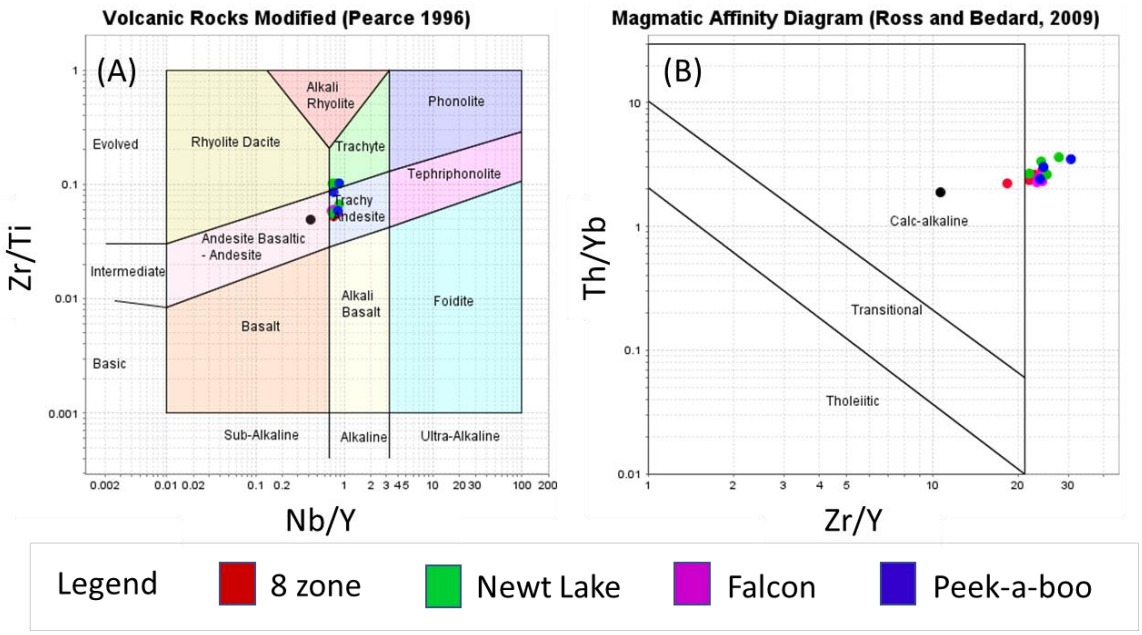

Figure 4.15: Volcanic rock classification (a) and magmatic affinity diagram (b) for the chaotic unit between the different zones. Black dot is from the Peek-a-Boo zone (sample #: ER-2022-WP-P-20).

On primitive mantle normalized spider diagrams the chaotic units is characterized by: (1) strongly enriched LREE (La/Sm_{pm} = 3.4-5.1); (2) moderately fractionated HREE (Gd/Yb_{pm} = 2.0-2.5); (3) negative Nb anomalies (Nb/Nb* = 0.3-0.5); (4) negative Ti anomalies (Ti/Ti* = 0.6-1.0); and (5) positive Zr anomalies (Zr/Zr* = 1.7-2.3; Fig. 4.16; Table 4.1). The classification for weak, moderate and strong is defined as weak (1-2), moderate (2-3), and strong (>3), which is used on all the primitive mantle normalized spider diagrams below. The Peek-a-Boo area has one sample (i.e., ER-

2022-WP-P-20 indicated by black color to distinguish the sample in Figure 4.15) that is characterized by higher absolute trace element values but a similar pattern to the other samples.

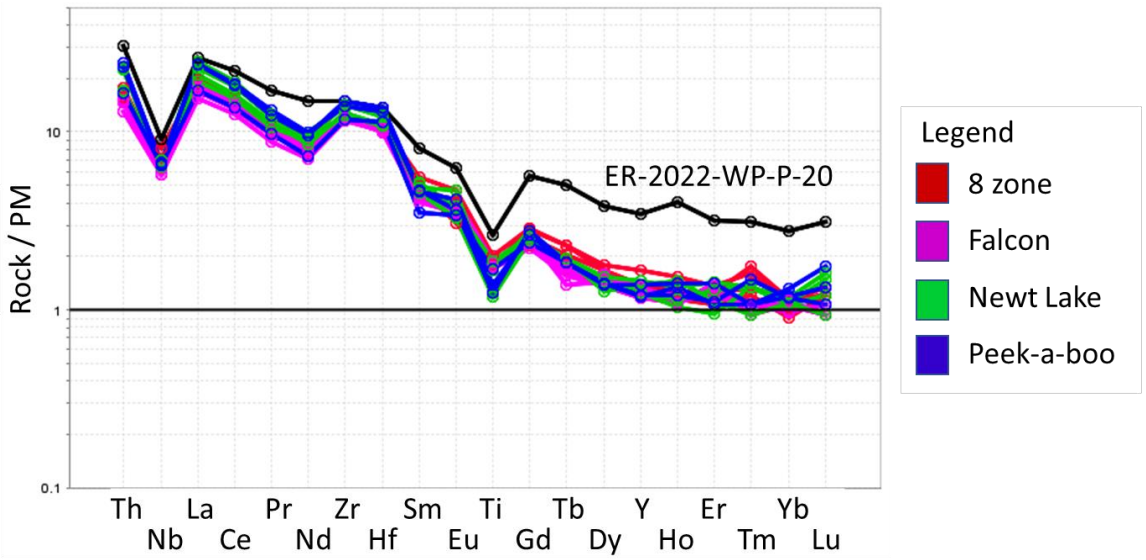

Figure 4.16: Primitive mantle normalized spider diagram for the chaotic unit per zone. The black line is from the Peek-a-Boo zone sample ER-2022-WP-P-20. Primitive mantle normalizing values are from Sun and McDonough (1989).

4.3.2 Laminated Unit

Based on the volcanic classification of Pearce (1996), the Laminated unit has been subdivided into two subgroups, which include: (A) calc-alkaline trachyte to andesite, and (B) a single tholeiitic basalt (Fig. 4.17 A and B).

Group A major elements are characterized by 61.7 to 71.3 wt.% SiO_2, 0.6 to 3.9 wt.% MgO, and 0.3 to 0.6 wt.% TiO_2. Trace element variations include 0.5 to 108 ppm Ni, and 9.5 to 28.89 Ti/Zr ratio. On primitive mantle normalized spider diagrams Group A are enriched in LREE with a negative slope towards the HREE. They are characterized by: (1) strongly enriched LREE (La/Sm_{pm} = 3.6-6.1); (2) weakly to moderately fractionated HREE (Gd/Yb_{pm} = 1.7-3.0); (3) negative Nb anomalies (Nb/Nb* = 0.3-0.4); (4) negative Ti anomalies (Ti/Ti* = 0.6-1.0); and (5) positive Zr anomalies (Zr/Zr* = 1.4-2.2; Fig. 4.18; Table 4.2).

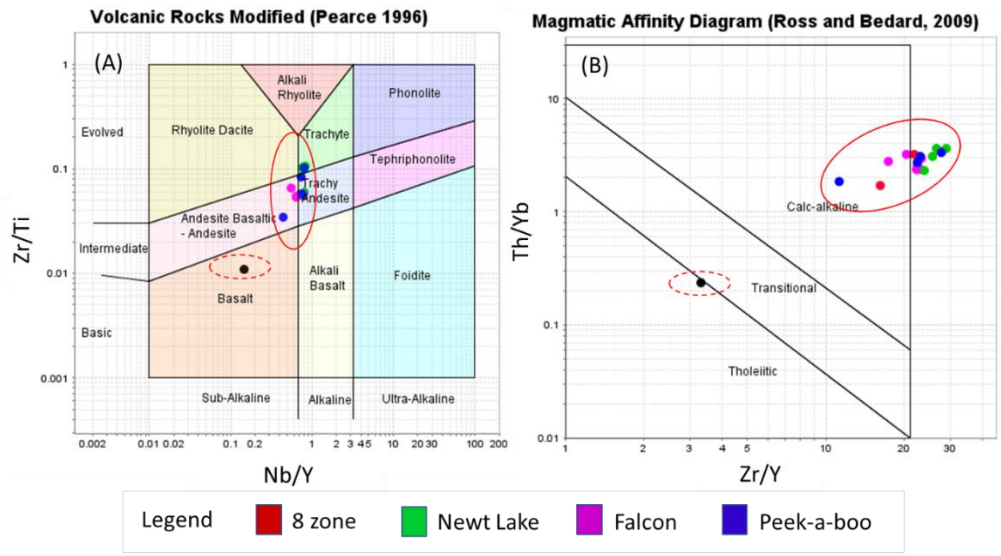

Figure 4.17: Volcanic rock classification (a) and magmatic affinity diagram (b) for the Laminated unit. Black dot is from the Peek-a-Boo zone. Solid red line represents group A, and dashed red line represents group B.

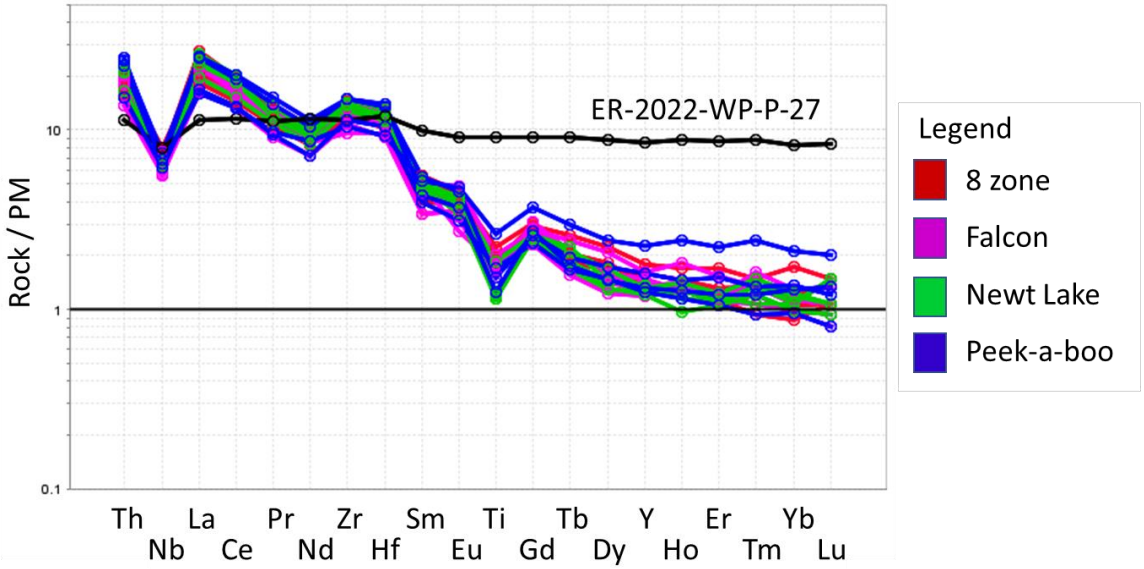

Figure 4.18: Primitive mantle normalized spider diagram for the Laminated unit per zone. The black line is from the Peek-a-Boo zone. Primitive mantle normalizing values are from Sun and McDonough (1989).

Group B major elements are characterized by 52.8 wt.% SiO_2, 4.3 wt.% MgO, and 1.96 wt.% TiO_2. Trace elements include 56 ppm Ni, and 90.7 Ti/Zr ratio. On primitive mantle normalized spider diagrams Group B has a flat pattern between LREE and HREE. The sample is characterized by: (1)

weakly enriched LREE (La/Sm_{pm} = 1.1); (2) nearly flat HREE (Gd/Yb_{pm} = 1.1); and (3) negative Nb anomalies (Nb/Nb* = 0.7; Fig. 4.18; Table 4.2).

4.3.3 Diorite

Based on the volcanic classification of Pearce (1996) and the primitive mantle normalized spider diagram, the diorite unit has been subdivided into two subgroups, which include: (a) calc-alkaline andesite basalt with higher abundance of trace elements, and (b) transitional to calc-alkaline basalt with lower abundance of LREE (Fig. 4.19 A and B).

Group A major elements are characterized by 58.3 to 65.9 wt.% SiO_2, 2.8 to 5.0 wt.% MgO, and 0.7 to 1.0 wt.% TiO_2. Trace element variations include 54 to 120 ppm Ni, and 20.1 to 40.5 Ti/Zr ratio. On primitive mantle normalized spider diagrams Group A are characterized by: (1) moderately to strongly enriched LREE (La/Sm_{pm} = 2.5-3.5); (2) moderately fractionated HREE (Gd/Yb_{pm} = 2.1-2.7); (3) negative Nb anomalies (Nb/Nb* = 0.3-0.4); (4) negative Ti anomalies (Ti/Ti* = 0.4-0.5); and (5) negative to positive Zr anomalies (Zr/Zr* = 0.9-1.4; Fig. 4.20; Table 4.3).

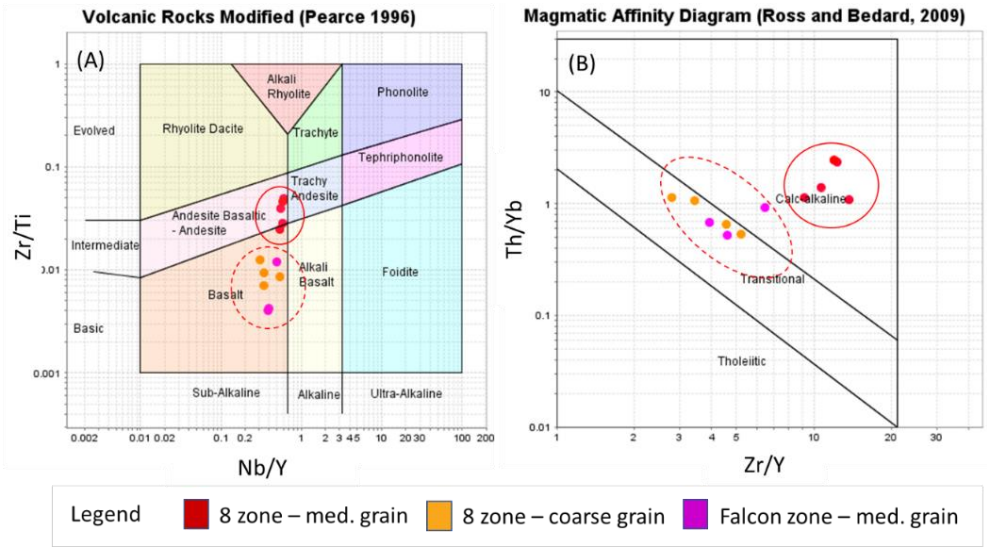

Figure 4.19: Volcanic rock classification (a) and magmatic affinity diagram (b) for the diorite unit. Solid red line represents group A, and dashed red line represents group B.

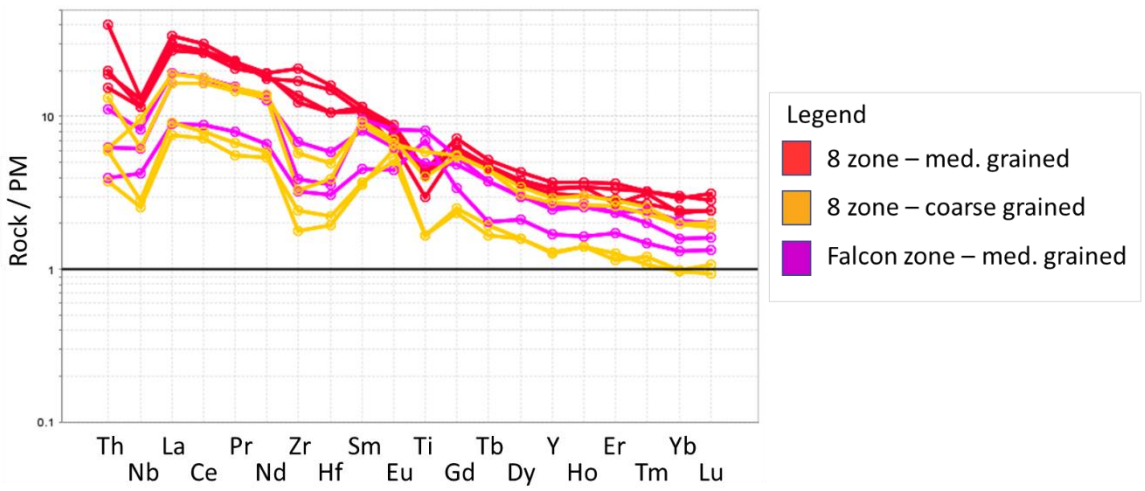

Figure 4.20: Primitive mantle normalized spider diagram for the diorite unit, including 8 zone – medium grained, 8 zone coarse grained, and Falcon zone – medium grained. Primitive mantle normalizing values are from Sun and McDonough (1989).

Group B major elements are characterized by 47.3 to 56.5 wt.% SiO_2, 3.7 to 6.2 wt.% MgO, and 0.4 to 1.8 wt.% TiO_2. Trace element variations include 68 to 170 ppm Ni, and 80.0 to 251.6 Ti/Zr ratio. On primitive mantle normalized spider diagrams Group B are characterized by: (1) weakly to moderately enriched LREE (La/Sm_{pm} = 1.7-2.5); (2) moderately to strongly fractionated HREE (Gd/Yb_{pm} = 2.1-3.5); (3) negative Nb anomalies (Nb/Nb* = 0.3-0.5); (4) negative to positive Ti anomalies (Ti/Ti* = 0.6-1.8); and (5) negative Zr anomalies (Zr/Zr* = 0.3-0.7; Fig. 4.20; Table 4.3).

4.3.4 Gabbro

Based on the volcanic classification of Pearce (1996), the gabbro unit plots within the tholeiitic basalt field (Fig. 4.21 A and B). The gabbros are characterized by 44.4 to 51.5 wt.% SiO_2, 5.8 to 11.2 wt.% MgO, and 0.5 to 1.0 wt.% TiO_2. Trace element variations include 82 to 338 ppm Ni, and 57.7 to 148.6 Ti/Zr ratio.

On primitive mantle normalized spider diagrams the gabbros are characterized by: (1) weakly depleted to weakly enriched LREE (La/Sm_{pm} = 0.9-1.1); (2) nearly flat HREE (Gd/Yb_{pm} = 1.0-1.4); (3)

negative Ti anomalies (Ti/Ti* = 0.5-1.2); and (4) negative Nb anomalies (Nb/Nb* = 0.7-0.9; Fig. 4.22; Table 4.4).

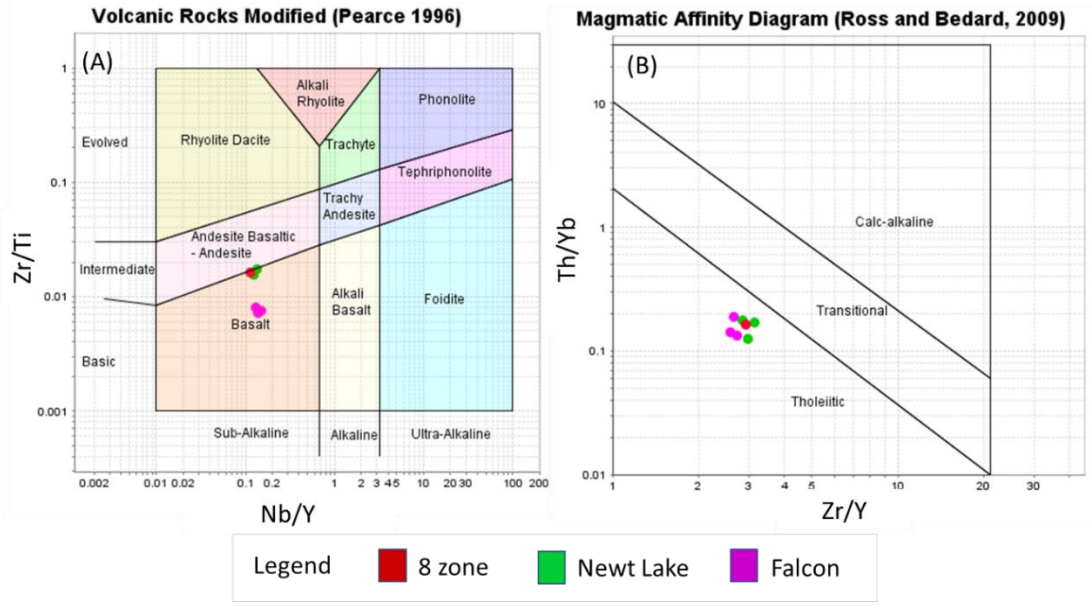

Figure 4.21: Volcanic rock classification (a) and magmatic affinity diagram (b) for the gabbro unit between the different zones. Black dot is from the Peek-a-Boo zone.

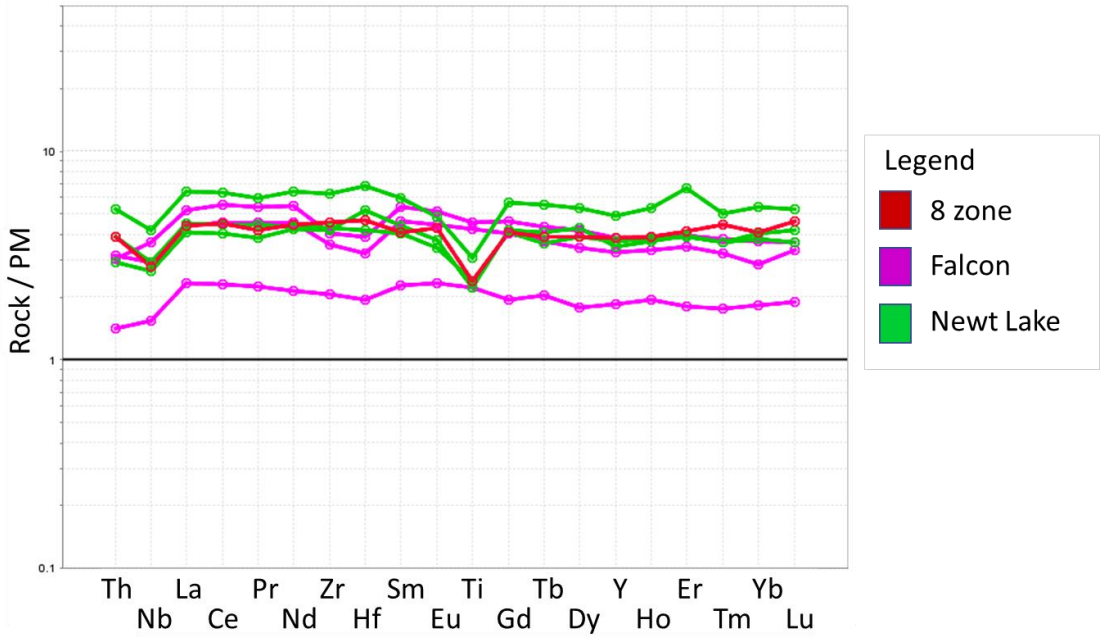

Figure 4.22: Primitive mantle normalized spider diagram for the gabbro unit per zone. Primitive mantle normalizing values are from Sun and McDonough (1989).

4.3.5 Granite and batholiths

Based on the volcanic classification of Pearce (1996), the upper granite from the Peek-a-Boo zone (n=2 of the 7) and the three granitic intrusions around the diorite (n=3 of the 7) plot within the syenite fields, whereas the lower granite from the Peek-a-Boo zone (n=2 of the 7) plots within the diorite field, with all units plotting as calc-alkaline (Fig. 4.23 A and B). The unit has been subdivided into two groups: (A) Central pluton and Bowman Lake batholith are characterized by elevated LREE elements, and (B) Floating Heart batholith and the Peek-a-Boo granites are characterized by less enriched LREE relative to Group A. Group B has been subdivided into two subgroups based on Ni content and Ti/Zr ratio, which include (B1) upper granite and Floating Heart batholith with low Ni and Ti/Zr ratio, and (B2) lower granite with elevated Ni and Ti/Zr ratio relative to Group B1.

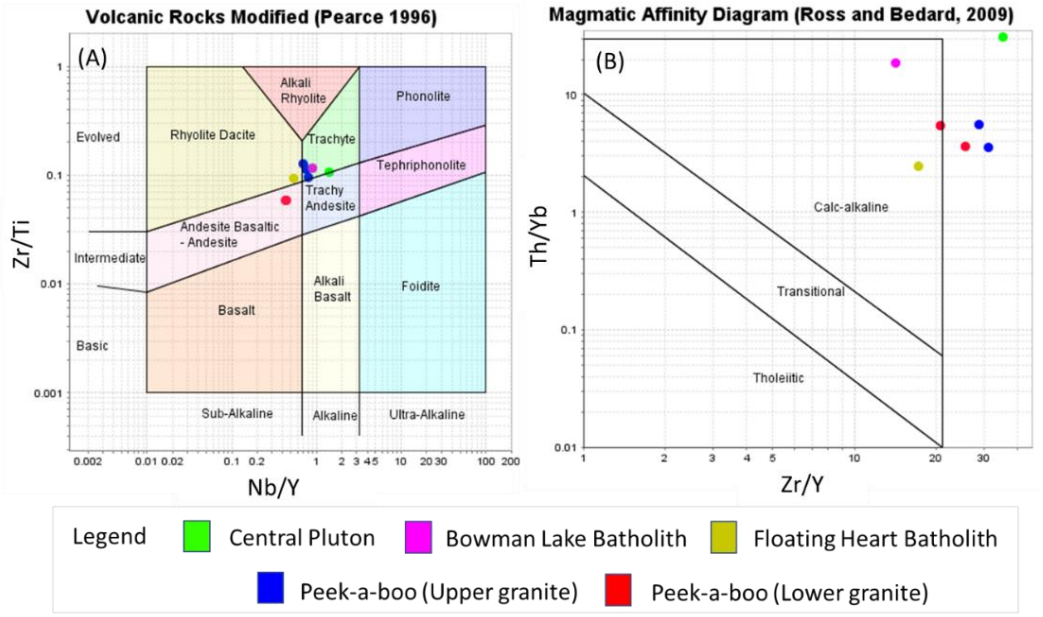

Figure 4.23: Volcanic rock classification (a) and magmatic affinity diagram (b) for the granite units within the Peek-a-Boo zone, and the three granitic intrusions around the diorite.

Group A is characterized by 71.7 to 72.6 wt.% SiO_2, 0.5 to 1.0 wt.% MgO, and 0.2 to 0.4 wt.% TiO_2. Trace element variations include 4 to 12 ppm Ni, and 8.6 to 9.3 Ti/Zr ratio. On the primitive mantle normalized spider diagrams the lower granite is characterized by: (1) strongly enriched LREE

(La/Sm_{pm} = 5.9-7.1); (2) strongly fractionated HREE (Gd/Yb_{pm} = 3.4-5.0); (3) negative Nb anomalies (Nb/Nb* = 0.1); (4) negative Ti anomaly (Ti/Ti* = 0.1-0.2); and (5) negative to positive Zr anomaly (Zr/Zr* = 0.8-1.3; Fig. 4.24; Table 4.5).

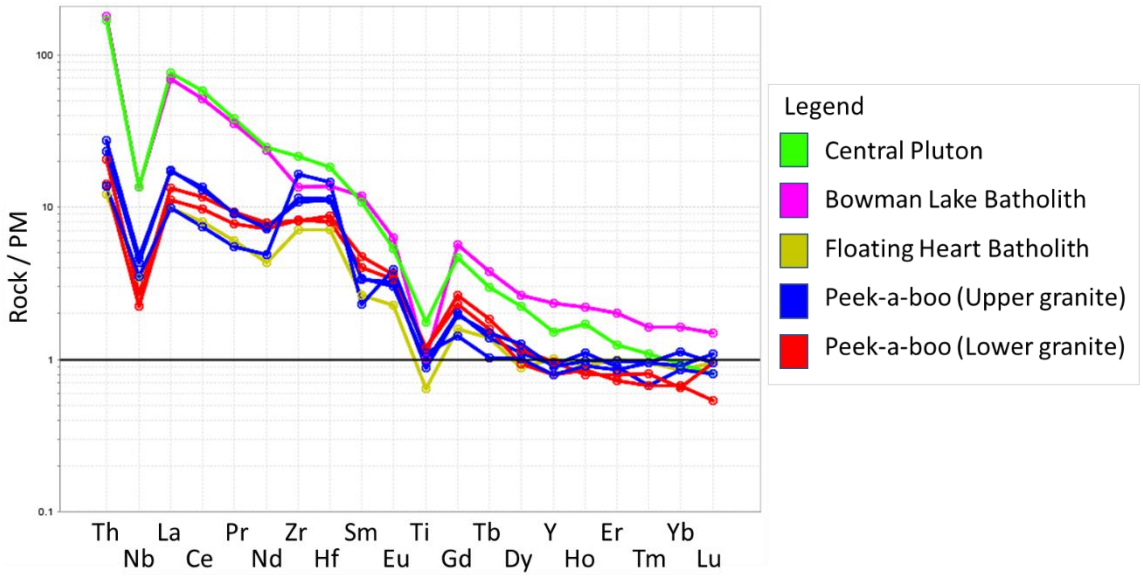

Figure 4.24: Primitive mantle normalized spider diagram for the granite units within the Peek-a-Boo zone, and the three granitic intrusions around the diorite. Primitive mantle normalizing values are from Sun and McDonough (1989).

Group B1 is characterized by 72.7 to 73.7 wt.% SiO_2, 0.5 to 0.6 wt.% MgO, and 0.1 to 0.2 wt.% TiO_2. Trace element variations include 0.5 to 4 ppm Ni, and 7.7 to 10.8 Ti/Zr ratio. On the primitive mantle normalized spider diagrams the lower granite is characterized by: (1) strongly enriched LREE (La/Sm_{pm} = 3.7-5.2); (2) weakly to moderately fractionated HREE (Gd/Yb_{pm} = 1.6-2.4); (3) negative Nb anomalies (Nb/Nb* = 0.2-0.3); (4) negative Ti anomaly (Ti/Ti* = 0.3-0.6); and (5) positive Zr anomaly (Zr/Zr* = 2.1-4.9; Fig. 4.24; Table 4.5).

Group B2 is characterized by 67.2 to 67.8 wt.% SiO_2, 1.04 to 1.06 wt.% MgO, and 0.3 wt.% TiO_2. Trace element variations include 16 ppm Ni, and 17.1-17.3 Ti/Zr ratio. On primitive mantle normalized spider diagrams the lower granite is characterized by: (1) moderately enriched LREE (La/Sm_{pm} = 2.8); (2) strongly fractionated HREE (Gd/Yb_{pm} = 3.5-4.1); (3) negative Nb anomalies

(Nb/Nb* = 0.2); (4) negative Ti anomaly (Ti/Ti* = 0.3-0.4); and (5) positive Zr anomaly (Zr/Zr* = 1.3-1.5; Fig. 4.24; Table 4.5).

4.3.6 Feldspar porphyry

Based on the volcanic classification of Pearce (1996), the feldspar porphyry unit has been subdivided into two subgroups, which include: (a) calc-alkaline andesite to trachy andesite; and (b) calc-alkaline basalts (Fig. 4.25 A and B). The 8 zone and the Falcon zone plot within Group B, the Peek-a-Boo zone within Group A, and Newt Lake zone has a mixture of both Group A (n=3: ER-2021-WP-N-04, ER-2021-WP-N-05, and ER-2021-WP-N-12) and Group B (n=2: ER-2021-WP-N-01 and ER-2021-WP-N-11).

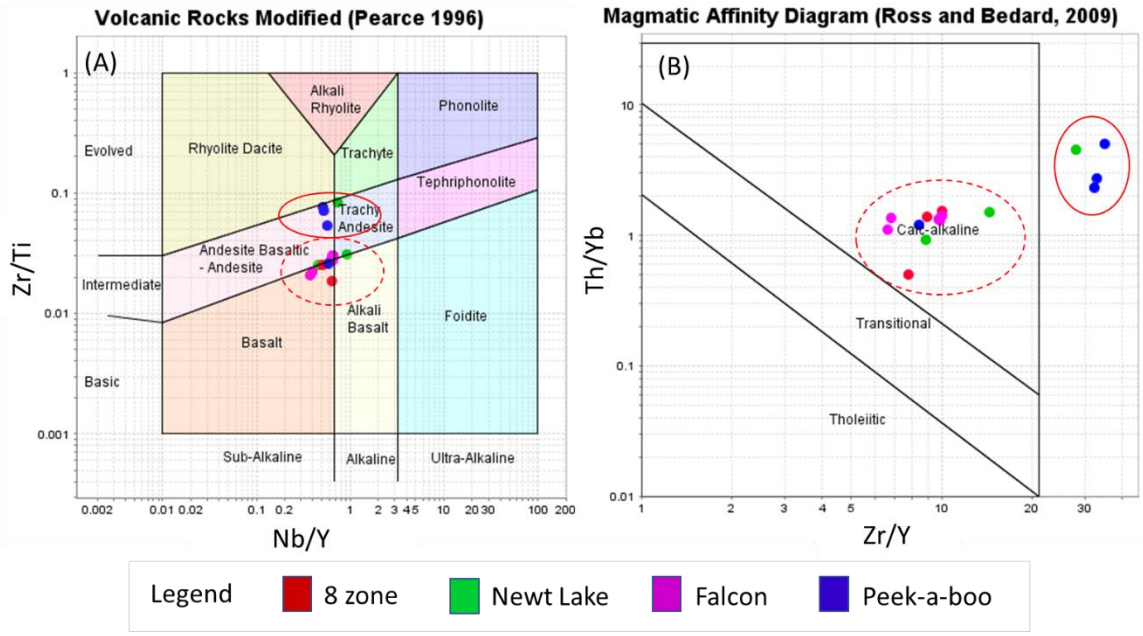

Figure 4.25: Volcanic rock classification (a) and magmatic affinity diagram (b) for the feldspar porphyry unit. Solid red line represents group A, and dashed red line represents group B.

Group A major elements are characterized by 67.2 to 72.0 wt.% SiO_2, 0.7 to 1.0 wt.% MgO, and 0.2 to 0.3 wt.% TiO_2. Trace element variations include 5 to 16 ppm Ni, and 11.6 to 18.9 Ti/Zr ratio. On primitive mantle normalized spider diagrams Group A are characterized by: (1) moderately to

strongly enriched LREE (La/Sm_{pm} = 2.7-4.6); (2) moderately to strongly fractionated HREE (Gd/Yb_{pm} = 2.5-5.0); (3) negative Nb anomalies (Nb/Nb* = 0.2-0.3); (4) negative Ti anomalies (Ti/Ti* = 0.3-0.4); and (5) positive Zr anomalies (Zr/Zr* = 1.6-2.0; Fig. 4.26; Table 4.6).

Group B major elements are characterized by 53.2 to 61.4 wt.% SiO_2, 2.7 to 7.7 wt.% MgO, and 0.7 to 1.5 wt.% TiO_2. Trace elements variations include 52 to 249 ppm Ni, and 31.9 to 53.8 Ti/Zr ratio. On primitive mantle normalized spider diagrams Group B are characterized by: (1) moderately enriched LREE (La/Sm_{pm} = 2.1-3.0); (2) weakly to moderately fractionated HREE (Gd/Yb_{pm} = 1.9-2.5); (3) negative Nb anomalies (Nb/Nb* = 0.3-0.6); (4) negative Ti anomalies (Ti/Ti* = 0.4-0.6); and (5) negative to positive Zr anomalies (Zr/Zr* = 0.7-1.4; Fig. 4.26; Table 4.6).

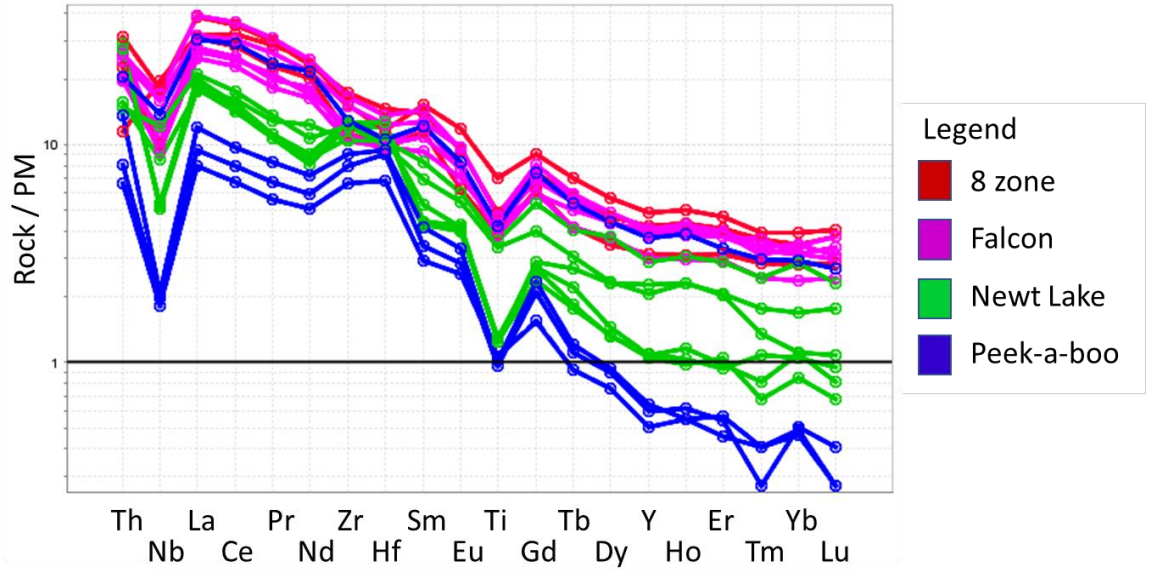

Figure 4.26: Primitive mantle normalized spider diagram for the feldspar porphyry unit per zone. Primitive mantle normalizing values are from Sun and McDonough (1989).

4.3.7 Volcanic Rocks

Based on the volcanic classification of Pearce (1996), the volcanic rocks plot within the tholeiitic basalt zone, with one outlier plotting with the tholeiitic to transitional rhyolite to dacite zone (n=1: ER-2021-WP-N-06; Fig. 4.27). Based on the primitive mantle normalized spider diagrams the chaotic

unit is more related to feldspar porphyry unit rather than the volcanic rocks, whereas the Laminated unit is more related to the rock that is being altered (i.e., volcanic rocks, or chaotic unit).

Volcanic rocks major elements are characterized by 47.3 to 54.3 wt.% SiO_2, 3.9 to 10.7 wt.% MgO, and 0.5 to 2.0 wt.% TiO_2. Trace element variations include 20 to 258 ppm Ni, and 56.1 to 98.5 Ti/Zr ratio. On primitive mantle normalized spider diagrams the Group A are characterized by: (1) weakly depleted to weakly enriched LREE (La/Sm_{pm} = 0.8-1.4); (2) weakly fractionated HREE (Gd/Yb_{pm} = 1.0-1.2); (3) negative Ti anomalies (Ti/Ti* = 0.5-1.0); (4) negative Nb anomalies (Nb/Nb* = 0.5-0.8); and (5) negative to positive Zr anomalies (Zr/Zr* = 0.8-1.1; Fig. 4.28; Table 4.7).

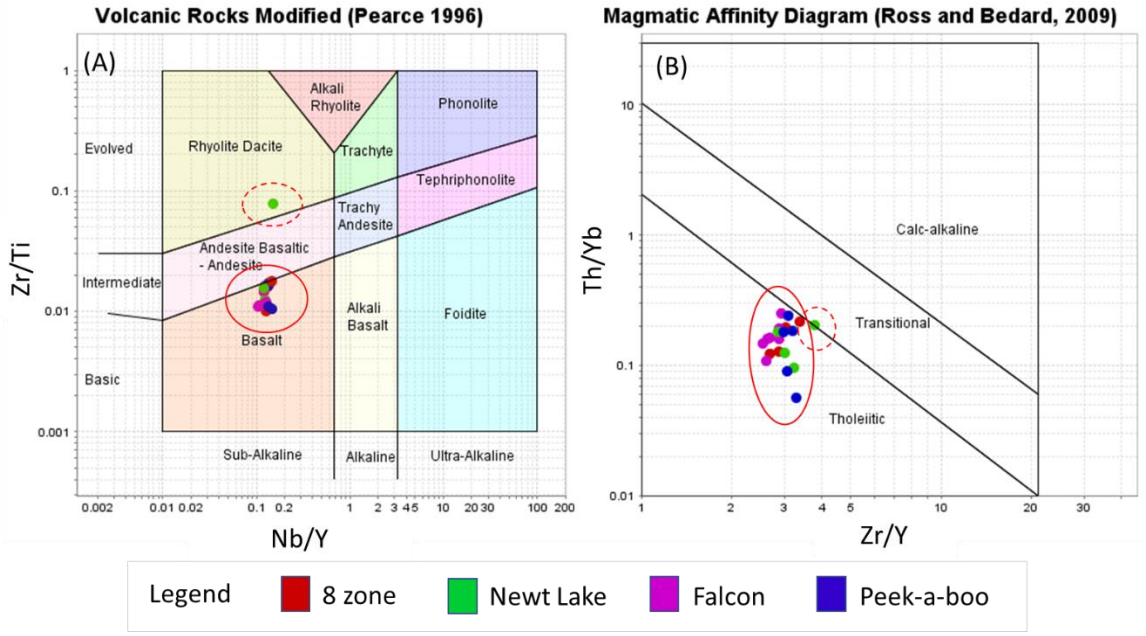

Figure 4.27: Volcanic rock classification (a) and the magmatic affinity diagram (b) for the volcanic rocks. Solid red line represents volcanic rocks, and dashed red line represents the outlier.

Volcanic rock outlier major elements are characterized by 69.5 wt.% SiO_2, 1.14 wt.% MgO, and 0.7 wt.% TiO_2. Trace element variations include 0.5 ppm Ni, and 12.5 Ti/Zr ratio. On primitive mantle normalized spider diagrams the outlier is characterized by: (1) weakly enriched LREE (La/Sm_{pm} = 1.1); (2) weakly fractionated HREE (Gd/Yb_{pm} = 1.1); (3) negative Ti anomalies (Ti/Ti* = 0.1); (4) negative Nb anomalies (Nb/Nb* = 0.7); and (5) positive Zr anomalies (Zr/Zr* = 1.2; Fig. 4.28; Table 4.7).

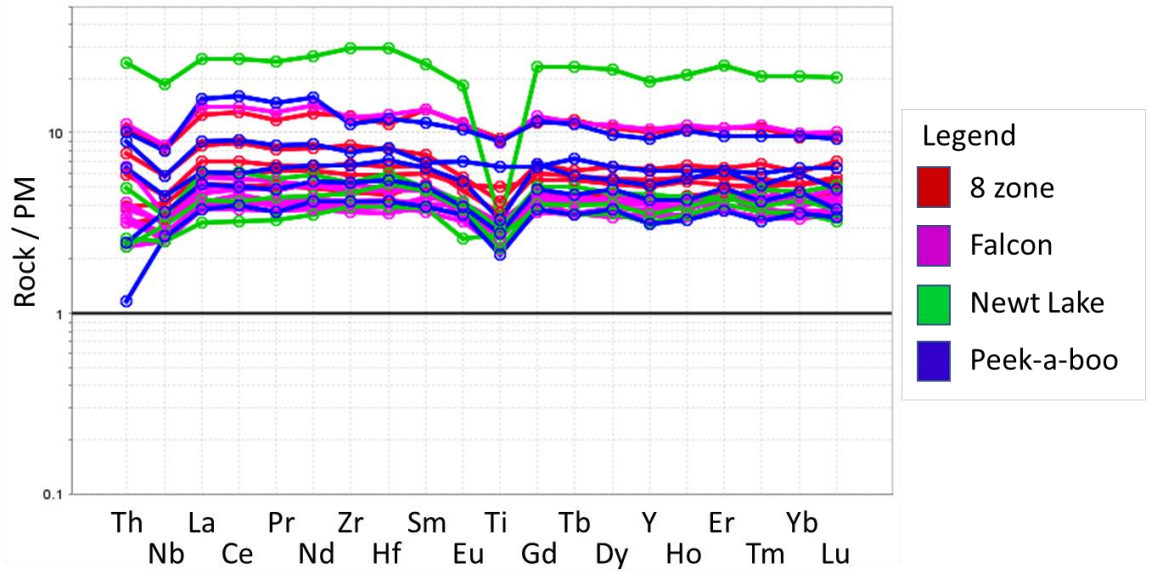

Figure 4.28: Primitive mantle normalized spider diagram for the volcanic rocks per zone. The outlier is from Newt Lake which is more enriched and has a strong negative Ti anomaly. Primitive mantle normalizing values are from Sun and McDonough (1989).

5. Paragenesis of the chaotic unit

The study of the chaotic unit was undertaken as it a host to part of the mineralization within the area. The categorization of the veining was undertaken to provide a better understanding of the unit and how it relates to mineralization.

Within the chaotic unit 15 different vein types were identified, five of which are quartz veining (Fig. 5.1, Table 5.1). The veins were characterized based on the type of infill (i.e., clinochlore, amphibole, etc.) and sub categorized based on the alteration (i.e., albite, potassic, etc.). Not all vein types are found within each area, and the abundance of each vein type varied between the zones (see Sections 5.2, 5.3, 5.4, and 5.5 paragenesis diagrams for the occurrence and abundances of the vein types within each zone). The alteration halo around the veins varied based on the orientation of the vein to the fabric. If the vein was parallel to fabric, the alteration halo was thinner, more consistent in thickness and weakly boudinaged (Fig. 5.2 A). If the vein was at a high angle to the fabric, the alteration thickness was highly variable (Fig. 5.2 B). The following text discusses the veins in order of formation.

5.1 Vein types

5.1.1 Q1

The veins are highly deformed, discontinuous, boudinaged and up to 2 cm in width. The vein consists of quartz with remnant altered orthoclase clasts with minor titanite, clinozoisite, clinochlore, and zircons (Fig. 5.3). The contacts of the vein are associated with higher accumulation of clinochlore and titanites. The quartz grains are anhedral up to 60 micrometers in width with undulatory extinction and strong recrystallization texture, with inclusions of anhedral clinozoisite up

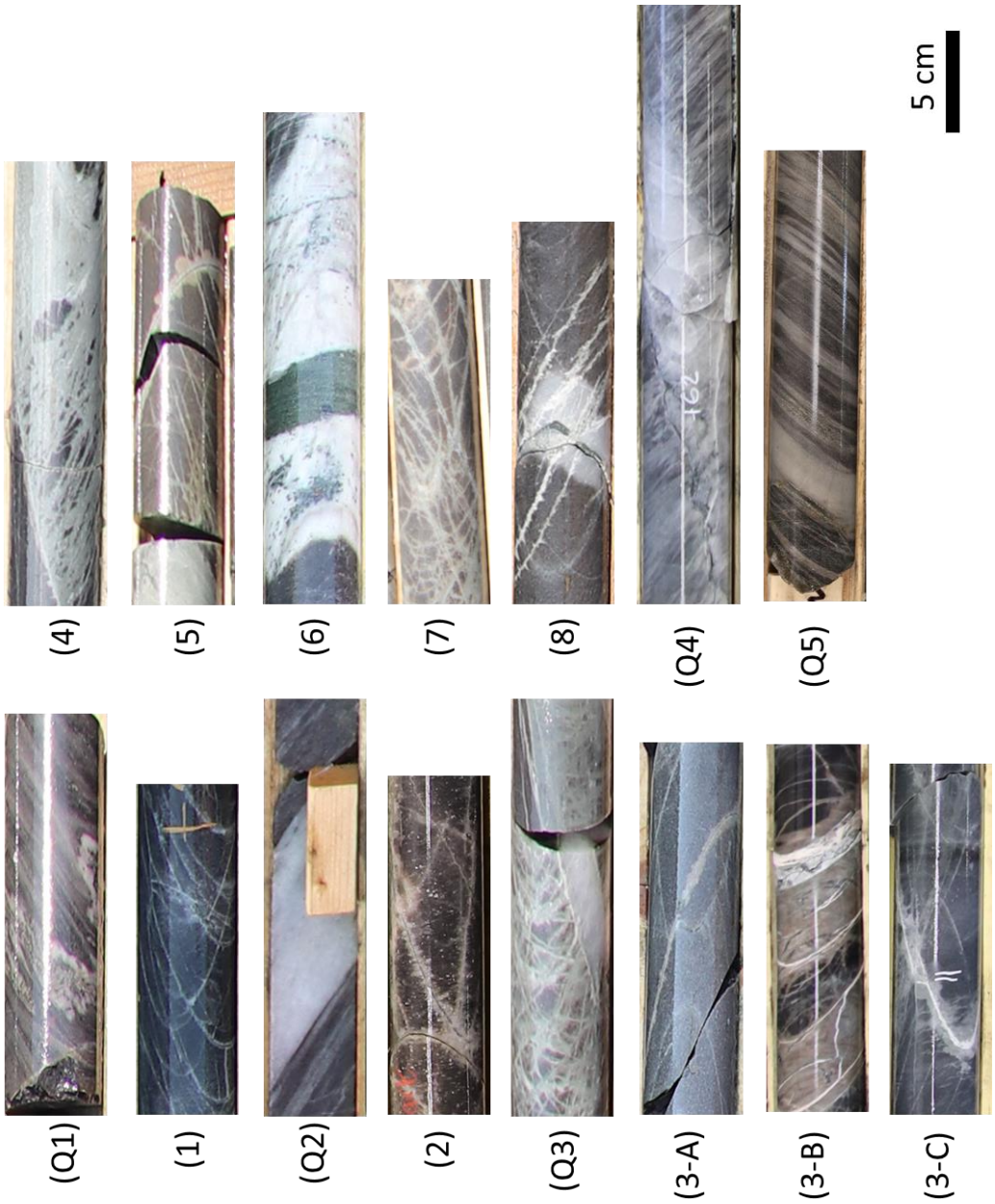

Figure 5.1: Characterization of different vein types found with the chaotic unit. (Q1) highly deformed quartz veining (700-E-01 @ 23m); (1) quartz infill with albite alteration (700-E-03 @ 5m); (Q2) quartz veining parallel to fabric (700-E-02 @ 6m); (2) orthoclase-quartz-carbonate infill with albite-prehnite- clinochlore alteration (ERX-2021-71 @ 139m); (Q3) quartz veining cross-cutting chaotic unit (700-E-07 @ 39m); (3-A) clinochlore-zeolite-muscovite infill with potassic alteration (700-E-03 @ 15m); (3-B) zeolite-clinozoisite infill with potassic alteration (ERM-2020-95 @ 518m); (3-C) alkali feldspar-carbonate-quartz with albite alteration (ERM-2020-79 @ 462m); (4) net-texture veins with albite alteration (700-E-06 @ 17m); (5) quartz-plagioclase-prehnite infill with albite and potassic alteration (700-E-01 @ 9m); (6) clinochlore infill with albite alteration (700-E-02 @ 46m); (7) clinozoisite with albite alteration (700-E-11A @ 71m); (8) clinochlore-muscovite infill with albite alteration (700-E-15 @ 21m); (Q4) quartz veining cutting fabric (ERM-2020-78 @ 62m); and (Q5) quartz veining parallel to fabric (ERX-2021-57 @ 96m).

Table 5.1: Summary of vein based on the paragenesis.

Vein ID	Vein infill major	Vein infill minor	Vein alteration	Macro identification
Q1	quartz	albite, clinochlore, prehnite	no alteration halio	milky quartz strongly deformed no alteration halo
1	quartz		albite, prehnite, clinzoisite sulfides accumalte at terminations of splays	mm-scale veins, commonly infill is not visible alteration halo is thin but can be variable if on an angle to fabric
Q2/Q5	quartz	carbonate, muscovite		milky quartz parallel to fabric no alteration halo
2	orthoclase	carbonate, quartz	albite, orthoclase,prehnite, pumpellyite, clinozoisite, clinochlore, carbonate,	mm-scale dark grey to black infill, straight to weakly undulating alteration halos is greenish-greyish in color with irregular darker patches, that can be irregular
Q3	quartz	muscovite	orthoclase, albite, prehnite, clinozoisite	clear to milky quartz range from mm- to cm-scale, dominantly straight local weak mm-scale light beige alteration halo
3-A	zeolite, clinochlore, muscovite	quartz, titanite, prehnite	orthoclase, albite, prehnite, clinozoisite	mm-scale veins, dark green in color alteration halo is beige and can be reddish away from the vein contact
3-B	zeolite	clinozoisite, muscovite, ilmenite	orthoclase, albite, prehnite, pumpellyite,	mm-scale veins, white infill alteration halo is dominantly broad and reddish
3-C	feldspar	carbonate, quart, hematite	orthoclase, albite, prehnite, pumpellyite	mm-scale vein with white infill alteration halo is light beige to light green and locally can have irregular patches of potassic alteration
4	plagioclase, albite, quartz, clinochlore	ilmenite, titanite, prehnite	albite, orthoclase, prehnite, pumpellyite	net-texture veinlets vein with the infill not visible alteration halo is irregular that is greenish-greyish
5	plagioclase, quartz	prehnite, hematite, clinochlore, titanite	albite, orthoclase, prehnite, pumpellyite	mm-scale vein with dark green to black infill alteration halo is light green-grey in proximity to vein and become potassic altered. Commonly alteration halo is variable in thickness.
6	clinochlore	quartz, muscovite, sphalerite, zircon, titanite	albite, orthoclase, prehnite, pumpellyite, carbonate	vein range from mm-scale to cm-scale infilled with medium to dark green clinochlore alteration halo is dominantly broad with sharp contact containing patches raning from light beige to dark green locally vein can be boudinaged and thin, with infills of quartz
7	clinozoisite	orthoclase, titanite	albite, orthoclase, prehnite, pumpellyite, carbonate	mm-scale vein that is dark green. The vein is dominantly straight but can have thin splays alteration halo is light-greenish to grey with abundant patches ranging from black to white. Often the alteration halo is variable in thickness.
8	clinochlore, muscovite	titanite, clinozoisite, quartz	albite, orthoclase, clinozoisite, carbonate	mm-scale vein with infill not visible alteration halo is variable in thickness and white in color only noted in zone 8
Q4	quartz	carboante, muscovite		clear to milky quartz that cut fabric. Commonly the vein contact are sharp but irregular.

to 10 micrometers wide. The clinochlore grains are anhedral up to 20 micrometers elongated subparallel to the contact. Zircon grains are subhedral up to 3 micrometers found along quartz grain boundaries. Subhedral to euhedral titanite grains are up to 15 micrometers wide dominantly found near the contact. The remnant orthoclase feldspars are strongly altered with medium to dark brown

alteration. The alteration consists of albite with the darker patches having higher accumulation of prehnite-pumpellyite. Within the clasts there are inclusions of subhedral clinozoisite up to 10 micrometers wide.

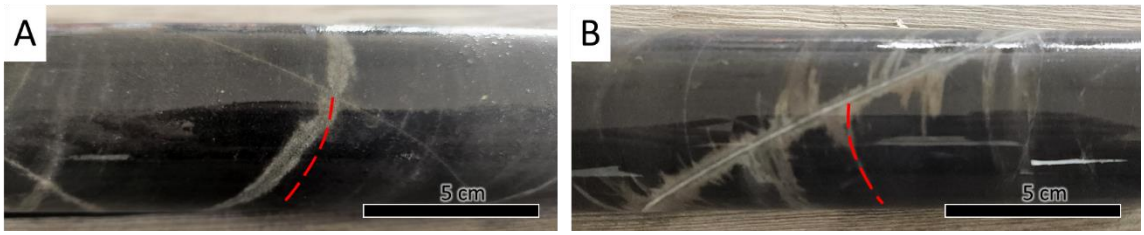

Figure 5.2: The veining in the chaotic unit showing the effect that fabric has on alteration. When the vein is parallel to fabric the alteration halo is thinner and less variable (A). When the vein is on an angle to the fabric, the alteration halo is thicker and more variable (B). The red dashed line indicates the fabric.

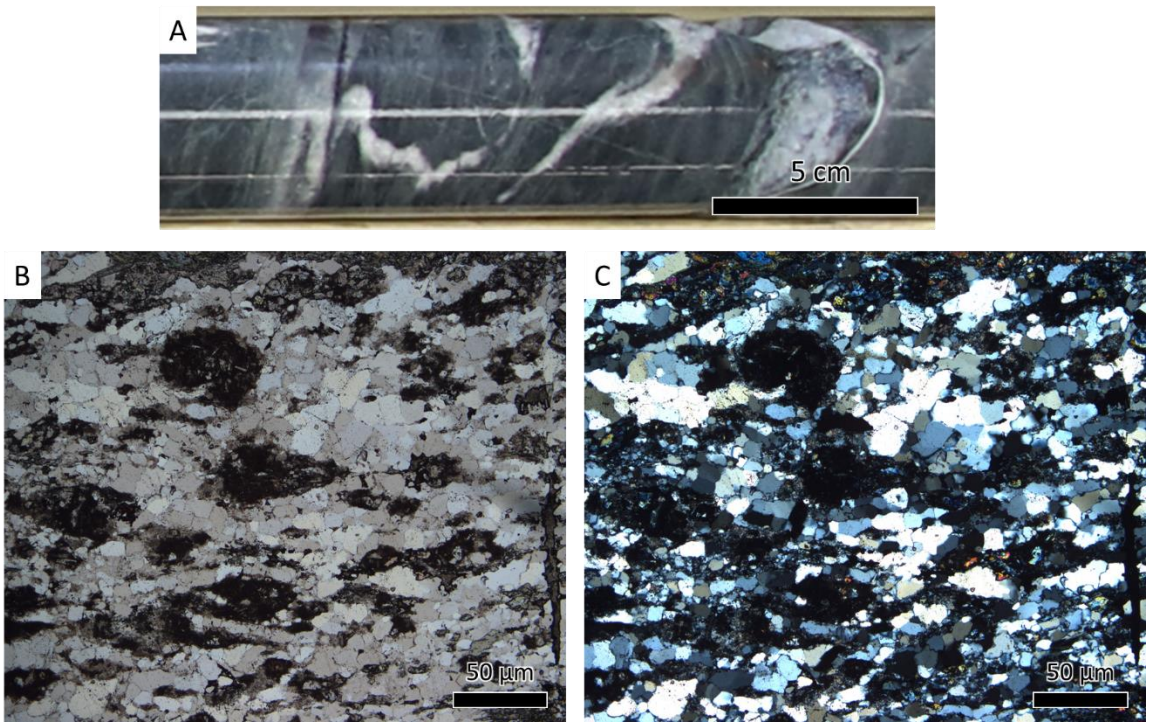

Figure 5.3: Quartz 1 vein in the core sample (a) and photomicrographs in plane polarized light (b) and cross polarized light (c) from ER-2022-WP-F-53.

5.1.2 Type 1

Type 1 veins are thin, variably oriented veins exhibiting weak deformation fabrics, ranging in thickness from 0.01 to 2 micrometers, and infilled with massive quartz (Fig. 5.4). The alteration halo

thickness and variability range from 1-4 mm and is composed of a light-medium brown destructive alteration. The lighter brown patches are dominantly composed of albite and darker patches dominated by prehnite. Anhedral clinozoisite up to 3 micrometers across occur in proximity to the vein. Locally anhedral clinochlore grains up to 30 micrometers across occur within the alteration halo, with the Fe# ranging from 69 to 74. Locally small splays occur which are associated with higher abundance of subhedral to euhedral pyrite, and trace chalcopyrite.

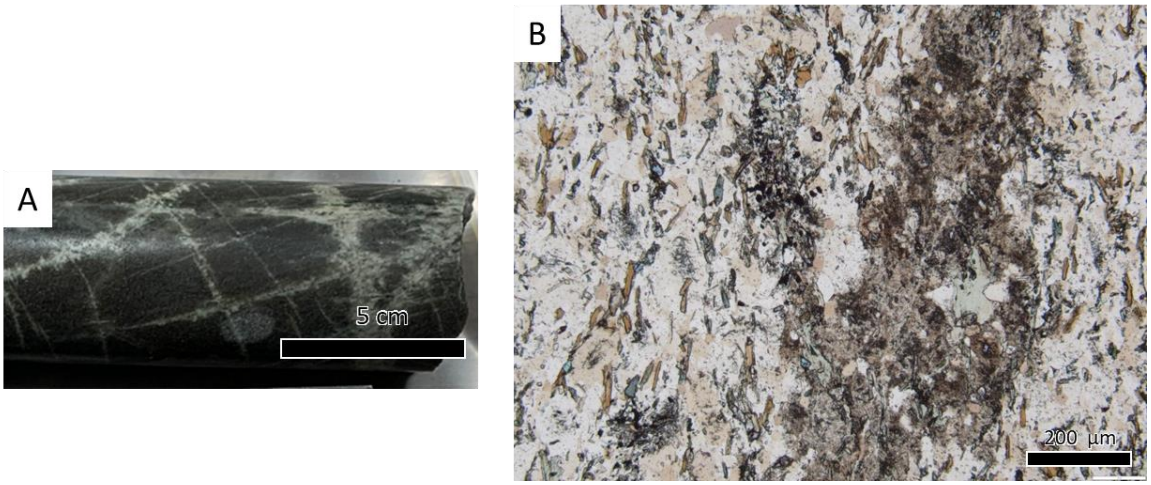

Figure 5.4: Type 1 vein in the core sample (a) and photomicrograph in plane polarized light (b) from ER-2021-WP-8Z-03A.

5.1.3 Q2

The quartz veining is parallel to the deformation fabric and are boudinaged, ranging from 100 micrometers to over 1 cm in width (Fig. 5.5). The vein is dominantly composed of recrystallized quartz with inclusions of clinochlore, carbonate, clinozoisite, muscovite, sphalerite, pyrite, pyrrhotite and chalcopyrite. The inclusions vary depending on the mineralogy of the deformed layers. The quartz grains have a bimodal distribution with the coarser grains over 150 micrometers across exhibiting undulatory extinction. The finer grains can be up to 30 micrometers across, but commonly less than 20 micrometers and are commonly found along coarse quartz grain boundaries. The clinochlore grains are subhedral up to 20 micrometers across and are oriented sub parallel to

the contact. The muscovite grains are subhedral up to 25 micrometers and are oriented sub parallel to the contact. The carbonate grains are anhedral and commonly found along grain boundaries of quartz. The sulphides are anhedral up to 30 micrometers and found along grain boundaries of quartz grains. They are dominated by pyrite with minor pyrrhotite and chalcopyrite. Locally along the contact subhedral coarse clinochlore or muscovite up to 60 micrometers can be found oriented parallel to the contact. The muscovite abundance and size increase in proximity to the vein contact. The quartz veins do not exhibit an alteration halo.

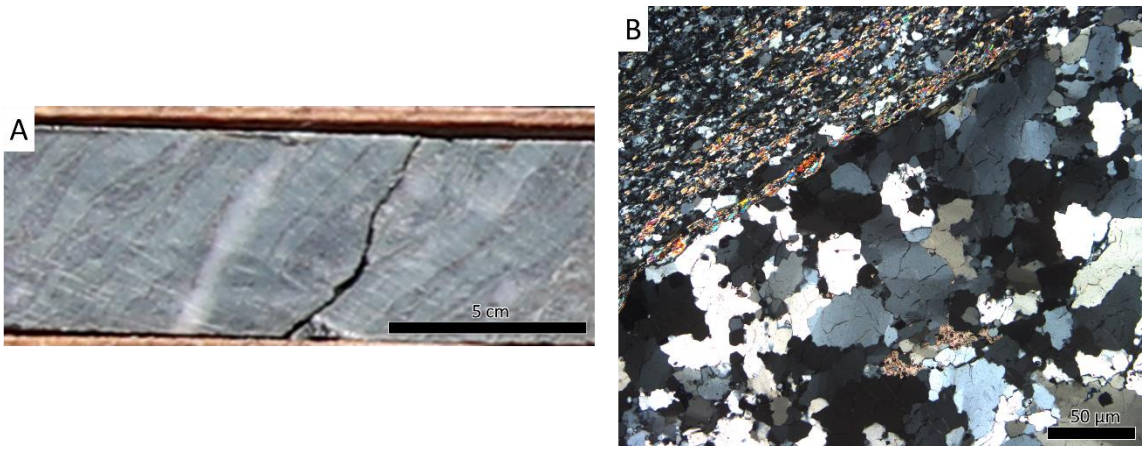

Figure 5.5: Quartz 2 vein in the drill core (a) and photomicrograph in cross polarized light (b) from ER-2021-WP-8z-53.

5.1.4 Type 2

Type 2 veins are weakly boudinaged veins infilled with orthoclase-carbonate-quartz (Fig. 5.6). The veins contain quartz, which can range from coarse-grained up to 50 micrometers with weak undulatory extinction, to fine-grained up to 20 micrometers with recrystallization textures. Orthoclase grains are subhedral ranging from 50 to 100 micrometers with weak to moderate sericite alteration, and inclusions of carbonate. The carbonate grains are anhedral up to 200 micrometers, commonly less than 100 micrometers, and can be found either as inclusions or along grain boundaries. The alteration halo is texturally destructive light to medium brown with patches of

darker brown, ranging from 3 to 10 mm. The lighter brown alteration areas are dominated by albite (An_{1-8}) and orthoclase with darker patches having higher abundance of prehnite-pumpellyite. Close to the vein within the alteration halo there are inclusions of clinochlore, apatite, carbonate and titanite grains. The clinochlore Fe# ranges from 66 to 73. The titanite grains are anhedral to subhedral up to 5 micrometers across distributed throughout the alteration halo, with some crystals found in contact with the clinochlore grains.

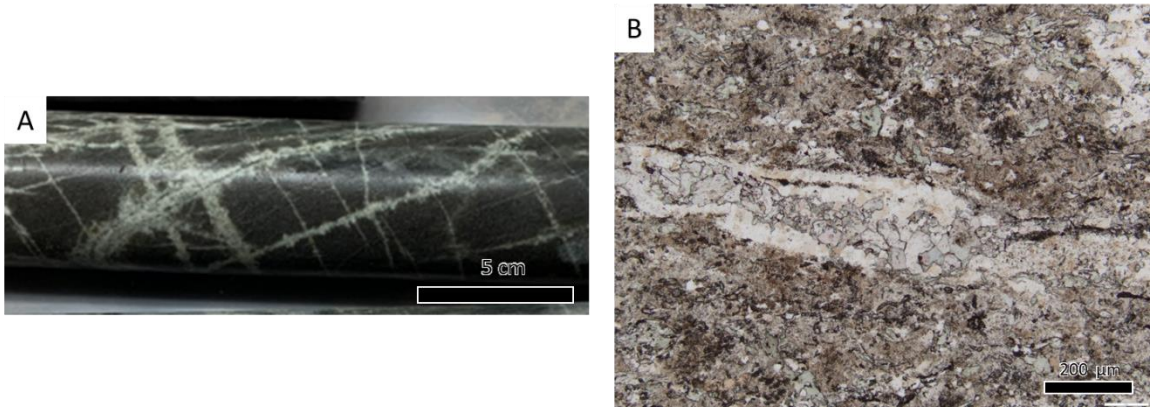

Figure 5.6: Type 2 vein in the core sample (a) and photomicrograph in plane polarized light (b) from ER-2021-WP-8Z-03B.

5.1.5 Q3

The quartz veins are associated with cross-cutting relationships with the chaotic units. The veins are of variable thickness ranging from 200 micrometers to over 1 cm in width (Fig. 5.7). The quartz grains are dominantly coarse up 500 micrometers across, with finer recrystallized grains up to 30 micrometers along the grain boundaries. The coarse quartz grains commonly exhibit undulating extinction with inclusions of surrounding host rock. The inclusions include muscovite, clinochlore, titanite, carbonate, pyrite, pyrrhotite, chalcopyrite. The finer grains are anhedral up to 20 micrometers across and commonly found along quartz grain boundaries or closer to the contact. Locally, along the contact there is an increased abundance of muscovite or clinochlore that is oriented parallel to sub-parallel to the contact. The clinochlore Fe# ranges from 65 to 70.

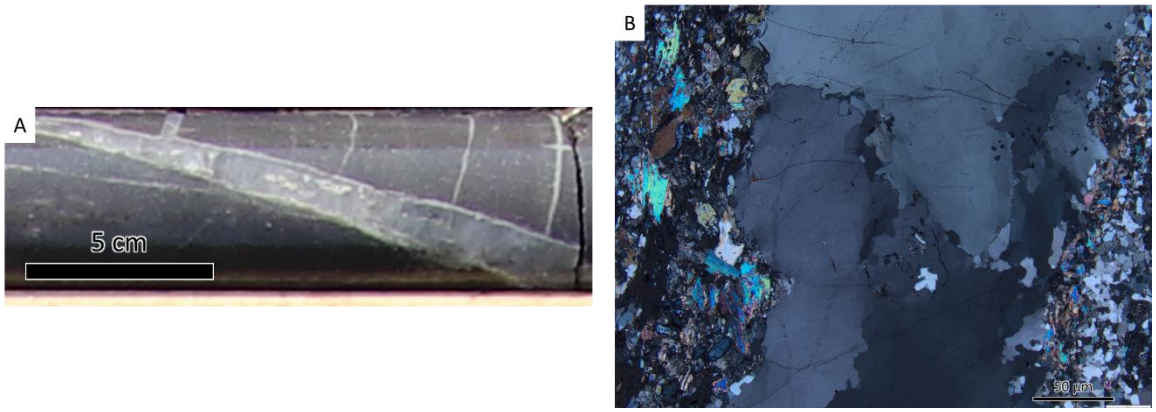

Figure 5.7: Quartz 3 vein in core sample cutting a younger quartz vein which is possibly Q2 (a) and photomicrograph in cross polarized light (b) from ER-2021-WP-8z-30.

5.1.6 Type 3-A

Type 3-A are found in both the 8 and Falcon zones, with the Falcon zone having the better exposure within the drillholes. The veins are boudinaged ranging from 20 to 60 micrometers in width, infilled with clinochlore, zeolite and muscovite with minor quartz, titanite, ilmenite, and sphalerite (Fig. 5.8)**.** The clinochlore grains are subhedral up to 25 micrometers, dominantly oriented sub-parallel to the vein, with inclusions of subhedral to anhedral titanite and sphalerite. The clinochlore is dominantly found along the edges of the vein. The zeolite grains are anhedral up to 20 micrometers across and are elongated sub parallel to the vein, and dominantly found within the core of the vein. The muscovite grains are subhedral up to 40 micrometers randomly oriented within the vein, containing inclusions of anhedral titanite. The quartz grains are anhedral up to 20 micrometers across with undulatory extinction and occur along the contact of the rock with the vein. The titanite grains are anhedral up to 20 micrometers but are commonly less than 10 micrometers. The sphalerite grains are anhedral up to 5 micrometers and are commonly found associated with clinochlore. The clinochlore Fe# ranges from 61 to 69. The alteration halo is highly variable ranging from 20 to 120 micrometers consisting of light to medium brown alteration with patches of darker brown. The lighter brown color is dominantly composed of albite (An_{0-5}) with minor orthoclase, and

darker patches are dominated by prehnite. The clinozoisite grains are anhedral up to 3 micrometers across and are distributed throughout the alteration halo.

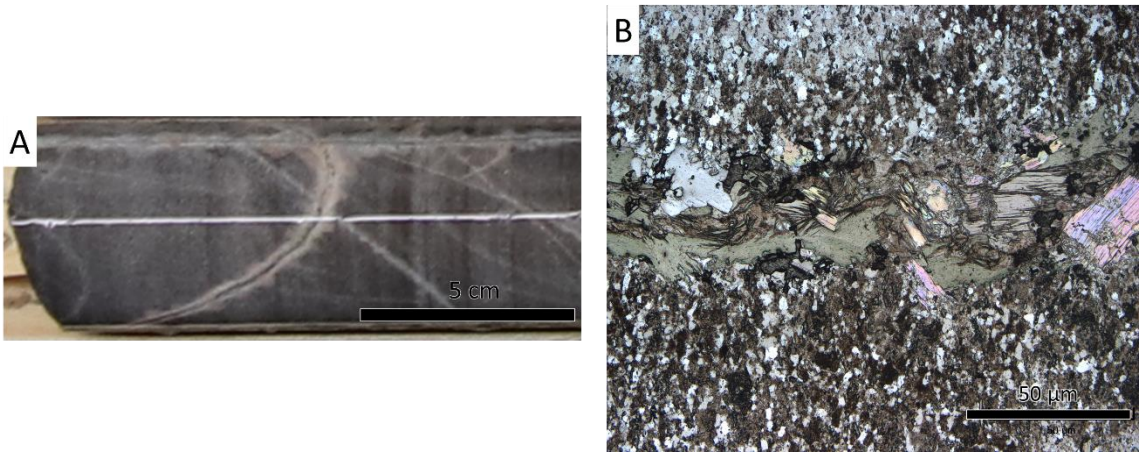

Figure 5.8: Type 3-A vein in core sample (a) and photomicrograph in plane polarized light (b) from ER-2021-WP-F-52.

5.1.7 Type 3-B

Type 3-B are found in all the zones, with the Falcon zone being the best locality for the vein type. The veins are weakly boudinaged ranging from 30 to 50 micrometers and infilled with zeolite and clinochlore with minor muscovite, clinozoisite, and titanite (Fig. 5.9). The zeolite grains are subhedral up to 10 micrometers across and are randomly oriented within the vein. The grains contain anhedral grains of titanite up to 4 micrometers wide. The clinochlore grains are anhedral up to 30 micrometers across and are dominantly found along the edges of the vein. The muscovite grains are anhedral up to 10 micrometers across and are dominantly found along the edges of the veins. The clinozoisite grains are anhedral up to 40 micrometers wide and are found along the contacts of the vein. The carbonate alteration is patchy along the contacts with inclusions of zeolite. The alteration halo is highly variable that can be up to 4 cm wide. The alteration halo is light brown with minor medium brown patches. The light brown alteration is dominated by albite (An_{0-10}), orthoclase and anorthoclase, with darker patches having a higher abundance of prehnite-

pumpellyite. Within the alteration halo there is a higher abundance of clinochlore elongated parallel to the fabric of the rock. Associated with the clinochlore grains are higher abundances of anhedral prehnite-pumpellyite. The clinochlore Fe# ranges from 63 to 71.

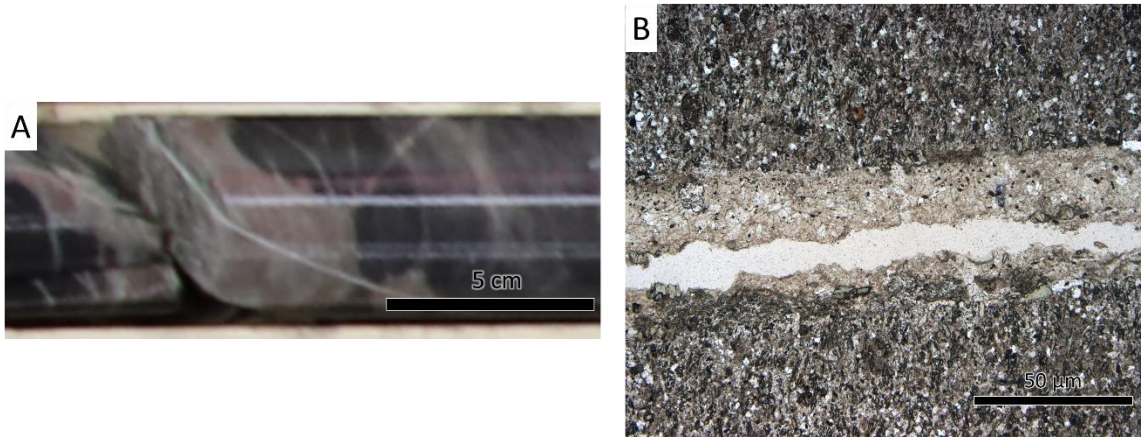

Figure 5.9: Type 3-B vein in core sample (a) and photomicrograph in plane polarized light (b) from ER-2021-WP-F-50.

5.1.8 Type 3-C

Type 3-C veins are boudinaged ranging from 5 to 20 micrometers in width and are infilled with plagioclase and alkali feldspar-carbonate-quartz (Fig. 5.10). The feldspars are anhedral, up to 10 micrometers across and are randomly oriented within the vein. The grains contain micro inclusions of titanite with weak hematite alteration. Anhedral carbonate grains are found throughout the vein with inclusions of titanite and feldspars. The abundance of carbonate tends to increase in thicker sections of the vein. Trace amounts of anhedral quartz grains up to 10 micrometers across are dominantly found along the contact with the host rock. Trace amounts of Fe-rich sphalerite are found along the edges of the vein. The sphalerite is anhedral up to 10 micrometers across. Trace amounts of subhedral inclusion-poor pyrite up to 5 micrometers across are found along the edges of the veins. The alteration is light brown in proximity to the vein and becomes medium brown distal to the vein. The light brown is dominated by albite (An_{2-6}) with alkali feldspars and prehnite-pumpellyite. The medium brown contains less orthoclase and an increase in the Ca content within

plagioclase (An_{4-24}). Darker brown patches are dominated by higher abundances of prehnite-pumpellyite.

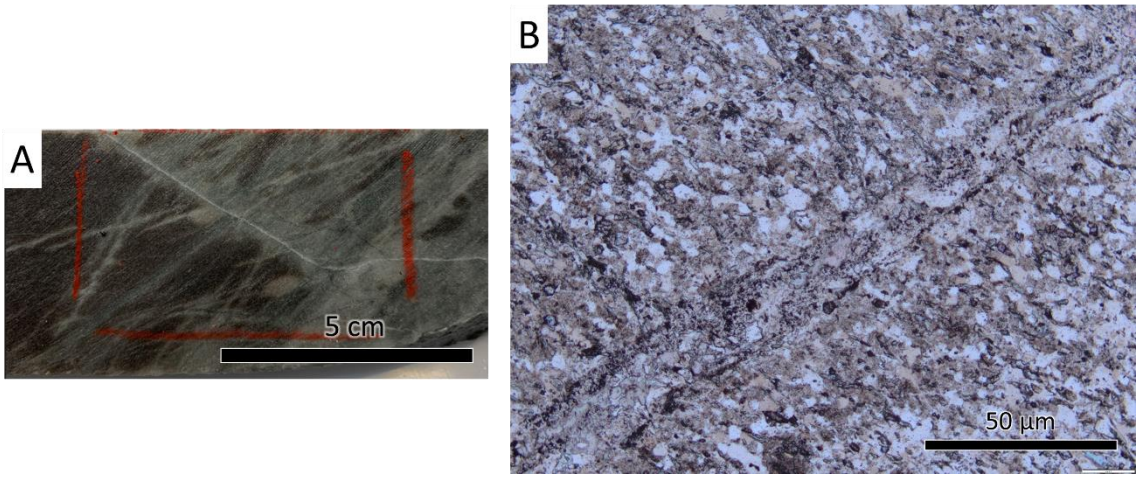

Figure 5.10: Type 3-C vein in core sample (a) and photomicrograph in plane polarized light (b) from ER-2021-WP-8z-17B.

5.1.9 Type 4

Type 4 veins are characterized as a network of tightly spaced veins with albite to andesine alteration (Fig. 5.11 A). The veins are boudinaged ranging from less than two micrometers up to 20 micrometers in width and can split into multiple offshoots (Fig. 5.11 B). The veins are infilled with very fine-grained albite, oligoclase, quartz, clinochlore, clinozoisite, ilmenite, titanite, and prehnite. The clinochlore Fe# ranges from 68 to 74. The quartz-clinozoisite grains are up to 10 micrometers across. Locally the infill is massive and isotropic in plane polarized light. The alteration halo is variable from 10 to 100 micrometers in width infilled with light to medium brown alteration. The lighter brown alteration is composed of albite (An_{4-9}) with minor orthoclase and anorthoclase, whereas the darker brown coloration is associated with an increase in abundance of prehnite-pumpellyite. In areas where the prehnite-pumpellyite is more abundant the Ca content in plagioclase increases to an_{20-50}.

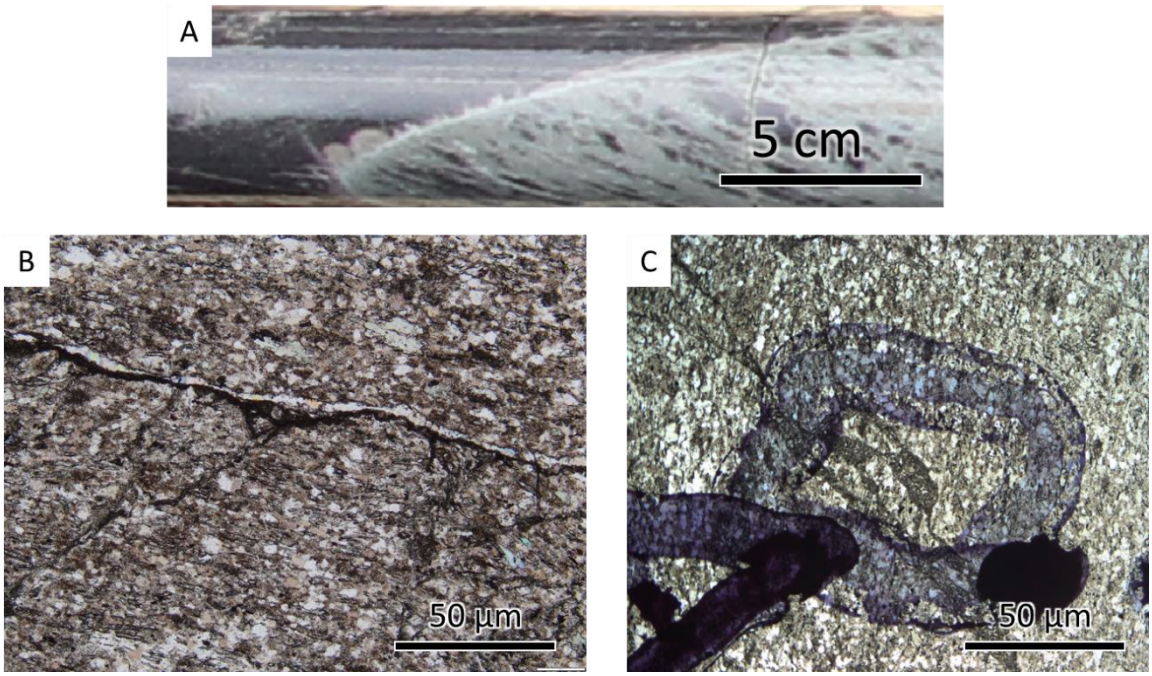

Figure 5.11: Type 4 vein in core sample (a) and photomicrograph in plane polarized light (b) from ER-2021-WP-8z-06. The vein can have quartz-clinozoisite infill along edges (b) or splitting into multiple offshoots (c).

5.1.10 Type 5

Type 5 veins are weakly boudinaged ranging from 10 to 20 micrometers across and are infilled with quartz, plagioclase, and prehnite with minor clinochlore, orthoclase, titanite, apatite, and xenocrystic zircon (Fig. 5.12). The quartz grains are anhedral up to 5 micrometers. The plagioclase grains are anhedral up to 5 micrometers across and are dominated by albite (An_{2-12}) with less commonly andesine (An_{40-61}). The orthoclase grains are anhedral up to 5 micrometers across. The vein infill has medium to dark brown alteration which is dominantly found along the edges of the vein, but also within the core of the vein. The medium to dark brown alteration is dominated by albite, prehnite and pumpellyite. Along the contact of the vein with the rock anhedral clinochlore up to 20 micrometers across is elongated parallel to the contact. The clinochlore Fe# ranges from 69 to 74. The alteration halo is highly variable ranging from 20 to over 200 micrometers wide. In proximity to the vein the alteration halo is lighter brown consisting of dominantly albite (An_{5-12}) with minor

darker patches of prehnite with minor pumpellyite. Distal to the vein the alteration halo changes and becomes richer in orthoclase and prehnite with minor pumpellyite.

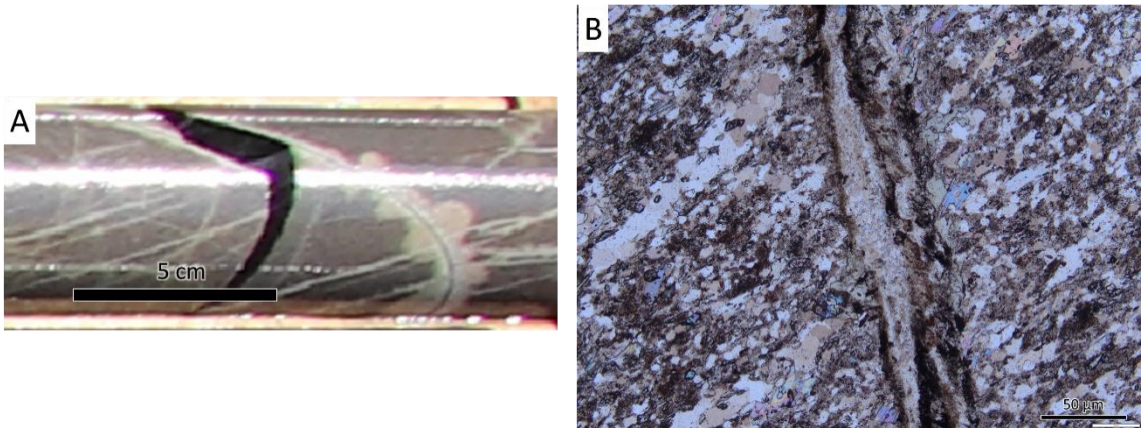

Figure 5.12: Type 5 vein cutting Type 1 vein in core sample (a) and photomicrograph in plane polarized light (b) from ER-2021-WP-8z-19.

5.1.11 Type 6

Type 6 veins are thicker boudinaged veins ranging from 0.5-3 cm in width with sharp boundaries that are either straight or undulating (Fig. 5.13). The veins are infilled with clinochlore and variable amounts of quartz. The quartz grains are concentrated along the contacts with the rock and are up to 2 mm wide with undulatory extinction and inclusions of muscovite (Fig. 5.14). The clinochlore grains range from 200 to 400 micrometers, and contain inclusions of sphalerite, titanite, and xenocrystic zircon. The titanite grains are anhedral up to 100 micrometers across, and dominantly found along the contact with the rock. The sphalerite grains are subhedral up to 100 micrometers wide and are zoned with the outer zone being composed of fine-grained sphalerite (Fig. 5.15). Along the contact with the rock there are discontinuous sections of subhedral muscovite up to 400 micrometers across oriented sub-parallel to the contact. On the macro scale the vein alteration halo is white to off white and up 8 cm wide with darker green to black patches (Fig. 5.16). The alteration halo is composed of quartz and plagioclase (An_{19-33}) with medium to dark brown patches of

alteration. The coarser quartz is up to 200 micrometers across and exhibits a weak undulatory extinction. The finer grains of quartz range from 30 to 50 micrometers across and make up the bulk of the alteration along with plagioclase that exhibits weak to moderate sericite alteration. The green patches consist of coarse anhedral clinochlore grains up to 600 micrometers across with inclusions of titanite, muscovite and pumpellyite. The clinochlore Fe# ranges from 64 to 73. The darker patches are dominated by prehnite-pumpellyite, and the Ca content in plagioclase increases to An_{53-68}. The patches are associated with higher abundances of anhedral sulphides up to 30 micrometers across, commonly less than 10, ranging from pyrite to chalcopyrite. When the alteration halo interacts with pre-existing type 1 veins, the veins are further altered to muscovite with minor pumpellyite, titanite and apatite changing the coloration of the vein to a whiter color (Fig. 5.16). Carbonate alteration can be found either along the vein contact with the rock, sometimes altering the carbonate to ankerite, or as anhedral patches found within the alteration halo.

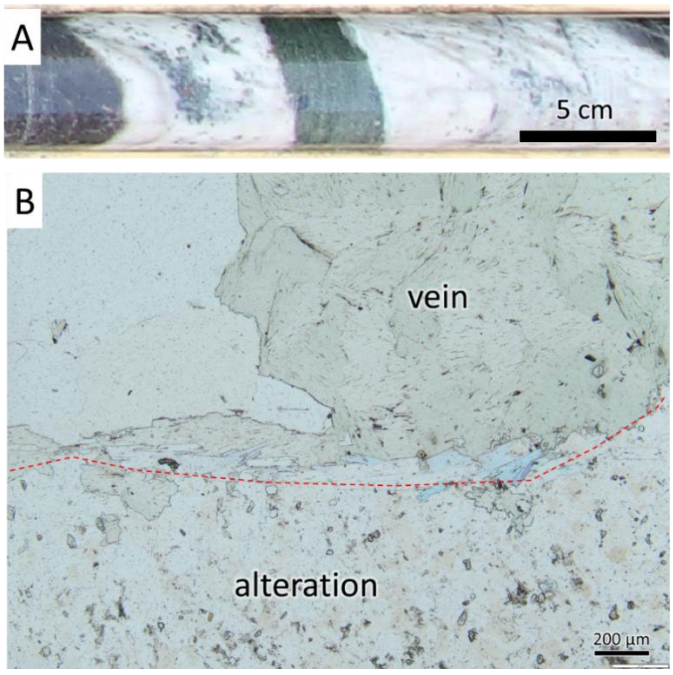

Figure 5.13: Type 6 vein in core sample (a) and photomicrograph in plane polarized light (b) from ER-2021-WP-8z-07. The photomicrograph image shows the contact between the vein infill and the host rock alteration. The dashed red line outlines the contact.

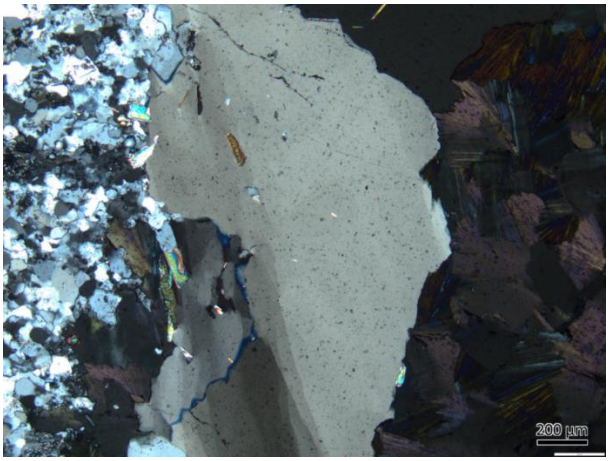

Figure 5.14: Photomicrograph in cross polarized light showing the undulatory extinction in quartz within a type 6 vein from ER-2021-WP-8z-07.

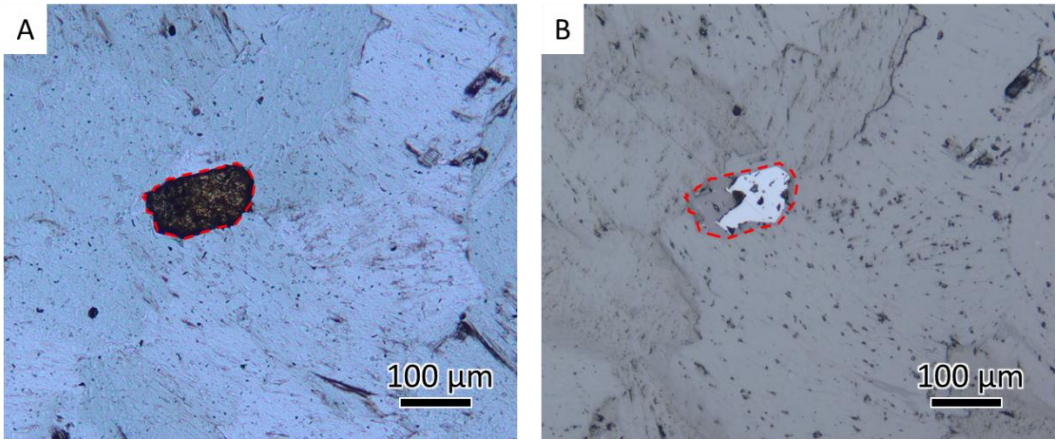

Figure 5.15: Photomicrograph in cross polarized light (a) and reflected light (b) showing the alteration halo of sphalerite within the type 6 vein from ER-2021-WP-8z-07. The dashed red line outline the grain boundary.

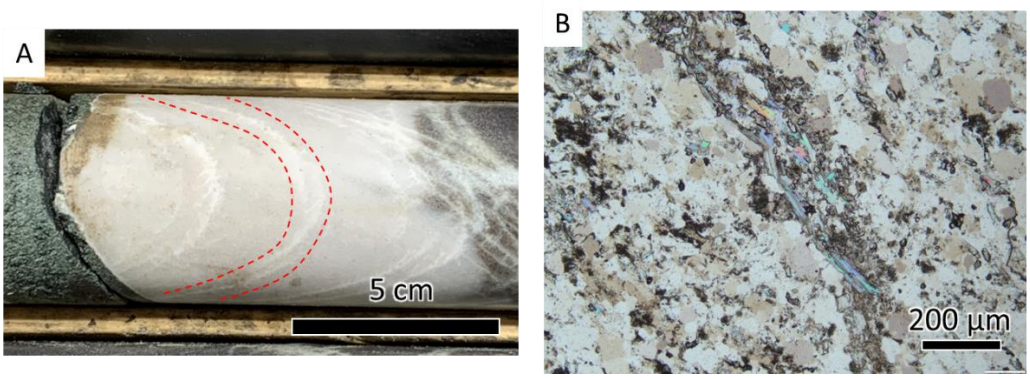

Figure 5.16: Interaction between type 1 vein and the alteration halo of type 6 vein on a macroscale. Type 1 vein is outlined by the dashed red line (a) and a Photomicrograph in cross polarized light showing the white type 1 veins (b) from ER-2021-WP-8z-07.

5.1.12 Type 7

Type 7 veins are boudinaged ranging from 20 to 50 micrometers across, infilled dominantly with clinozoisite with alkali feldspar and minor carbonate alteration, which can split into thinner offshoots (Fig. 5.17). The clinozoisite has a bimodal distribution with finer grained crystals less than 5 micrometers across, and coarser grains up to 20 micrometers. The coarser grains tend to be along the core of the vein but can also be found along the contacts. The alkali feldspar grains are anhedral up to 100 micrometers across and tend to be found along the edge of the vein elongated parallel to the contact. The carbonate grains are anhedral up to 20 micrometers across and are dominantly found along the edges of the vein. The titanites are anhedral up to 5 micrometers across and are found along the edges of the vein elongated parallel to the margin. The clinochlore are discontinuous along the contacts of the vein as anhedral grains up to 20 micrometers across, but within the alteration halo the grains tend to coarser up to 40 micrometers. The clinochlore Fe# ranges from 67 to 73. The alteration halo is variable up to 350 micrometers wide and is light to medium brown with minor patches of darker brown. The lighter brown color is dominated by albite (An_{2-16}) with darker patches dominated by prehnite-pumpellyite. In more intense zones of prehnite-pumpellyite the Ca content in plagioclase increases to an_{31-53}.

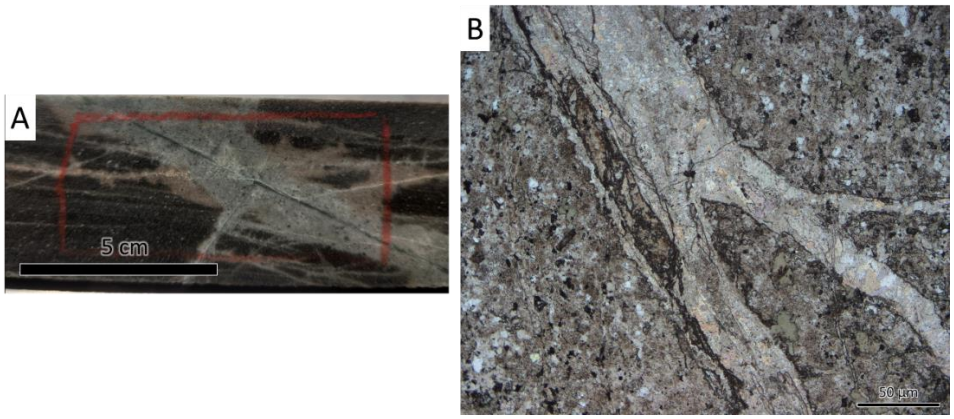

Figure 5.17: Type 7 vein in core sample (a) and photomicrograph in plane polarized light (b) from ER-2021-WP-8z-61.

5.1.13 Type 8

Type 8 veins are weakly boudinaged ranging from 10 to 40 micrometers wide infilled with clinochlore-muscovite and minor quartz-clinozoisite-titanite (Fig. 5.18). The clinochlore grains are up to 30 micrometers wide elongated sub parallel to the vein and are found dominantly along the rims of the vein. The clinochlore Fe# ranges from 66 to 68. Anhedral to subhedral inclusions of clinozoisite and titanite are found within the clinochlore grains. Anhedral muscovite tends to be found within the core of the vein, up to 30 micrometers across, oriented parallel to the orientation of the vein. Anhedral inclusions of clinozoisite are found within the muscovite grains. Trace amounts of anhedral quartz up to 5 micrometers across are found along the contact of the vein. The alteration halo is variable ranging from 10 to 20 micrometers across and is generally medium brown with dark brown patches. The alteration halo is dominated by variable amounts of prehnite-pumpellyite with plagioclase (An_{3-14} and An_{40-52}). Minor anhedral clinozoisite and ilmenite are found within the alteration halo.

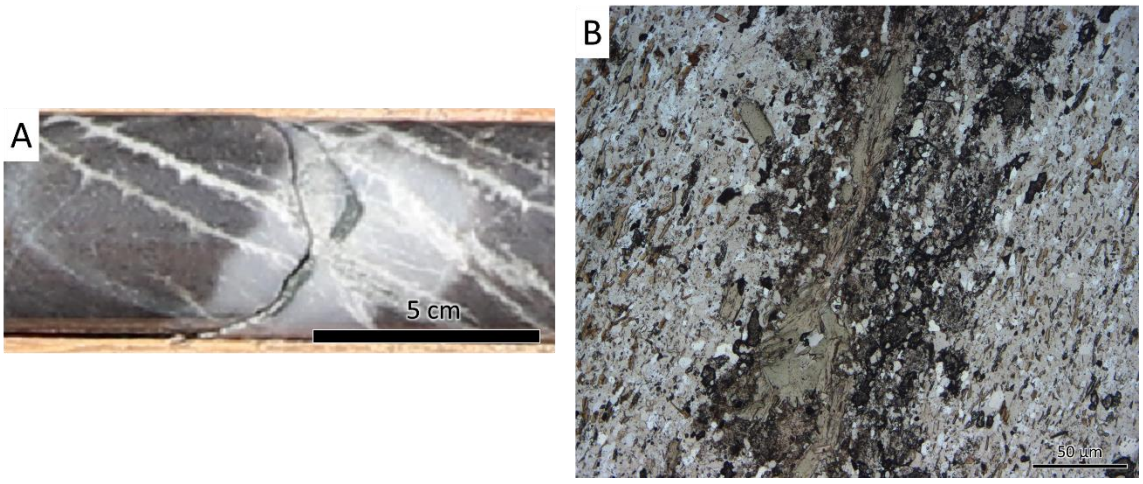

Figure 5.18: Type 8 vein cutting type 6 vein in core sample (a) and photomicrograph in plane polarized light (b) from ER-2021-WP-8z-63.

5.1.14 Q4

The vein is composed of coarse-grained quartz with recrystallization texture (Fig. 5.19). The coarse-grained quartz grains are up to 200 micrometers wide that exhibit undulatory extinction and contain micro inclusions. The finer quartz grains are up to 30 micrometers wide and are either associated with quartz grain boundaries or along late-stage fractures. The quartz grain boundaries contain anhedral clinochlore grains up to 40 micrometers wide. Fractures are associated with prehnite and pumpellyite with minor amounts of sphalerite containing zonation of titanite. The veins locally contain medium brown albite alteration halos up to 60 micrometers wide. The vein contact contains coarse-grained clinochlore and clinozoisite oriented to the contact.

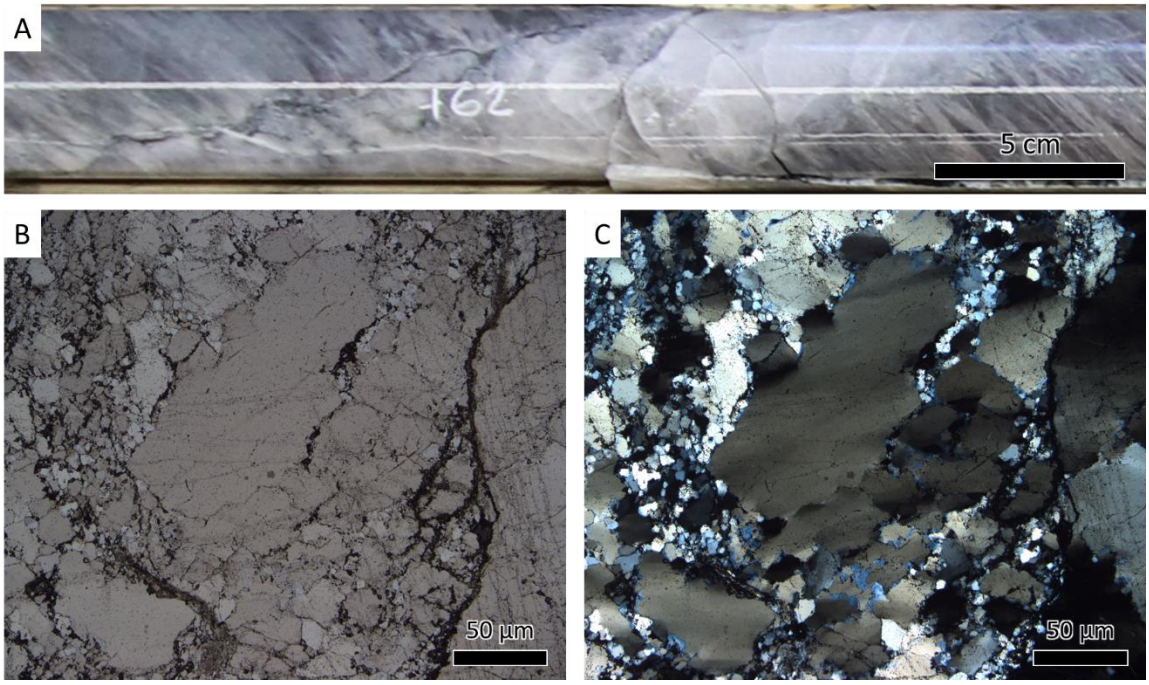

Figure 5.19: Quartz 4 vein in core sample (a) and photomicrograph in plane polarized light (b) and cross polarized light (c) from ER-2022-WP-F-54.

5.1.15 Q5

The quartz veins resemble the Q2 vein types in terms of characteristics, appearance, and orientation. The veins are separated based on timing relationships with occurrences of the quartz veins cutting the Laminated unit that overprints the chaotic unit.

5.2 8 zone

The 8 zone represents the most complete record of the vein types as it is the only zone with all the vein types and as such has been used to best constrain the paragenesis. The chaotic unit is dominantly hosted within a fine-grained felsic volcanic rock, and less commonly within the feldspar porphyry unit (Fig. 5.20).

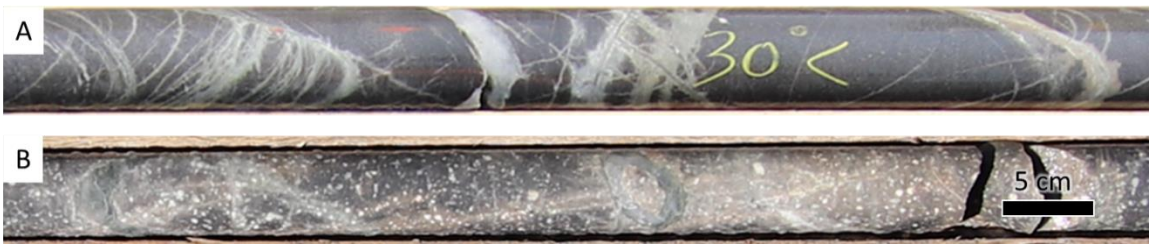

Figure 5.20: Chaotic unit hosted within a typical volcanic rock (a) and less commonly within the feldspar porphyry unit (425-1 @ 165m) (b).

Type 1 veins are dominantly straight with weak undulation, and variable alteration halos. These veins have the highest abundance of cross cutting relationships and are always cut by later veins (Fig. 5.21 A, B, C, D, E, and F), and they are overprinted by the Laminated unit (Fig. 5.21 Q). Type 2 veins are straight and weakly undulating. These veins are commonly cut by the rest of the veins (Fig. 5.21 A). Type 3 veins are straight and can either be found as isolated veins or as groups of veins. When occurring in groups type 3 veins usually have thicker alteration halos. These veins consistently cut vein types 1 and 2 but are only cut by type 6 veins (Fig. 5.21 B). Type 4 veins form a tightly spaced network of veins that cut type 1 and 2 veins, but relationships with younger veins are not

visible within the 8 zone. Type 4 cross-cutting relationship with type 3 veins is found in the Falcon zone. Younger cross-cutting relationships are noted within the Falcon zone. Type 5 veins are dominantly straight with only cross cutting relationship noted with types 1, 2, and 4 veins and cutting the Laminated unit (Fig. 5.21 C, D, and R). Type 6 veins are dominantly straight to weakly undulating with well-developed alteration halos (Fig. 5.21 E), but less commonly can also be found

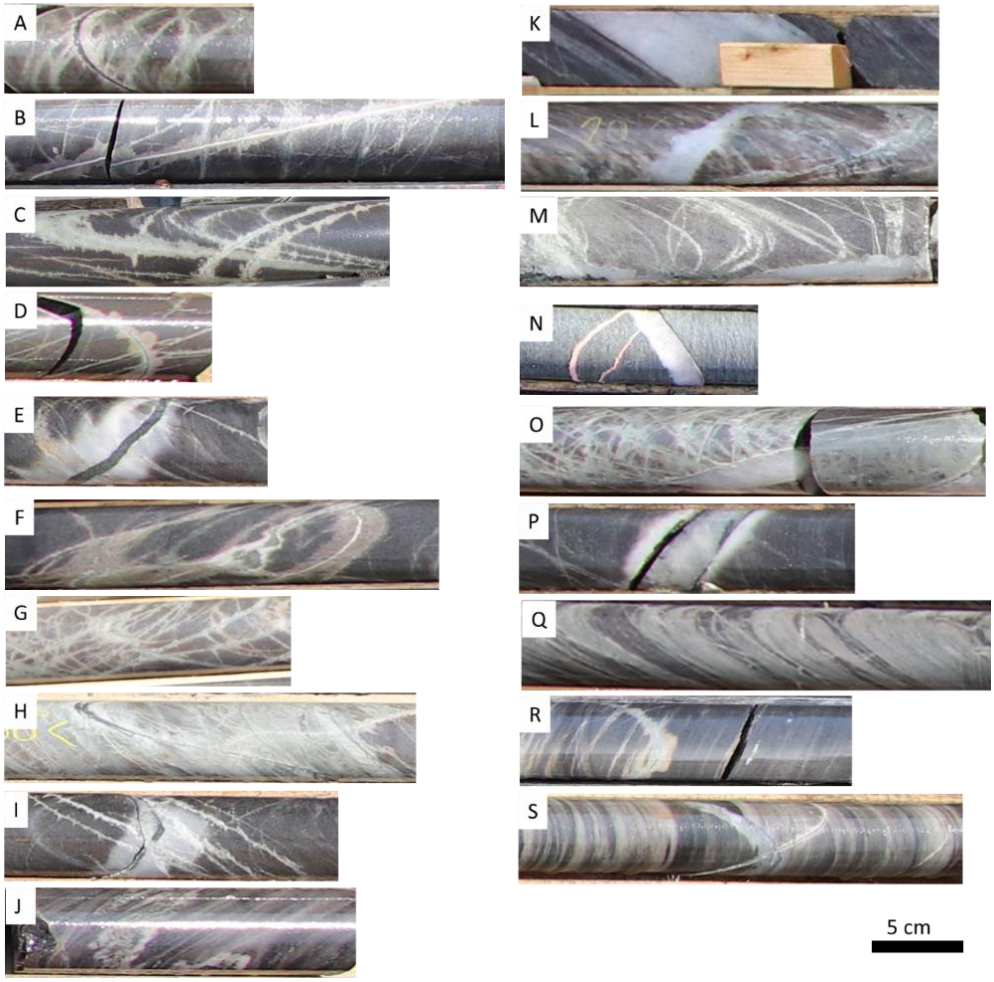

Figure 5.21: Cross-cutting relationships found within the 8 zone. (a) type 2 cuts 1 (700-e-03 @ 5m); (b) type 3-B cuts 1 and 2 (2009-248 @ 373m); (c) type 5 cuts 2 and 4 (700-E-11A @ 117m); (d) type 5 cuts 1 (700-E-01 @ 9m); (e) type 6 cuts 1 and 2 (700-E-15 @ 21m); (f) type 6 cuts 1 and 3-B (700-E-23 @ 9m); (g) type 7 cuts 1 and K alteration (700-E-11A @ 71m); (h) type 7 cuts 4 (700-E-01 @ 15m); (i) type 8 cuts 6 (700-E-15 @ 21m); (j) Q1 veining (700-E-01 @ 23m); (k) Q2/Q5 veins parallel to the fabric (700-E-02 @ 6m); (l) Q4 vein cuts fabric (700-E-06 @ 119m); (m) Q3 vein cuts type 1 and 2 (700-E-01 @ 61m); (n) Q3 vein cuts type 3-B (220-E-01 @ 231m); (o) Q3 vein cuts type 4 (700-E-07 @ 39m); (p) Q3 vein cuts type 6 (700-E-13 @ 31m); (q) Laminated unit cuts type 1 (700-E-02 @ 85m); (r) type 5 cuts the Laminated unit; and (s) type 7 cuts the Laminated unit and quartz vein.

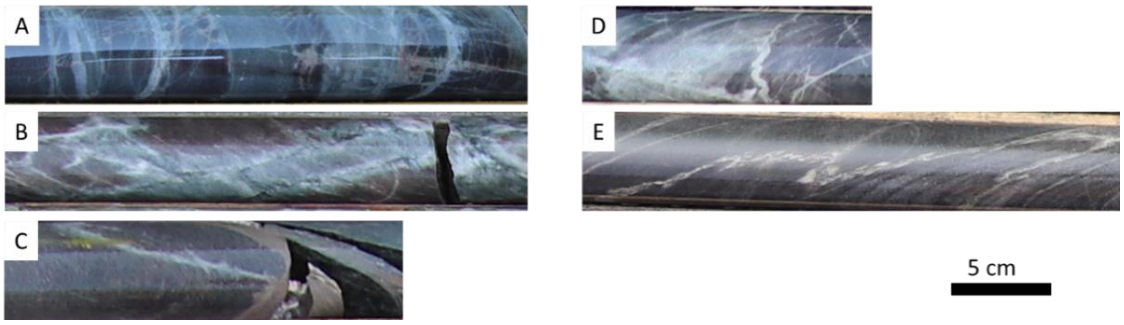

Figure 5.22: Rare vein types found within the 8 zone. (a) pervasive chlorite/amphibole infill with no alteration halo (2009-249 @ 369m); (b) undulating and deformed chlorite/clinozoisite infill with rim of amphibole and albite alteration (700-E-06 @ 115m); (c) hematite infill with no alteration halo (700-E-03 @ 34m); (d) and (e) pre-fabric veining (700-E-06 @ 22m).

as deformed boudinage veins (Fig. 5.21 F). These veins cut type 1, 2, 3-B, and 4 veins. Type 7 veins are rare and straight with small alteration halos. These veins cut type 1, 4, Q2 veins and the Laminated unit (Fig. 5.21 G, H, and S). Type 8 veins are rare and cross-cutting relationships were only observed cutting type 6 veins (Fig. 5.21 I). Cross-cutting relationship between types 6 and 7 veins were not observed. All five types of quartz veins are found within the 8 zone, where they range from clear to milky with minimal inclusions that have generally sharp contacts. The Q1 veins have discontinuous sections of deformed veinlets (Fig. 5.21 J). The Q2 and Q5 veins are parallel to the fabric, and Q4 veins cut the fabric (Fig. 5.21 K and L). The Q3 veins cut types 1, 2, 3-B, 4, and 6 veins (Fig. 5.21 M, N, O, and P).

Based on the cross-cutting relationships a paragenesis of the veins is shown in Figure 5.23. The cross-cutting relationship are limited, but the sequence of younging is dominantly unidirectional. The exception is Q3 vein type which cuts type 1, 2, 3-B, 4 and 6 veins, and Q4 which has minimal cross-cutting relationships.

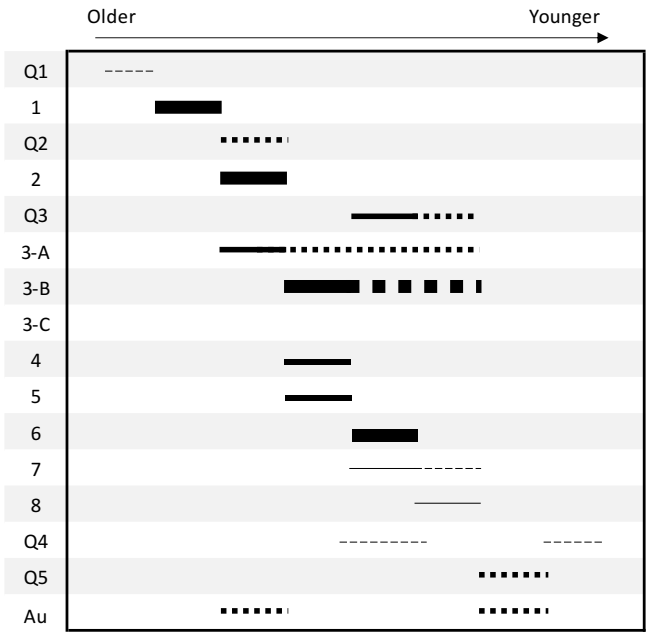

Figure 5.23: Paragenesis of veining within the chaotic unit in the 8 zone. The thicker the line the more abundant the vein type. Solid lines indicate higher confidence of cross-cutting relationships, and dashed line indicate non-constrained cross-cutting relationships.

5.3 Falcon zone

The Falcon zone is similar to the 8 zone in terms of the vein types and host lithology which can also be hosted within the feldspar porphyry unit (Fig. 5.24 A). The veins within the feldspar porphyry unit can either cut the host rocks (Fig. 5.24 A and B) or be cut off along the contact (Fig. 5.24 C). Within the chaotic unit the alteration halo is variable depending on whether or not it interacts with the chaotic unit or the volcanic rocks. Within the chaotic unit the alteration halo is more distinguishable and is more intense, whereas if the same vein is hosted within the volcanic rock the alteration halo is generally less pronounced (Fig. 5.24 A and B). This relationship was also noted in the Newt Lake and the Peek-a-Boo areas.

Figure 5.24: Different characteristics of chaotic unit within Falcon Zone. (a) associated with intrusions of feldspar porphyry. Note the vein changes characteristics between volcanic rock and feldspar porphyry (ERM-2022-81 @ 554m); (b) change in appearance of veins between volcanic and feldspar porphyry (ERM-2020-96 @ 541.4m); and (c) chaotic veins that do not cross the contact between volcanic rock (ERS-2022-031 @ 471m).

The Falcon zone has similar vein types to the 8 zone with the addition of type 3-C vein but lacks type 8 veins. Type 1 and 2 veins look very similar to the 8 zone with no noticeable differences (Fig. 5.25 A). Also, the Laminated unit cuts type 1 veins (Fig. 5.25 N). Type 3 veins look like the 8 zone but are more common. These veins can appear as a group or less commonly as isolated veins. The alteration halos tend to be broader compared to the 8 zone, especially when in more tightly spaced groups. Locally hematite staining is noted overprinting the veins, which are commonly associated with a nearby hematite bearing faulting. Type 3 veins were only observed cutting type 1 and 2 veins and the Laminated unit (Fig. 5.25 B, C, D, and O). Type 4 veins are similar to those in the 8 zone but are more abundant than in the 8 zone. These veins cut type 1, 2, and 4 veins (Fig. 5.25 E). Type 5 veins look like those in the 8 zone with similar abundance, and they cut type 1 and 2 veins**.** Type 6 vein types tend to be irregular and less commonly straight relative to the 8 zone with thinner vein infill and noted cutting type 1 and 2 (Fig. 5.25 F). The quartz infill of the veins was not seen in this zone. Type 7 veins are rare and cut type 6 veins and the Laminated unit (Fig. 5.25 G and P). Like the quartz veining within the 8 zone, the four types of quartz veining are also found within the Falcon zone. The veins are variable ranging from milky to clear to smoky quartz with minimal inclusions and generally have sharp contacts, locally the veins have ankerite alteration along the contacts with the rock. The contacts tend to have an increasing abundance of muscovite and clinochlore sub-parallel to the contacts. The Q1 veins look similar to the ones found in the 8 zone (Fig. 5.25 H). The Q2 and Q5

veins are parallel to the fabric, and the Q3 veins are cutting the fabric (Fig. 5.25 I and J). The Q3 veins cut types 1, 2, and 3-B veins, and are cut by type 3-C veins (Fig. 5.25 K, L and M).

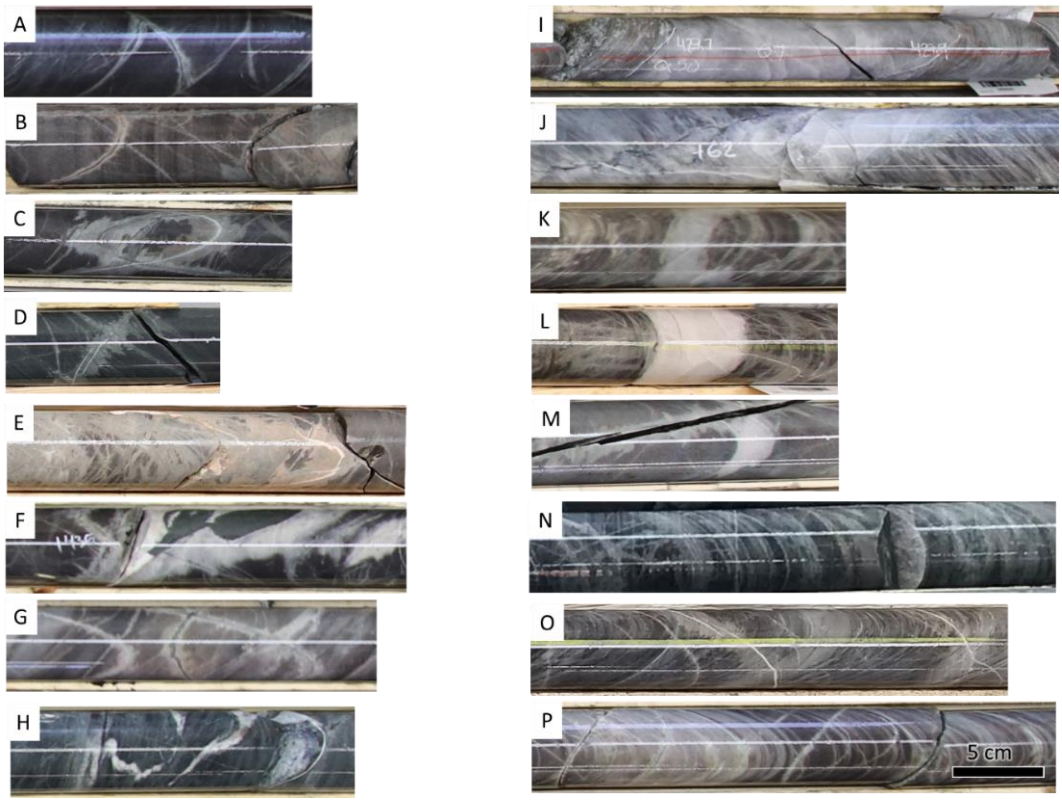

Figure 5.25: Cross-cutting relationships found within the Falcon Zone. (a) type 2 cuts 1 (E|RM-2020-79 @ 413m); (b) type 3-A cuts 1 (ERM-2020-77 @ 135m); (c) type 3-B cuts 2 (ERM-2020-77 @ 117m); (d) type 3-C cuts 2 (ERM-2020-92 @ 486m); (e) type 4 cuts 3-B (ERS-2022-032 @ 155m); (f) type 5 cuts 1 and 2 (ERM-2020-79 @ 436m); (g) type 7 cuts 6 (ERM-2020-84 @ 519m); (h) Q1 vein (ERM-2020-79 @ 402m); (i) Q2/Q5 veins parallel to the fabric (ERM-2020-79 @ 430m); (j) Q4 vein cuts fabric (ERM-2020-78 @ 62m); (k) Q3 vein cuts types 1 and 2 (ERM-2020-96 @ 476m); (l) Q3 vein cuts type 3-B (ERS-2022-055 @ 332m); (m) Q3 vein cut by type 3-C (ERM-2020-78 @ 203m); (n) Laminated unit cuts type 1 (ERM-2019-07 @ 570m); (o) type 3-B cuts the Laminated unit (ERM-2019-59 @ 317.5m); and (p) type 7 cuts the Laminated unit (ERM-2020-85 @ 520.5m).

Like the 8 zone, the Falcon zone also has rare veins (Fig. 5.26) which have a very limited to localized occurrence within the Falcon zone. These veins include clinochlore infilled with strong albitization, quartz with tourmaline and albite alteration, amphibole infill with epidote-albite alteration, strong pervasive albitization, irregular network of clinochlore albite veining with patchy potassic alteration.

Based on the cross-cutting relationships a paragenesis of the veins is shown in Figure 5.27. The cross-cutting relationship are limited, but as with the 8 zone the sequence of younging is dominantly

unidirectional. The exceptions are Q3 which cut types 1, 2, and 3-B veins, but is cut by 3-C veins so they are interpreted to form coeval to type 3 veins. Also, Q2 veins are only noted cutting fabric and no cross-cutting relationships with the veins are noted.

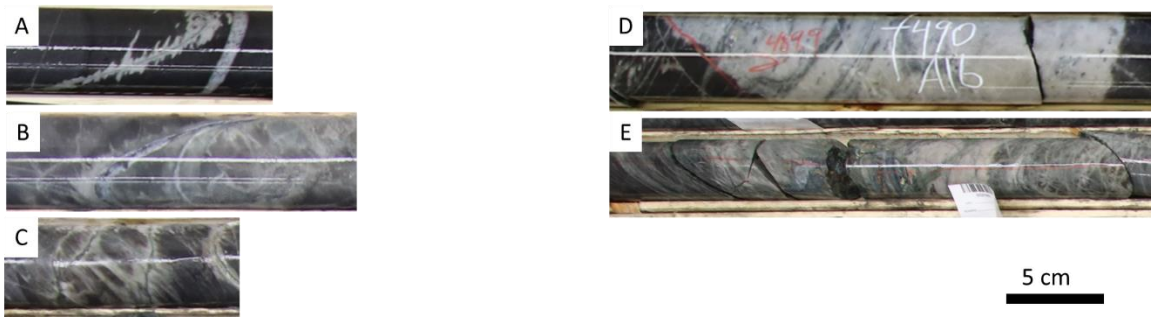

Figure 5.26: Rare vein types found within Falcon Zone. (a) chlorite infilled with strong albitization (EM-2020-79 @ 469m); (b) quartz with tourmaline and albite alteration (ERM-2020-83 @ 461m); (c) amphibole infill with epidote-albite alteration (ERM-2020-95 @ 435m); (d) strong pervasive albitization (ERM-2020-90 @ 490m); (e) irregular network of chlorite albite veining with patchy potassic alteration (ERM-2020-77 @ 162m).

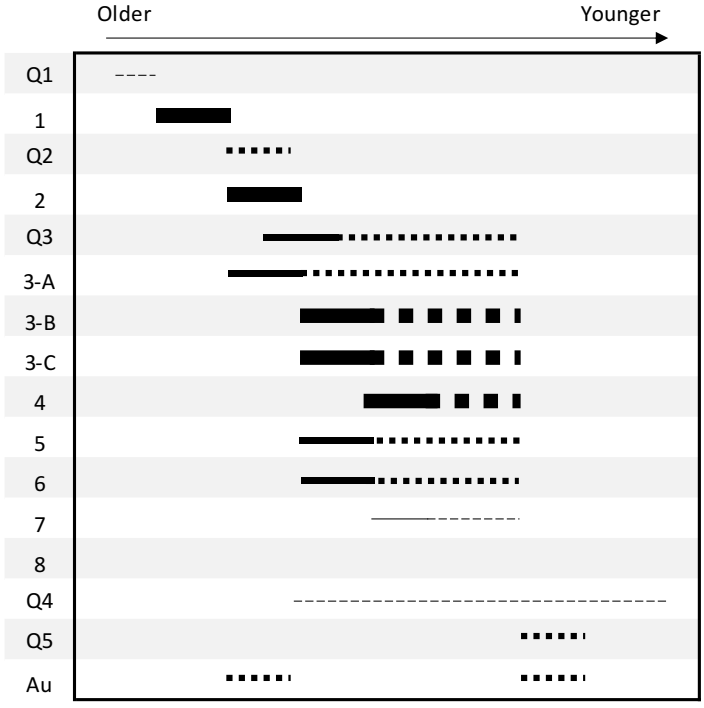

Figure 5.27: Paragenesis of veining within the chaotic unit in the Falcon zone. The thicker the line the more abundant the vein type. Solid lines indicate higher confidence of cross-cutting relationships, and dashed line indicate non-constrained cross-cutting relationships.

5.4 Newt Lake zone

The abundance of the chaotic unit with the Newt Lake zone is lower relative to the 8 and Falcon zones. The unit is mostly concentrated on the east side of the zone, or in proximity to the Laminated unit. Like the 8 and Falcon zones, the chaotic unit is hosted within the volcanic rocks and the feldspar porphyry unit (Fig. 5.28 A). As with the other zones, the alteration halo within the chaotic unit varies depending on if it is hosted in the volcanic rock or feldspar porphyry, with the alteration more pronounced in the feldspar porphyry (Fig. 5.28 B).

Figure 5.28: Chaotic unit hosted within feldspar porphyry unit (ERX-2021-56 @ 251m; a); and alteration variability as it progresses from the feldspar porphyry unit into the volcanic rock (ERX-2021-71 @ 139m; b).

Type 1 and 2 veins are very similar to the 8 zone and the Falcon zone and are the most abundant type throughout the zone. They are consistently cut by younger veins. Type 2 veins cut type 1 veins and the Laminated unit (Fig. 5.29 A and L). Type 3 veins are similar to the 8 zone and are thinner than those in the Falcon zone, they cut types 1 and 2 and the Laminated unit (Fig. 5.29 B, C, L, and N). Type 4 veins are rare in the Newt Lake zone and are dominantly associated with the feldspar porphyry unit. They are less frequent relative to the Falcon zone and tend to have thinner alteration halos. Type 5 veins are like the Falcon and 8 zones, with no additional cross-cutting relationships noted. Type 6 veins look like the Falcon zone but are more erratic and tend to be thinner than in the Falcon zone. They crosscut type 1 veins (Fig. 5.29 D). Like the 8 zone, type 6 veins are infilled with quartz veining. Type 7 veins are rare but resemble those in the Falcon and 8 zones. They crosscut type 3-B veins and the Laminated unit (Fig. 5.29 E, F, and O). Like the other zones all five types of

quartz veining are found within the Newt Lake zone. The veins tend to be clear to milky with less common smoky quartz infill. The contact with the rock tends to be straight and sharp. The Q1 veins look similar to those found in the Falcon and 8 zones (Fig. 5.29 G). The Q2, Q4 and Q5 veins have a higher association with pyrite that can be either parallel or cutting the fabric (Fig. 5.29 H and I). The Q3 veins cut type 1 and 6 veins (Fig. 5.29 J and K).

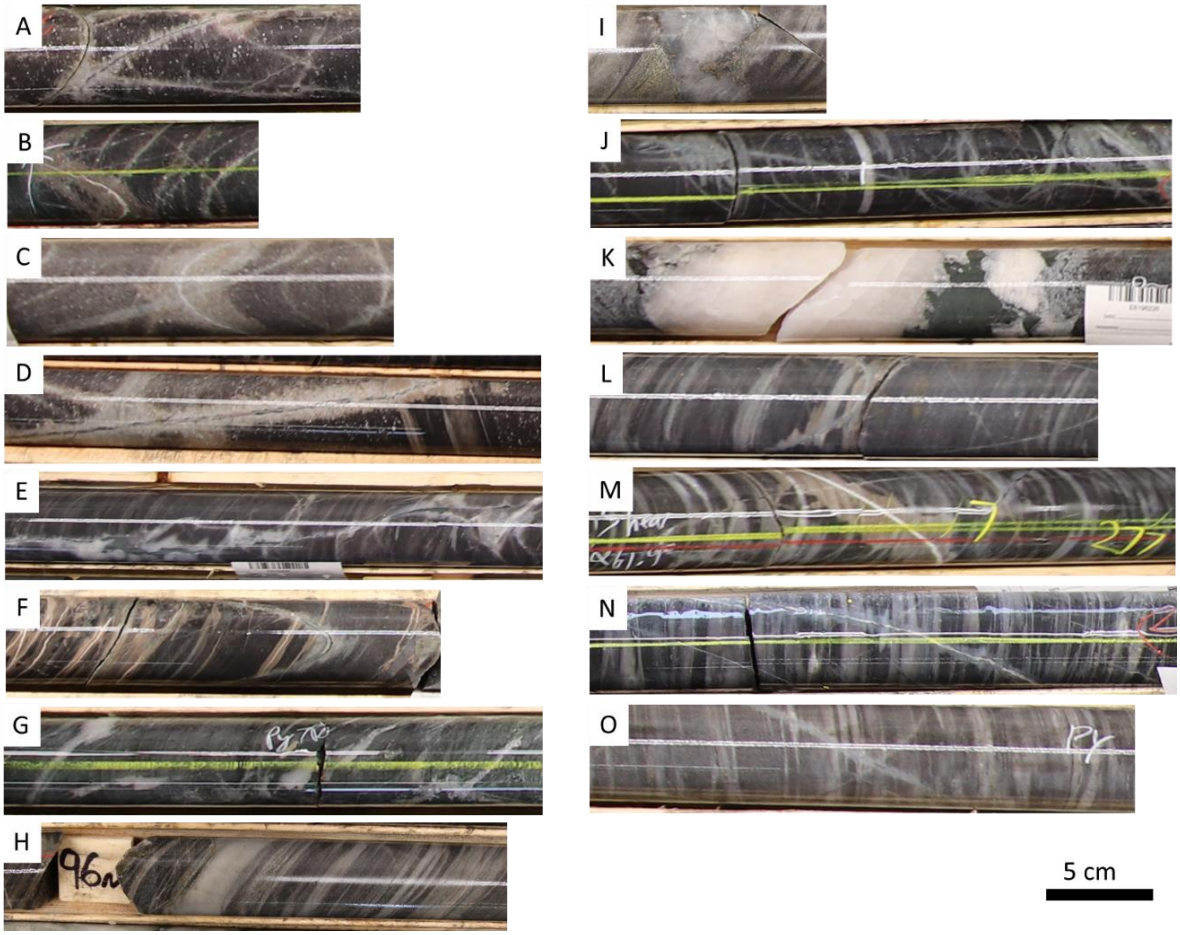

Figure 5.29: Cross-cutting relationships found within the Newt Zone. (a) type 2 cuts 1 (ERX-2021-71 @ 139.5m); (b) type 3-B cuts 1 (ERX-2021-56 @ 245m); (c) type 3-B cuts 2 (ERX-2021-70 @ 177m); (d) type 6 cuts 1 (ERX-2021-70 @ 214m); (e) type 7 cuts 1 (ERX-2021-59 @ 104m); (f) type 7 cuts 3-B and Laminated unit (ERX-2021-70 @ 111m); (g) Q1 vein (ERS-2022-014 @ 160m); (h) Q2/Q5 veins parallel to the fabric (ERX-2021-57 @ 96m); (i) Q4 vein cuts the fabric with a pyrite halo (ERX-2021-57 @ 90m); (j) Q3 vein cuts type 1 vein (ERX-2021-056 @ 120m); (k) Q3 vein infills type 6 vein (ERX-2021-68 @ 296m); (l) type 2 cuts the Laminated unit (ERX-2021-59 @ 100.5m); (m) type 3-B cuts the Laminated unit (ERX-2021-57 @ 120m); (n) type 3-C cuts the Laminated unit (ERX-2021-56 @ 127.5m); and (o) type 7 cuts the Laminated unit (ERX-2021-59 @ 110.5m).

Like the rest of the zones, the Newt Lake zone also has several rare veins (Fig. 5.30). These include light grey infill, and albite-epidote infilled veins with no alteration halos.

Based on the cross-cutting relationships a paragenesis of the veins is developed in Figure 5.31. The cross-cutting relationship are limited, but the sequence of younging is dominantly unidirectional up to type 3 veins. Type 4 veins and younger (except type 7) have limited cross-cutting relationships and are only noted cutting type 1 veins.

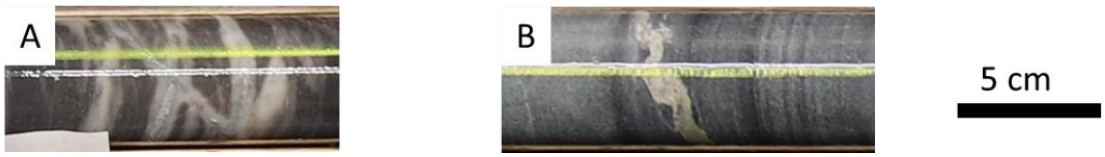

Figure 5.30: Rare vein types found within Newt Zone. (a) grey infill (ERM-2021-59 @ 103m); and (b) epidote infill (ERM-2021-59 @ 310m).

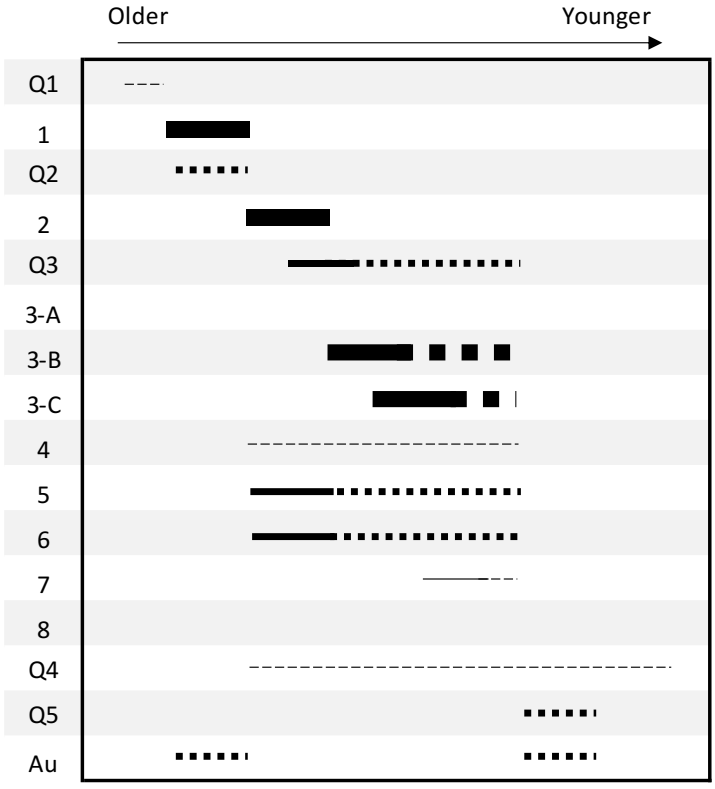

Figure 5.31: Paragenesis of veining within the chaotic unit in the Newt zone. The thicker the line the more abundant the vein type. Solid lines indicate higher confidence of cross-cutting relationships, and dashed line indicate non-constrained cross-cutting relationships.

5.5 Peek-a-Boo zone

The chaotic unit is less abundant and thinner in Peek-a-Boo zone compared to the rest of the zones. The unit ranges from 0.2-1 m, but can be up to 36 m, with the thickest intersections on the east side of the zone. Like the other zones, the unit can also be hosted within the feldspar porphyry unit, with the alteration intensity being more intense within the feldspar porphyry unit relative to the volcanic rock (Fig. 5.32). Due to the limited exposure of the unit cross-cutting relationships are limited within the zone. Type 1, 2 and 3-B veins are the most common types, with the rest of the vein types being relatively rare. Type 6 and 8 veins are also not noted within the zone.

Figure 5.32: Chaotic unit hosted within the Peek-a-Boo zone (ERX-2020-21 @ 337m).

Type 1 and 2 veins are very similar to the rest of the zones. Type 3 veins look more like the 8 and Newt Lake zones, in that they are thinner than in the Falcon zone and ranging from straight to weakly irregular. They cut the Laminated unit and Q2 veins (Figs. 5.33 H and I). Type 6 veins look like the Newt Lake zone, but are thinner, and sparser. The veins cut type 1 veins (Fig. 5.33 A). Type 7 veins are similar to those in other zones and cut type 1 veins and the Laminated unit (Fig. 5.33 B and J). Like the other zones, the quartz veins occur as veinlets that are either deformed veinlets (Q1), parallel to the fabric (Q2 or Q5), or cutting the fabric (Q4; Fig. 5.33 C, D and E). The quartz veins range from milky to clear quartz veins with variable carbonate alteration, and sharp contacts. The Q3 veins cut type 1, and 3-B veins (Fig. 5.33 F and G).

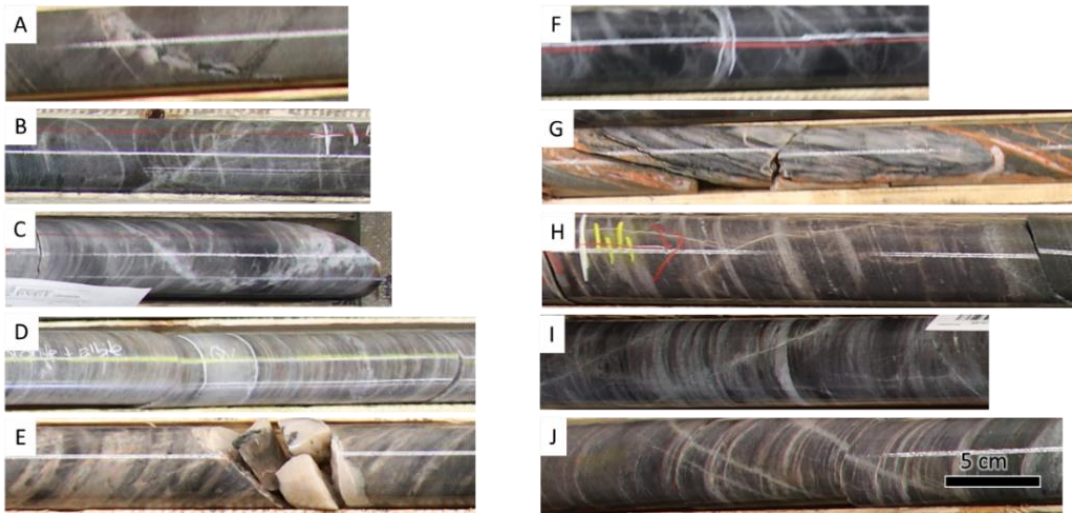

Figure 5.33: Cross-cutting relationships found within the Peek-a-Boo Zone. (a) type 6 cuts 1 (ERX-2021-99 @ 174m); (b) type 7 cuts 1 (ERX-2020-23 @ 155m); (c) Q1 vein (ERX-2020-22 @ 11m); (d) Q2/Q5 veins parallel to the fabric (ERX-2020-24 @ 101m); (e) Q4 vein cutting fabric (ERX-2021-96 @ 23m); (f) Q3 vein cuts type 1 vein; (g) Q3 vein cuts type 3-B vein (ERX-2021-99 @ 111m); (h) type 3-B cuts the Laminated unit (ERX-2021-85 @ 44m); (i) type 3-C cuts the Laminated unit and Q2 vein parallel to fabric (ERX-2021-88 @ 91m); and (j) type 7 cuts the Laminated unit (ERX-2021-93 @ 147m).

Based on the cross-cutting relationships a paragenesis of the veins is developed in Figure 5.34. The cross-cutting relationship are very limited, and thus the younging direction is unknown as the veins appear to be coeval.

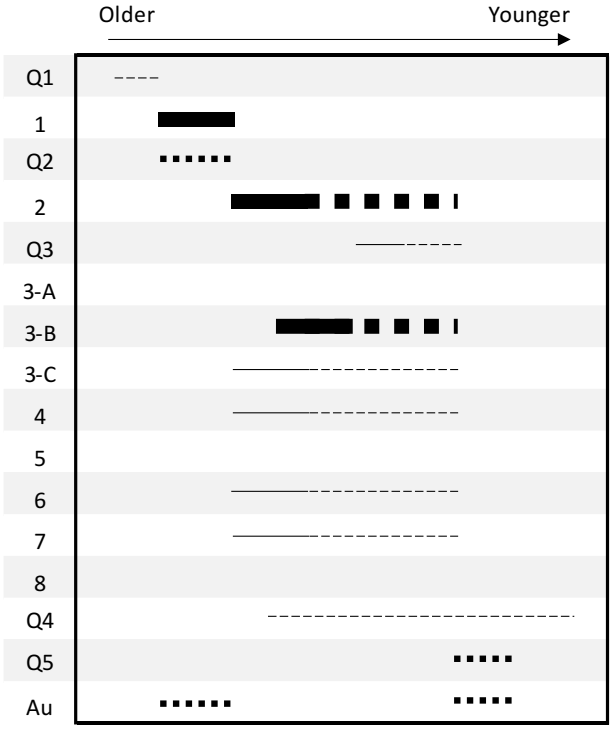

Figure 5.34: Paragenesis of veining within the chaotic unit in the Falcon zone. The thicker the line the more abundant the vein type. Solid lines indicate higher confidence of cross-cutting relationships, and dashed line indicate non-constrained cross-cutting relationships.

6. Discussion

6.1 Constraints on age of Eagle River complex rocks and mineralization

The new U-Pb dates from this study include the Central pluton (ER-2021-WP-G1: 2656.38 ± 0.41 Ma) to the north-west, the Bowman Lake batholith (ER-2021-WP-G2: 2658.35 ± 0.41 Ma) to the north-east, the Floating Heart batholith (Pilot Harbour granite; ER-2021-WP-G3: 2687.26 ± 0.42 Ma) to the south, and the mine diorite (ER-2021-WP-G4: 2716.22 ± 0.41 Ma) central to the batholiths (Fig. 6.1). The Central pluton and the Bowman Lake granite are very similar in age and potentially are part of the same event.

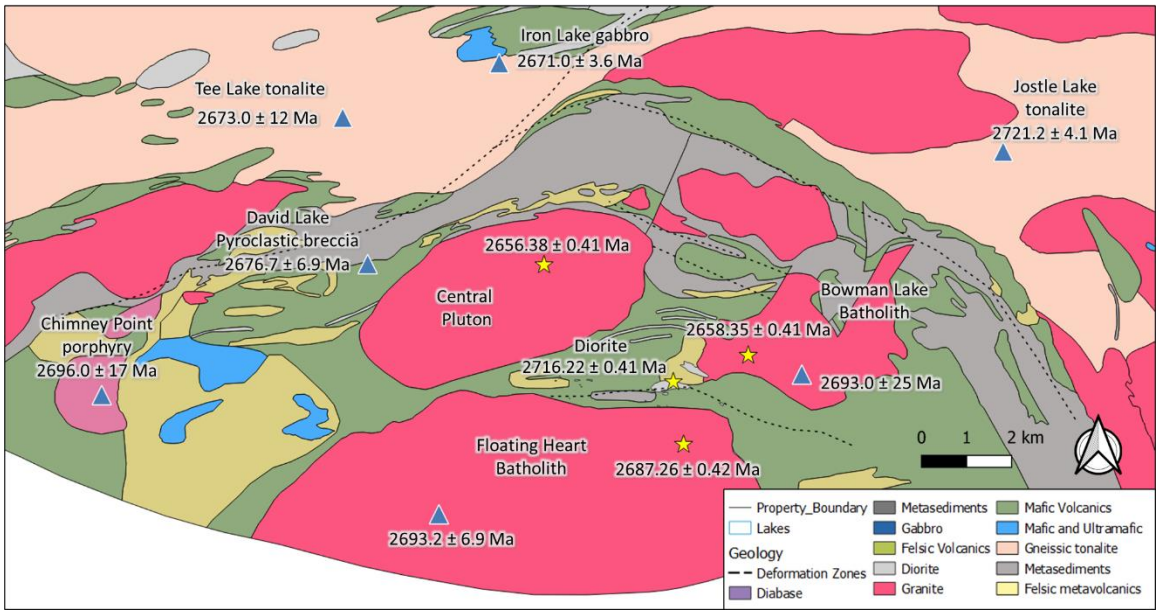

Figure 6.1: Geological map of the region showing the new (stars) and published (triangle) ages by Keller (1989) (Map courtesy of Wesdome Gold Ltd.)

The Bowman Lake batholith and the Floating Heart batholith had previously published ages of 2693.0 ± 25 Ma and 2693.2 ± 6.9 Ma, respectively (Keller, 1989) but due to the relatively high errors

new samples were acquired to better constrain the age. The new dates are within error of the previously published dates but provide a much tighter age constraint. The oldest intrusive date within the region is the Jostle Lake tonalite (2721.2 ± 4.1 Ma) which predates the diorite, as well as younger intrusions including the Tee Lake tonalite (2673.0 ± 12 Ma) and the Iron Lake gabbro (2671.0 ± 3.6 Ma; Turek et al., 1982; Fig. 6.1). These ages are broadly coeval with the new ages from this study. The new ages acquired for the Central pluton (2656.38 ± 0.41 Ma) and the Bowman Lake batholith (2658.35 ± 0.41 Ma) provides a tighter constraint on the plutonism in the belt.

The David Lakes pyroclastic breccia (2676.7 ± 6.9 Ma) is located west of the Central pluton (Fig. 6.1), with the age reported by Turek et al. (1982) is younger than the mine diorite (2716.22 ± 0.41 Ma) and the Floating Hearth batholith (2687.26 ± 0.42 Ma) that intrude it. The David Lakes pyroclastic breccia lies along the contact with the top of the metasedimentary rocks without any associated mafic and intermediate volcanic rocks and it is possible that the age is related to a younger sedimentation event rather than volcanism (Turek et al., 1982), or that the volcanic activity in the belt started before the diorite and continued to 2676 Ma with potential unconformities along the way.

Turek et al. (1984) classified the Michipicoten plutonic-volcanic terrane into six different events, which include: (I) 2888 Ma – plutonism and formation of older granitic rocks; (II) ca. 2743 Ma (2737-2749 Ma) – extrusion of lower volcanic rocks and plutonism; (III) ca. 2717 Ma (2713-2722 Ma) – extrusion of middle volcanic rocks and plutonism; (IV) ca. 2696 Ma (2694-2698 Ma) – extrusion of upper volcanic rocks and intrusion of external plutons; (V) ca. 2668 Ma (2662-2675 Ma) – renewed plutonism following by cessation of volcanism (Kenoran Orogeny); and (VI) 2615 Ma – tectonic activity, faulting and plutonism. Based on this model for the evolution of the Michipicoten area, the mine diorite (2716 Ma) would be part of event III. Although the Floating Heart batholith (2687 Ma) falls outside the range of the event IV, it would represent a younger limit of the plutonism. Similarly,

the Central pluton (2656 Ma) along with the Bowman Lake batholith (2658 Ma) fall outside the range of event V, as such they too would represent a younger limit of the plutonism.

Additional to the ages acquired around the vicinity of the mine site, a more regional scale comparison was completed to investigate how the data from this study fit within the district. These ages are summarized in Figures 6.2 and 6.3. The Eagle River rock ages were compared to: (1) The Manitouwadge greenstone belt (Zaleski et al., 1999) where volcanism and subvolcanic plutonism are associated with massive sulphide deposits and hydrothermal alteration from 2720 Ma to 2689-2687 Ma and synkinematic plutonism from 2680-2677 Ma. Greywackes were deposited after 2693 Ma, post-dating local volcanism by at least 25 m.y.; (2) The Hemlo Gold Deposit (Muir, 2003) which is bounded by metamorphic batholiths (~2720 Ma), internal granitoid intrusions (2690-2684 Ma and 2678 Ma), and plutons (~2697 Ma and 2678 Ma); (3) The Missinabie-Renabie area (Turek et al., 1996) where the felsic volcanism is constrained by the Renabie crystal tuff at 2740 ± 8 Ma and the Cradle Lakes porphyry at 2736 ± 4 Ma. A deformed quartz-feldspar porphyry at Conboy Lake has yielded an age of 2675 ± 6 Ma, and the Conboy Lake tonalite has an age of 2688 ± 14 Ma. The Ogasiwi Lake granitoid complex borders the southern flank of the greenstone belt with an age of 2723 Ma. The belt contains four internal plutons including the 2661 ± 11 Ma Ruby Lake stock, 2670 ± 8 Ma Lochalsh Bay stock, 2679 ± 5 Ma Ash Lake pluton, and the 2668 Ma Rennie Lake stock; (4) The Island Gold deposit (Jellicoe, 2019) is hosted in the Wawa assemblage which is composed of tholeiitic mafic to intermediate volcanic rocks ranging from 2749 ± 2 Ma to 2728.8 ± 2.7 Ma. The Catfish assemblage is the youngest volcanic package with ages of 2710 ± 7.7 Ma and 2701 ± 7.7 Ma. The Dore metasedimentary rocks are the youngest supracrustal rocks with sedimentation occurring between 2682 ± 3 Ma to 2698 ± 2 Ma, and unconformably overlie the Catfish and Wawa assemblage; (5) the Gamitagama greenstone belt (Krogh & Turek, 1981) which is bounded by metamorphic batholiths (~2720 Ma), internal granitoid intrusions (2690-2684 Ma, and 2678 Ma),

and plutons (~2697 Ma and 2678 Ma; Muir, 2003). The gold mineralization is hosted along a regional east trending shear zone within the hanging wall of a transition between the volcanic and sedimentary rocks, that formed between 2693 Ma and 2680-2690 Ma (Jackson et al., 1998); and (6) the Batchawana greenstone belt (Corfu & Grunsky, 1987) where the greenstone belt formed between 2730 and 2670 Ma. The 2729 ± 3 Ma tholeiitic metavolcanic rocks were intruded by a 2716 ± 2 Ma tonalite. Additional ages of stratigraphic levels of mixed tholeiitic to calc-alkaline metavolcanic rocks include 2720 ± 10 Ma, 2709 ± 2 Ma, 2711 ± 2 Ma, 2701 ± 2 Ma, and 2698 ± 2 Ma. The internal syn- to late- plutons have yielded ages of 2678 ± 4 Ma, 2677 ± 2 Ma, 2677 ± 3 Ma and 2676 ± 2 Ma.

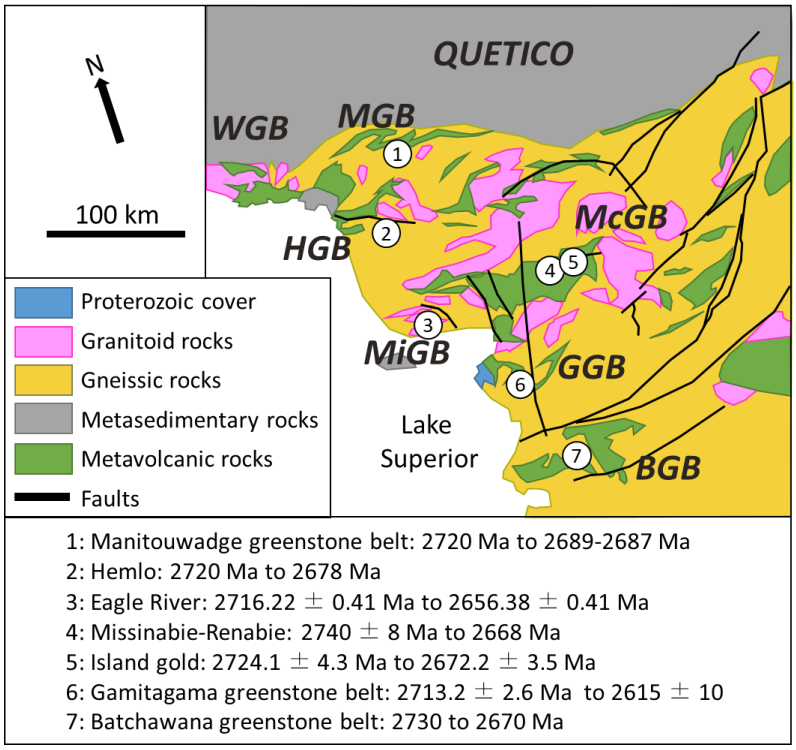

Figure 6.2: Geographical locations of geochronological dates relative to the greenstone belts (modified from Card and Poulsen, 1998 and Turek et al., 1995). Abbreviations: MGB - Manitouwadge greenstone belt; WGB - Winston Lake greenstone belt; McGB – Michipicoten Greenstone belt; MiGB – Mishibishu Lake greenstone belt; HGB – Hemlo greenstone belt; GGB – Gamitagama greenstone belt; BGB – Batchawana greenstone belt.

The volcanism within the Eagle River complex is not currently constrained, but since the 2716.22 ± 0.41 Ma mine diorite intrudes the volcanic rocks, the volcanic rocks must be older than the mine diorite. The Eagle River plutonism is bracketed between 2716.22 ± 0.41 Ma to 2656.38 ± 0.41 Ma at a similar timeframe to the plutonism in the surrounding regions. The Pilot Harbour granite and the Central pluton are closely related to the oldest and youngest internal plutons in the Missinabie-Renabie area, respectively. Additionally, the Pilot Harbour granite correlates with 2720 Ma to 2689-2687 Ma volcanism and subvolcanic plutonism in the Manitouwadge belt (Fig. 6.3).

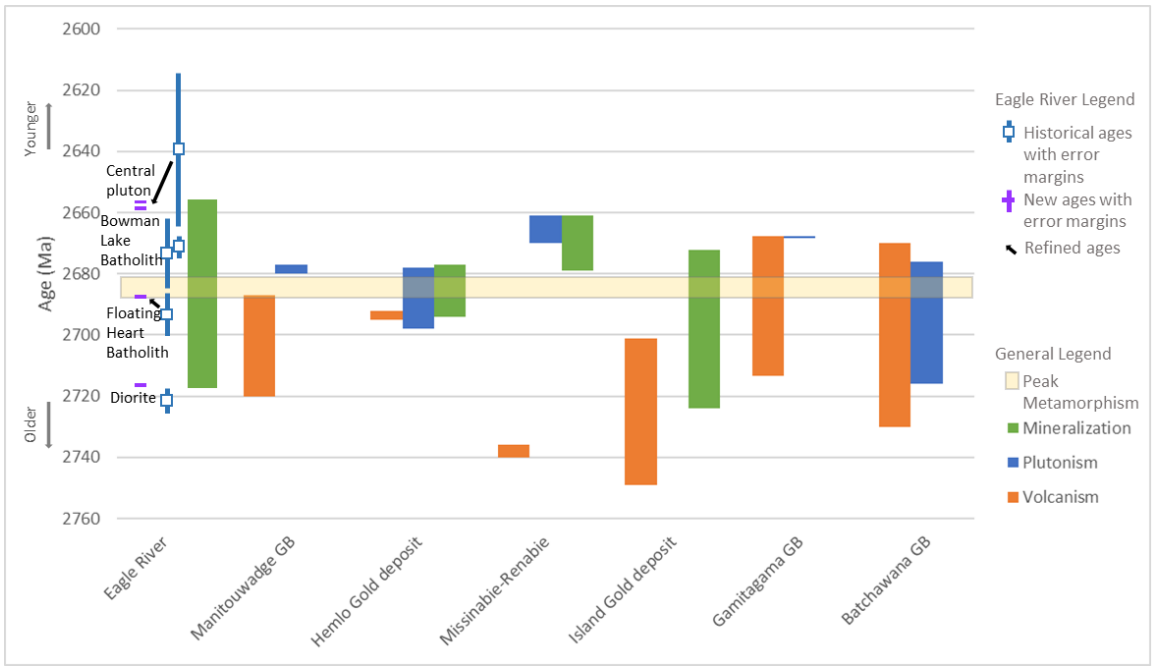

Figure 6.3: Geochronological compilation from different greenstone belts in relation to volcanism, plutonism, and mineralization. Abbreviations: GB: Greenstone belt. The black arrows point towards the new revised age for the unit determined in this study. Peak metamorphism is based on Hemlo Gold mineralization (Muir, 2002). Source of ages is given in the text.

In addition to the volcanism and plutonism, three mineralization ages have been acquired from: (1) The Hemlo Gold deposit where the mineralization is hosted along a regional east trending shear zone within the hanging wall of a transition between the volcanic and sedimentary rocks, occurring between 2693 Ma and 2680 to 2690 Ma (Jackson et al., 1998); (2) the Missinabie-Renabie area where a period of late deformation related to gold mineralization is bracketed between 2661 ± 11

Ma and 2679 ± 5 Ma (Turek et al., 1996); and (3) the Island Gold deposit where the Webb Lake Stock has yielded a weighted mean $^{207}Pb/^{206}Pb$ age of 2724.1 ± 4.3 Ma, representing the older limit of mineralization (Jellicoe, 2019). The younger limit of mineralization is represented by the barren monzonite intrusion that cross cuts the ore zone with a weighted $^{207}Pb/^{206}Pb$ age of 2672.2 ± 3.5 Ma (Jellicoe, 2019).

The lower limit of mineralization in Eagle River is bounded by the 2716.22 Ma diorite that hosts the mineralization, but the upper limit of mineralization is currently not constrained. The mineralization is cut by younger northeast and northwest striking late Precambrian diabase dykes. To have a better constraint on the upper limit of mineralization, the regional compilation of mineralization (i.e., the Hemlo, Missinabie-Renabie and Island Gold deposits) and peak metamorphism (based on Hemlo deposit) are used (Fig. 6.3). All three regional mineralization ages occur at similar times and have overlapping intervals, which implies a broad mineralizing event. The Hemlo mineralization has lower confidence relative to Island Gold and Missinabie-Renabie as the mineralization is hosted in different rock types relative to the Eagle River deposit and is the most distal mineralization in this study relative to the Eagle River. The Island Gold mineralization overlaps with the regional metamorphism, similar to that of the Hemlo deposit. The Missinabie-Renabie mineralization is hosted in quartz veins within high-strain zones that postdate the peak metamorphism and are related to late deformation (Turek et al., 1996). Based on three regional mineralization ages, the timing of the mineralization overlaps with the mine diorite and the Floating Heart batholith intrusions. Since the Floating Heart batholith also overlaps with the peak metamorphism, it has a higher potential to be linked with mineralization than the mine diorite, which is potentially the interpreted age of mineralization. The upper limit of mineralization within Eagle River is currently undefined and would require additional dating to constrain it, such as younger units that cut it, or the age of the shearing that hosts it.

6.2 Tectonic setting of Eagle River complex rocks

The mafic volcanic rocks do not show any significant chemical variations within the major and trace elements between the four zones (i.e., 8, Falcon, Newt Lake, and Peek-a-Boo zones). They exhibit good correlation with REE and HFSE plotted against Zr (Fig. 6.4 A-H). This suggests that the elements exhibit relative low mobility during deformation and alteration. The mafic volcanic rocks also have near-flat primitive mantle normalized spider diagrams with negative Nb and Ti anomalies as outlined in section 4.3.7. These negative Nb and Ti anomalies are indicative of a magmatic arc origin (Polat et al., 1998). The arc signature is further supported by plotting Zr/Y vs Nb/Nb* with all the rock types plotting away from the MORB signature and following the arc trend within a slab dehydration zone (Figs. 6.5 and 6.6). The negative Nb anomalies are indicative of fluid transport of trace elements under relatively low pressures in the shallow part of the subduction zone (Baier et al., 2008) and are a strong indication of magmas generated in the subduction-zone setting (Pearce, 1982; 1996). The negative Ti anomalies are indicative of fractionation of a Ti-phase such as ilmenite, titanite or rutile (Polat et al., 1998). The Nb anomalies form by fractionation of Nb from Th and Ce during

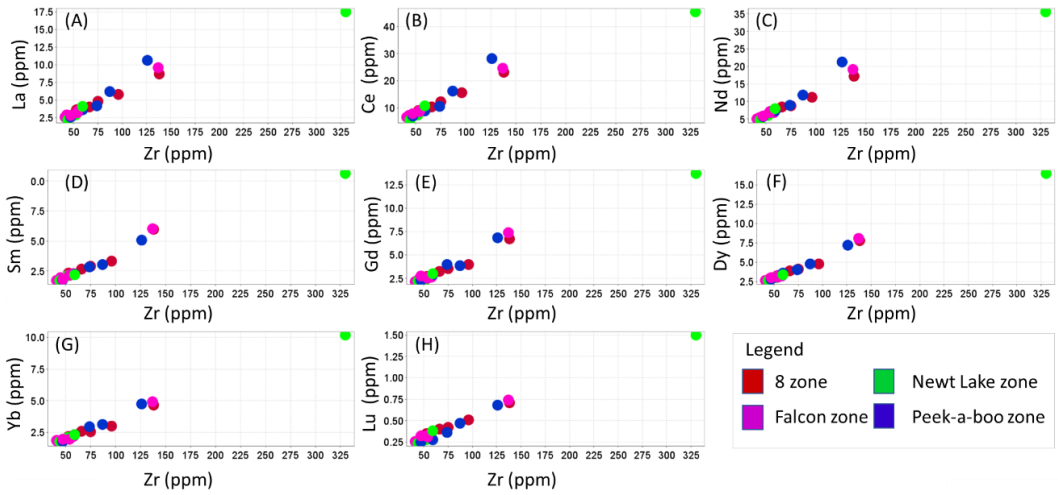

Figure 6.4: Trace element scatter plots in the mafic volcanic rocks dehydration and partial melting of the subducted crust and are retained within amphiboles and minor Ti phases such as titanite and rutile (Pearce, 1996). Thorium contents vary depending on the contribution from subducted sediments, with higher Th/Ta and Th/Nb ratios during partial melting.

of subducted sediments or assimilation of crust (Hawkesworth et al., 1997). The low Th/Nb values seen in rocks from this study suggest that crustal contamination was not an important feature during petrogenesis (Mills & Sandeman, 2018).

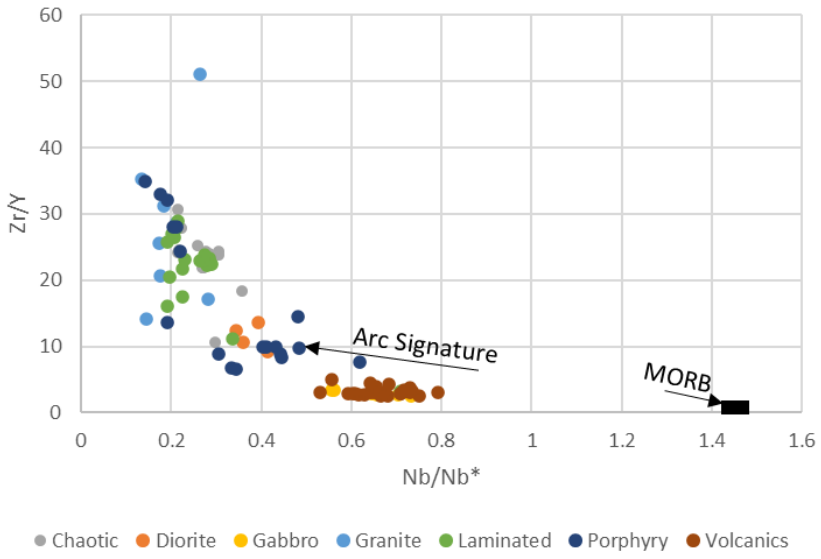

Figure 6.5: Zr/Y vs Nb/Nb diagram for rocks from the four study areas. The black arrows indicate an arc trend, and the position of MORB. The rocks suites in this study show an arc signature. Fields for MORB and arc signature after Polat et al. (1998).*

The gabbro unit shows no significant chemical variations of the major and trace elements across the four zones. There is a moderate correlation between the REE and HFSE plotted against Zr (Fig. 6.7). The correlation with REE plotted against Zr is weaker relative to the mafic volcanic rocks suggestive of increased mobility of the REE and HFSE elements. The gabbro and the Laminated Group B units both show similar near-flat primitive mantle normalized patterns with negative Nb and Ti anomalies to the mafic volcanic rocks (Fig. 6.8). Like the mafic volcanic rocks, both the gabbro and the Laminated Group B unit show an arc affinity with a slab dehydration signature (Figs. 6.5 and 6.6). Due to similarities of the primitive mantle normalized patterns, negative Nb and Ti anomalies, and the same arc affinity from a dehydrated slab, the gabbro, Laminated Group B unit, and mafic volcanic rocks are interpreted to have formed from a similar source.

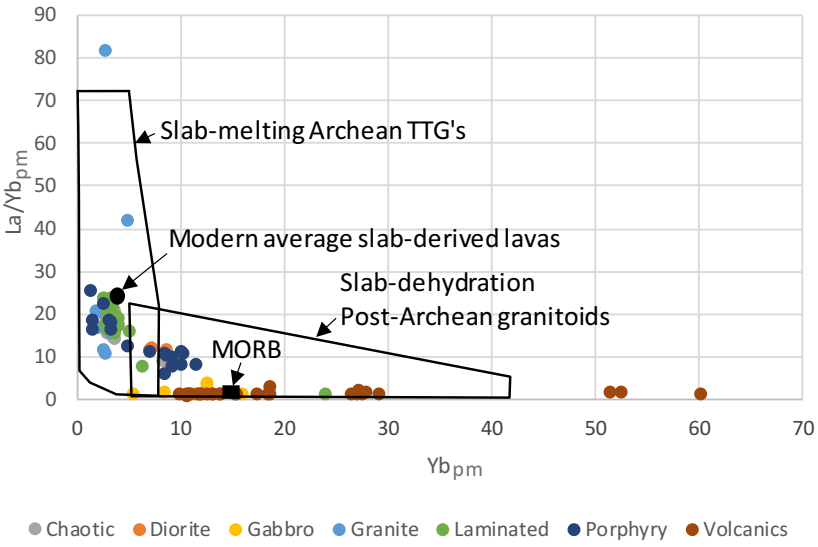

Figure 6.6: Primitive mantle normalized La/Yb_{pm} vs Yb_{pm} for the suite of rocks in the study area. The regions for slab-melting and slab-dehydration are shown on the diagram. The Laminated unit and the granite have a dominantly slab-melting signature, the volcanic rocks and the gabbro have a dominantly slab-dehydration signature, and the diorite, porphyry, and chaotic unit have a mixed signature between slab-melting and slab-dehydration. Modified after Polat et al. (1998).

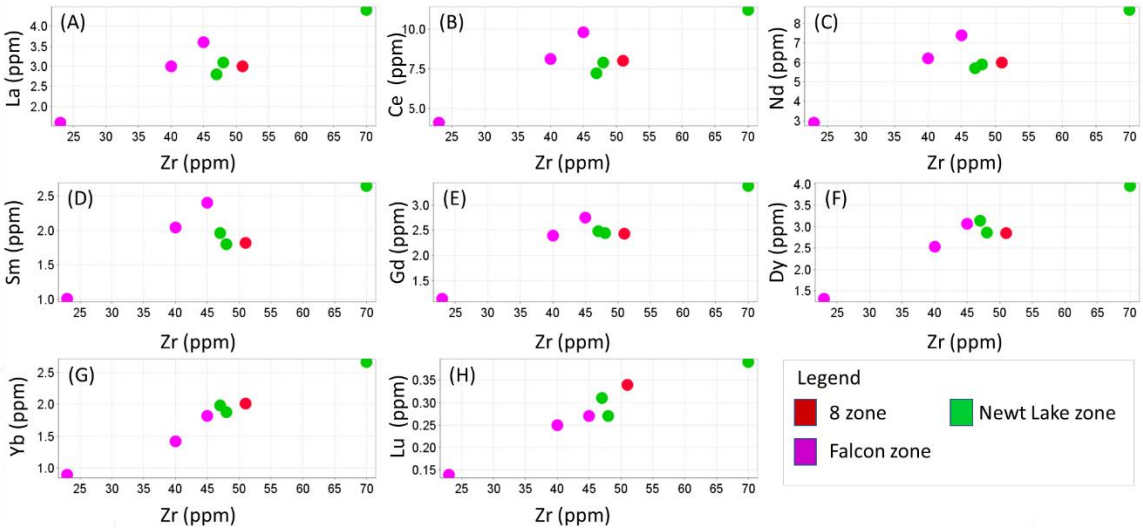

Figure 6.7: Trace element scatter plots for the gabbro unit.

The granitoids have highly fractioned HREE, high Zr/Y (14-51), high Sr/Y (35-143), low K/Rb (180-425) ratios, and negative Nb anomalies (0.13-0.28; Fig. 6.9). Based on Zr, Hf, Nb, Ta, Y, Zr and Rb values they are consistent with an arc origin (Pearce et al., 1984). The granitoids have high Na_2O values

(3.82-5.66 wt. % Na_2O) and are metaluminous (Fig. 6.10). The Eagle River granites have been classified as I-type granites based on the high Na_2O values (>3.2 %), CIPW normative diopside or <1% normative corundum (Chappell & White, 2010), metaluminous with a wide

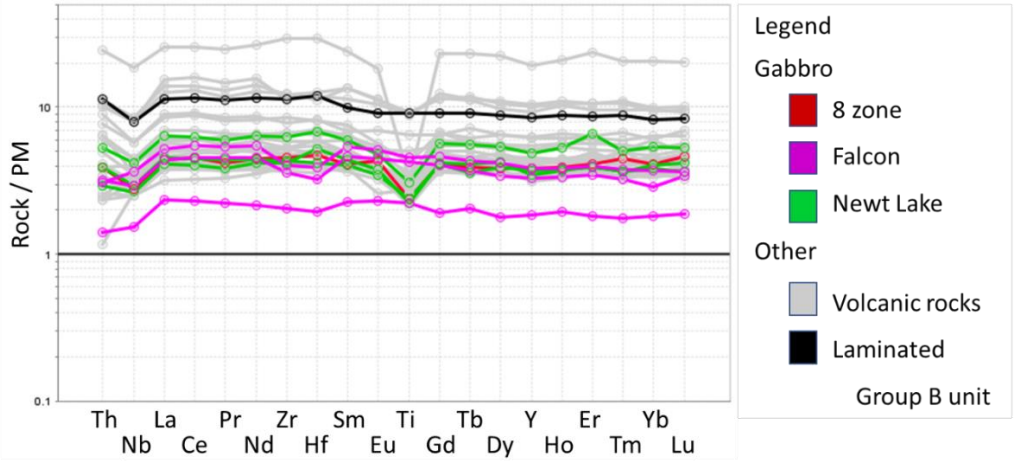

Figure 6.8: Primitive mantle normalized spider diagram for the gabbro unit by zone relative to the mafic volcanic rocks and the Laminated Group B unit. Primitive mantle normalizing values are from Sun and McDonough (1989).

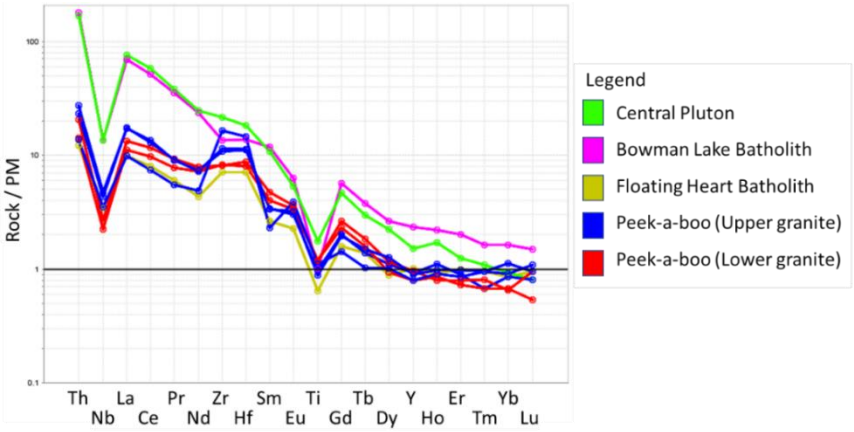

Figure 6.9: Primitive mantle normalized spider diagram for the three pluton/batholith intrusions from the geochronological samples and the granitic samples from the Peek-a-Boo zone. Primitive mantle normalizing values are from Sun and McDonough (1989).

range of silica contents (56-77 wt. % SiO_2; Frost et al., 2001). Plotting the Nb + Y against Rb values shows a volcanic arc granite association (Fig. 6.11). The granites from the Central pluton and the Bowman Lake batholith (Group A) show a different trend relative to the Floating Heart batholith and

the Peek-a-Boo zone granite (Group B), with Group B subdivided into two groups based on Ni and the Ti/Zr ratio as discussed in Section 4.3.5. Group A granites are ~30 m.y. younger than Group B granites and have elevated Th, Nb, La and LREE relative to Group B.

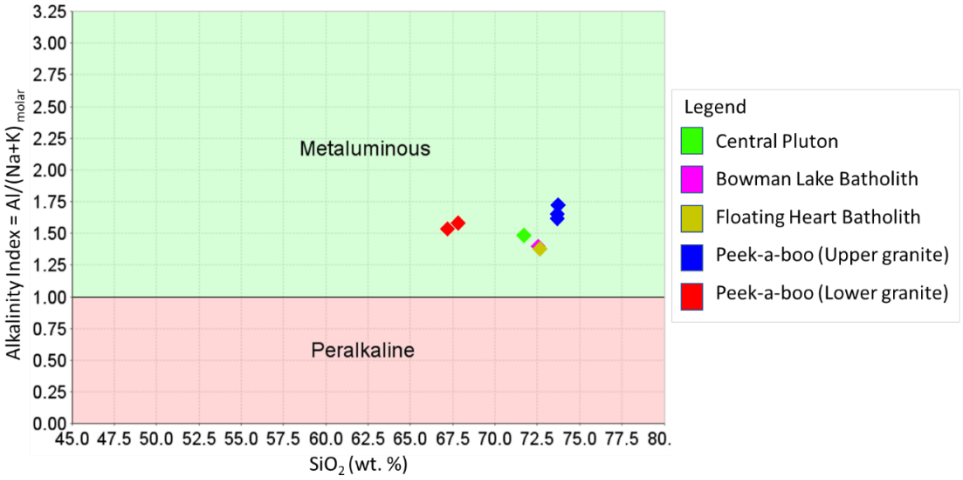

Figure 6.10: Alkalinity Index versus SiO_2 for the granitoids. Modified after Frost and Frost (2008).

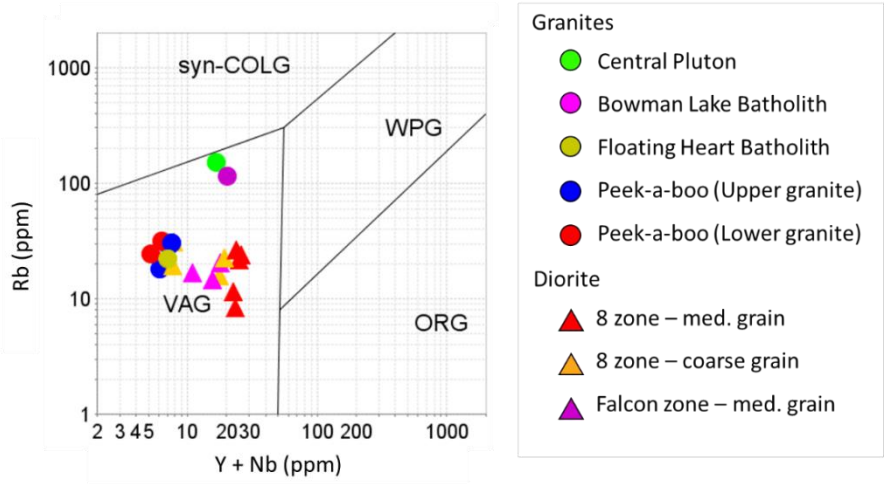

Figure 6.11: Nb + Y vs Rb (ppm) classification diagram for granitoids. Modified after Pearce et al. (1984). Syn-COLG: syn-collisional granite; VAG: volcanic arc granites; WPG: within plate granites; ORG: ocean-ridge granites.

The diorite unit shows a poor to moderate correlation between CaO and LOI plotted against SiO_2 (Fig. 6.12 A and B). This is suggestive of alteration, with more altered samples having higher LOI. The development of kaolinite, chlorite and carbonates results increased values of LOI, with altered

samples having LOI > 2% (Laouar, 2002). There is a poor to moderate correlation for the major elements and moderate correlation for La, Ce, Yb and Lu plotted against Zr (Fig. 6.12 C, D, E, and F). This suggests immobility of the REE elements during alteration and deformation. The diorite has highly fractionated primitive mantle normalized patterns, moderate Zr/Y (3-14), high Sr/Y (19-97), low K/Rb (254-359) ratios, and negative Nb anomalies (0.26-0.48). Relative to the granitoids, the diorite has more fractionated HREE and a dominantly negative Zr anomaly, whereas the granitoids have dominantly positive Zr anomalies (Fig. 6.13). Additionally, the Ti anomaly can be either positive or negative in the diorite, whereas the granitoids have a strong negative Ti anomaly. The difference in the Ti and Zr anomalies can either mean the same source of magma with different fractionation history, or two different sources of magmas. Based on spatial association of the diorite and batholiths, as well as the similar ages, the same source of magma is assumed. On a La/Yb_n against

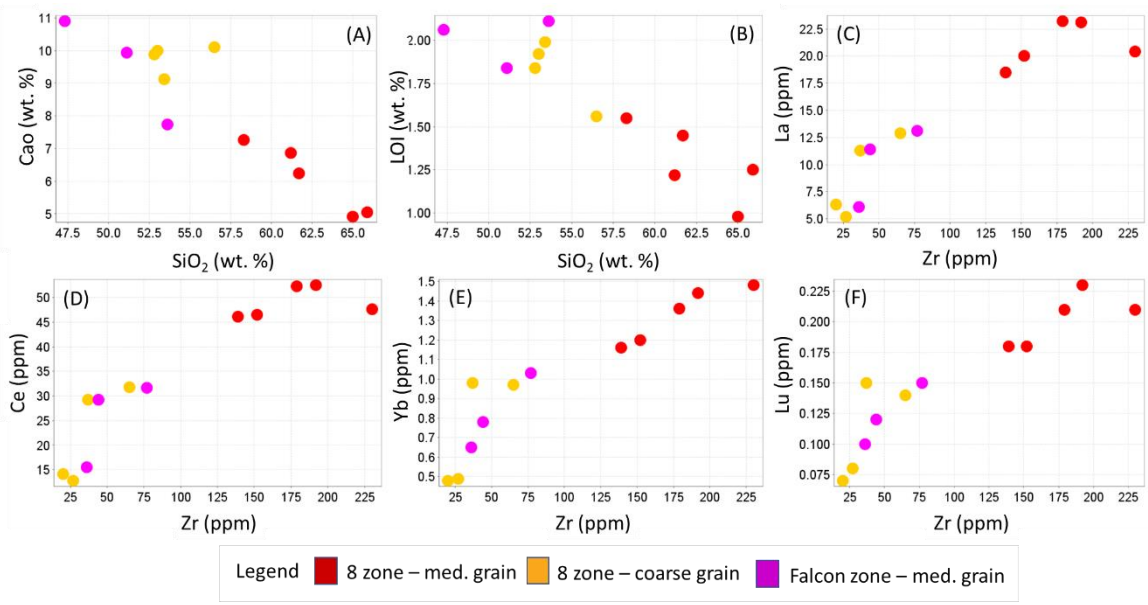

Figure 6.12: Major and trace element scatter plots for the diorite unit.

Yb_n plot, the diorite plots in the mixing zone between the slab melting and slab-dehydration field, whereas the granite plots within the slab melting field (Fig. 6.6). Based on geochemical differences

between the rock types, it suggests either a switch between slab melting and slab-dehydration during the evolution of the greenstone belt or melting of garnet-bearing rocks.

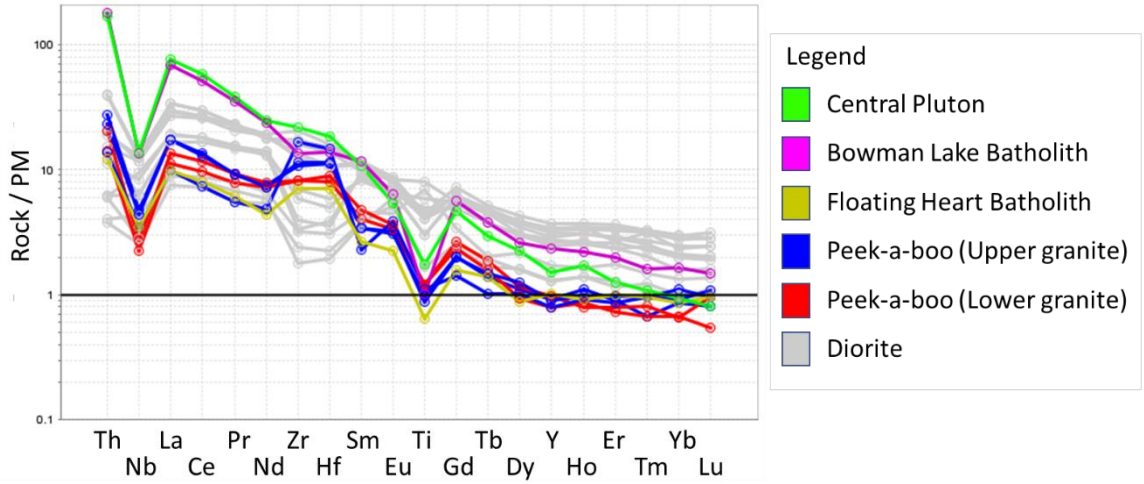

Figure 6.13: Primitive mantle normalized spider diagram for the three pluton/batholith intrusion from the geochronological samples, the granitic samples from the Peek-a-Boo zone, and the diorite. Primitive mantle normalizing values are from Sun and McDonough (1989).

Polat et al. (1998) classified the volcanic sequences of the Archean Schreiber-Hemlo and White River-Dayohessarah greenstone belts into multiple groups including (1) ultramafic volcanic rocks (komatiites; Group 1A and Group 1B); (2) Mafic volcanic rocks (Group 2A and Group 2B); (3) intermediate volcanics rocks (andesites); (4) granitoids (TTG's); and (5) siliciclastic sedimentary rocks (sandstones and shales). The geodynamic setting proposed by Polat et al. (1998) involved the accretion of ocean plateaus, ocean arcs and trench turbidities through a series of out-of-sequence thrusting and orogen-parallel strike-slip faulting. Within the Polat et al. (1998) study the Group 2B basalts are tectono-stratigraphically higher than Group 2A basalts, which suggests plume-type volcanism overprinted by arc volcanism. They argued that changes in relative plate-motion resulted in the initiation of intra-oceanic subduction along the edge of an oceanic plateau similar to the modern-day Caribbean oceanic plateau and the Greater Antilles subduction zone. They proposed that metasedimentary rocks are consistent with foreland basins developed in response to

lithospheric down flexure under the loading of SSE-verging greenstone-granitoid nappes. The rocks from Polat et al. (1998) show similarities to the rocks from the Eagle River complex, including (1) the volcanic rocks matching Group 2B basalts, and (2) the granitoids matching the Dacite-Rhyodacites group. No komatiites or sedimentary rocks have been sampled within this study. The similarities between the rocks of Eagle River to those from the study of Polat et al. (1998) suggest that the rocks likely formed in a similar geodynamic setting.

The stratigraphy within the Eagle River complex strikes east-west to east-southeast and is steeply dipping to the north. The rocks consist of volcanic rocks that range between calc-alkaline and tholeiitic, with intrusive bodies consisting of diorite, granites, and feldspar porphyry. All these rocks have an arc signature with the magma either generated by slab dehydration or slab melting. Within the subduction zone the subducting slab would dehydrate and release fluids which would trigger melting that formed in the volcanic rocks and the gabbros. The continued subduction of the slab would have eventually reached conditions (e.g., pressures, temperatures, etc.) to cause the slab to melt, resulting in the geochemical signature seen in the granitoids, diorite and the feldspar porphyry. The crustal contamination of the assimilating magma based on the Th/Yb ratio (chaotic – 1.88-3.60, diorite – 0.52-2.45, gabbro - 0.13-0.66, granite Group A – 2.45-5.57, granite Group B – 18.77-30.98, Laminated Group A – 1.72-3.64, Laminated Group B - 0.24-0.24, feldspar porphyry Group A – 2.33-5.33, feldspar porphyry Group B - 0.5-1.53, volcanic rocks - 0.06-0.25) is generally low, suggesting low degrees of crustal contamination, with the highest crustal contamination being associated with the granites. This would suggest a deeper source of the granites. The Laminated unit would have been created by the deformation and alteration of various units.

6.2.1 Geochemical constraints on alteration and evolution of feldspar porphyries

Based on the cross-cutting relationship of the feldspar porphyry with the alteration, the feldspar porphyry has been subdivided into three groups, which include: (1) Feldspar porphyry with no or minimal veining which show more fractionated HREE patterns (Figs. 6.14C, 6.15); (2A) Feldspar porphyry with veining and alteration cutting across the contact with the volcanic rocks that has steeper HREE patterns (Figs. 6.14A, 6. 15); and (2B) Feldspar porphyry with the veining and alteration cut off at the contact with the volcanic rocks (Figs. 6.14B, 6.15). Group 2B (Gd/Yb_{pm} = 1.9-2.5) has similar HREE patterns as Group 2A (Gd/Yb_{pm} = 2.5-5.0) but has more fractionated HREE. The cross-cutting relationship suggests at least two different feldspar porphyry intrusions. Group 1 feldspar porphyry has the lowest SiO_2 content, and is generally enriched in Fe_2O_3, MgO and CaO, Cr, Ni and V relative to Group 2A and 2B (Fig. 6.16). The differences between the major and trace elements are consistent with two separate intrusions. A study by Heather (1986) on the Mishibishu Lake greenstone belt identified two types of porphyry (i.e., quartz-feldspar porphyry and feldspar porphyry) that are associated with gold mineralization within zones of intense hydrothermal alteration. These quartz-feldspar and feldspar porphyry dikes cut the mineralization, while also

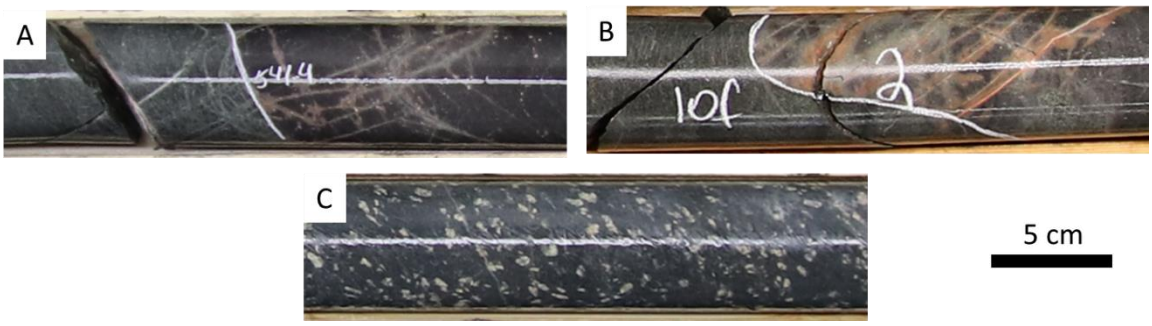

Figure 6.14: Chaotic unit contact with feldspar porphyry unit, showing the alteration cutting through the contact with volcanic rocks (ERM-2020-96 @ 541.4m) (a) and alteration being terminated at the volcanic rock contact (ERS-2022-031 @ 471m) (b). Feldspar porphyry with no or minimal veining (c).

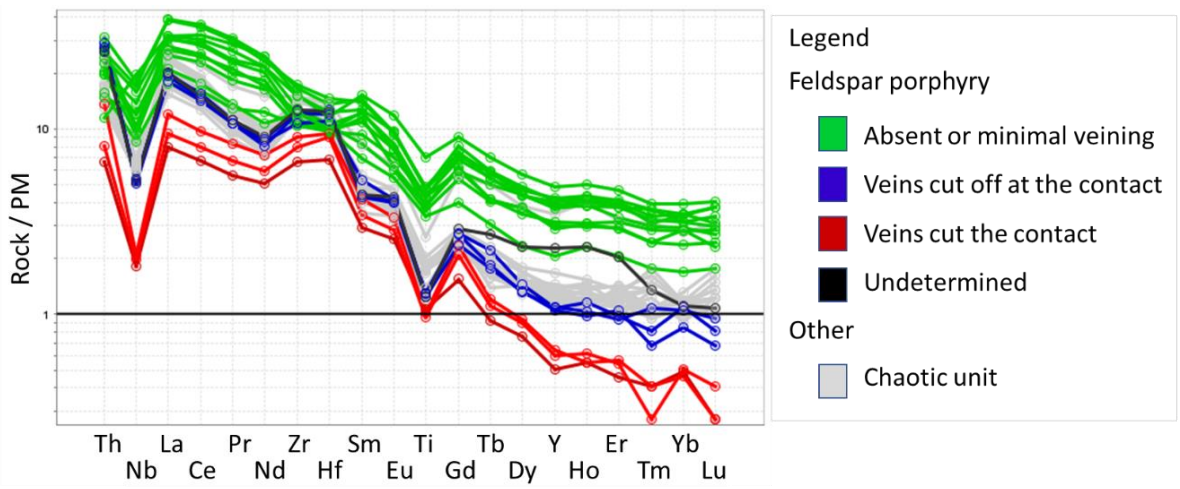

Figure 6.15: Primitive mantle normalized spider diagram for the feldspar porphyry unit relative to the alteration, veining, and the chaotic unit. Primitive mantle normalizing values are from Sun and McDonough (1989).

being cut by the mineralization, which suggests a spatial and potentially a temporal relationship between the hydrothermal alteration, porphyry dikes and the gold mineralization (Heather, 1986).

Within Eagle River the feldspar porphyry with veining and alteration (Groups 2A and 2B) would be suggestive of hydrothermal alteration. Since the alteration is cut off at the contact between volcanic rock and the feldspar porphyry and also cuts the contact between volcanic rock and feldspar porphyry it is suggestive of a long-lived hydrothermal system, and a temporal relationship with the hydrothermal alteration and the feldspar porphyry. Similar to the Mishibishu Lake greenstone belt feldspar porphyry from the Heather (1986) study, the feldspar porphyry within the Eagle River is associated with hydrothermal alteration and is in proximity to the gold mineralization. Within the Falcon zone the mineralization cuts the feldspar porphyry, but feldspar porphyry cutting the mineralization was not noted within this study. Establishing the cross-cutting relationship can provide further insight into mineralization and provide constraint on the temporal relationship with the feldspar porphyry and the mineralization.

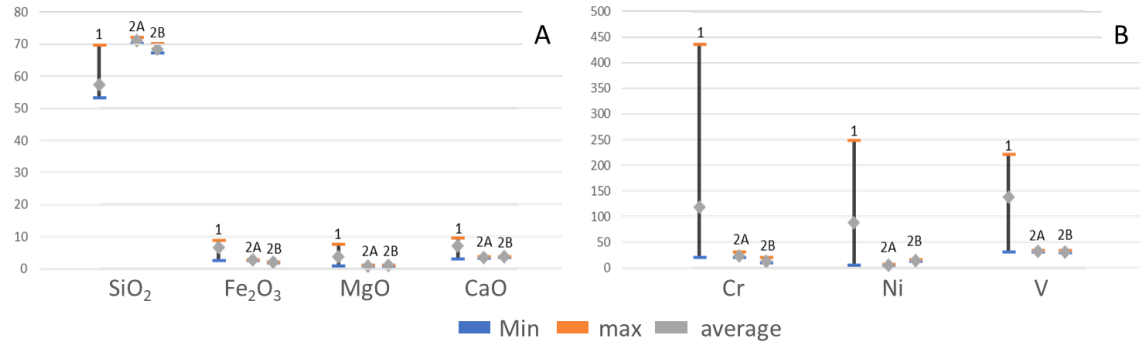

Figure 6.16: Feldspar porphyry geochemistry variations based on major elements (a) and trace elements (b).

The visual change in alteration as it progresses from feldspar porphyry to the volcanic rock is shown in Figure 6.14 A (Group 1 n = 12, Group 2A n = 3, Group 2B n = 3). Elemental maps of the contact from Figure 6.14 A are shown in Figure 6.17. The main elemental differences are with Na, Fe, and Mg, where the upper part of image (feldspar porphyry) is dominated by Na, and the lower part of the image (volcanic rock) is dominated by Fe and Mg. Within the feldspar porphyry (right side of Fig. 6.14 A, top of Fig. 6.17) the alteration is reddish and is dominated by albite, anorthoclase, quartz and minor prehnite and biotite, whereas within the volcanic rock (left side of Fig. 6.14 A, bottom of Fig. 6.17) the alteration color is greenish grey and is dominated by clinochlore, prehnite, and clinozoisite with minor biotite, pumpellyite, pyrite, and quartz. The red coloration noticed within alkali feldspar is due to the inclusions of hematite, with the intensity of coloration correlating with the amount of hematite present (Hofmeister & Rossman, 1984; Nakano et al., 2019). During alteration the Fe^{3+} within the feldspar porphyry would have been dominantly associated with albite and anorthoclase, giving the alteration a reddish coloration. The substitution of iron for aluminum has been shown for clinozoisite (Graham, 1983), prehnite (Akasaka et al., 2003), and clinochlore (Wang & Greenwood, 1988). Within the volcanic rock, the Fe^{3+} would have substituted for Al^{3+} within clinochlore, prehnite, or clinozoisite giving the alteration a greenish-grey color. The color change of the alteration as noted above, is due to a mineralogical difference between the feldspar

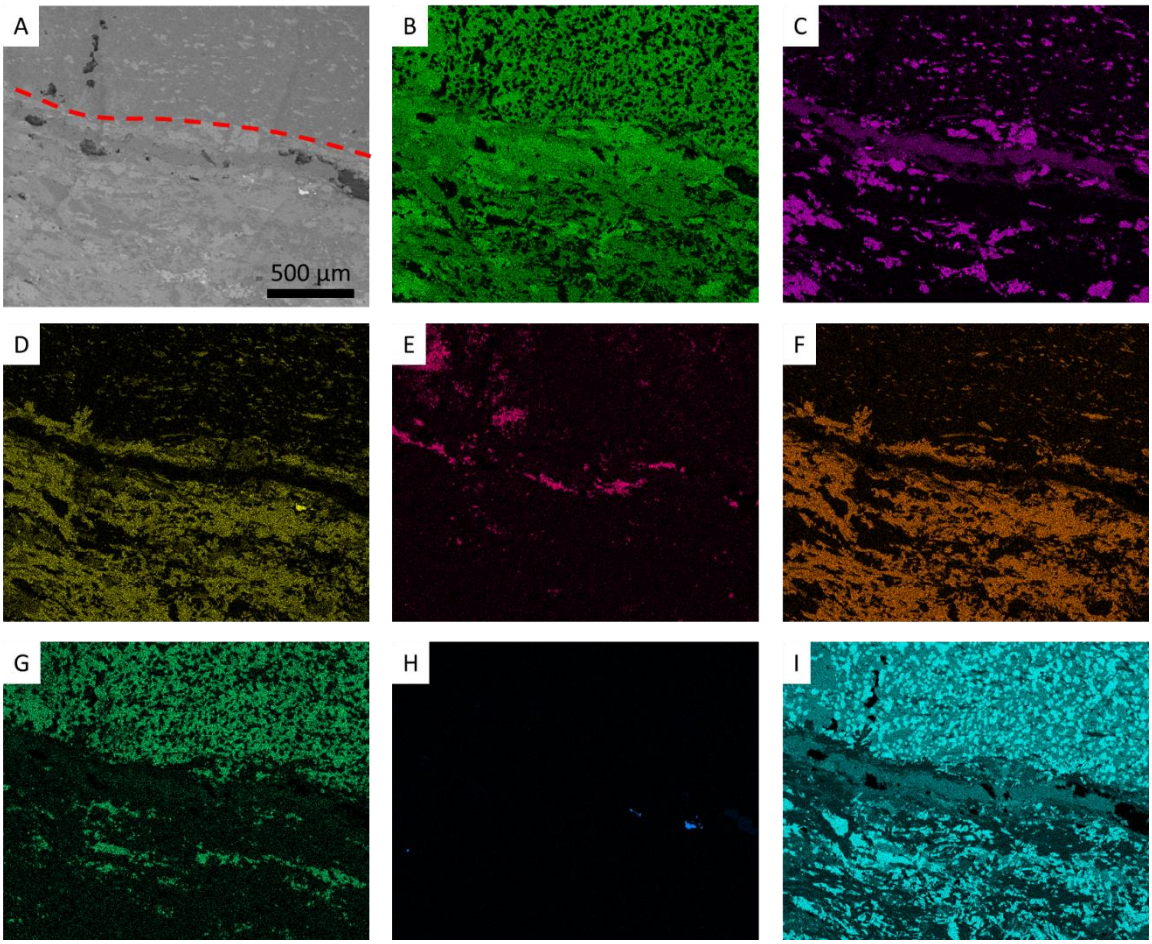

Figure 6.17: SEM elemental maps of the alteration along the contact between the chaotic and the feldspar porphyry units from Figure 6.14 A. SEM image of the section with the red dash line outlining the contact (a), aluminum (b), calcium (c), iron (d), potassium (e), magnesium (f), sodium (g), sulfur (h), and silicon (i).

porphyry and the volcanic rock, providing different minerals for the iron to associate with. The implication of this study is that the extent of potassic or hematite alteration is more widespread and can be more complicated to map out due to the variable coloration.

The feldspar porphyry unit shows no significant chemical variations between the four zones. It can be divided into two groups which include: (A) calc-alkaline andesite to trachy andesite; and (B) calc-alkaline basalts as discussed in Section 4.3.6. The feldspar porphyry unit shows a moderate correlation between TiO_2 and Fe_2O_3 plotted against SiO_2, which is suggestive of fractionation of Ti-phases such as ilmenite, titanite, or rutile (Fig. 6.18 A and B). Additionally, there is a moderate

correlation between La and Ce plotted against Zr (Fig. 6.18 C and D). On a primitive mantle normalized spider diagram the feldspar porphyry have enriched LREE relative to HREE with negative Nb and Ti anomalies consistent with a magmatic arc origin (Polat et al., 1998). The feldspar porphyry Group A has higher Th/Ta (Group A = 5.6-11.6, Group B = 1.39-6.37) and Th/Nb (Group A = 0.43-0.77, Group B = 0.07-0.31) relative to Group B, suggesting a higher contribution from recycled sediments (Polat et al., 1998). Pearce (2008) showed that the Th/Yb ratio (Group A = 2.33-5.33, Group B = 0.50-1.53) can be used to investigate crustal contamination, and the TiO_2/Yb ratio (Group A = 0.49-0.96, Group B = 0.55-0.88) can be used to investigate the depth of melting for the magma. Ascending magmas that have interacted with the crust, or have a subduction component, have higher Th/Yb values compared to MORB and OIB (Pearce, 2008; Varol et al., 2014). Due to the partition coefficients of Ti and Yb during crystallization, the Ti/Yb ratio can be used as a proxy for melting depth, with higher ratios suggesting deeper depths of melting (Pearce, 2008). Plotting Th/Yb and TiO_2/Yb against Nb/Yb shows that the rocks from Eagle River plot within the volcanic arc field above the enriched source (Fig. 6.19 A) with melting at shallower depths (2.5 GPa or below; Fig. 6.19 B). The Sr/Y or La/Yb ratios are another proxy that can be used to approximate crustal depths with increasing ratios suggestive of deeper depths (Moyen, 2009). The Sr/Y (Group A = 22.5-176.67, Group B = 13.06-34.68) and La/Yb (Group A = 22.92-35.65, Group B = 8.58-17.35) ratios for the feldspar porphyry unit show two different groupings which is suggestive of partial melting at different depths. Based on the two feldspar porphyry subgroups is suggested that there are two separate intrusions of feldspar porphyry based on crustal depths and degree of partial melting within an arc setting, where feldspar porphyry Group A has a higher crustal contamination component originating from deeper depths.

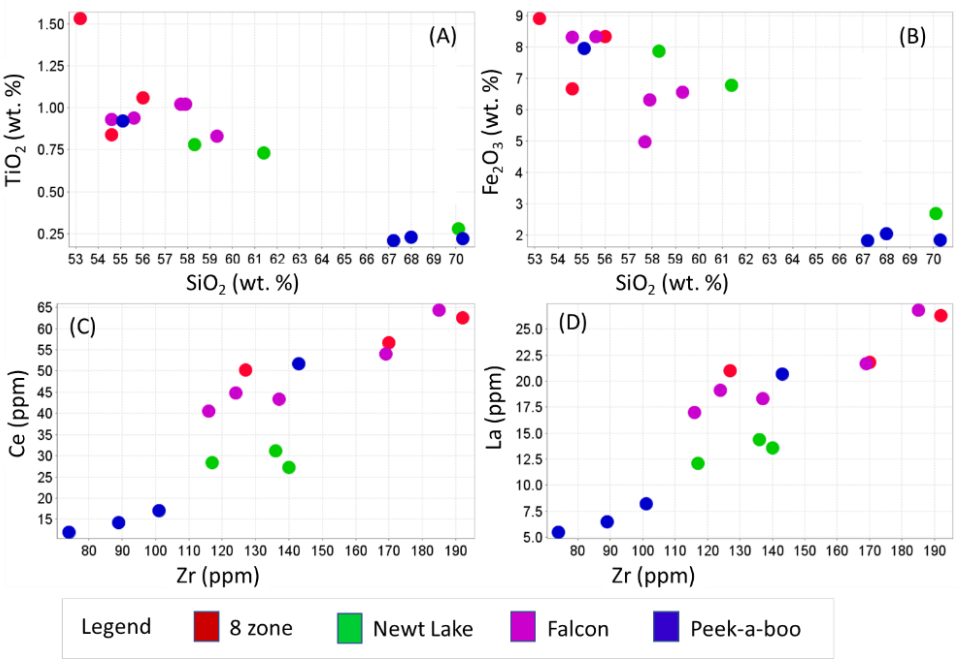

Figure 6.18: Major and trace element scatter plots for the feldspar porphyry unit.

The chaotic unit shows no significant chemical variations between the four zones. The chaotic unit shows poor correlation with REE when plotted against Zr, except for moderate to poor correlation with the La, Ce, and Nd (Fig. 6.20 A-C). Plotting TiO_2 against Zr shows two different trends between the zones. The Newt Lake and Peek-a-Boo zones have a negative slope, whereas the 8 and Falcon zones have a positive slope (Fig. 6.20 D). This trend may indicate two different intrusions. The chaotic unit shows a similar primitive mantle normalized pattern to the feldspar porphyry Group A unit with enriched LREE, negative Nb and Ti anomalies (Fig. 6.21). They also have similar Zr/Ti ratios relative to the feldspar porphyry unit, which would imply a similar geochemical source. This suggests that at feldspar porphyry can be the least altered protolith to the chaotic unit.

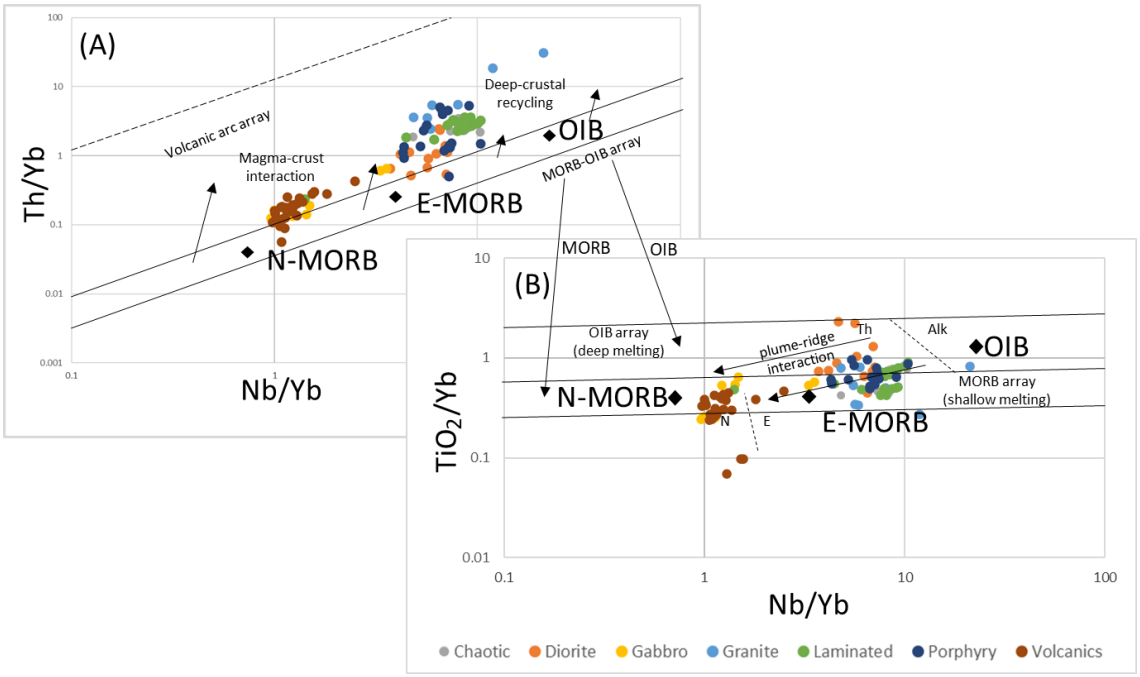

Figure 6.19: Plots to distinguish depleted vs enriched source using Th/Yb (a) and TiO_2/Yb (b) vs Nb/Yb. Modified after Pearce (2008).

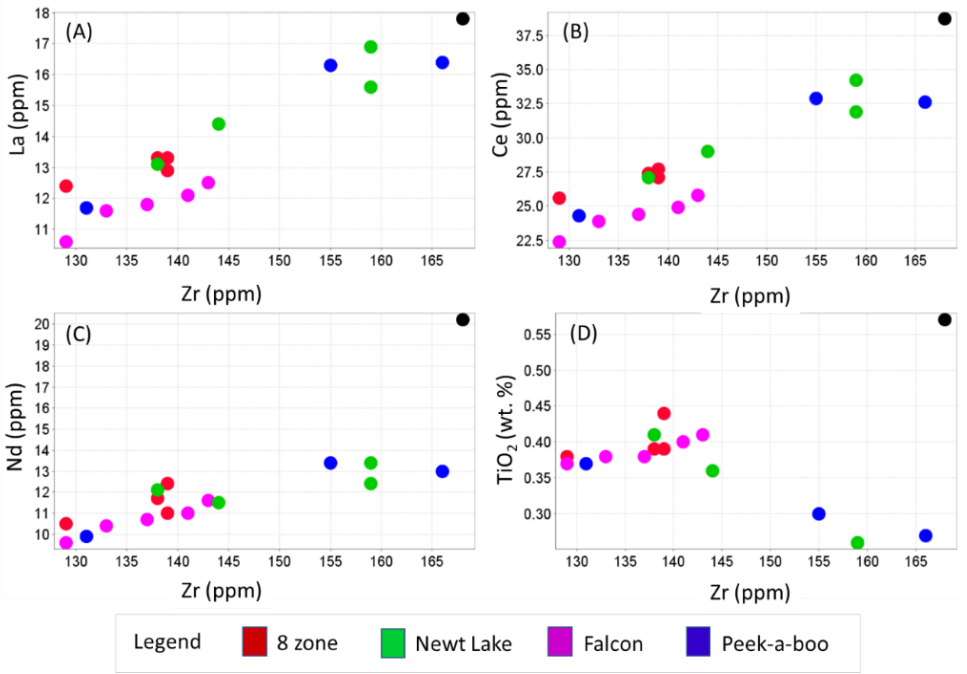

Figure 6.20: Major and trace element scatter plots in the chaotic unit. Black dot is from Peek-a-Boo zone.

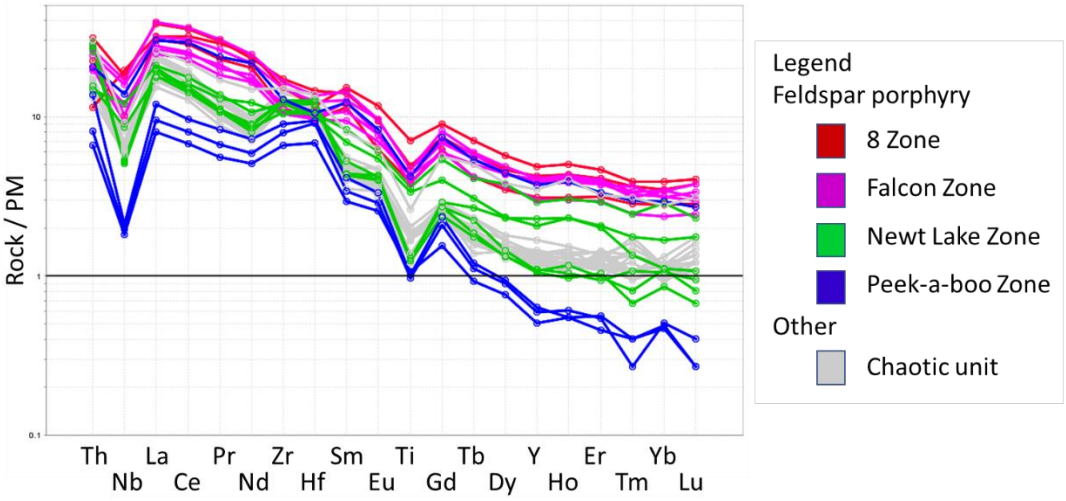

Figure 6.21: Primitive mantle normalized spider diagram for the feldspar porphyry unit per zone relative to the chaotic unit. Primitive mantle normalizing values are from Sun and McDonough (1989).

The Laminated unit shows poor correlation with major elements, but moderate to poor correlation with REE and HFSE plotted against Zr (Fig. 6.22). The Laminated Group A unit has similar primitive mantle normalized patterns to the chaotic unit and the feldspar porphyry Group A unit, with similar Zr/Ti ratios implying a similar geochemical source. The Laminated unit, as stated in section 4.3.2, consists of two groups that either resemble the chaotic unit (Laminated Group A; Fig. 6.23) or the volcanic rocks (Laminated Group B; Fig. 6.8) on a primitive mantle normalized spider diagram. Due to geochemically similar REE patterns, similar values of major and trace elements, the Laminated unit is interpreted to have formed either as (1) a response to deformation such as shearing or faulting, or (2) alteration of heterogenous host rock. During deformation (i.e., faulting or shearing) phases such as feldspar or epidote are replaced by sericite, with the strongest intensity in proximity to the core of deformation, which results in a preferred growth of phyllosilicates subparallel with deformation (Simpson, 1986; Holdsworth et al., 2014). In general, the development of phyllosilicates is widespread, and decreases in intensity and thickness away from the center of deformation (Holdsworth et al., 2014). The preferred mechanism of formation of the Laminated unit is based on the alignment of the phyllosilicates due to deformation as they are commonly found in proximity to

the deformation/shear zones. The variability of the Laminated unit is based on the protolith that is being deformed or altered. Since the protolith (i.e., volcanic rocks, chaotic unit, etc.) can vary, any pre-existing heterogeneity, alteration, or structure that were there pre deformation would have been incorporated into the Laminated unit, giving the Laminated unit variable appearance (Fig. 2.1).

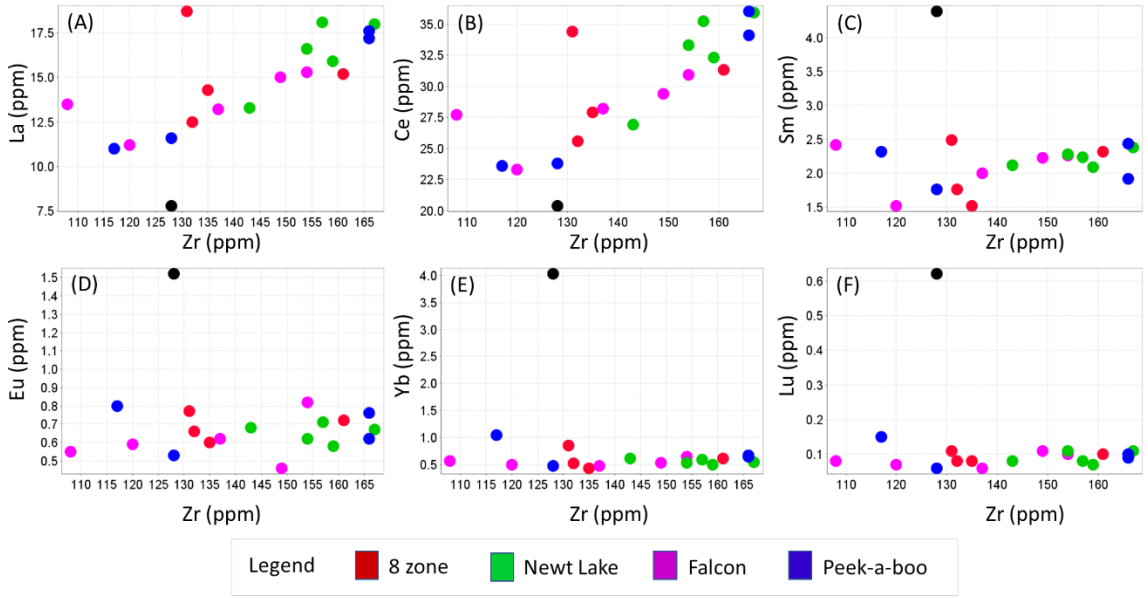

Figure 6.22: Trace element scatter plots in the Laminated unit. Black dot is from Peek-a-Boo zone.

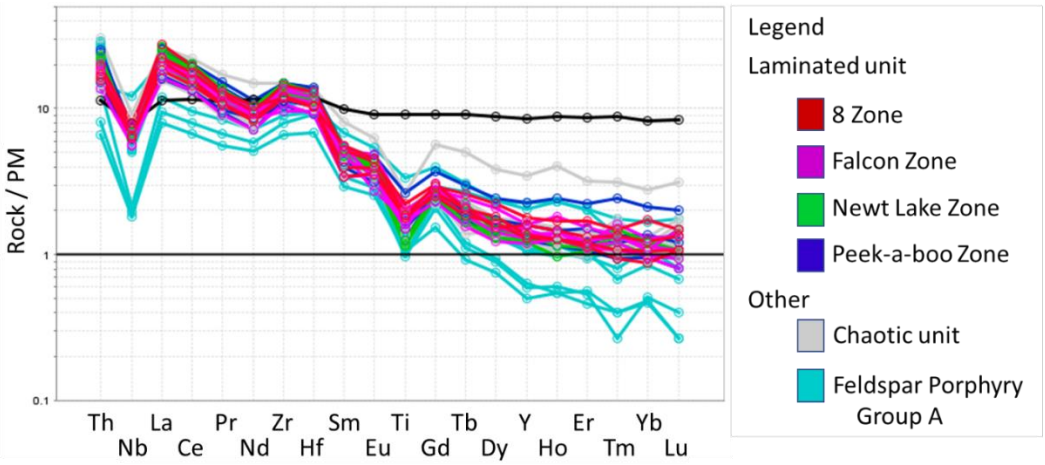

Figure 6.23: Primitive mantle normalized spider diagram for the Laminated unit per zone relative to the chaotic unit. The black line is from the Peek-a-Boo zone. Primitive mantle normalizing values are from Sun and McDonough (1989).

6.2.2 Gain and loss of elements during alteration

Gain and loss of elements during alteration can provide further insight into the formation of alteration during hydrothermal activity. These calculations were performed on the Laminated Group A, and chaotic units in the feldspar porphyry to quantify the gain and losses of elements during alteration of the feldspar porphyry. The mass balance equation used is based on the simplified Gresens mass transfer equation below (Mathieu, 2018).

$$X_n = w \{[(X^b_n)(X^a_{immobile} / X^b_{immobile})] - X^a_n\}$$

where :

- X_n = mass change of component n expressed in g per 100 g of precursor;
- w = weight of precursor (=100g);
- X^a_n, X^b_n = component n in rocks A and B;

The least altered precursor was selected by comparing the primitive mantle normalized patterns, and further assessing the degree of alteration in the samples based on coloration and veining. Once the least altered sample was identified mass balance (gain-loss) calculations were performed for the chaotic and the Laminated units. Within the Falcon zone the chaotic and Laminated units are both proximal to the mineralization and consequently do not provide a distal to proximal expression of the gain-loss alteration relative to the mineralization.

Due to the similarities between the feldspar porphyry, and the host rocks to the chaotic and Laminated Group A units and the similar Zr/Ti ratios, the feldspar porphyry was chosen as the least altered equivalent to the chaotic and the Laminated Group A units (Figs. 6.24 and 6.25). The feldspar porphyry sample was chosen based on the closest primitive mantle normalized spider diagram pattern, which was then narrowed down further based on the photos of the samples that contained

the least amount of veining/alteration. Both the chaotic and the Laminated Group A units show similar gain-loss results to each other, and relative to the least altered feldspar porphyry, except for the LREE (La, Ce, Nd) which show a gain in the chaotic unit but a loss in the Laminated unit. Relative to the feldspar porphyry the chaotic unit gain-loss results show (1) gain in LOI, and Y; (2) the majority of the samples show a gain with a small amount of samples showing a minor loss in Fe_2O_3, MgO, CaO, K_2O, Co, and Sc; (3) loss in Ga; and (4) the majority of the samples show a loss with a small amount of samples showing a minor gain in Na_2O, Sr, La, Ce, and Nd (Fig. 6.24). Relative to the feldspar porphyry the Laminated Group A unit gain-loss results show (1) gain in LOI, and Y; (2) the

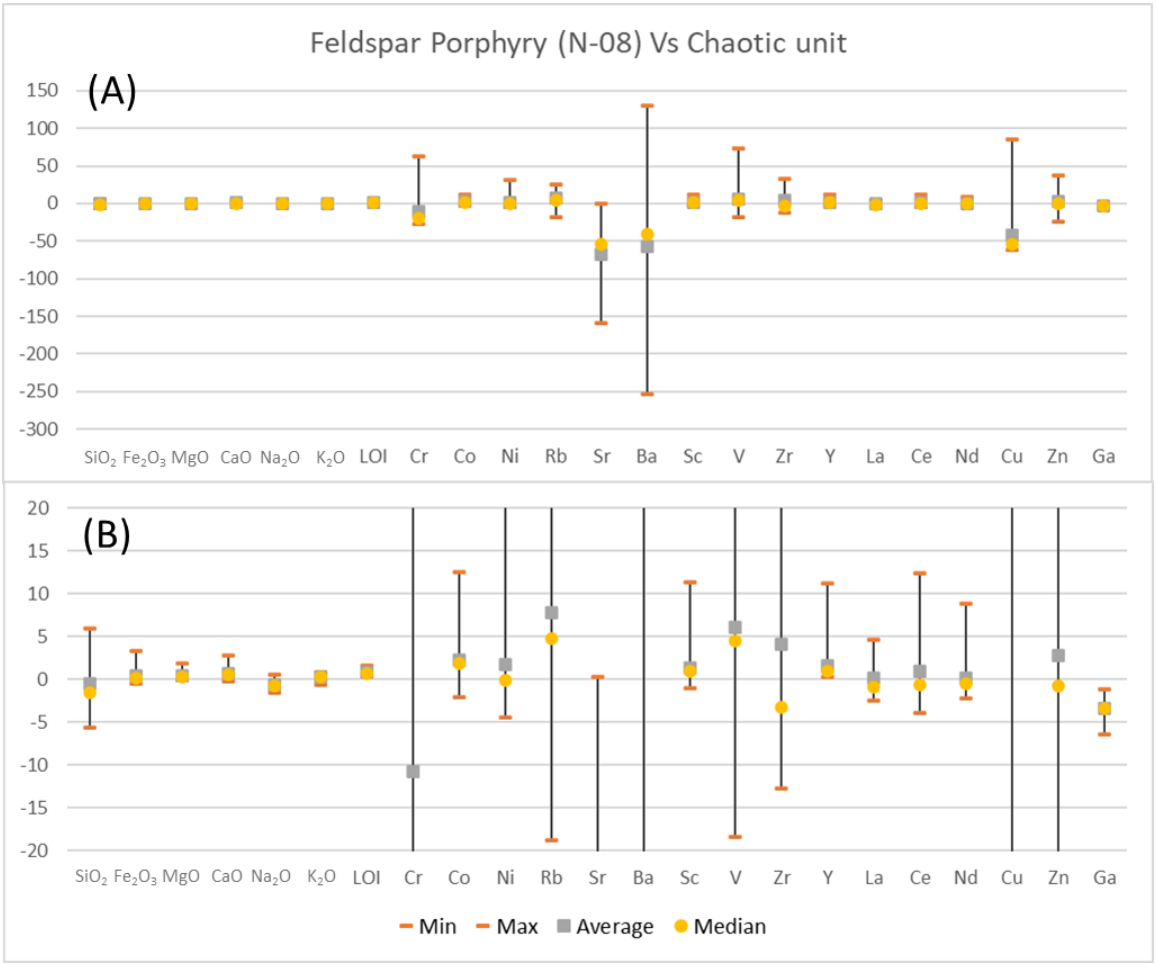

Figure 6.24: Calculated mass change of elements for the chaotic unit relative to a least altered feldspar porphyry (a) and a modified y-axis to show the smaller variations (b).

majority of the samples show a gain with a small amount of samples showing a minor loss in Fe_2O_3, MgO, CaO, K_2O, Co, Sc, La, Ce, and Nd; (3) the majority of the samples show a loss with a small amount of samples showing a minor gain in Na_2O, and Ga (Fig. 6.25).

The breakdown of amphibole in the feldspar porphyry could cause a decrease in Fe_2O_3, CaO and MgO, which can potentially crystalize to biotite, epidote, chlorite, and magnetite (Naney & Swanson, 1980), or portions of the elements be substituted into clinochlore, biotite and minor prehnite, pumpellyite, and Fe-rich sphalerite. The Sr can substitute for various minerals which include plagioclase, hornblende, apatite, epidote minerals, sphene, prehnite, thomsonite and Sr-minerals

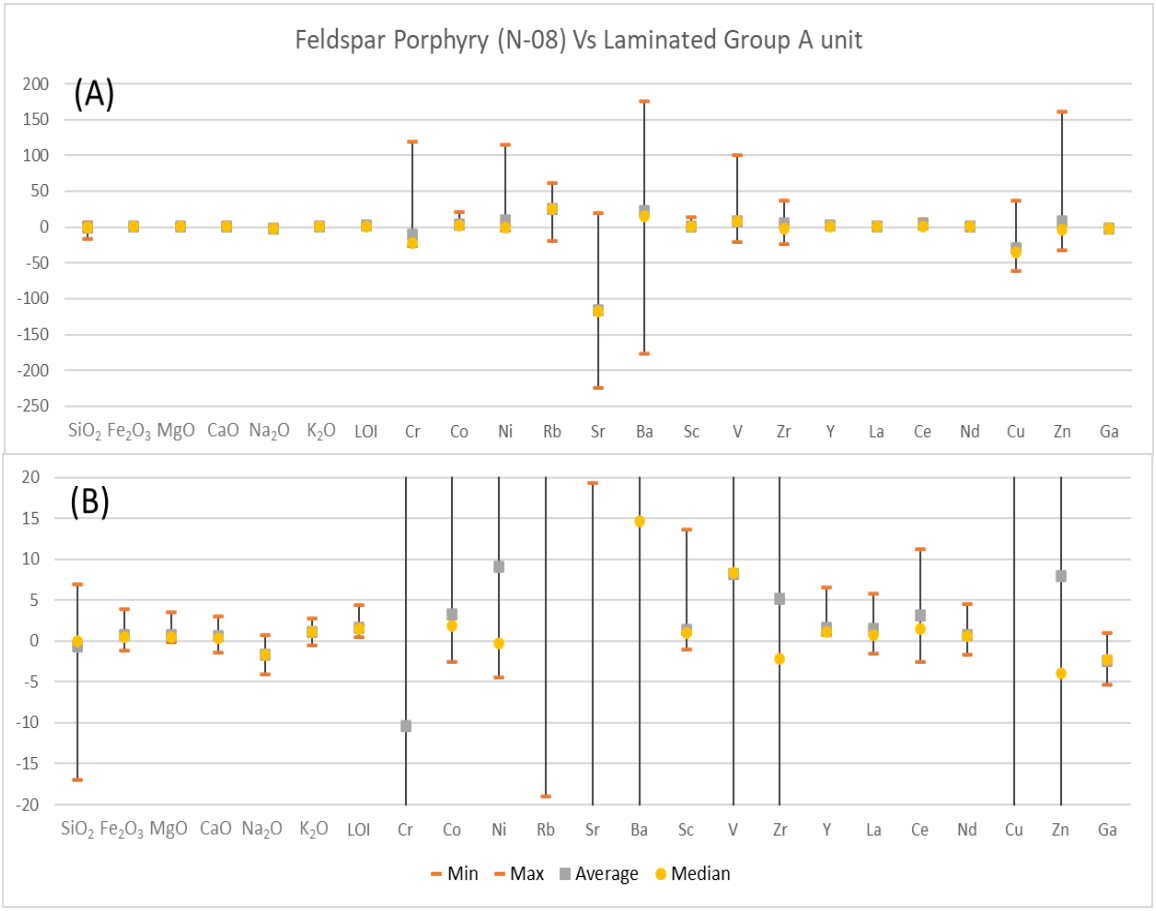

Figure 6.25: Calculated mass change of elements for the Laminated Group A unit relative to a least altered feldspar porphyry (a) and a modified y-axis to show the smaller variations (b).

(Brastad, 1985). Based on petrography the feldspar porphyry contain plagioclase, hornblende with minor titanite and prehnite, and the Laminated Group B unit contains plagioclase, clinozoisite with minor titanite, and prehnite. In plagioclase, clinozoisite, prehnite and titanite Sr^{2+} substitutes for Ca^{2+}, whereas in hornblende Sr^{2+} substitutes for Ca^{2+} and Na^{+} within M4 site (Brastad, 1985). Consequently, the loss of Sr is attributed to breakdown of amphiboles from the feldspar porphyry. The gain in K_2O is attributed to an increased abundance of biotite and muscovite relative to the feldspar porphyry unit. The work by Abdelnasser et al. (2018) on hydrothermal alteration of a granitoid-hosted orogenic gold deposit showed that there is minor mobility of LREE relative to HREE during sericite alteration. The increase of LREE can thus be attributed to sericite alteration found within the Laminated unit. The increase in LOI is attributed to an increased abundance of carbonate alteration associated with the chaotic and Laminated units, and quartz-carbonate veining.

6.3 Paragenesis and mineralization

Based on the comparison of the vein types between the four zones, they are broadly similar, with similar cross-cutting relationships. This suggests that the veins correlate between the zones and the chaotic unit is continuous between the zones. Based on continuity of the chaotic unit a regional paragenesis has been created for all the zones (Fig. 6.26). In the 8 zone the chaotic unit is dominantly found within the footwall of the 8 zone vein, where the mineralized vein is in proximity to the contact of the diorite and the volcanic rocks, with minor chaotic unit intervals in the hanging wall. The Laminated unit is dominantly associated with the quartz veining. The highest abundance and the thickest intervals of the chaotic unit are found within the Falcon zone, with a few sections of the Laminated unit structurally overlying the chaotic unit and cutting the chaotic unit. Within the Newt Lake zone the chaotic unit occupies three discontinuous volcanic horizons. The middle horizon is thickest and is commonly associated with the Laminated unit that either structurally overlies,

underlies, or cuts the chaotic unit. The upper and lower horizon is generally not associated with the Laminated unit. The Peek-a-Boo zone has the thinnest and lowest abundance of the chaotic unit that consists of various thin intervals as opposed to a thick package and is not always associated with the Laminated unit. The changes of the chaotic and the Laminated unit from the 8 and Falcon zones towards the Peek-a-Boo zone likely signify a greater distance away from the most significant mineralization.

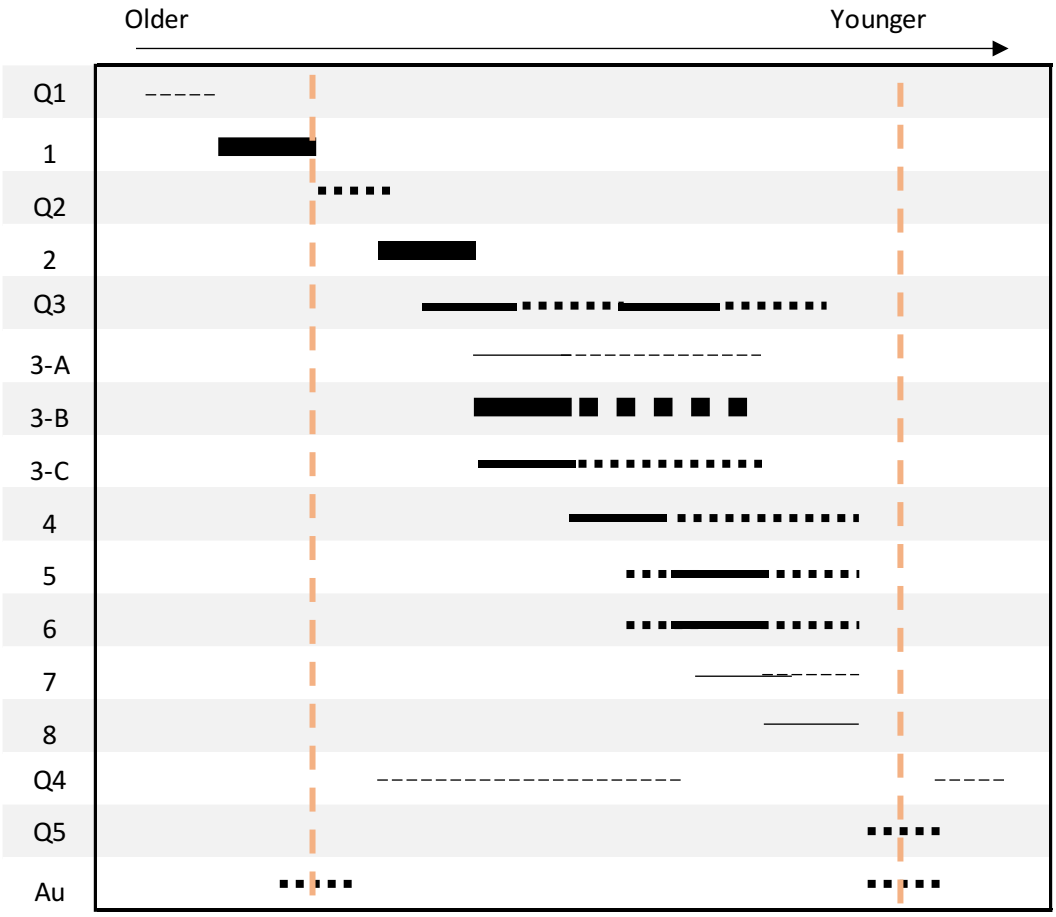

Figure 6.26: Combined paragenesis of veining within the chaotic unit between all the zones. The thicker the line the more abundant the vein type. Solid lines indicate higher confidence of cross-cutting relationships, and dashed lines indicate poorly constrained cross-cutting relationships. The orange dashed vertical line represents the timing of the Laminated unit.

Type 1 veins are the most common and are found within all the zones, and are cut by all the vein types, as well as by the Laminated unit. Type 2 veins are also common between all the zones, and are cut by all the younger vein types, but also cuts the Laminated unit.

Type 3 vein infill is dominated by zeolite (potentially laumontite based on Raman spectrometry) infill which would suggest formation under the zeolite metamorphic facies. The zeolite facies form in conditions between diagenesis and regional metamorphism, and are characterized by mineral assemblages including laumontite, heulandite, or analcite with quartz (Zen, 1961). Natural laumontite is stable up to temperatures of 250°C (Rykl & Pechar, 1984), but laumontite has been synthesized in temperatures ranging between 30°C and 450°C, with the habit dependent on the temperature. The habit changes from long prismatic crystal shapes at low temperatures (<250°C), to equant to platy habit at higher temperatures (Ghobarkar & Schaf, 1998). The habit of zeolite within the type 3 veins from this study is anhedral and cannot be used to assess the temperatures of formation. The type 3 veins are cut by veins that were affected by the greenschist metamorphic facies. In general, greenschist facies is characterized by the mineral assemblage actinolite, chlorite, epidote, calcite, ankerite, quartz and albite (Harte & Graham, 1975). The overprinting of the greenschist facies over the zeolite facies poses a timing problem as the zeolite facies should not have been preserved and instead recrystallized to higher grade greenschist facies minerals. There are a number of possible explanations for this including: (1) metamorphism where the P-T conditions hover around the upper zeolite facies and the lower greenschist facies; (2) the zeolite minerals are not the primary vein infill, but instead are an alteration that occurred post greenschist metamorphic facies during retrograde metamorphism; or (3) by changing the temperature and/or pressure the chemical potential of H_2O relative to that of CO_2 can change the stability of zeolites (Zen, 1961). At high values of H_2O and low values of CO_2 the zeolite facies are stable, but with increasing values of CO_2 the zeolite minerals become unstable (Zen, 1961). Zeolite minerals can be

produced by a number of alteration styles, which include: (A) alteration of calcite and pyrophyllite in the presence of water (Zen, 1961); (B) alteration of calcite, kaolinite and quartz in the presence of water (Zen, 1961); or (C) alteration of plagioclase during albitization (Helmold & Kamp, 1984). Based on this study, the formation of zeolite is likely due to retrograde metamorphism based on the formation of ilmenite, rutile and titanite, which will be discussed later in the Section. It is possible that the primary mineral within type 3 veins was dominated by alkali feldspars and abundance of albitization based on type 3-C veins. Different methods such as x-ray powder diffraction (XRD), and short-wave infrared (SWIR) spectroscopy can be used to better identify the types of zeolites that are present. Since zeolites can form under various geological environments, under variable geochemical and temperature conditions, identifying the proper type of zeolite can constrain the environment of formation of the zeolites.

Within the chaotic unit there are multiple generations of quartz veining, which have been distinguished based on cross-cutting relationships with the host rocks and the vein types. One additional cross-cutting relationship to note is from the Peek-a-Boo zone which has quartz veins along the contact between the granite and the volcanic rocks, as well as quartz veins (possibly Q5 veins) cutting the granite (Fig. 6.27). The quartz veins that cut the granite (Floating Heart Batholith - 2687.26 ± 0.42 Ma) indicate that the veining continued post emplacement of the Peek-a-Boo granite, but the timing of the quartz veins relative to the Laminated unit is currently unknown. The chaotic vein types that would be of higher importance to mineralization are (A) veins altered by chlorite, siderite or white mica (sericite) as they can be associated with quartz vein mineralization (Sillitoe, 2020), (B) contain inclusions of galena and sphalerite as they are associated with gold grades within the mine (Jennifer Moscalli, personal communication, 2022), and (C) veins that have been infilled or overprinted by quartz as gold is hosted within quartz veins. Based on the above criteria all the vein types have potential to be associated with gold mineralization, and they are

commonly associated with various alteration types, sulphides, such as pyrite, pyrrhotite, chalcopyrite and sphalerite, and can be infilled by quartz veining.

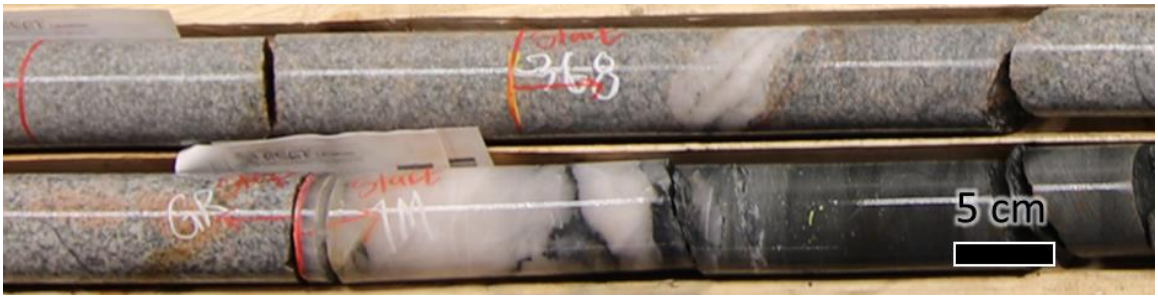

Figure 6.27: Cross-cutting relationships with quartz veins and the lower granite found in Peek-a-Boo zone from hole ERX-2021-75 @ 368m.

There are two forms of sulphides that are found within the Eagle River complex (1) coarse-grained porous anhedral sulphide, and (2) finer grained subhedral to euhedral sulphides. The sulphides can be either pyrite- or pyrrhotite-dominant. Craig and Vokes (1993) suggested that the two forms of sulphides can imply two generations of growth, which includes coarse-grained anhedral sulphide that have an igneous origin, and finer grained subhedral to euhedral grained sulphide that have a metamorphic origin. This is the method of formation assumed to be responsible for the formation of pyrite and pyrrhotite within this study.

6.3.1 Sulphides and gold

Six occurrences of gold were found within the 8 and Falcon zones (Fig. 6.28). The occurrences include (1) 8 zone: hosted in massive pyrite associated with a sheared quartz vein in proximity to a hematite fault. The gold occurs as an inclusion within a pyrite grain (Fig. 6.28 A); (2) Falcon zone 5: hosted in Laminated unit associated with layers of pyrite and boudinaged quartz. The gold occurs along pyrite-pyrite grain boundaries with chalcopyrite and quartz in proximity (Fig. 6.28 B). The composite value for the gold mineralization yielded 1.42 g/t Au over 3.5m, with the interval where the sample was collected yielding 0.16 g/t Au; (3-6) Falcon zone 5: hosted in the Laminated unit

associated with quartz veining and sulphides along vein boundaries. The gold can be found either along pyrite-pyrite grain boundaries associated with sphalerite (Fig. 6.28 C), pyrite-pyrite grain boundaries (Fig. 6.28 D), quartz-clinochlore grain boundaries (6.28 E), or along quartz-pyrite grain boundaries (Fig. 6.28 E). The sample interval yielded 1.72 g/t Au with barren samples above and below the interval. The gold occurrences are consistent with a previous study by Clemson (1989) and SGS in 2017 which showed that gold can occur along gangue-gangue contacts, sulphide grain margins in contact with gangue, pyrite-pyrite grain contacts, inclusions within sulphides and gangue.

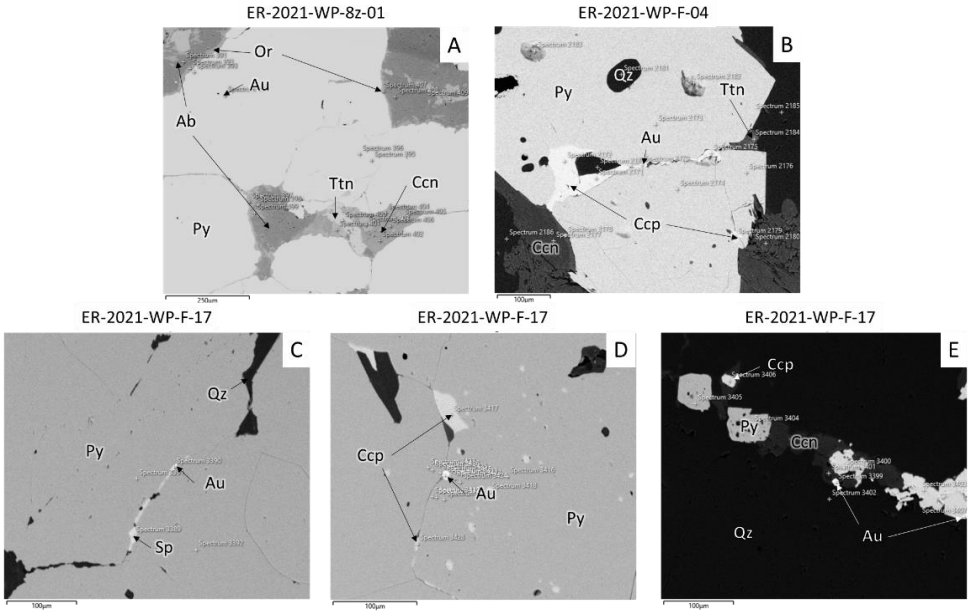

Figure 6.28: SEM images of samples that have Au mineralization. Gold can be situated as an inclusion within a pyrite grain (a), pyrite-pyrite grain boundaries close to chalcopyrite (b), pyrite-pyrite grain boundaries associated with sphalerite (c), pyrite-pyrite grain boundaries (d), and quartz-clinochlore grain boundaries or quartz-pyrite grain boundaries (e). Ab = Albite, Au = Gold, Ccn = Clinochlore, Ccp = Chalcopyrite, Or = Orthoclase, Py = Pyrite, Sp = Sphalerite, Ttn = Titanite, Qz = Quartz.

The gangue minerals are dominated by quartz with minor phyllosilicates. The gold inclusions are associated with either inclusion-poor or inclusion-rich pyrite, whereas the gold along pyrite-pyrite grain boundaries is associated with the inclusion-poor subhedral to euhedral pyrite. Clemson (1989) suggested that the coarser gold grains tend to occur within the core of the quartz veins, whereas finer gold grains are found along narrow micaceous shears, and suggestive of gold mobilization

during deformation. Based on the gold occurrence from this study, gold is commonly found with inclusion-poor pyrite or associated with quartz and/or phyllosilicates (Fig. 6.28). These textures imply depositional traps for Au during syn-metamorphic and syn-deformation events (Dubosq et al., 2018). The vein types associated with sulphides include types 1, Q2, 3-C, 6, Q3 and Q5 veins. Also, gold is associated with quartz and phyllosilicates, which implies an association with quartz veining and deformation. The vein types that have quartz and phyllosilicates associated with them include types Q2, 6, Q3, and Q5 veins. Since gold is hosted within the quartz veins that are parallel to the deformation (i.e., Laminated unit), it suggests that the mineralization is syn deformation.

From the gold occurrences found with this study, the gold is associated with the quartz veins that are parallel to the bands within the Laminated unit, which are the Q2 or Q5 veins. Based on the assay values the entire Laminated unit is not mineralized and contains barren sections (Fig. 6.29). The areas that contain higher Au values are associated with quartz veining, which can either be thin veinlets or thicker veins. Commonly thicker veins carry higher Au values relative to thin veinlets and can have sulphides in proximity. Based on the cross-cutting relationships there are two occurrences of the Laminated unit (1) the Laminated unit that cuts vein type 1, and is cut by subsequent vein types (i.e., vein type 2 and younger); and (2) the Laminated that unit overprints the chaotic unit. This is suggestive of more complex deformation history, with multiple deformation events that have potential to host gold mineralization. Gold transported in fluids will remain in solution until changing chemical conditions trigger precipitation of the metals (Goldfarb & Groves, 2015). The intensity and variability of the chaotic and Laminated units can provide changing conditions for migrating fluids and potential to precipitate metals. The Q1 veins are found to be least prospective as they are discontinuous, have rare occurrences within the zones, have no interactions with the alteration vein types, and there was no gold found within the veins. The Q3 veins crosscut the chaotic unit veining

and occur post the first occurrence of the Laminated unit and have potential to be associated with gold mineralization.

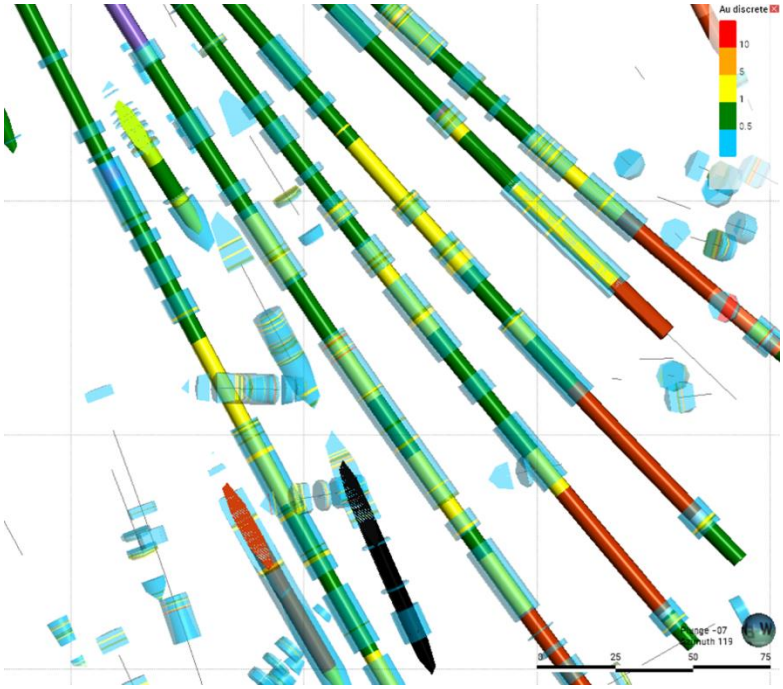

Figure 6.29: Drillholes overlayed with assay values from the Falcon zone (Map courtesy of Wesdome Gold Ltd.). Dark green = volcanic rocks, purple = feldspar porphyry, yellow = Laminated unit, red = chaotic unit.

6.3.2 Constraints on mineralizing conditions

To gain further insight into the mineralization and the conditions of formation of the rocks, the Fe/Mg ratio of the clinochlore can be used. The Fe/Mg ratio of the clinochlore is dominantly controlled by the fluid composition, pH, and temperature (Herdianita, 2022). In general, with decreasing Fe# (Fe/Fe+Mg) in chlorite the temperature of formation of chlorite increases (Herdianita, 2022). To assess the Fe# ratios of clinochlore, the grains were analyzed from the different rock types. The Fe# within the Eagle River complex range from 49 to 59 in the volcanic rocks, 51 to 56 in the gabbro, 47 to 52 in the granite, 59 to 67 in the diorite, 60 to 66 in the feldspar porphyry, 61 to 74 in the chaotic unit, and 49 to 78 in the Laminated unit. The barren rocks have generally lower Fe# relative to the chaotic and Laminated units, which implies lower temperature of

formation for the clinochlore within the chaotic and Laminated units. This suggests that the chaotic and Laminated units formed later and were one of the last units to be formed.

The temperature of formation of host rocks can be further constrained by the formation of titanite, ilmenite, and rutile which are stable at different pressures and temperatures (Meinhold, 2010). Within this study the ilmenite grains with minor inclusions of rutile are anhedral and have a zone of titanite around them that are commonly elongated parallel to the fabric (Fig. 6.30). Commonly the zonation of titanite around ilmenite-rutile grains tends to increase in proximity to all types of alteration within the chaotic unit. This is common throughout all the zones. Based on work by Meinhold (2010) on the P-T conditions for the formation of rutile, titanite and ilmenite showed that rutile is the stable mineral at high pressures (13 kbar @ 550°C and 16 kbar @ 1000°C). At lower pressures and temperatures, the titanite and ilmenite phases are stable, with titanite being stable at lower temperatures (1 kbar at 550°C and 13 kbar at 800°C; Meinhold, 2010). Titanite stability was further constrained by overlaying metamorphic facies which showed that titanite is stable below 1 GPa (10 kbar, 30 km depth) and temperatures below 530°C (Angiboust & Harlov, 2017). Based on the P-T conditions of formation by Mainhold (2010), within Eagle River the ilmenite grains with minor inclusions of rutile formed at higher temperature and pressures, and were subsequently overprinted by titanites that formed at lower temperatures and pressures relative to ilmenite and rutile, which is suggestive of retrograde metamorphism. Yardley et al. (2014) showed different examples of retrograde metamorphism such as replacement of hornblende by chlorite and/or actinolite, and the replacement of plagioclase by sericite or epidote, both of which are found within the Eagle River complex consistent with retrograde metamorphism. Additionally, the zeolite formation within type 3 veins would have formed during the retrograde metamorphism when the temperatures dropped below 250°C.

The gold mineralization within Eagle River is associated with quartz veins that are parallel to the Laminated unit, dominantly as gold trapped between grain boundaries with minor gold as inclusions within pyrite. Within this study the gold is dominantly associated with inclusion-poor sulphides, but can also be associated with inclusion-rich sulphides. There are two occurrences of the Laminated unit which, which occur at the beginning of the formation of the chaotic unit, and a second occurrence post formation of the chaotic unit. Both the chaotic and the Laminated units formed latter relative to rest of the units within Eagle River at lower temperatures and pressures during or post retrograde metamorphism. Both occurrences of the Laminated unit are prospective for gold mineralization.

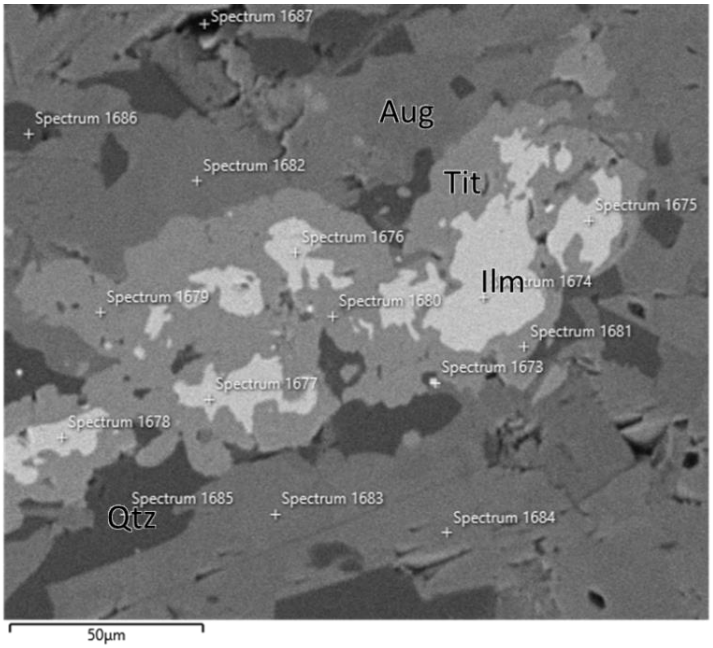

Figure 6.30: Ilmenite being replaced by titanite under SEM from sample ER-2021-WP-F-13. The lighter gray is ilmenite and darker grey around is titanite. The image is taken from Falcon zone. Aug = Aegerine-augite, Tit = Titanite, Ilm = Ilmenite, Qtz = Quartz.

6.4 Deposit type and exploration

The current classification of the Eagle River deposit is an orogenic gold deposit hosted within Archean greenstone belt (Mannard & Ng, 2016; Kilbourne, 2020). In general, orogenic gold deposits consist of an array of quartz-carbonate veins that display vertical continuity with no significant zoning, the ores have Au:Ag ratios > 5, the dominant sulphide mineral is either pyrite or pyrrhotite,

and the mineralization is spatially associated with regional shear zones that occur in greenschist-grade rocks (Robert et al., 2007). Within Eagle River the characteristics that are in favor of orogenic gold deposit include (1) array of quartz-carbonate veins which display vertical continuity containing several mineralized zones that are either hosted in the diorite or volcanic rocks. Along strike the mineralized pods within the quartz-carbonate veins are spaced ~400m apart; (2) the sulphides are dominated by pyrite and/or pyrrhotite with minor galena, sphalerite and chalcopyrite; and (3) the quartz-carbonate veins are hosted within a shear zone (Eagle River Deformation Zone) hosted within Archean Mishibishu Lake greenstone belt. The current metal zonation is not well constrained but based on this study the Au:Ag ratios range from 2.6-37.3, commonly between 5.5-6.5 (n=4 of 6).

A study by Hart and Goldfarb (2005) showed that there are differences between the orogenic and intrusion-related (IR) gold deposits. Intrusion related deposits can be distinguished based on: (1) zoning where the cooling plutons result in concentric metal zones that develop outwards whereas orogenic gold deposits show minimal zoning, except for Hg- and Sb-rich zones in their epizonal parts; (2) diverse deposit styles where fluids exsolved cool quickly in numerous geological settings resulting in veins, stockworks, skarns, hydrothermal breccia, replacements characterized by wide range of gold grades. In contrast, orogenic gold deposits lack diversity of styles and commonly have consistent gold grades; (3) sheeted arrays of parallel, low-sulphide content, single stage quartz veins; (4) metal association where significant copper is lacking and gold correlates with Bi and Te geochemical signatures; (5) pluton features have a “smoking gun” characteristic that indicate generation of hydrothermal and mineralizing fluids, including high volatile contents, evidence of fractionation and fluid exsolution, associated skarns, presence of aplites/pegmatites, tourmaline veins, greisen alteration, and cupola hosted mineralization; (6) redox states that are associated with felsic, ilmenite-series plutons that lack magnetite, have low magnetic susceptibility and low

ferric:ferrous ratios (<0.3); (7) timing of the plutons with the deposits are coeval (±2 m.y.) that develop after the regional metamorphic and deformation episodes.

Within the Eagle River complex the characteristics that are similar to intrusion related deposit include: (1) diversity of deposit styles which include laminated veins (Falcon zone 7), stockwork zone (Falcon zone 5), and hydrothermal breccia found within 8 zone characterized by variable gold grades, and (2) arrays of low-sulphide quartz veins. Although there are some similarities to intrusion related gold, the majority of the characteristics are not in favor of it or are not well constrained. Based on current data the Eagle River is classified as an orogenic gold deposit. Another possibility is to incorporate both deposit types, with an earlier intrusion related mineralization event that has been overprinted by a later hydrothermal event that is orogenic in nature. A study by McDivitt (2016) on gold mineralization within Missanabie-Renabie district showed that the mineralization is interpreted to be both intrusion-related and metamorphic-hydrothermal in origin. Within the Missanabie-Renabie deposit the laminated veins pre-date regional deformation and localized shear zones that created pathways for fluids. These laminated veins formed during an early intrusion-related gold event, with subsequent hydrothermal events are orogenic in nature as a product of metamorphic fluids. To test this hypothesis at the Eagle River complex a better constrained fault and shear model would need to be established as it would provide potential pathways for fluids and any offset along geology.

Finding gold deposits is a challenging task with no direct methods being able to accurately pin point their locations, but using hydrothermal alteration zones can help narrow down the search and utilize minerals such as clay minerals, iron oxides, sericite as indicator minerals for gold occurrences in general (Amer et al., 2016; Lypaczewski et al., 2019). Different deposit types have different alteration zones associated with the model, which can help to narrow down where in the alteration system the assay samples are located. Within Archean intrusion related or orogenic gold deposit the

alteration zones are poorly constrained, with different deposits having variable alterations, which include (i) Hemlo having feldspar (K, Na) and sericite alteration (Cameron & Hattori, 1985); (ii) the Malartic camp ranging from potassic alteration (microcline, albite, phlogopite, quartz, carbonate, pyrite) to potassic-sericite (phengitic white mica, Mg-rich biotite, microcline, albite, quartz, calcite and pyrite; Lypaczewski et al., 2019); (iii) Island Gold mineralization associated with silicic alteration and potassic alteration (Jellicoe, 2019); and (iv) Missanabie-Renabie mineralization associated with saussuritization, phyllic alteration, and retrograde alteration including K-feldspar, hematite, chlorite, titanite and albite (McDivitt, 2016). The alteration type that is common between the deposits is K-feldspar and commonly sericite and albite alteration.

The Eagle River complex contains various types of alteration, including saussuritization, albitization, K-feldspar alteration, sericitisation, sulphidation, silicification, carbonatisation, chloritisation, and tourmalisation. The most common being albitization, K-feldspar alteration, chloritisation and carbonatization. The potassic and hematite alteration is commonly associated with the quartz veining within the mine zone and was noted up to 350m away from the quartz veining. The potassic or hematite alteration intensity is variable and does not always increase towards mineralization. The potassic and hematite alteration is also associated with faults that consist of a series of discontinuous sections that appear in all four zones at different lithological horizons, and commonly cut diabase dykes. Where faults are present, the alteration intensity generally increases towards the fault. Sericite alteration is commonly associated with the Laminated unit and combined can be used as a tool in exploration. The Laminated unit can be categorized based on thickness, alteration intensity and associated minerals (i.e., sulphides or gangue minerals). Since the thickness of the shear zones get thinner away from the center of the deformation, categorizing the Laminated unit can point towards the center of the deformation zone. Also, the thicknesses of the Laminated unit can potentially be used as markers to tell the displacements of the unit that is cut by a younger

fault, which can aid in constraining the fault model. Like the potassic-hematite alteration, the sericite alteration intensity does not consistently increase towards mineralization. Albite alteration is dominantly associated with the chaotic unit, with the thickest and highest intensity associated with the Falcon zone, but it does not consistently increase towards the mineralization. In general, Eagle River has various alteration types associated with the mineralization lithology and mineralization, but they are not always associated with mineralization or increase towards it and hence cannot be used as a reliable vector towards it. Even though alteration intensity does not always increase towards mineralization, it can still be a useful in identifying areas that have higher hydrothermal activity. Combined with the fault and shear model would increase the potential for the areas to host mineralization.

7. Conclusions

Four geochronological samples were taken to help constrain the plutonism within the Eagle River complex. These include the Central pluton (2656.38 ± 0.41 Ma), the Bowman Lake batholith (2658.35 ± 0.41 Ma), the Floating Heart batholith (2687.26 ± 0.42 Ma), and the mine diorite (2716.22 ± 0.41 Ma). These new ages provided a tighter age constraint for the Bowman Lake batholith (previously published age of 2639.0 ± 25 Ma) and the Floating Heart batholith (previously published age of 2693.2 ± 6.9 Ma). Based on the regional comparison (Manitouwadge greenstone belt, Hemlo gold deposit, Missinabie-Renabie deposit, Island gold deposit, Gamitagama greenstone belt, Batchawana greenstone belt) of volcanism and plutonism, the Eagle River rocks formed at a similar time. Within the Eagle River complex the maximum age of mineralization is bound by the mine diorite (2716.22 ± 0.41 Ma) which hosts the mineralization. Based on regional comparison of the mineralization, the mine diorite and the Floating Hearth batholith both overlap which the ages of mineralization in other belts, and the Floating Hearth batholith also overlaps with the peak metamorphism. The maximum age of mineralization within Eagle River is currently undefined and would require additional geochronological dating to constrain it, such as feldspar porphyry or the diabase dykes.

On primitive mantle normalized plots, the Eagle River rocks have either near-flat (i.e. volcanic rocks, gabbro, and Laminated Group B unit) or variably enriched LREE with variably fractionated HREE patterns (i.e., the rest of the rocks). All the rocks have a negative Nb anomaly, which is indicative of a magmatic arc geodynamic setting, this is consistent with the conclusions of Polat et al. (1998). On a La/Yb_{pm} versus Yb_{pm} diagram the rocks plot either within the slab dehydration area, the slab melting area, or overlap between the two fields. The volcanic rocks plot within the slab dehydration area, gabbro dominantly in the slab dehydration field, diorite and feldspar porphyry have a mix

between slab dehydration and slab melting areas, and granite in the slab melting area. This suggests that there was either a switch between slab melting and slab-dehydration in the arc source, melting in the garnet-bearing source rock, or indicates multiple sources at broadly the same time, but further dating would be required to better constrain the timing.

The feldspar porphyry has been subdivided into three groups based on the cross-cutting relationships between the feldspar porphyry and alteration, which include (1) Feldspar porphyry with no or minimal veining; (2A) Feldspar porphyry with veining and alteration that cuts the contact with the volcanic rocks; and (2B) Feldspar porphyry with the veining and alteration that is cut off at the contact with the volcanic rocks. These different cross-cutting relationships are supportive of separate intrusions of the feldspar porphyry unit. Within the Group 2A feldspar porphyry there is a visual change of color in the alteration as it progresses from a reddish coloration (dominated by albite, anorthoclase, quartz and minor prehnite and biotite) within the feldspar porphyry to a greenish-grey (dominated by clinochlore, prehnite, and clinozoisite with minor biotite, pumpellyite, pyrite, and quartz) coloration within the volcanic rocks. The change in coloration is likely due to Fe^{3+}, which can be found as inclusions within albite and anorthoclase giving it a reddish coloration in the feldspar porphyry, or substituted for Al^{3+} within clinochlore, prehnite, or clinozoisite giving it a greenish-grey color. Since the visual appearance of Fe alteration changes based on the rock type that is being altered, it suggests that color alone cannot be used to properly identify the extent of Fe alteration and mineralogy needs to be included as well to map out the extent of alteration. Heather (1986) study showed that the Mishibishu Lake greenstone belt has a spatial and potentially a temporal relationship between the hydrothermal alteration, porphyry dikes and the gold mineralization. Within Eagle River the feldspar porphyry cuts the alteration and also is cut by alteration, which suggests a long-lived hydrothermal system, and a temporal relationship between the feldspar porphyry and hydrothermal alteration. The mineralization cutting the feldspar porphyry

has been noted in the Falcon zone, but felspar porphyry cutting the mineralization was not noted in this study. Establishing the cross-cutting relationship can provide insight into the temporal relationship with the feldspar porphyry and the mineralization.

The feldspar porphyry has geochemical similarities to the chaotic unit, which suggests that the feldspar porphyry may be the least altered equivalent of the chaotic unit. Similarly, the Laminated Group A unit also resembles the chaotic unit and the feldspar porphyry, implying a similar geochemical source. The Laminated unit has two separate primitive mantle normalized patterns which are either similar to the volcanic rocks or the chaotic unit. The preferred mechanism of formation for the Laminated unit is based on the alignment of phyllosilicates as they are commonly found in proximity to the deformation/shear zones. The deformation signature is of two different rock types.

Gain and loss calculations were performed to gain further insight into the formation of the altered units. Relative to the feldspar porphyry the chaotic and Laminated units gain-loss results show (1) gain in LOI, and Y; (2) the majority of the samples show a gain with a small amount of samples showing a minor loss in Fe_2O_3, MgO, CaO, K_2O, Co, and Sc; (3) loss in Ga; and (4) the majority of the samples show a loss with a small amount of samples showing a minor gain in Na_2O, Sr. Additionally, the La, Ce, and Nd which show a gain in the chaotic unit but a loss in the Laminated Group A unit. Some of these differences are attributed to the breakdown of amphiboles in the feldspar porphyry, causing a decrease in Fe_2O_3, MgO, and CaO. These elements can recrystallize to pyroxene, biotite, hornblende, epidote, or magnetite, or be substituted into clinochlore, biotite, prehnite, pumpellyite, or clinozoisite. The gain in K_2O is attributed to an increase in abundance of biotite and muscovite relative to the feldspar porphyry unit. The gain in LOI is attributed to the increased abundance of carbonate alteration associated with the chaotic and Laminated units, and quartz-carbonate veining.

The chaotic unit consists of variable striking veining associated with variable alteration and is found within all four zones. There were eight different vein types found within the chaotic unit based on the infill and alteration type, as well as five different generations of quartz veining, which based on cross-cutting relationships are dominantly unidirectional. Within the Falcon zone the chaotic unit is associated with mineralization that is hosted within the Laminated unit in quartz-carbonate veins, which are parallel to the Laminated unit suggesting that mineralization was syn-deformation. The gold is dominantly found between grain boundaries with minor inclusions within pyrite, consistent with a previous study by Clemson (1989) and SGS in 2017. Based on the gold occurrences from this study, gold is dominantly associated with inclusion-poor pyrite or associated with quartz and/or phyllosilicates. Since the gold is dominantly associated with pyrite grains within this study, it suggests that the presences of sulphides within the drill core can have higher potential for mineralization. There are two occurrences of the Laminated unit, which occur post vein type 1 but pre vein type 2, and a second occurrence of the Laminated unit that overprints the chaotic unit. This is suggestive a more complex deformation history, with multiple deformation events that have potential to host gold mineralization. Based on the Fe# within clinochlore, it suggests that the chaotic and Laminated units were formed later and were one of the last phases to be formed relative to the rest of the rocks.

The Eagle River deposit is classified as a mesothermal orogenic gold deposit hosted within an Archean greenstone belt. The characteristics that are in favor of orogenic gold defined by Robert et al. (2007) include: (1) array of quartz-carbonate veins which display vertical continuity; (2) the sulphides are dominated by pyrite and/or pyrrhotite; (3) hosted within a shear zone hosted within Archean Mishibishu Lake greenstone belt; and (4) Au:Ag metal associations are generally > 5. The deposit does have some characteristics that resemble intrusion related gold as outlined by Hart and

Goldfarb (2005) but these are not well constrained. Since orogenic gold deposits are hosted within quartz-carbonate veins in shear zones, this can define horizons for exploration targets.

Within the Eagle River complex there are various alteration styles that are dominated by albitization, K-feldspar alteration, chloritisation and carbonatization. In general, the alteration intensities do not consistently increase towards the gold mineralization, and are not always mineralized, so they do not serve as reliable vectors. The potassic and hematite alteration is commonly associated with quartz veining within the mine, and is commonly associated with faults, and where present the alteration intensity generally increases towards the hematite faults. Sericite alteration is commonly associated with the Laminated unit, which can be categorized based on thickness, alteration intensity, and associated minerals. The categorized Laminated unit can serve as vectors towards the center of deformation zone or can be used as markers across younger lithologies or faulting.

There are still questions left to be explored which include: (1) with a completed fault and shear model, can alteration halos be used as rough vectors towards mineralization? and (2) is there any dominant orientation trend between the chaotic unit veining, and if there is how it relates to the formation of the unit and potentially mineralization. Now that the chaotic unit veining has been categorized, they can be measured and categorized using tools like the Reflex IQLogger. Compilation of this data could be used to show if any of the vein types have a preferred orientation.

8. References

Abdelnasser, A., Kumral, M., Zoheir, B., Karaman, M., Weihed, P., 2018. REE geochemical characteristics and satellite-based mapping of hydrothermal alteration in Atud gold deposit, Egypt. Journal of African Earth Sciences, Accepted Manuscript, pp.1-26.

Angiboust, S. & Harlov, D.E., 2017. Ilmenite breakdown and rutile-titanite stability in metagranitoids: Natural observations and experimental results. *American Mineralogist*, 102, pp.1696-708.

Akasaka, M., Hashimoto, H., Makino, K., Hino R., 2003. 57Fe Mossbauer and X-ray Rietveld studies of ferrian prehnite from Kouragahana, Shimane Peninsula, Japan. Journal of Mineralogical and Petrological Sciences, 998, pp.31-40.

Amer, R., Mezayen, A.E., Hasanein, M., 2016. ASTER spectral analysis for alteration minerals associated with gold mineralization. Ore Geology Reviews, 75, pp.239-251.

Ayer, J., Amelin, Y., Corfu, F., Kamo, S., Ketchum, J., Kwok, K., Trowell, N., 2002. Evolution of the southern Abitibi greenstone belt based on U-Pb geochronology: autochthonous volcanic construction followed by plutonism, regional deformation and sedimentation. Precambrian Research, 115, pp.63-95.

Bates, W. & Miree, H., 1991. Geologic Report, Mishi Lake Joint Venture Project, Mishibishu Lake, Abbie Lakes Areas, and St. Germain Township, Ontario. *Granges Inc. 72 pages. Internal Report*.

Beakhouse, G.P. & Davis, D.W., 2005. Evolution and tectonic significance of intermediate to felsic plutonism associated with the Hemlo greenstone belt, Superior Province, Canada. 137, pp. 61-92.

Bennet, G. & Thurston, P.C., 1977. Geology of the Pukaskwa River - University River Area, Ontario Division of Mines. *Geoscience Report*, p.153.

Bodnar, R.J., Lecumberri-Sanchez, P., Moncada, D. & Steele-MacInnis, M., 2014. Fluid Inclusions in Hydrothermal Ore Deposits. *Treatise on Geochemistry 2nd Edition*, pp.119-42.

Brastad, K., 1985. Sr Metasomatism, and Partition of Sr Between the Mineral Phases of a Meta-Eclogite from Bjorkedalen, West Norway. TMPM Tschermaks Mineralogische und Petrographische Mitteilungen, 34, pp.87-103.

Brousseau, K., Gauthier, N. & Poirier, S., 2011. *Technical report and pre-feasability study for the Mishi Project (according to Regulation 43-101 and Form 43-101F1)*.

Burrows, D.R. & Spooner, E.T.C., 1987. Generation ofa magmatic H20-CO2 fluid enriched in Au, Mo and W within an Archean sodic granodiorite stock, Mink Lake, northwestern Ontario. *Economic Geology*, 82, pp.1931-57.

Cameron, E.M., 1988. Archean gold: relation to granulite formation and redox zoning m the crust. *Geology*, 16, pp.109-12.

Cameron, E.M. & Hattori, K., 1985. The Hemlo gold deposit, Ontario: A geochemical and isotopic study. Geochimica et Cosmochimica Acta, 49, pp. 2041-2050.

Card, K.D. & Poulsen, K.H., 1998. Geology of Precambrian Superior and Grenville Provinces and Precambrian fossils in North America. *Geological Survey of Canada, Geology of Canada*, 7, pp.13-194.

Card, K.D., Poulsen, K.H. & Robert, F., 1989. The Archean Supetior Province and its lode gold deposits. *Economic Geology Monograph*, 6, pp.11-28.

Chappell, B.W. & White, A.J.R., 2010. Two contrasting granite types: 25 years later. Australian Journal of Earth Sciences, 48(4), pp.489-499

Claoue-Long, J.C., King, R.W. & Kerrich, R., 1990. Archaean hydrothermal zircons in the Abitibi greenstone belt: constraints on the timing of gold mineralisation. *Earth Planetary Science*, 98, pp.109-28.

Clemson, E., 1989. Mineralogical Investigation of Mineralized Rocks from the Central Crude Limited - Hemlo Gold Mines Joint Venture Project. Memorandum, pp.1-17.

Colvine, A.C., 1989. An empirical model for the formation of Archean gold deposits: products of final cratonization of the Superior Province, Canada. *Economic Geology Monograph*, 6, pp.37-53.

Colvine, A.C., Fyon, J.A., Heather, K.B., Marmont, S., Smith, P.M., Troop, D.G., 1988. Archean lode gold deposits in Ontario. *Ontario Geological Survey Miscellanous Paper*, 139, p.136.

Condon, D.J., Schoene, B., McLean, N.M., Bowring, S.A., Parrish, R.R., 2015. Metrology and traceability of U-Pb isotope dilution geochronology (EARTHTIME Tracer Calibration Part I): Geochimica et Cosmochimica Acta, 164, pp.464–480.

Corfu, F. & Grunsky, E.C., 1987. Igneous and Tectonic Evolution of the Batchawana Greenstone Belt, Superior Province: A U-Pb Zircon and Titanite Study. *Journal of Geology*, 95, pp.87-105.

Craig, J.R. & Vokes, F.M., 1993. The metamorphism of pyrite and pyritic ores: an overview. *Mineralogical Magazine*, 57, pp.3-18.

Crowley, J.L, Schoene, B., Bowring, S.A., 2007. U-Pb dating of zircon in the Bishop Tuff at the millennial scale. Geology, 35(12), pp.1123-1126.

Davis, D.W. & Lin, S., 2003. Unraveling the Geologic History of the Hemlo Archean Gold Deposit, Superior Province, Canada: A U-Pb Geochronological Study. 98(51-67).

Dubé, B. & Gosselin, P., 2007. Greenstone-Hosted Quartz-Carbonate Vein Deposits. *Geological Survey of Canada*, pp.49-73.

Dubosq, R., Lawley, C.J.M., Rogowitz, A., Schneider, D.A., Jackson, S., 2018. Pyrite deformation and connections to gold mobility: Insight from micro-structural analysis and trace element mapping. Lithos, Accepted Manuscript, pp.1-57.

Evans, E.L., 1942. Geology of the Mishibishu Lake Area. *Department of Mines*, p.Vol. 49.

Forslund, N., 2020. *Report on 2017 Diamond Drilling: Eagle River Mine Surface Project 100 and Eagle River North Project 105, Point Isacor Township, Sault Ste. Marie Mining District, Province of Ontario, Canada*. Wesdome Gold Mines Ltd.

Forslund, N., 2022. *2020 Diamond Drilling for Surface Exploration Eagle River Mine*. Thunder Bay: Wesdome Gold Mines Ltd.

Ghobarkar, H. & Schaf, O., 1998. Hydrothermal synthesis of laumontite, a zeolite. Microporous and Mesoporous Materials, 23, pp.55-60.

Goldfarb, R.J., Baker, T., Dube, B., Groves, D.I., Hart, C.J.R., Gosselin, P., 2005. Distribution, Character, and Genesis of Gold Deposits in Metamorphic Terranes. *Society of Economic Geologists*, 100th Anniversary Volume, pp.407-50.

Goldfarb, R.J. & Groves, D.I., 2015. Orogenic gold: Common or evolving fluid and metal sources through time. *U.S. Geological Survey*, pp.2-26.

Graham, C., 1983. The epidote jigsaw. Nature, 305, pp.279.

Groves, D., Barnicoat, A. C., Barley, M., Cassidy, K. F., Fare, R. J., Hagemann, S. G., Ho, S. E., Hronsky, J. M. A., Mikucki, E. J., Mueller, A. G., Mcnaughton, N., Perring, C. S., Ridley, J. R., & Vearncombe, J. R., 1992. Sub-greenschist to granulite-hosted Archean lode-gold deposits of the Yilgarn Craton: a depositional continuum from deep-sourced hydrothermal fluids in the crustal-scale plumbing systems. *J.E. Glover and S.E Ho (Editors), The Archaean: Terrains, Processes and Metallogeny. Geol. Dep. (Key Centre) and Univ. Extension. Univ. West. Aust.*, 22, pp.325-37.

Groves, D.I., Goldfarb, R.J., Gebre-Mariam, M., Hagemann, S.G., Robert F., 1998. Orogenic gold deposits: A proposed classification in the context of their crustal distribution and relationship to other gold deposit types. *Ore Geology Reviews*, pp.7-27.

Groves, D.I., Goldfarb, R.J., Robert, F. & Hart, C.J.R., 2003. Gold Deposits in Metamorphic Belts: Overview of Current Understanding, Outstanding Problems, Future Research, and Exploration Significance. *Economic Geology*, 98, pp.1-29.

Groves, D.I, Ridley, J.R., Bloem, E.M.J., Mintesnot, G., Hagemann, S., Hronsky, J.M.A., Knight, J.T., McNaughton, N.J., Ojala, J., Vielreicher, R.M., McCuaig, T.C., Holyland, P., 1995. Lode-gold deposits of the Yilgarn Block: Products of Late-Archean crustal-scale overpressured bydrothermal systems. *Journal of Geological Society of London*.

Hanes, J.A., Archibald, D.A. & Hodgson, C.J., 1992. Dating of Archean auriferous quartz vein deposits in the Abitibi greenstone belt, Canada: 40Ar/39Ar evidence for a 70- to 100-m.y. time gap between plutonism-metamorphism and mineralization. *Economic Geology*, 87, pp.1849-61.

Hart, C.J. & Goldfarb, R.J., 2005. Distinguishing intrusion-related from orogenic gold systems. *Yukon Geological Survey*.

Harte, B. & Graham, C.M., 1975. The Graphical Analysis of Greenschist to Amphibolite Facies Mineral Assemblages in Metabasites. Journal of Petrology, 16(2), pp.347-370.

Hawkesworth, C.J., Turner, S.P., McDermott, F., Peate, D.W., van Calsteren, P., 1997. U-Th Isotopes in Arc Magmas: Implications for Element Transfer from the Subducted Crust. *Science*, 276, pp.551-55.

Heather, K.B., 1986. Mineralization of the Mishibishu Lake Greenstone Belt. Miscellaneous Paper 132.

Herdianita, N.R., 2022. Variation of Fe and Mg in Hydrothermal Altered Chorite. Proceedings, pp.1-5.

Hiess, J., Condon, D.J., McLean, N., Roble, S.R.,2012. 238U/235U Systematics in terrestrial uranium-bearing minerals. Science (New York, N.Y.), 335, pp.1610-4.

Hodgson, C.J., Hamilton, J.V. & Hanes, J.A., 1989. The late emplacement of gold in the Archean Abitibi greenstone belt: a consequence of thermal equilibration following collisional orogeny. *Geological Asscіation of Canada; Mineral Association of Canada*, 14, p.A45.

Hofmeister, A.M. & Rossman, G.R., 1984. Determination of Fe3+ and Fe2+ concentrations in feldspar by optical absorption and EPR spectroscopy. Physics and Chemistry of Minerals, 11, pp.213-224.

Holdsworth, R.E., Stewart, M., Imber, J., Strachan, R.A., 2014. The structure and rheological evolution of reactivated continental fault zones: a review and case study. Geological Society, London, Special Publications, 184, pp.115-137.

Jackson, J.E., 2000. Mishibishu Lake Area High Density Regional Lake Sediment and Water Geochemical Survey, Northern Ontario. Open File Report 6039, pp.74.

Jackson, S.L., Beakhouse, G.P. & Davis, D.W., 1998. Regional Geological Setting of the Hemlo Gold Deposit; an Interim Progress Report. Open File Report 5977, pp.121.

Jaffey, A.H., Flynn, K.F., Glendenin, L.E., Bentley, W.C., and Essling, A.M., 1971, Precision measurements of half-lives and specific activities of 235U and 238U: Physical Review C, 4, pp. 1889-1906.

Jamielita, R.A., Davis, D.W. & Krogh, T.E., 1990. U-Pb evidence for Abitibi gold mineralization postdating greenstone magmatism and metamorphism. *Nature*, 346, pp.831-34.

Jellicoe, K., 2019. *Structural Controls and Deformation History of the Orogenic Island Gold Deposit, Michipicoten Greenstone Belt, Ontario*. Waterloo: University of Waterloo Masters Paper.

Keller, R.J., 1989. *The evolution of the Mishibishu greenstone belt, near Wawa, Ontario*. Electronic Theses and Dissertations 3985.

Kerrich, R., Goldfarb, R., Groves D., Garwin, S., Jia, Y., 2000. The characteristics, origins, and geodynamic settings of supergiant gold metallogenic provinces. *Science in China (Series D)*, 43, pp.1-68.

Kerrich, R. & Cassidy, K.F., 1994. Temporal relationships of ldoe gold mineralization to accretion, magmatism, metamorphism and deformation - Archean to present: A review. Ore Geology Reviews, 9, pp. 263-310.

Kerrich, R. & Wyman, D.A., 1993. The mesothermal gold-lamprophyre association: Significance for an accretionary geodynamic setting, supercontinent cycles, and metallogenic processes. *Mineral Petrology, 51, pp.147-172*.

Kilbourne, M., 2020. *Technical Report on the Wawa property Sault Ste. Marie Mining Division, Ontario, pp.1-56*.

Krogh, T.E., 1973. A Low-Contamination Method for Hydrothermal Dissolution of Zircon and Extraction of U and Pb for Isotopic Age Determinations. *Geochimica et Cosmochimica Acta, 37, pp. 485-494*.

Krogh, T.E. & Turek, A., 1981. Precise U-Pb zircon ages from the Gamitagama greenstone belt, southern Superior Province. *Canadian Journal of Earth Sciences, 19(4), pp.859-867*.

Laouar, R, 2002. Petrogenetic and metallogenitic studies of the tertiary igenous complexes of northeast Algeria: A stable isotope study. Thesis for doctoral d-etat for University Badji Mokhtar Annaba, pp.1-188.

Lodge, R.W.D., 2012. Winston Lake and Manitouwadge Revisited: Modern views of two Volcanogenic Massive Sulphide (VMS)- endowed greenstone belts. A field trip guidebook; *Ontario Geological Survey, Open File Report 6282, pp.34*.

Ludden, J., Hubert, C. & Gariepyt, C., 1986. The tectonic evolution of the Abitibi greenstone belt of Canada, 123, pp. 153-166.

Lypaczewski, P., Rivard, B., Gaillard, N., Perrouty, S., Piette-Lauziere, N., Berube, C.L., Linnen, R.L., 2019. Using hyperspectral imaging to vector towards mineralization at the Canadian Malartic gold deposit, Quebec, Canada. Ore Geology Reviews, 111, pp.102945.

Mathieu, L., 2018. Quantifying Hydrothermal Alteration: A Review of methods. Geosciences, 8, pp. 245-272.

Mannard, G. & Ng, P., 2016. *Technical report for the Eagle River Mining Complex including the Eagle River Gold Mine, the Mishi Gold Mine and related infrastructure*. pp. 1-84.

McDivitt, J.A., 2016. Gold Mineralization in the Missanabie-Renabie District of the Wawa Subprovince (Missanabie, Ontario, Canada). Thesis for Master of Science in Geology in Laurnetian University.

Meinhold, G., 2010. Rutile and its applications in earth sciences. *Earth-Science Reivews*, pp.1-28.

Mercier-Langevin, P., Gibson, H.L., Hannington, M.D., Goutier, J., Monecke, T., Dube, B., Houle, M.G., 2013. A Special Issue on Archean Magmatism, Volcanism, and Ore Deposits: Part 2. Volcanogenic Massive Sulfide Deposits. 109(1).

Michaud, M., 2019. *Eagle River Complex*. [Online] Available at: https://www.wesdome.com/operations/eagle-river/default.aspx.

Mills, A.J. & Sandeman, H.A.I., 2017. Lithogeochemistry of mafic intrusive rocks from the Bonavista Penninsula, Avalon Terrane, Northeastern Newfoundland. Geological Survey, Report 17-1, pp.19-39.

Mordaunt, P., 1986. Geology Report: Magnacon Project, Sault Saint Marie, pp.1-20.

Moyen, J.F., 2009. High Sr/Y and La/Yb ratios: The meaning of the "adakitic signature". Lithos, 112, pp.556-574.

Muir, T.L., 2003. Structural evolution of the Hemlo greenstone belt in the vicinty of the world-class Hemlo gold deposit Journal. 40, pp. 395-430.

Nakano, S., Makino, K., Yoshida, I., Maniwa, K., Sawada, K., Sakashita, F., Kohno, T., 2019. Combined influences of iron-oxides and micropores on reddish coloration of alkali feldspars in granitic rocks. Journal of Geological Sciences, Japan, 125(10), pp.759-773.

Naney, M. & Swanson, S.E., 1980. The effect of Fe and Mg on crystallization in granitic systems. American Mineralogist, 65, pp.639-653.

Pearce, J.A., 1996. A User's Guide to Basalt discrimination diagrams. *Trace Element Geochemistry of Volcanic Rocks: Applications for Massive Sulphide Exploration*, 12, pp.79-113.

Pearce, J.A., 2008. Geochemical fingerprinting of oceanic basalts with applications to ophiolite classification and the search for Archean oceanic crust. Lithos, 100, pp.14-48.

Pearce, J.A., Harris, N.B. & Tindle, A.G., 1984. Trace Element Discrimination Diagrams for the Tectonic Interpretation of Granitic Rocks. *Journal of Petrology*, 25, Part 4, pp.956-83.

Pearce, J.A. & Peate, D.W., 1995. Tectonic implications of the composition of volcanic arc magmas. *Annual Review of Earth Planet Science*, 23, pp.251-85.

Percival, J.A., Sanborn-Barrie, M., Skulski, T., Stott, G.M., Helmsteadt, H., White, D.J., 2006. Tectonic evolution of the western Superior Province from NATMAP and Lithoprobe studies. *Canadian Journal of Earch Science*, 43(7), pp.1085-1117.

Percival, J.A., Skulski, T., Sanborn-Barrie, M., Stott, G., Leclair, A.D., Corkery, T., Boily, M., 2012. Geology and tectonic evolution of the Superior Province, Canada; in Tectonic Styles in Canada: THe Lithoprobe Perspective. Special Paper 49, pp. 321-378.

Polat, A., 2009. The geochemistry of Neoarchean (ca. 2700 Ma) tholeiitic basalts, transitional to alkaline basalts, and gabbros, Wawa Subprovince, Canada: Implications for petrogenetic and geodynamic processes. Precambrian Research, 168, pp.83-105.

Polat, A. & Kerrich, R., 2000. Magnesian andesites, Nb-enriched basalt-andesites, and adakites from late-Archean 2.7-Ga Wawa greenstone belts, Superior Province, Canada: implications for late Archean subduction zone petrogenetic processes. *Department of Geological Sciences, University of Saskatchewan, 141, pp.36-52*.

Polat, A., Kerrich, R. & Wyman, D.A., 1998. The late Archean Schreiber-Hemlo and White River-Dayohessarah greenstone belts, Superior Province: collages of oceanic plateaus, oceanic arcs, and subduction-accretion complexes. *Tectonophysics*, 289(4), pp.295-326.

Robert, F., Brommecker, R., Bourne, B., Dobak, P.J., Mcewan, C., Rowe, R.R., Zhour, X., 2007. Models and exploration methods for major gold deposit types. Proceedings of Exploration 07: Fifth Decennial International Conference on Mineral Exploration, pp. 691-711.

Robert, F., Poulsen, H.K., Cassidy, K.F. & Hodgson, C.J., 2005. Gold metallogeny of the Superior and Yilgarn Cratons. *Economic Geology 100th Anniversary Volume,* pp.1001-33.

Rock, N.M.S., Groves, D.I. & Perring, C.S., 1989. Gold, lamprophyes and porphyries: What does their association mean? *Economic Geology Monograph*, 6, pp.609-25.

Ross, P. & Bedard, J.H., 2009. Magmatic affinity of modern and ancient subalkaline volcanic rocks determined from trace element discriminant diagrams. *Canadian Journal of Earth Sciences*, 46 (11), pp.823-39.

Rykl, D. & Pechar, F., 1984. Study relating to temperature stability of the natural laumontite zeolite. Crystal Research and Technology, 19(4), pp.549-555.

Sage, R.P., 1994. Geology of Michipicoten Greenstone Belt. Open File Report 5888, pp.592.

Saunders, J.A., Hofstra, A.H., Goldfarb, R.J. & Reed, M.H., 2014. Geochemistry of Hydrothermal Gold Deposits. *Treatise on Geochemistry 2nd Edition*, pp.383-424.

Schmitz, M.D., Schoene, B., 2007, Derivation of isotope ratios, errors and error correlations for U-Pb geochronology using 205Pb-235U-(233U)-spiked isotope dilution thermal ionization mass spectrometric data: Geochemistry, Geophysics, Geosystems, 8, pp. 1-20.

Sillitoe, R.H., 2020. Gold Deposit Types: An Overview. *Society of Economic Geologists*, 10, pp.1-28.

Simpson, C., 1986. Fabric development in brittle-to-ductile shear zones. Pure and Applied Geophysics, 124, pp. 269-288.

SRK, 2022. *Technical Report for the Eagle River Gold Mining Complex, Canada, pp.1-246*.

Stott, G.M., Corkery, M.T., Percival, J.A., Simard, M., Goutier, J., 2010. Project Units 98-006 and 98-007. A Revised Terrane Subdivision of the Superior Province. Open File Report 6260, pp. 20-1 to 20-10.

Sun, S.S., & McDonough, W.F., 1989. Chemical and isotopic systematics of oceanic basalts: implications for mantle composition and processes. Geological Society, London, Special Publications, 42, pp.313-345.

Thurston, P.C., 2015. Greenstone Belts and Granite−Greenstone Terranes: Constraints on the Nature of the Archean World, 42, pp. 437-484.

Thurston, P.C., Williams, H.R., Sutcliffe, R.H. & Stott, G.M., 1991. Geology of Ontario. Special Volume 4, Part 1, pp.26-57.

Turek, A., Heather, K.B., Sage, R.P. & Van Schmus, W.R., 1996. U-Pb zircon ages for the Missanabie-Renabie area and their relation to the rest of the Michipicoten greenstone belt, Superior Province, Ontario, Canada. *Precambrian Research*, 76, pp.191-211.

Turek, A., Keller, R. & Van Schmus, W.R., 1990. U-Pb zircon ages of volcanism and plutonishm in the Mishibishu greenstone belt neare Wawa, Ontario. *Canadian Journal of Earth Science*, 24, pp. 649-656.

Turek, A., Sage, R.P. & Van Schmus, W.R., 1992. Advances in the U-Pb zircon geochronology of the Michipicoten greenstone belt, Superior Province, Ontario. *Canadian Journal of Earth Sciences*, 29(6), pp.1154-65.

Turek, A., Smith, P.E. & Schmus, W.R., 1982. Rb-Sr and U-Pb ages of volcanism and granite emplacement in the Michipicoten belt - Wawa, Ontario, 19, pp. 1608-1626.

Turek, A., Smith, P.E. & Schmus, W.R., 1984. U-Pb zircon ages and the evolution of the Michipicoten plutonic - volcanic terrane of the Superior Province, Ontario. Canadian Journal of Earth Sciences, 21, pp.457-464.

Varol, E., Temel, A., Yurur, T., Gourgaud, A., Bellon, H., 2014. Petrogenesis of the Neogene bimodal magmatism of the Galatean Volcanic Province, Central Anatolia, Turkey. Journal of Volcanology and Geothermal Research, 280, pp.14-29.

Wall, C.J., Scoates, J.S., Weis, D., Friedman, R.M., Amini, M., Meurer, W.P., 2018. The Stillwater Complex: Integrating Zircon Geochronological and Geochemical Constraints on the Age, Emplacement History and Crystallization of a Large, Open-System Layered Intrusion. Journal of Petrology, 59, pp. 153–190.

Wang, X. & Greenwood, H.J., 1988. An experimental study of the equilibrium: Grossular + Clinochlore = 3 Diopside + 2 spinel + 4 H2O. Canadian Mineralogist, 26, pp.269-281.

Williams, H.R., Heather, G.M., Muir, K.B. & Sage, R.P., 1991. Wawa Subprovince. Special Volume 4, Part 1, pp. 485-539.

Wong, L., Davis, D.W., Krogh, T.E. & Robert, F., 1991. U-Pb zircon and futile chronology of Archean greenstone formation and gold mineralization in the Val d'Or region, Quebec. *Earth Planetary Science Letters*, 104, pp.325-36.

Wyman, D.A. & Kerrich, R., 1988. Alkaline magmatism, major structures, and gold deposits: Implications for greenstone belt gold metallogeny. *Economic Geology*, 83, pp.451-58.

Yardley, B.W.D., Rhede, D., Heinrich, W., 2014. Rates of Retrograde Metamorphism and their Implications for the Rheology of the Crust: an Experimental Study. Journal of Petrology, 55(3), pp.623-641.

Zaleski, E., Breemen, O.V. & Peterson, V.L., 1999. Geological evolution of the Manitouwadge greenstone belt and Wawa-Quetico subprovince boundary, Superior Province, Ontario, constrained by U-Pb zircon dtes of supracrustal and plutonic rocks. 36, pp.945-66.

Zen, E., 1961. The zeolite facies: An interpretation. American Journal of Science, 259, pp.401-409.

Zweng, P.L., Mortensen, J.K. & Dalrymple, G.B., 1993. Thermochronology of the Camflo Gold Deposit, Malartic, Quebec: implications for magmatic underplating and the formation of gold-bearing quartz veins. *Economic Geology*, 88, pp.1700-21.

Appendix A: Major and trace element lithogeochemistry

Table 4.1: Major (wt. %) and trace element (ppm) data for the chaotic unit.

SampleID	LOD	8z-33	8z-34	8z-35	8z-36	F-28	F-29	F-30	F-31	F-32	N-13	N-14	N-15	N-16	P-18	P-19	P-20	P-21
SiO_2	0.01	67.80	69.50	68.40	70.10	71.20	69.60	70.70	70.40	70.60	67.60	73.60	69.00	71.30	69.60	70.50	64.90	69.60
TiO_2	0.01	0.44	0.39	0.39	0.38	0.38	0.37	0.40	0.38	0.41	0.36	0.26	0.41	0.26	0.27	0.37	0.57	0.30
Al_2O_3	0.01	15.75	15.80	15.75	15.55	15.75	14.85	16.00	15.75	15.85	15.30	15.00	16.60	14.60	15.90	15.95	15.10	14.40
Fe_2O_3	0.01	3.78	3.06	2.85	2.77	2.88	2.86	2.98	3.17	2.96	2.99	2.08	3.07	2.63	2.47	3.06	5.78	3.05
MnO	0.01	0.05	0.06	0.05	0.04	0.03	0.03	0.02	0.02	0.03	0.03	0.03	0.04	0.04	0.05	0.05	0.08	0.04
MgO	0.01	1.46	1.24	1.08	1.20	0.97	1.36	1.10	1.17	1.27	1.13	0.63	1.13	0.64	0.83	1.10	2.62	0.93
CaO	0.01	6.22	3.88	3.97	4.04	3.78	3.35	4.65	3.19	4.47	3.03	3.31	4.55	3.18	3.62	4.58	5.09	3.47
Na_2O	0.01	3.71	4.48	4.29	4.16	4.91	3.92	4.22	5.60	4.07	4.92	4.57	4.67	4.19	3.99	3.55	3.58	4.32
K_2O	0.01	0.22	0.92	1.20	1.26	0.94	1.54	0.76	0.88	0.97	1.42	0.94	1.10	1.40	1.65	1.08	1.44	1.09
P_2O_5	0.01	0.11	0.11	0.11	0.11	0.11	0.11	0.12	0.11	0.11	0.10	0.09	0.11	0.09	0.09	0.11	0.12	0.11
LOI	0.01	0.91	1.39	1.00	0.91	0.94	1.84	0.84	1.08	0.88	1.19	0.86	1.14	1.06	1.80	1.17	1.28	0.96
Sum		100.49	100.89	99.17	100.59	101.95	99.88	101.85	101.79	101.68	98.13	101.44	101.88	99.44	100.33	101.57	100.62	98.32
Cr	10	31	8	9	9	23	10	13	13	10	9	50	10	8	3	6	90	22
Co	1	9	6	7	6	7	7	9	11	7	7	3	7	4	3	7	17	6
Ni	1	18	5	5	4	4	5	5	7	7	3	1	2	1	1	1	36	10
Rb	0.2	8	26	28	43	31	39	29	30	41	42	36	34	44	53	30	43	29
Sr	0.1	318	300	269	275	238	211	283	185	284	233	274	342	222	165	272	205	221
Cs	0.01	0.27	0.76	0.49	0.59	1.87	2.70	0.77	0.75	1.50	0.82	0.94	0.82	0.81	0.91	1.12	1.27	0.72
Ba	0.5	69.2	305.0	459.0	349.0	238.0	231.0	245.0	142.5	212.0	344.0	308.0	300.0	274.0	327.0	147.0	315.0	229.0
Sc	1	6.0	4.0	4.0	4.0	4.0	4.0	4.0	4.0	4.0	4.0	2.0	4.0	2.0	2.0	4.0	14.0	3.0
V	5	57.0	47.0	41.0	41.0	37.0	33.0	38.0	40.0	39.0	37.0	16.0	44.0	16.0	15.0	38.0	104.0	24.0
Ta	0.1	0.40	0.30	0.40	0.30	0.30	0.30	0.30	0.30	0.30	0.30	0.40	0.30	0.30	0.40	0.30	0.50	0.40
Nb	0.1	5.76	4.66	4.68	4.47	4.37	4.12	4.37	4.12	4.61	4.96	4.82	4.61	4.53	4.75	4.62	6.54	4.72
Zr	2	139.0	138.0	139.0	129.0	137.0	129.0	141.0	133.0	143.0	144.0	159.0	138.0	159.0	166.0	131.0	168.0	155.0
Hf	0.1	3.31	3.27	3.08	3.23	3.27	3.11	3.38	3.08	3.24	3.41	3.77	3.33	3.83	4.22	3.51	4.24	4.02
Th	0.05	1.25	1.34	1.49	1.28	1.27	1.11	1.24	1.28	1.29	1.43	1.94	1.44	1.91	2.08	1.40	2.56	1.95
U	0.05	0.34	0.35	0.38	0.37	0.35	0.31	0.37	0.37	0.32	0.44	0.54	0.38	0.51	0.47	0.38	0.66	0.46
Y	0.1	7.6	6.3	6.1	5.3	5.7	5.3	5.9	5.7	6.1	5.7	6.6	6.3	5.7	5.4	5.5	15.8	6.3
La	0.1	12.90	13.30	13.30	12.40	11.80	10.60	12.10	11.60	12.50	14.40	16.90	13.10	15.60	16.40	11.70	17.80	16.30
Ce	0.1	27.70	27.40	27.10	25.60	24.40	22.40	24.90	23.90	25.80	29.00	34.20	27.10	31.90	32.60	24.30	38.70	32.90
Pr	0.02	3.04	2.73	3.07	2.83	2.70	2.41	2.66	2.64	2.83	3.12	3.48	2.92	3.34	3.41	2.68	4.67	3.63
Nd	0.1	12.40	11.70	11.00	10.50	10.70	9.60	11.00	10.40	11.60	11.50	13.40	12.10	12.40	13.00	9.90	20.20	13.40
Sm	0.03	2.48	2.07	2.21	2.21	2.06	1.90	1.94	1.78	1.99	2.28	2.17	2.30	2.03	2.07	1.56	3.57	2.05
Eu	0.02	0.79	0.68	0.67	0.52	0.57	0.59	0.59	0.59	0.70	0.64	0.79	0.61	0.55	0.61	0.57	1.06	0.70
Gd	0.05	1.72	1.52	1.68	1.37	1.49	1.33	1.48	1.53	1.40	1.65	1.51	1.55	1.47	1.65	1.42	3.35	1.57
Tb	0.01	0.25	0.22	0.25	0.18	0.17	0.17	0.18	0.15	0.19	0.20	0.21	0.21	0.20	0.20	0.20	0.54	0.20
Dy	0.05	1.32	1.24	1.24	1.01	1.17	1.01	1.09	1.05	1.15	1.00	1.13	0.94	1.06	1.04	1.04	2.82	1.03
Ho	0.01	0.25	0.21	0.21	0.19	0.18	0.18	0.19	0.20	0.19	0.19	0.22	0.24	0.17	0.22	0.20	0.66	0.23
Er	0.03	0.65	0.59	0.60	0.52	0.68	0.62	0.58	0.57	0.65	0.62	0.69	0.54	0.46	0.52	0.53	1.54	0.68
Tm	0.01	0.12	0.10	0.13	0.09	0.08	0.08	0.08	0.08	0.07	0.10	0.10	0.07	0.10	0.08	0.11	0.23	0.08
Yb	0.03	0.56	0.57	0.57	0.45	0.49	0.48	0.52	0.56	0.53	0.54	0.58	0.54	0.53	0.59	0.58	1.36	0.65
Lu	0.01	0.10	0.09	0.09	0.09	0.08	0.08	0.07	0.07	0.07	0.11	0.12	0.07	0.09	0.10	0.08	0.23	0.13
Cu	1	4.0	0.5	0.5	0.5	9.0	8.0	40.0	150.0	5.0	2.0	5.0	20.0	17.0	5.0	29.0	47.0	10.0
Zn	2	25.0	41.0	54.0	28.0	31.0	68.0	18.0	22.0	43.0	30.0	19.0	68.0	61.0	60.0	62.0	77.0	36.0
Mo	1	0.50	1.00	1.00	1.00	0.50	0.50	2.00	16.00	0.50	1.00	1.00	0.50	0.50	0.50	0.50	1.00	1.00
Ag	0.5	0.25	0.25	0.25	0.25	0.25	0.25	0.25	0.25	0.25	0.25	0.25	0.25	0.25	0.25	0.25	0.25	0.25
Tl	0.02	0.01	0.01	0.03	0.04	0.05	0.04	0.04	0.07	0.05	0.05	0.05	0.07	0.09	0.06	0.05	0.09	0.05
Pb	2	1.00	1.00	2.00	1.00	1.00	12.00	1.00	2.00	1.00	1.00	1.00	2.00	3.00	1.00	1.00	1.00	1.00
Sn	1	0.60	0.60	0.70	0.50	0.60	0.50	0.60	0.25	0.50	0.70	0.80	0.80	0.80	0.70	0.50	0.90	0.70
Sb	0.05	0.03	0.03	0.03	0.03	0.03	0.03	0.03	0.03	0.03	0.03	0.03	0.03	0.03	0.03	0.03	0.03	0.03
Ga	0.1	19.40	20.10	20.60	21.30	19.10	17.20	19.30	16.80	19.90	21.50	19.10	20.90	19.60	20.60	18.40	18.30	19.90
Ge	5	1.00	1.20	1.00	1.00	0.80	0.80	0.70	0.90	0.90	1.20	1.30	1.10	0.90	0.90	0.70	1.20	1.00
As	0.1	0.20	0.30	0.10	0.10	1.40	36.80	0.30	1.50	0.30	0.10	0.20	0.10	0.30	0.05	0.10	0.05	0.10
W	1	0.25	1.10	0.90	0.60	1.10	1.50	0.70	3.90	0.25	0.60	0.50	0.50	0.50	0.60	0.70	0.50	0.25
Bi	0.01	0.01	0.01	0.01	0.01	0.08	0.01	0.01	0.02	0.01	0.01	0.01	0.02	0.02	0.03	0.01	0.02	0.01
La/Sm (PM)		3.36	4.15	3.89	3.63	3.70	3.61	4.03	4.21	4.06	4.08	5.03	3.68	4.97	5.12	4.85	3.22	5.14
Gd/Yb (PM)		2.54	2.21	2.44	2.52	2.52	2.29	2.35	2.26	2.19	2.53	2.15	2.37	2.29	2.31	2.03	2.04	2.00
Nb/Nb*		0.36	0.27	0.27	0.28	0.29	0.31	0.28	0.27	0.28	0.26	0.22	0.27	0.22	0.21	0.31	0.30	0.22
Ti/Ti*		0.50	0.52	0.48	0.52	0.50	0.55	0.55	0.54	0.57	0.45	0.34	0.51	0.36	0.35	0.58	0.39	0.40
Zr/Zr*		1.74	1.94	1.95	1.85	2.02	2.09	2.11	2.14	2.06	1.95	2.04	1.81	2.19	2.22	2.31	1.37	2.05

Table 4.2: Major (wt. %) and trace element (ppm) data for the Laminated unit.

SampleID	LOD	8z-41 (A)	8z-42 (A)	8z-43 (A)	8z-44 (A)	F-34 (A)	F-35 (A)	F-36 (A)	F-37 (A)	F-38 (A)	N-17 (A)	N-18 (A)	N-19 (A)	N-20 (A)	N-21 (A)	P-25 (A)	P-26 (A)	P-28 (A)	P-29 (A)	P-27 (B)
SiO_2	0.01	67.00	69.10	65.20	69.10	70.50	67.70	69.70	67.10	63.60	71.30	69.30	67.60	70.50	69.90	61.70	69.80	70.40	71.00	52.80
TiO_2	0.01	0.41	0.39	0.48	0.40	0.38	0.39	0.36	0.33	0.44	0.25	0.27	0.40	0.26	0.25	0.57	0.37	0.33	0.27	1.96
Al_2O_3	0.01	15.10	15.75	19.00	16.05	15.55	15.40	14.35	14.40	17.05	14.35	15.35	16.10	14.55	14.50	14.00	14.80	14.50	15.65	12.85
Fe_2O_3	0.01	3.84	2.90	1.88	3.29	3.71	3.23	2.91	4.82	4.17	2.02	2.86	3.24	2.99	3.36	5.93	3.23	3.17	2.77	16.55
MnO	0.01	0.03	0.09	0.01	0.04	0.03	0.02	0.04	0.04	0.04	0.04	0.04	0.04	0.05	0.03	0.09	0.06	0.06	0.03	0.23
MgO	0.01	1.97	1.18	1.00	1.25	1.58	1.08	2.33	1.88	3.51	0.64	0.97	1.28	0.83	0.75	3.90	1.76	1.52	0.79	4.30
CaO	0.01	4.49	4.43	5.65	4.08	3.15	4.02	3.42	3.46	2.04	3.22	3.41	3.79	3.32	2.80	5.71	3.74	5.29	2.87	8.91
Na_2O	0.01	5.34	3.67	3.82	3.63	0.88	2.92	1.44	1.75	3.48	3.64	4.51	3.13	3.72	3.94	3.77	1.32	2.43	5.74	2.33
K_2O	0.01	0.29	1.85	2.47	2.05	3.65	1.95	2.85	2.19	2.00	1.85	0.98	2.48	1.74	1.97	1.04	3.44	1.48	1.20	0.22
P_2O_5	0.01	0.14	0.13	0.14	0.13	0.12	0.11	0.11	0.09	0.12	0.09	0.09	0.11	0.10	0.09	0.13	0.11	0.12	0.09	0.18
LOI	0.01	1.20	1.93	1.59	1.30	2.33	1.85	1.87	2.23	3.63	1.78	0.79	1.58	1.51	1.63	4.26	1.81	1.63	1.32	0.87
Sum		99.86	101.50	101.30	101.38	101.92	98.72	99.43	98.33	100.15	99.24	98.63	99.81	99.63	99.28	101.17	100.51	100.99	101.79	101.24
Cr	10	18	6	5	5	18	9	6	19	7	13	8	7	7	6	135	6	47	10	41
Co	1	14	7	3	7	10	11	6	9	13	3	4	9	4	5	23	9	6	3	43
Ni	1	29	4	4	4	22	7	5	16	6	1	1	4	2	1	108	6	20	1	56
Rb	0.2	8	36	63	48	67	55	64	48	61	66	48	61	52	39	27	84	44	46	5
Sr	0.1	286	198	255	283	94	251	148	142	144	217	335	190	193	133	221	122	186	217	149
Cs	0.01	0.49	0.77	0.58	0.71	0.97	1.08	0.80	0.65	1.81	1.39	0.64	1.34	1.02	0.82	1.01	1.94	1.41	0.92	0.24
Ba	0.5	141.0	485.0	222.0	281.0	260.0	305.0	357.0	281.0	523.0	381.0	244.0	380.0	388.0	437.0	296.0	474.0	289.0	347.0	56.3
Sc	1	5.0	4.0	4.0	4.0	5.0	4.0	4.0	4.0	5.0	2.0	2.0	4.0	2.0	2.0	15.0	4.0	4.0	2.0	34.0
V	5	69.0	42.0	50.0	41.0	48.0	41.0	39.0	42.0	53.0	15.0	14.0	43.0	16.0	13.0	120.0	40.0	32.0	13.0	406.0
Ta	0.1	0.30	0.30	0.40	0.30	0.30	0.30	0.30	0.30	0.40	0.30	0.30	0.30	0.30	0.30	0.30	0.30	0.40	0.40	0.40
Nb	0.1	5.20	4.44	5.65	4.59	4.05	4.73	4.02	3.96	5.36	4.52	4.90	4.84	4.58	4.79	4.62	4.38	5.29	4.84	5.66
Zr	2	131.0	135.0	161.0	132.0	149.0	137.0	120.0	108.0	154.0	159.0	167.0	143.0	154.0	157.0	117.0	128.0	166.0	166.0	128.0
Hf	0.1	3.18	3.19	4.00	3.23	3.66	3.37	2.79	2.97	3.99	3.65	4.01	3.51	3.74	3.44	2.86	3.22	4.12	4.32	3.66
Th	0.05	1.46	1.39	1.66	1.34	1.71	1.40	1.16	1.57	1.53	1.77	1.90	1.41	1.93	1.82	1.92	1.28	2.07	2.13	0.96
U	0.05	0.44	0.34	0.41	0.36	0.49	0.44	0.31	0.45	0.44	0.47	0.50	0.36	0.46	0.42	0.43	0.34	0.48	0.52	0.25
Y	0.1	8.1	6.2	7.2	5.9	7.3	5.9	5.4	6.2	6.7	5.5	6.2	6.0	5.8	6.1	10.4	5.7	7.2	6.0	38.6
La	0.1	18.70	14.30	15.20	12.50	15.00	13.20	11.20	13.50	15.30	15.90	18.00	13.30	16.60	18.10	11.00	11.60	17.60	17.20	7.80
Ce	0.1	34.40	27.90	31.30	25.60	29.40	28.20	23.30	27.70	30.90	32.30	35.90	26.90	33.30	35.20	23.60	23.80	36.00	34.10	20.40
Pr	0.02	3.57	2.96	3.39	2.91	3.30	2.99	2.52	3.07	3.44	3.24	3.73	3.05	3.38	3.77	2.70	2.62	4.19	3.82	3.10
Nd	0.1	14.00	11.50	12.90	11.10	12.60	12.40	9.70	11.60	13.10	12.30	13.80	11.30	12.80	13.30	11.70	9.80	15.40	14.20	15.50
Sm	0.03	2.49	1.52	2.32	1.76	2.23	2.00	1.52	2.42	2.26	2.09	2.38	2.12	2.28	2.24	2.32	1.76	2.44	1.92	4.39
Eu	0.02	0.77	0.60	0.72	0.66	0.46	0.62	0.59	0.55	0.82	0.58	0.67	0.68	0.62	0.71	0.80	0.53	0.76	0.62	1.52
Gd	0.05	1.75	1.57	1.81	1.50	1.67	1.53	1.38	1.82	1.62	1.50	1.56	1.54	1.48	1.54	2.21	1.40	1.54	1.63	5.43
Tb	0.01	0.28	0.22	0.22	0.20	0.26	0.20	0.17	0.23	0.23	0.20	0.24	0.23	0.18	0.20	0.32	0.18	0.21	0.19	0.99
Dy	0.05	1.64	1.33	1.14	1.22	1.54	1.04	0.91	1.13	1.18	0.98	1.05	1.23	0.96	1.06	1.78	1.10	1.28	1.08	6.48
Ho	0.01	0.28	0.21	0.24	0.21	0.30	0.23	0.21	0.23	0.21	0.16	0.19	0.23	0.21	0.21	0.40	0.19	0.24	0.21	1.45
Er	0.03	0.81	0.54	0.63	0.57	0.74	0.55	0.53	0.59	0.57	0.51	0.53	0.59	0.56	0.53	1.07	0.51	0.73	0.58	4.12
Tm	0.01	0.11	0.07	0.10	0.08	0.10	0.09	0.08	0.10	0.12	0.09	0.10	0.11	0.08	0.10	0.18	0.07	0.10	0.09	0.65
Yb	0.03	0.85	0.43	0.61	0.52	0.53	0.47	0.49	0.56	0.64	0.49	0.54	0.61	0.53	0.59	1.04	0.47	0.67	0.64	4.03
Lu	0.01	0.11	0.08	0.10	0.08	0.11	0.06	0.07	0.08	0.10	0.07	0.11	0.08	0.11	0.08	0.15	0.06	0.09	0.10	0.62
Cu	1	9.0	37.0	0.5	4.0	14.0	51.0	15.0	53.0	109.0	17.0	26.0	27.0	18.0	39.0	59.0	58.0	32.0	5.0	75.0
Zn	2	14.0	59.0	10.0	29.0	25.0	16.0	58.0	25.0	41.0	34.0	29.0	57.0	61.0	58.0	66.0	193.0	31.0	48.0	157.0
Mo	1	0.50	1.00	1.00	0.50	1.00	0.50	1.00	1.00	1.00	1.00	0.50	1.00	1.00	0.50	1.00	3.00	1.00	0.50	1.00
Ag	0.5	0.25	0.25	0.25	0.25	0.25	0.25	0.25	0.25	0.25	0.25	0.25	0.25	0.25	0.25	0.25	0.25	0.25	0.25	0.25
Tl	0.02	0.02	0.04	0.10	0.07	0.11	0.07	0.14	0.04	0.01	0.05	0.06	0.14	0.12	0.04	0.04	0.11	0.07	0.01	0.06
Pb	2	1.00	2.00	2.00	1.00	6.00	1.00	2.00	3.00	1.00	1.00	1.00	2.00	1.00	8.00	1.00	2.00	1.00	1.00	3.00
Sn	1	0.25	0.90	0.90	0.25	0.60	0.25	0.70	0.50	0.90	0.70	0.70	0.50	1.20	0.70	0.50	1.00	0.60	0.70	1.10
Sb	0.05	0.03	0.03	0.03	0.03	0.03	0.03	0.03	0.03	0.03	0.03	0.03	0.03	0.03	0.03	0.03	0.03	0.03	0.03	0.03
Ga	0.1	23.30	19.40	25.00	20.50	21.50	21.50	18.00	19.40	23.10	19.90	21.00	20.70	20.20	19.80	15.90	18.30	18.70	19.30	21.60
Ge	5	1.30	0.90	1.10	1.10	2.00	0.80	0.70	0.90	0.60	0.90	1.00	1.00	1.00	0.80	0.90	1.10	1.00	0.80	1.60
As	0.1	1.80	0.20	0.70	0.05	0.20	0.20	0.20	0.60	0.40	0.30	0.05	0.20	0.30	0.20	0.50	0.05	0.10	0.05	0.05
W	1	0.60	1.50	3.60	1.60	2.50	5.10	3.60	2.50	0.70	0.70	0.50	0.50	0.60	1.00	0.25	1.40	0.50	0.60	1.70
Bi	0.01	0.01	0.01	0.01	0.01	0.01	0.01	0.01	0.02	0.03	0.02	0.01	0.01	0.02	0.04	0.01	0.01	0.01	0.02	0.01
La/Sm (PM)		4.85	6.08	4.23	4.59	4.35	4.27	4.76	3.61	4.38	4.92	4.89	4.05	4.71	5.22	3.06	4.26	4.66	5.79	1.15
Gd/Yb (PM)		1.70	3.02	2.45	2.39	2.61	2.69	2.33	2.69	2.09	2.53	2.39	2.09	2.31	2.16	1.76	2.46	1.90	2.11	1.11
Nb/Nb*		0.19	0.23	0.29	0.28	0.20	0.29	0.28	0.22	0.26	0.22	0.20	0.27	0.21	0.19	0.34	0.29	0.23	0.21	0.71
Ti/Ti*		0.47	0.59	0.55	0.58	0.46	0.54	0.59	0.38	0.55	0.34	0.34	0.53	0.34	0.32	0.59	0.56	0.40	0.36	0.94
Zr/Zr*		1.54	2.24	2.04	2.07	1.95	1.90	2.16	1.41	1.96	2.17	2.02	2.02	1.97	1.99	1.55	2.13	1.87	2.20	1.07

Table 4.3: Major (wt. %) and trace element (ppm) data for the diorite unit.

SampleID	LOD	8z-11 (A)	8z-16 (A)	G4 (A)	8z-37 (A)	8z-38 (A)	F-01 (B)	F-12 (B)	F-33 (B)	8z-12 (B)	8z-26 (B)	8z-39 (B)	8z-40 (B)
SiO_2	0.01	65.90	61.20	65.00	58.30	61.70	51.10	53.60	47.30	56.50	53.00	53.40	52.80
TiO_2	0.01	0.65	0.89	0.65	0.94	0.97	1.75	1.07	1.50	0.87	0.36	1.27	0.36
Al_2O_3	0.01	14.75	15.65	14.95	15.35	15.00	19.00	15.10	17.70	15.85	19.90	18.20	20.30
Fe_2O_3	0.01	5.35	6.89	5.41	6.80	6.51	7.99	8.31	11.95	5.49	4.38	7.04	5.06
MnO	0.01	0.07	0.09	0.07	0.10	0.09	0.09	0.12	0.11	0.08	0.06	0.10	0.07
MgO	0.01	2.75	4.04	2.79	4.96	3.53	3.68	6.21	3.99	5.77	4.67	4.69	4.21
CaO	0.01	5.05	6.86	4.92	7.26	6.24	9.94	7.74	10.90	10.10	10.00	9.13	9.89
Na_2O	0.01	4.27	3.89	3.94	4.17	4.29	3.58	3.05	3.10	4.22	4.00	3.75	4.61
K_2O	0.01	0.91	0.50	1.04	0.32	0.89	0.55	0.69	0.58	0.57	0.94	0.78	0.64
P_2O_5	0.01	0.17	0.27	0.16	0.31	0.32	0.73	0.37	0.09	0.25	0.06	0.57	0.09
LOI	0.01	1.25	1.22	0.98	1.55	1.45	1.84	2.11	2.06	1.56	1.92	1.99	1.84
Sum		101.18	101.59	99.99	100.14	101.06	100.34	98.46	99.34	101.34	99.38	100.99	99.95
Cr	10	90	120	101	202	93	30	240	24	70	70	126	64
Co	1	16	22	19	26	21	29	33	47	25	20	26	22
Ni	1	54	87	55	120	72	68	170	124	148	124	118	115
Rb	0.2	22	11	27	8	24	15	20	17	16	31	23	19
Sr	0.1	303	422	324	409	387	561	323	414	399	564	409	561
Cs	0.01	1.11	0.97	1.21	0.40	1.03	0.90	1.47	2.16	0.54	0.91	0.83	2.81
Ba	0.5	217.0	171.5	259.0	126.5	182.5	100.0	108.0	83.9	93.2	113.5	118.5	127.0
Sc	1	10.0	12.0	10.0	15.0	13.0	13.0	17.0	23.0	19.0	10.0	15.0	13.0
V	5	94.0	129.0	105.0	160.0	135.0	405.0	176.0	572.0	158.0	76.0	185.0	90.0
Ta	0.1	0.60	0.40	0.50	0.40	0.50	0.30	0.30	0.20	0.30	0.10	0.40	0.10
Nb	0.1	9.40	8.30	8.77	8.24	9.24	4.40	5.90	3.04	4.50	2.00	6.78	1.82
Zr	2	192.0	152.0	179.0	139.0	230.0	44.0	77.0	36.0	37.0	20.0	65.0	27.0
Hf	0.1	4.60	3.30	4.21	3.26	4.95	1.10	1.80	0.95	1.20	0.60	1.53	0.69
Th	0.05	3.39	1.69	3.33	1.31	1.60	0.53	0.95	0.34	1.12	0.51	0.52	0.32
U	0.05	0.95	0.42	0.86	0.40	0.44	0.15	0.28	0.09	0.27	0.07	0.15	0.08
Y	0.1	15.6	14.3	15.0	15.2	16.8	11.2	11.9	7.8	13.2	5.8	12.5	5.9
La	0.1	23.10	20.00	23.20	18.50	20.40	11.40	13.10	6.10	11.30	6.30	12.90	5.20
Ce	0.1	52.50	46.50	52.30	46.10	47.60	29.20	31.70	15.50	29.20	14.10	31.80	12.80
Pr	0.02	6.35	6.12	6.34	5.65	6.28	4.24	4.30	2.20	4.02	1.86	4.24	1.53
Nd	0.1	23.90	24.50	24.00	25.70	26.00	18.50	17.40	9.00	17.90	7.90	18.90	7.30
Sm	0.03	4.74	5.11	4.29	4.82	5.14	4.23	3.61	2.01	4.08	1.60	3.89	1.66
Eu	0.02	1.11	1.35	1.10	1.32	1.47	1.39	1.06	0.75	1.18	1.01	1.10	0.86
Gd	0.05	3.59	3.73	3.61	3.74	4.29	3.25	2.90	2.04	3.26	1.50	3.30	1.41
Tb	0.01	0.49	0.50	0.52	0.52	0.56	0.41	0.41	0.22	0.48	0.21	0.48	0.18
Dy	0.05	2.83	2.70	2.77	2.84	3.18	2.23	2.18	1.57	2.57	1.17	2.27	1.18
Ho	0.01	0.57	0.50	0.55	0.57	0.61	0.42	0.44	0.27	0.50	0.23	0.43	0.23
Er	0.03	1.62	1.38	1.58	1.28	1.74	1.13	1.12	0.83	1.35	0.61	1.25	0.55
Tm	0.01	0.24	0.20	0.23	0.23	0.24	0.15	0.18	0.11	0.19	0.08	0.17	0.09
Yb	0.03	1.44	1.20	1.36	1.16	1.48	0.78	1.03	0.65	0.98	0.48	0.97	0.49
Lu	0.01	0.23	0.18	0.21	0.18	0.21	0.12	0.15	0.10	0.15	0.07	0.14	0.08
Cu	1	10.0	21.0	7.0	8.0	35.0	29.0	68.0	120.0	3.0	2.0	14.0	7.0
Zn	2	46.0	60.0	51.0	52.0	66.0	59.0	83.0	70.0	34.0	39.0	68.0	50.0
Mo	1	2.00	1.00	1.00	0.50	21.00	1.00	2.00	2.00	1.00	1.00	2.00	8.00
Ag	0.5	0.25	0.25	0.25	0.25	0.25	0.25	0.25	0.25	0.25	0.25	0.25	0.25
Tl	0.02	0.06	0.04	0.11	0.01	0.04	0.05	0.02	0.08	0.01	0.01	0.03	0.06
Pb	2	5.00	2.00	3.00	3.00	5.00	3.00	3.00	2.00	1.00	3.00	4.00	2.00
Sn	1	1.00	1.00	1.00	0.50	0.80	0.50	1.00	0.50	0.50	0.50	0.25	0.25
Sb	0.05	0.03	0.03	0.03	0.03	0.03	0.03	0.03	0.03	0.03	0.03	0.05	0.03
Ga	0.1	18.50	18.80	19.60	19.90	19.30	20.80	16.70	21.20	16.80	20.10	21.20	21.10
Ge	5	2.50	2.50	1.10	1.10	1.00	2.50	2.50	1.30	2.50	2.50	1.20	1.20
As	0.1	1.00	0.20	0.20	0.20	1.00	0.40	0.30	0.70	0.50	0.30	1.40	1.40
W	1	1.00	0.50	0.25	1.00	0.70	6.00	1.00	1.10	1.00	0.50	0.90	0.90
Bi	0.01	0.01	0.01	0.01	0.01	0.01	0.01	0.01	0.02	0.01	0.01	0.04	0.06
La/Sm (PM)		3.15	2.53	3.50	2.48	2.57	1.74	2.35	1.96	1.79	2.54	2.14	2.02
Gd/Yb (PM)		2.06	2.57	2.20	2.67	2.40	3.45	2.33	2.60	2.75	2.58	2.81	2.38
Nb/Nb*		0.34	0.36	0.32	0.41	0.39	0.37	0.41	0.47	0.38	0.26	0.48	0.32
Ti/Ti*		0.37	0.48	0.39	0.52	0.49	1.12	0.80	1.77	0.56	0.56	0.83	0.56
Zr/Zr*		1.25	0.94	1.22	0.86	1.38	0.34	0.67	0.59	0.30	0.39	0.52	0.54

Table 4.4: Major (wt. %) and trace element (ppm) data for the gabbro unit.

SampleID	LOD	8z-48	F-23	F-24	F-25	N-02	N-07	N-09
SiO_2	0.01	51.20	44.40	46.80	46.40	51.50	50.10	51.40
TiO_2	0.01	0.52	0.92	0.99	0.48	0.52	0.48	0.67
Al_2O_3	0.01	16.00	16.80	14.85	17.50	14.50	15.65	13.60
Fe_2O_3	0.01	9.11	9.43	12.50	9.34	9.81	9.21	12.05
MnO	0.01	0.15	0.15	0.18	0.13	0.15	0.15	0.16
MgO	0.01	7.79	5.77	9.09	11.20	8.79	7.89	6.91
CaO	0.01	12.70	11.20	10.70	11.25	11.20	12.60	11.20
Na_2O	0.01	1.76	2.01	1.73	1.17	1.81	1.41	1.42
K_2O	0.01	0.16	0.24	0.17	0.08	0.35	0.17	0.24
P_2O_5	0.01	0.04	0.12	0.16	0.03	0.04	0.04	0.06
LOI	0.01	1.76	1.77	1.89	3.51	1.78	1.69	1.70
Sum		101.24	92.90	99.13	101.14	100.53	99.44	99.43
Cr	10	277	470	360	290	500	300	50
Co	1	37	35	56	55	42	37	45
Ni	1	98	82	259	338	104	111	84
Rb	0.2	4	7	3	1	13	4	6
Sr	0.1	102	147	126	119	118	84	89
Cs	0.01	0.42	0.30	0.17	0.18	2.18	0.31	0.55
Ba	0.5	35.2	21.1	27.4	11.9	39.5	34.6	17.1
Sc	1	38.0	26.0	22.0	14.0	32.0	34.0	42.0
V	5	231.0	192.0	213.0	175.0	213.0	235.0	290.0
Ta	0.1	0.10	0.10	0.20	0.10	0.10	0.10	0.20
Nb	0.1	1.99	2.10	2.60	1.10	2.10	1.90	3.00
Zr	2	51.0	40.0	45.0	23.0	48.0	47.0	70.0
Hf	0.1	1.45	1.00	1.20	0.60	1.30	1.60	2.10
Th	0.05	0.33	0.27	0.26	0.12	0.33	0.25	0.45
U	0.05	0.10	0.07	0.07	0.03	0.10	0.13	0.18
Y	0.1	17.4	15.0	17.4	8.4	16.8	15.8	22.3
La	0.1	3.00	3.00	3.60	1.60	3.10	2.80	4.40
Ce	0.1	8.00	8.10	9.80	4.10	7.90	7.20	11.20
Pr	0.02	1.15	1.26	1.49	0.62	1.22	1.06	1.64
Nd	0.1	6.00	6.20	7.40	2.90	5.90	5.70	8.70
Sm	0.03	1.82	2.04	2.40	1.01	1.80	1.96	2.64
Eu	0.02	0.72	0.75	0.86	0.39	0.58	0.63	0.81
Gd	0.05	2.43	2.39	2.75	1.15	2.44	2.48	3.37
Tb	0.01	0.42	0.40	0.47	0.22	0.39	0.44	0.60
Dy	0.05	2.85	2.53	3.07	1.32	2.86	3.14	3.95
Ho	0.01	0.64	0.55	0.63	0.32	0.62	0.61	0.87
Er	0.03	1.98	1.67	1.89	0.87	1.86	1.90	3.18
Tm	0.01	0.33	0.24	0.28	0.13	0.27	0.27	0.37
Yb	0.03	2.01	1.42	1.82	0.90	1.88	1.98	2.66
Lu	0.01	0.34	0.25	0.27	0.14	0.27	0.31	0.39
Cu	1	84.0	73.0	77.0	51.0	80.0	80.0	165.0
Zn	2	61.0	77.0	92.0	54.0	57.0	60.0	52.0
Mo	1	0.50	1.00	1.00	1.00	1.00	2.00	1.00
Ag	0.5	0.25	0.25	0.25	0.25	0.25	0.25	0.25
Tl	0.02	0.01	0.01	0.02	0.01	0.03	0.01	0.04
Pb	2	1.00	4.00	2.00	1.00	2.00	2.00	1.00
Sn	1	0.50	0.50	0.50	0.50	0.50	0.50	0.50
Sb	0.05	0.03	0.03	0.03	0.03	0.03	0.03	0.03
Ga	0.1	15.20	15.40	15.80	14.30	14.30	15.10	16.00
Ge	5	1.70	2.50	2.50	2.50	2.50	2.50	2.50
As	0.1	2.60	0.30	0.20	0.20	0.80	2.50	0.20
W	1	0.25	0.50	0.50	0.50	0.50	0.50	0.50
Bi	0.01	0.01	0.01	0.01	0.01	0.01	0.01	0.01
La/Sm (PM)		1.07	0.95	0.97	1.02	1.11	0.92	1.08
Gd/Yb (PM)		1.00	1.39	1.25	1.06	1.07	1.04	1.05
Nb/Nb*		0.66	0.70	0.73	0.66	0.64	0.65	0.65
Ti/Ti*		0.58	1.06	0.92	1.05	0.59	0.52	0.54
Zr/Zr*		1.07	0.78	0.74	0.93	1.02	0.97	1.01

Table 4.5: Major (wt. %) and trace element (ppm) data for the granitoids, plutons, and batholiths.

SampleID	LOD	P-02 (upper)	P-08 (upper)	P-22 (lower)	P-23 (lower)	P-24 (upper)	G2 (Bowman Lake)	G1 (Central)	G3 (Floating Heart)
SiO_2	0.01	73.70	73.60	67.20	67.80	73.60	72.60	71.70	72.70
TiO_2	0.01	0.24	0.19	0.26	0.26	0.21	0.22	0.38	0.14
Al_2O_3	0.01	15.20	14.55	15.95	16.05	14.45	14.60	14.75	14.55
Fe_2O_3	0.01	2.38	2.16	2.15	2.19	2.14	2.40	2.77	1.37
MnO	0.01	0.03	0.03	0.02	0.02	0.03	0.06	0.03	0.02
MgO	0.01	0.54	0.46	1.04	1.06	0.46	0.54	1.00	0.56
CaO	0.01	3.52	2.81	3.79	3.69	2.89	1.75	1.98	1.34
Na_2O	0.01	4.94	4.70	5.39	5.37	4.73	3.87	3.82	5.66
K_2O	0.01	0.68	1.02	1.40	1.22	1.05	3.73	3.30	1.12
P_2O_5	0.01	0.05	0.04	0.08	0.09	0.06	0.10	0.12	0.03
LOI	0.01	0.51	0.87	1.58	1.54	0.56	0.67	0.78	0.56
Sum		101.88	100.51	98.97	99.40	100.26	100.67	100.76	98.14
Cr	10	10	10	20	20	12	20	33	20
Co	1	3	2	7	7	3	3	6	2
Ni	1	1	2	16	16	1	4	12	4
Rb	0.2	18	29	32	24	31	116	152	22
Sr	0.1	464	336	513	514	323	370	286	433
Cs	0.01	1.27	0.57	1.23	1.41	0.99	2.03	5.46	0.76
Ba	0.5	239.0	372.0	464.0	438.0	361.0	823.0	921.0	381.0
Sc	1	2.0	2.0	3.0	3.0	2.0	3.0	4.0	2.0
V	5	19.0	14.0	36.0	35.0	15.0	26.0	39.0	14.0
Ta	0.1	0.30	0.20	0.10	0.10	0.30	0.90	0.80	0.20
Nb	0.1	2.50	3.10	1.91	1.59	3.36	9.60	9.71	2.46
Zr	2	184.0	128.0	91.0	92.0	121.0	152.0	243.0	79.0
Hf	0.1	4.50	3.50	2.72	2.46	3.46	4.27	5.65	2.19
Th	0.05	1.16	1.96	1.74	1.20	2.34	15.20	14.25	1.03
U	0.05	0.64	0.26	0.38	0.36	0.63	2.92	1.22	0.32
Y	0.1	3.6	4.1	4.4	3.6	4.2	10.7	6.9	4.6
La	0.1	6.80	12.00	9.20	7.70	11.90	47.40	52.50	6.80
Ce	0.1	13.10	22.90	20.80	17.30	23.90	91.00	102.50	14.20
Pr	0.02	1.51	2.54	2.57	2.15	2.50	9.69	10.45	1.67
Nd	0.1	6.60	9.70	10.60	9.80	10.10	32.10	33.20	5.90
Sm	0.03	1.02	1.50	2.09	1.79	1.52	5.22	4.77	1.18
Eu	0.02	0.65	0.54	0.61	0.56	0.51	1.06	0.90	0.38
Gd	0.05	0.85	1.17	1.58	1.38	1.20	3.37	2.76	0.94
Tb	0.01	0.11	0.16	0.20	0.17	0.15	0.41	0.32	0.15
Dy	0.05	0.75	0.93	0.85	0.69	0.82	1.93	1.65	0.65
Ho	0.01	0.15	0.16	0.13	0.14	0.18	0.36	0.28	0.15
Er	0.03	0.41	0.47	0.38	0.35	0.43	0.96	0.60	0.48
Tm	0.01	0.07	0.07	0.06	0.05	0.05	0.12	0.08	0.07
Yb	0.03	0.45	0.55	0.32	0.33	0.42	0.81	0.46	0.42
Lu	0.01	0.08	0.07	0.07	0.04	0.06	0.11	0.06	0.07
Cu	1	2.0	3.0	14.0	12.0	4.0	6.0	17.0	3.0
Zn	2	44.0	45.0	52.0	50.0	48.0	65.0	68.0	30.0
Mo	1	0.50	0.50	0.50	0.50	1.00	0.50	0.50	0.50
Ag	0.5	0.25	0.25	0.25	0.25	0.25	0.25	0.25	0.25
Tl	0.02	0.07	0.02	0.04	0.02	0.07	0.10	0.31	0.01
Pb	2	3.00	4.00	2.00	5.00	3.00	32.00	17.00	5.00
Sn	1	1.00	0.50	0.50	0.25	0.50	1.70	2.30	0.50
Sb	0.05	0.03	0.03	0.03	0.03	0.03	0.03	0.03	0.03
Ga	0.1	20.40	19.40	20.40	20.60	18.20	18.80	24.20	21.10
Ge	5	2.50	2.50	0.60	0.70	0.80	1.10	0.70	0.80
As	0.1	0.20	0.20	0.20	0.30	0.05	0.30	0.50	0.50
W	1	0.50	0.50	1.90	0.50	0.25	0.25	0.25	0.25
Bi	0.01	0.01	0.01	0.02	0.01	0.02	0.09	0.25	0.02
La/Sm (PM)		4.31	5.17	2.84	2.78	5.06	5.87	7.11	3.72
Gd/Yb (PM)		1.56	1.76	4.08	3.46	2.36	3.44	4.96	1.85
Nb/Nb*		0.26	0.18	0.18	0.17	0.21	0.15	0.13	0.28
Ti/Ti*		0.60	0.34	0.34	0.40	0.37	0.12	0.25	0.32
Zr/Zr*		4.91	2.32	1.34	1.52	2.14	0.81	1.34	2.07

Table 4.6: Major (wt. %) and trace element (ppm) data for the feldspar porphyry unit.

SampleID	LOD	N-04 (A)	N-05 (A)	N-08 (A)	N-12 (A)	P-06 (A)	P-12 (A)	P-16 (A)	8z-04 (B)	8z-23 (B)	8z-45 (B)	F-05 (B)	F-15 (B)	F-16 (B)	F-39 (B)	F-40 (B)	N-01 (B)	N-11 (B)	P-30 (B)
SiO_2	0.01	71.10	72.00	70.10	69.70	70.30	67.20	68.00	56.00	53.20	54.60	59.30	57.70	57.90	54.60	55.60	61.40	58.30	55.10
TiO_2	0.01	0.27	0.28	0.28	0.27	0.22	0.21	0.23	1.06	1.53	0.84	0.83	1.02	1.02	0.93	0.94	0.73	0.78	0.92
Al_2O_3	0.01	15.45	15.50	15.50	15.40	16.40	16.55	16.10	16.40	17.85	17.15	16.65	18.10	17.00	17.20	16.95	16.10	14.40	14.55
Fe_2O_3	0.01	2.51	2.62	2.68	2.59	1.83	1.82	2.03	8.33	8.90	6.66	6.56	4.96	6.31	8.31	8.32	6.78	7.86	7.95
MnO	0.01	0.03	0.03	0.03	0.03	0.03	0.02	0.03	0.11	0.11	0.07	0.09	0.05	0.06	0.11	0.11	0.09	0.11	0.12
MgO	0.01	0.77	0.88	0.80	0.74	0.81	0.87	1.03	3.43	3.65	3.34	4.29	2.67	2.73	4.18	4.25	3.75	6.99	7.68
CaO	0.01	3.21	3.57	3.31	2.95	3.61	3.47	3.57	7.10	9.53	7.36	7.15	8.58	7.85	7.96	7.84	7.82	6.94	7.75
Na_2O	0.01	5.13	4.80	4.95	5.48	6.28	5.64	5.83	3.67	3.53	6.46	3.84	4.43	3.63	4.37	4.20	2.96	3.34	4.04
K_2O	0.01	0.78	0.88	0.83	0.93	0.90	1.40	0.75	0.65	0.45	0.26	0.61	0.33	0.44	0.47	0.59	0.36	0.17	0.22
P_2O_5	0.01	0.07	0.08	0.08	0.08	0.07	0.07	0.07	0.32	0.47	0.24	0.27	0.32	0.35	0.21	0.23	0.16	0.19	0.31
LOI	0.01	0.54	0.57	0.36	0.98	1.13	0.77	1.03	1.13	1.12	3.68	1.13	1.05	0.89	0.86	0.97	0.79	1.77	1.66
Sum		99.92	101.29	98.98	99.20	101.68	98.13	98.79	98.28	100.41	100.71	100.81	99.29	98.25	99.28	100.07	101.03	100.93	100.38
Cr	10	20	20	30	20	10	10	20	40	50	103	150	60	40	91	89	110	330	435
Co	1	5	5	5	6	5	6	5	24	27	22	23	15	19	28	28	22	31	34
Ni	1	5	6	5	6	12	16	16	57	71	60	109	54	52	86	82	81	227	249
Rb	0.2	26	26	27	26	32	33	19	26	16	7	15	10	12	12	15	8	2	6
Sr	0.1	296	309	319	234	468	477	375	371	436	243	415	528	442	456	375	326	211	222
Cs	0.01	0.97	0.81	1.51	0.50	0.67	1.15	0.59	0.83	2.08	0.49	0.73	0.82	1.24	0.52	0.57	0.36	0.16	2.62
Ba	0.5	278.0	281.0	321.0	281.0	471.0	586.0	370.0	197.0	99.8	55.8	164.0	99.9	117.0	140.5	158.0	227.0	35.8	28.9
Sc	1	3.0	3.0	3.0	3.0	2.0	2.0	3.0	15.0	17.0	14.0	12.0	11.0	11.0	18.0	18.0	11.0	17.0	17.0
V	5	30.0	31.0	33.0	31.0	34.0	31.0	29.0	167.0	221.0	152.0	131.0	137.0	141.0	185.0	181.0	104.0	140.0	168.0
Ta	0.1	0.40	0.30	0.30	0.30	0.10	0.10	0.10	0.70	0.70	0.30	0.40	0.60	0.60	0.30	0.40	0.50	0.40	0.40
Nb	0.1	3.80	3.60	3.70	3.70	1.50	1.40	1.30	12.80	13.90	7.21	8.50	11.30	12.10	6.60	7.29	8.60	6.10	9.87
Zr	2	135.0	119.0	140.0	141.0	101.0	89.0	74.0	192.0	170.0	127.0	137.0	169.0	185.0	116.0	124.0	136.0	117.0	143.0
Hf	0.1	3.70	3.40	3.90	3.80	2.90	2.80	2.10	4.50	3.60	2.96	3.10	3.80	4.20	2.98	3.03	3.10	3.20	3.25
Th	0.05	2.24	2.46	2.35	2.21	1.16	0.69	0.56	2.64	0.97	1.91	1.66	2.06	2.22	1.70	2.29	1.25	1.32	1.73
U	0.05	1.20	0.87	0.92	0.91	0.49	0.14	0.12	0.67	0.37	0.46	0.44	0.48	0.60	0.40	0.45	0.31	0.45	0.44
Y	0.1	4.8	4.9	5.0	10.4	2.9	2.7	2.3	19.2	22.0	14.2	13.7	17.3	18.7	17.6	18.3	9.4	13.2	17.0
La	0.1	13.20	12.40	13.60	13.90	8.20	6.50	5.50	26.30	21.80	21.00	18.30	21.70	26.80	17.00	19.10	14.40	12.10	20.70
Ce	0.1	26.00	25.10	27.30	26.70	17.10	14.20	12.00	62.50	56.70	50.20	43.40	54.00	64.30	40.50	44.80	31.10	28.40	51.70
Pr	0.02	2.97	2.94	3.07	3.06	2.30	1.85	1.54	8.21	7.90	6.29	5.83	7.25	8.43	5.03	5.48	3.76	3.56	6.51
Nd	0.1	10.90	11.50	11.90	12.20	9.80	8.00	6.90	31.50	33.10	27.20	22.90	29.20	33.10	22.20	24.80	14.40	16.60	29.20
Sm	0.03	1.91	2.34	1.95	1.95	1.84	1.52	1.30	6.23	6.76	5.06	4.80	5.63	6.37	4.15	5.48	3.05	3.69	5.40
Eu	0.02	0.67	0.70	0.68	0.72	0.56	0.48	0.43	1.58	1.97	1.05	1.30	1.62	1.61	1.17	1.30	0.91	1.01	1.39
Gd	0.05	1.42	1.62	1.61	1.73	1.40	1.24	0.92	4.43	5.37	3.66	3.57	4.23	4.81	3.54	4.08	2.37	3.21	4.39
Tb	0.01	0.19	0.24	0.20	0.29	0.13	0.12	0.10	0.62	0.76	0.45	0.45	0.63	0.64	0.54	0.59	0.33	0.44	0.58
Dy	0.05	0.98	1.07	0.97	1.71	0.69	0.66	0.56	3.42	4.18	2.57	2.73	3.26	3.56	3.23	3.20	1.73	2.77	3.25
Ho	0.01	0.16	0.19	0.17	0.38	0.09	0.10	0.09	0.71	0.82	0.51	0.49	0.63	0.70	0.66	0.68	0.38	0.50	0.64
Er	0.03	0.50	0.47	0.45	0.97	0.27	0.26	0.22	1.97	2.23	1.51	1.41	1.81	1.91	1.80	1.88	0.99	1.39	1.60
Tm	0.01	0.05	0.06	0.08	0.10	0.03	0.02	0.03	0.27	0.29	0.21	0.18	0.24	0.25	0.27	0.23	0.13	0.18	0.22
Yb	0.03	0.42	0.54	0.52	0.55	0.23	0.25	0.24	1.72	1.93	1.38	1.17	1.55	1.70	1.54	1.68	0.83	1.41	1.44
Lu	0.01	0.05	0.06	0.07	0.08	0.02	0.03	0.02	0.28	0.30	0.21	0.18	0.22	0.23	0.25	0.28	0.13	0.17	0.20
Cu	1	9.0	20.0	62.0	10.0	13.0	14.0	13.0	18.0	67.0	0.5	28.0	2.0	5.0	95.0	75.0	42.0	31.0	49.0
Zn	2	54.0	59.0	41.0	43.0	49.0	56.0	52.0	80.0	36.0	56.0	59.0	23.0	24.0	89.0	82.0	109.0	88.0	78.0
Mo	1	0.50	1.00	0.50	0.50	0.50	0.50	0.50	1.00	1.00	1.00	1.00	1.00	1.00	1.00	1.00	1.00	1.00	1.00
Ag	0.5	0.25	0.25	0.25	0.25	0.25	0.25	0.25	0.25	0.25	0.25	0.25	0.25	0.25	0.25	0.25	0.25	0.25	0.25
Tl	0.02	0.07	0.10	0.10	0.05	0.02	0.06	0.04	0.07	0.08	0.01	0.04	0.03	0.05	0.01	0.03	0.02	0.01	0.01
Pb	2	3.00	2.00	3.00	3.00	3.00	4.00	4.00	3.00	4.00	1.00	1.00	1.00	3.00	1.00	1.00	5.00	3.00	1.00
Sn	1	1.00	1.00	1.00	1.00	1.00	1.00	1.00	1.00	0.50	1.30	1.00	1.00	1.00	0.50	0.70	1.00	1.00	0.80
Sb	0.05	0.03	0.03	0.03	0.10	0.03	0.03	0.03	0.03	0.03	0.03	0.03	0.03	0.03	0.03	0.03	0.03	0.03	0.03
Ga	0.1	21.60	20.60	22.90	21.80	23.30	22.60	18.10	21.90	21.20	20.30	19.50	20.90	20.10	20.90	21.50	19.50	17.20	18.20
Ge	5	2.50	2.50	2.50	2.50	2.50	2.50	2.50	2.50	2.50	1.50	2.50	2.50	2.50	1.10	1.20	2.50	2.50	1.20
As	0.1	0.40	0.10	0.20	1.20	0.20	0.20	0.20	0.70	0.20	0.05	0.20	0.30	0.20	0.05	0.05	0.10	0.30	0.10
W	1	0.50	0.50	0.50	0.50	0.50	0.50	0.50	1.00	1.00	0.90	0.50	0.50	1.00	0.50	0.25	4.00	0.50	0.70
Bi	0.01	0.01	0.01	0.01	0.02	0.02	0.01	0.01	0.02	0.01	0.01	0.01	0.01	0.01	0.01	0.01	0.02	0.01	0.01
La/Sm (PM)		4.47	3.42	4.51	4.61	2.88	2.76	2.73	2.73	2.08	2.68	2.46	2.49	2.72	2.65	2.25	3.05	2.12	2.48
Gd/Yb (PM)		2.80	2.48	2.56	2.60	5.04	4.10	3.17	2.13	2.30	2.19	2.52	2.26	2.34	1.90	2.01	2.36	1.88	2.52
Nb/Nb*		0.21	0.22	0.20	0.19	0.14	0.18	0.19	0.43	0.62	0.31	0.41	0.48	0.40	0.34	0.33	0.48	0.44	0.44
Ti/Ti*		0.39	0.34	0.38	0.35	0.32	0.37	0.51	0.49	0.60	0.46	0.47	0.50	0.45	0.58	0.47	0.64	0.53	0.45
Zr/Zr*		2.05	1.59	2.01	2.00	1.65	1.77	1.71	0.95	0.79	0.75	0.90	0.91	0.88	0.84	0.74	1.42	1.03	0.79

Table 4.7: Major (wt. %) and trace element (ppm) data for the volcanic rocks.

SampleID	LOD	8z-09	8z-13	8z-24	8z-46	8z-47	F-06	F-14	F-19	F-22	F-26	F-41	F-42	F-43	N-03	N-06	N-10	N-22	P-03	P-09	P-10	P-31	P-32
SiO_2	0.01	50.60	51.10	50.70	50.50	54.30	51.00	51.10	49.70	50.80	51.10	50.80	47.30	51.00	50.50	69.50	50.10	51.30	50.90	49.70	47.90	49.80	52.90
TiO_2	0.01	1.10	0.78	0.61	0.90	2.02	0.56	0.49	0.61	0.59	0.69	0.61	0.70	1.92	0.50	0.70	0.59	0.63	0.72	0.60	0.46	1.40	1.94
Al_2O_3	0.01	14.30	13.65	13.85	13.95	12.85	13.90	14.05	13.95	13.90	14.20	14.35	14.65	12.45	14.90	10.85	14.50	14.80	13.90	15.05	14.70	12.60	12.25
Fe_2O_3	0.01	14.15	12.35	10.75	11.10	15.95	10.35	9.52	11.00	10.55	9.97	10.65	11.70	17.55	9.70	11.65	11.05	10.50	11.95	9.81	10.05	16.95	17.05
MnO	0.01	0.21	0.17	0.15	0.15	0.23	0.16	0.15	0.17	0.16	0.13	0.17	0.15	0.20	0.15	0.16	0.17	0.13	0.17	0.16	0.15	0.24	0.25
MgO	0.01	6.92	7.69	8.53	7.52	4.05	8.23	9.07	8.42	8.12	8.15	7.77	8.93	4.34	8.34	1.14	8.65	8.36	6.84	7.17	10.65	6.25	3.89
CaO	0.01	11.10	10.15	11.70	8.95	7.23	11.00	10.75	11.45	10.50	11.40	12.00	11.60	7.49	11.25	4.10	11.50	11.50	10.75	11.40	10.45	9.49	6.70
Na_2O	0.01	1.63	2.07	2.02	2.45	3.98	1.72	2.32	2.27	1.66	2.77	1.63	2.06	2.49	1.85	3.16	1.41	1.88	2.05	2.46	1.93	1.66	3.59
K_2O	0.01	0.13	0.18	0.33	0.15	0.16	0.17	0.42	0.22	0.52	0.33	0.20	0.20	0.17	0.13	0.22	0.20	0.19	0.10	0.16	0.45	0.27	0.16
P_2O_5	0.01	0.09	0.06	0.05	0.08	0.33	0.05	0.03	0.04	0.04	0.03	0.04	0.05	0.31	0.04	0.19	0.04	0.06	0.05	0.06	0.04	0.12	0.32
LOI	0.01	1.17	1.04	1.33	4.29	0.47	1.47	1.41	1.16	1.93	1.22	1.96	1.34	0.63	1.82	0.29	2.11	1.44	0.64	0.96	1.85	0.83	0.27
Sum		101.44	99.28	100.08	100.08	101.59	98.68	99.39	99.06	98.84	100.06	100.25	98.75	98.56	99.26	101.98	100.39	100.86	98.10	97.58	98.70	99.63	99.34
Cr	10	220	190	370	233	28	420	420	390	380	370	414	439	23	480	10	380	436	140	250	360	85	33
Co	1	49	44	44	40	37	43	42	45	45	37	43	43	38	38	5	45	41	44	41	53	58	39
Ni	1	109	78	134	75	20	98	107	134	95	100	115	100	22	100	1	124	91	88	93	258	88	20
Rb	0.2	1	3	9	4	1	4	11	3	18	9	5	2	2	2	2	6	4	1	3	15	11	3
Sr	0.1	107	86	110	142	107	84	100	93	98	131	102	138	119	86	99	87	85	121	98	99	110	137
Cs	0.01	0.09	0.19	0.48	0.26	0.10	0.23	0.20	0.45	0.31	0.35	0.18	0.25	0.08	0.24	0.20	0.17	0.35	0.04	0.17	1.45	0.44	0.47
Ba	0.5	18.8	23.3	26.0	15.2	51.3	17.8	61.3	18.9	59.5	31.1	19.8	28.3	35.1	17.8	60.2	37.7	23.6	12.9	30.0	61.9	42.3	72.5
Sc	1	41.0	37.0	34.0	33.0	34.0	32.0	36.0	34.0	33.0	41.0	39.0	45.0	36.0	28.0	20.0	36.0	34.0	39.0	34.0	22.0	37.0	36.0
V	5	345.0	293.0	255.0	293.0	193.0	241.0	208.0	274.0	238.0	280.0	264.0	306.0	203.0	220.0	2.5	285.0	256.0	326.0	264.0	206.0	398.0	199.0
Ta	0.1	0.20	0.20	0.10	0.30	0.30	0.20	0.10	0.10	0.20	0.10	0.10	0.10	0.40	0.10	0.90	0.20	0.10	0.20	0.20	0.20	0.20	0.40
Nb	0.1	2.90	3.20	2.40	4.12	5.79	2.30	1.90	1.80	2.50	1.80	2.24	1.97	6.02	2.20	13.20	1.80	2.47	3.20	2.60	1.90	4.13	5.67
Zr	2	66.0	75.0	53.0	96.0	138.0	54.0	43.0	41.0	58.0	45.0	54.0	47.0	137.0	52.0	330.0	44.0	59.0	74.0	59.0	47.0	87.0	126.0
Hf	0.1	1.80	2.00	1.40	2.48	3.44	1.50	1.20	1.10	1.50	1.20	1.48	1.32	3.91	1.60	9.10	1.20	1.83	2.20	1.70	1.30	2.56	3.67
Th	0.05	0.33	0.50	0.27	0.65	0.88	0.32	0.27	0.20	0.55	0.29	0.35	0.29	0.95	0.20	2.08	0.22	0.42	0.54	0.21	0.10	0.76	0.86
U	0.05	0.11	0.14	0.10	0.17	0.25	0.09	0.08	0.06	0.11	0.09	0.09	0.07	0.26	0.03	0.76	0.12	0.10	0.31	0.03	0.03	0.18	0.25
Y	0.1	23.0	24.8	19.7	28.4	46.1	18.7	16.0	15.7	19.8	17.1	18.6	18.5	47.4	16.1	87.2	14.6	20.6	23.2	19.2	14.3	28.1	42.1
La	0.1	4.00	4.80	3.60	5.80	8.70	3.40	2.90	2.60	3.90	2.70	3.20	2.80	9.60	2.90	17.50	2.20	4.10	4.20	3.60	2.60	6.20	10.60
Ce	0.1	10.50	12.40	9.10	15.70	23.10	9.10	7.30	6.70	9.90	7.40	8.70	8.00	24.70	7.40	45.40	5.70	10.80	10.60	9.00	7.00	16.20	28.20
Pr	0.02	1.69	1.82	1.41	2.25	3.26	1.33	1.10	1.02	1.48	1.16	1.37	1.16	3.58	1.22	6.86	0.91	1.53	1.75	1.35	1.01	2.34	4.06
Nd	0.1	8.40	8.80	6.70	11.20	17.20	7.20	5.30	5.10	6.90	5.60	6.90	5.80	19.10	6.10	35.60	4.80	8.00	8.90	7.30	5.70	11.80	21.30
Sm	0.03	2.66	2.91	2.32	3.33	5.96	2.12	1.63	1.72	2.29	1.95	2.19	1.80	6.01	2.12	10.65	1.71	2.18	2.82	2.23	1.73	3.03	5.06
Eu	0.02	0.86	0.80	0.66	0.95	1.87	0.63	0.54	0.58	0.69	0.69	0.57	0.66	1.91	0.63	3.06	0.44	0.70	0.91	0.66	0.59	1.17	1.76
Gd	0.05	3.27	3.53	2.68	3.99	6.74	2.58	2.19	2.19	2.67	2.44	2.53	2.75	7.40	2.40	13.70	2.23	2.99	4.00	2.90	2.26	3.87	6.85
Tb	0.01	0.59	0.62	0.49	0.67	1.26	0.43	0.39	0.38	0.45	0.39	0.49	0.45	1.23	0.43	2.49	0.38	0.54	0.62	0.49	0.38	0.77	1.20
Dy	0.05	3.85	4.09	3.24	4.78	7.80	3.29	2.52	2.66	3.24	2.83	3.05	2.97	8.08	2.99	16.45	2.66	3.39	4.03	3.57	2.80	4.79	7.20
Ho	0.01	0.89	0.93	0.73	1.09	1.72	0.69	0.57	0.58	0.71	0.65	0.72	0.62	1.80	0.64	3.40	0.58	0.72	0.91	0.70	0.54	1.01	1.68
Er	0.03	2.47	2.73	2.24	3.08	5.07	2.07	1.78	1.77	2.16	1.90	1.79	2.08	5.12	2.12	11.35	1.95	2.11	2.98	2.38	1.78	2.97	4.60
Tm	0.01	0.37	0.41	0.33	0.50	0.79	0.31	0.25	0.25	0.33	0.28	0.32	0.37	0.81	0.29	1.52	0.27	0.36	0.38	0.31	0.24	0.44	0.71
Yb	0.03	2.58	2.56	2.18	3.01	4.66	2.01	1.66	1.85	2.17	1.80	1.97	1.96	4.92	2.08	10.20	1.77	2.30	2.94	2.33	1.76	3.13	4.74
Lu	0.01	0.40	0.42	0.35	0.51	0.71	0.33	0.26	0.26	0.36	0.28	0.31	0.32	0.74	0.28	1.50	0.24	0.38	0.36	0.28	0.25	0.47	0.68
Cu	1	128.0	37.0	17.0	92.0	66.0	85.0	54.0	104.0	92.0	12.0	103.0	0.5	65.0	5.0	14.0	112.0	30.0	139.0	158.0	34.0	128.0	62.0
Zn	2	103.0	128.0	47.0	80.0	140.0	61.0	59.0	71.0	66.0	80.0	73.0	81.0	91.0	68.0	187.0	73.0	40.0	88.0	69.0	82.0	129.0	151.0
Mo	1	1.00	1.00	2.00	0.50	1.00	0.50	0.50	1.00	0.50	2.00	2.00	0.50	1.00	2.00	1.00	0.50	0.50	0.50	0.50	0.50	0.50	0.50
Ag	0.5	0.25	0.25	0.25	0.25	0.25	0.25	0.25	0.25	0.25	0.25	0.25	0.25	0.25	0.25	0.25	0.25	0.25	0.25	0.25	0.25	0.25	0.25
Tl	0.02	0.01	0.01	0.01	0.01	0.01	0.01	0.01	0.02	0.01	0.01	0.02	0.01	0.01	0.01	0.01	0.01	0.01	0.01	0.01	0.03	0.02	0.02
Pb	2	2.00	4.00	1.00	2.00	2.00	2.00	1.00	3.00	2.00	5.00	1.00	3.00	1.00	1.00	1.00	2.00	1.00	1.00	1.00	1.00	1.00	1.00
Sn	1	1.00	1.00	0.50	0.70	0.90	1.00	0.50	0.50	0.50	1.00	0.25	0.80	1.30	0.50	2.00	0.50	0.60	1.00	1.00	0.50	0.80	0.80
Sb	0.05	0.03	0.03	0.03	0.03	0.03	0.03	0.03	0.03	0.05	0.03	0.03	0.03	0.03	0.03	0.03	0.03	0.03	0.05	0.03	0.03	0.03	0.03
Ga	0.1	18.40	15.60	14.80	17.70	22.50	15.10	13.70	15.10	15.00	15.10	15.90	17.20	23.10	14.70	24.50	14.20	15.00	17.20	15.70	14.10	18.10	19.70
Ge	5	2.50	2.50	2.50	1.70	1.80	2.50	2.50	2.50	2.50	2.50	2.00	2.30	2.10	2.50	2.50	2.50	1.60	2.50	2.50	2.50	1.50	1.50
As	0.1	0.50	0.10	0.20	0.20	0.10	0.20	0.10	0.20	1.40	0.20	1.00	0.20	0.10	0.20	0.30	0.30	0.10	0.20	0.10	0.05	0.20	0.10
W	1	0.50	0.50	0.50	0.25	0.25	0.50	0.50	0.50	0.50	0.50	0.25	0.70	0.50	1.00	1.00	132.00	0.60	0.50	0.50	0.50	0.25	0.25
Bi	0.01	0.01	0.01	0.01	0.01	0.01	0.01	0.01	0.01	0.01	0.01	0.01	0.01	0.01	0.01	0.01	0.01	0.01	0.01	0.01	0.01	0.01	0.01
La/Sm (PM)		0.97	1.07	1.00	1.13	0.94	1.04	1.15	0.98	1.10	0.89	0.94	1.01	1.03	0.88	1.06	0.83	1.22	0.96	1.04	0.97	1.32	1.35
Gd/Yb (PM)		1.05	1.14	1.02	1.10	1.20	1.06	1.09	0.98	1.02	1.12	1.06	1.16	1.24	0.95	1.11	1.04	1.08	1.13	1.03	1.06	1.02	1.20
Nb/Nb*		0.71	0.64	0.63	0.72	0.66	0.68	0.62	0.67	0.61	0.68	0.71	0.75	0.60	0.72	0.73	0.79	0.59	0.72	0.67	0.73	0.65	0.53
Ti/Ti*		0.87	0.58	0.58	0.59	0.74	0.58	0.62	0.75	0.57	0.75	0.61	0.76	0.69	0.53	0.13	0.71	0.58	0.52	0.57	0.56	0.97	0.79
Zr/Zr*		0.97	1.03	0.93	1.09	0.94	0.96	1.01	0.96	1.01	0.94	0.96	1.01	0.89	1.00	1.17	1.06	0.98	1.02	1.01	1.04	1.01	0.84

Appendix B: Thin section petrography

Table10.1: Thin section association with the drillhole and the depth intervals.

Zone	HoleID	SampleID	Depth From	Depth To
8 zone	758-E-07	ER-2021-WP-8z-01	323.3	323.5
8 zone	758-E-07	ER-2021-WP-8z-02	245.4	245.45
8 zone	700-E-06	ER-2021-WP-8z-03A	110.3	110.75
8 zone	700-E-06	ER-2021-WP-8z-03B	110.3	110.75
8 zone	700-E-06	ER-2021-WP-8z-06	17.3	17.75
8 zone	700-E-02	ER-2021-WP-8z-07	45.65	45.85
8 zone	700-E-02	ER-2021-WP-8z-08	45.85	45.95
8 zone	700-E-01	ER-2021-WP-8z-14	60.4	60.9
8 zone	700-E-05	ER-2021-WP-8z-15	33.9	34.1
8 zone	700-E-01	ER-2021-WP-8z-17A	15.3	15.6
8 zone	700-E-01	ER-2021-WP-8z-17B	15.3	15.6
8 zone	700-E-01	ER-2021-WP-8z-18	23.2	23.4
8 zone	700-E-01	ER-2021-WP-8z-19	8.7	8.8
8 zone	700-E-05	ER-2021-WP-8z-20	19	19.3
8 zone	700-E-03	ER-2021-WP-8z-21	95.8	96
8 zone	700-E-05	ER-2021-WP-8z-22	7.95	8.2
8 zone	700-E-13	ER-2021-WP-8z-25A	42.8	43.05
8 zone	700-E-13	ER-2021-WP-8z-25B	42.8	43.05
8 zone	700-E-01	ER-2021-WP-8z-29	22.55	22.65
8 zone	700-E-07	ER-2021-WP-8z-30	51.2	51.35
8 zone	700-E-07	ER-2021-WP-8z-31	39	39.7
8 zone	700-E-07	ER-2021-WP-8z-32	39	39.7
8 zone	EU-764	ER-2022-WP-8z-49	282.2	282.4
8 zone	EU-674	ER-2022-WP-8z-50	188.3	188.4
8 zone	ERX-2021-72	ER-2022-WP-8z-51	213.3	213.4
8 zone	2009-249	ER-2022-WP-8z-52	398	398.4
8 zone	2009-249	ER-2022-WP-8z-53	398	398.4
8 zone	2009-249	ER-2022-WP-8z-54	399.5	399.9
8 zone	700-E-40	ER-2022-WP-8z-55	10.2	10.4
8 zone	700-E-11A	ER-2022-WP-8z-56	69.1	69.3
8 zone	700-E-3	ER-2022-WP-8z-57	9	9.3
8 zone	700-E-16	ER-2022-WP-8z-58	18	18.3
8 zone	700-E-23	ER-2022-WP-8z-59	8.3	8.6
8 zone	700-E-07	ER-2022-WP-8z-60	39.6	39.8
8 zone	700-E-11A	ER-2022-WP-8z-61	70.3	71
8 zone	700-E-03	ER-2022-WP-8z-62	53.6	53.8
8 zone	700-E-15	ER-2022-WP-8z-63	20.2	20.4
8 zone	ERM-2020-96	ER-2022-WP-8z-64	541.3	541.5

Zone	HoleID	SampleID	Depth From	Depth To
Falcon	ERM-2020-84	ER-2021-WP-F-02	519.45	519.7
Falcon	ERM-2020-84	ER-2021-WP-F-03	469.2	469.3
Falcon	ERM-2020-86	ER-2021-WP-F-04	419.15	419.25
Falcon	ERM-2020-91	ER-2021-WP-F-07	403.45	403.55
Falcon	ERM-2020-88	ER-2021-WP-F-08	383.35	383.45
Falcon	ERM-2020-88	ER-2021-WP-F-10	378.5	378.6
Falcon	ERM-2020-88	ER-2021-WP-F-11	382.15	382.25
Falcon	ERM-2020-81	ER-2021-WP-F-13	541	541.2
Falcon	ERM-2020-81	ER-2021-WP-F-17	383.45	383.65
Falcon	ERM-2020-81	ER-2021-WP-F-18	509.1	509.6
Falcon	ERM-2020-90	ER-2022-WP-F-44	348.3	348.4
Falcon	ERM-2020-81	ER-2022-WP-F-45	494.1	494.2
Falcon	ERX-2020-06	ER-2022-WP-F-46	85.5	85.6
Falcon	ERM-2019-68	ER-2022-WP-F-47	486	486.1
Falcon	2009-248	ER-2022-WP-F-48	248	248.2
Falcon	ERM-2020-86	ER-2022-WP-F-49	460.5	460.6
Falcon	ERM-2020-83	ER-2022-WP-F-50	461.3	461.5
Falcon	ERM-2020-79	ER-2022-WP-F-51	436.5	436.7
Falcon	ERM-2020-77	ER-2022-WP-F-52	135	135.2
Falcon	ERM-2020-79	ER-2022-WP-F-53	406.3	406.6
Falcon	ERM-2020-78	ER-2022-WP-F-54	61.8	62.1
Newt Lake	ERX-2021-60	ER-2022-WP-N-23	143	143.2
Newt Lake	ERX-2021-57	ER-2022-WP-N-24	125	125.1
Newt Lake	ERX-2021-57	ER-2022-WP-N-25	184	184.1
Newt Lake	ERX-2021-74	ER-2022-WP-N-26	267.4	267.5
Newt Lake	ERX-2021-57	ER-2022-WP-N-27	137.1	137.7
Newt Lake	ERX-2021-59	ER-2022-WP-N-28	147.2	147.6
Peek-a-boo	ERX-2021-81	ER-2021-WP-P-14	122.5	122.75
Peek-a-boo	ERX-2021-75	ER-2022-WP-P-33	364	364.1
Peek-a-boo	ERX-2021-96	ER-2022-WP-P-34	53.6	53.7
Peek-a-boo	ERX-2021-77	ER-2022-WP-P-35	137.5	137.6
Peek-a-boo	ERX-2021-85	ER-2022-WP-P-36	46	46.1
Peek-a-boo	ERX-2021-75	ER-2022-WP-P-37	506.6	506.7
Peek-a-boo	ERX-2020-22	ER-2022-WP-P-38	9.7	9.8
Peek-a-boo	ERX-2020-22	ER-2022-WP-P-39	10.2	10.4
Peek-a-boo	ERX-2021-94	ER-2022-WP-P-40	183.3	183.9

ID: ER-2021-WP-8z-01

Rock type: Quartz-amphibole-biotite-plagioclase mylonite

Basic description:

- The host rock consists of plagioclase, quartz, amphibole, and biotite.
- The host rock is associated with various veins/vein:
    - 1 - Cut by a massive quartz vein with pyrite massive pyrite and shear fabric along the contact with the host rock.
    - 2 – Cut by massive pyrite vein. Finer grained quartz grains are associated with grain boundaries or with veins. Patchy carbonate alteration with higher concentrations around the core of the vein and weaker around the contacts.
    - 3 - Late-stage vein cuts the host rock, quartz vein and pyrite vein infill and exhibits different characteristics depending on the host. Within the pyrite vein: the vein has a dark brownish coloration, which cuts through the pyrite grains. Within the host rock and quartz vein: the vein is dominantly carbonate altered.
- A segment of the host rock is trapped between a massive quartz vein and massive pyrite vein. The segment has a fabric composed of amphibole and biotite and quartz alternating layers. The carbonate-chlorite alteration is strongest near the proximity of the vein.
- The reddish alteration within the rock is characterized as light to medium brown patchy alteration within the thin section.

Paragenesis:

- plagioclase -> amphibole -> quartz -> vein 2 (pyrite) = vein 1 (quartz) -> shear (amphibole-biotite) -> carbonate = chlorite -> vein 3 (carbonate-hematite)

Mineralogy:

Primary:

- Quartz (30%)
    - Within host rock (23%): Recrystallized grains up to 100 micrometers.
    - Within vein 1 (4%): Very coarse grains up to 3,000 micrometers exhibiting undulating extinction. Near veins and grain boundaries there are finer-grained quartz up to 100 micrometers.
    - Within vein 2 (2%): Recrystallized quartz veins up to 1,500 micrometers, with finer grained quartz up 500 micrometers in proximity to pyrite grains.
    - Within vein 3 (1%): massive quartz infill
- Biotite (15%): Bimodal distribution up to 400 micrometers and finer grains commonly less than 100 micrometers. The finer-grained crystals tend to be discordant and coarser aligned to contact orientation.
- Plagioclase (8%): Altered plagioclase with remnant twinning planes. In contact with quartz and biotite. Contact with quartz is sharp to gradational. Altered by carbonates.
- Amphibole (7%): Bimodal distribution up to 400 micrometers and finer grains commonly less than 100 micrometers. One large grain within the carbonate schist, cut by the late-stage carbonate vein. Green in coloration with sharp grain boundaries, includes smaller minerals. Biotite alteration around the rim of the grain and through it. Opaque minerals found within the grain (pyrite). Carbonate altered.

Alteration:

- Pyrite (25%)

    - Euhedral to subhedral grains with grains up to 900 micrometers. Pyrite grains have two different zonation around the grains. Massive black irregular alteration that can be up to 10 micrometers in width. Brownish alteration which has a similar characteristic to late-stage vein. Contains inclusions of chalcopyrite and Bi-Te.
- Carbonate (15%)
    - Within vein 2: Anhedral grains found along grain boundaries with highest concentrations in the core of the vein.
- Chlorite (trace): Bladed chlorite, replacing biotite dominantly found along the contact with quartz vein and host rock. Sometimes found a clusters within quartz vein (can be either blueish or yellowish hues)
- Titanite (trace): Subhedral grains of titanite up to 50 micrometers, usually associated with higher abundance of amphibole and biotite.
- Chalcopyrite (trace): Found as anhedral grains within pyrite that are either fully enclosed within the pyrite grain (no apparent veins attached) or along pyrite grain boundaries.

ID: ER-2021-WP-8z-02

Rock type: massive quartz vein

Basic description:

- Massive quartz with bimodal distribution ranging from coarser grains up to 500 micrometers exhibiting undulatory extinction, and finer grains up to 200 micrometers.
- The quartz vein is cut by multiples veins.
    - 1 – Boudinage vein infilled with carbonate with no alteration halo present.
    - 2 – Boudinage vein infilled with massive quartz-feldspar with hematite staining. Cuts vein 1.
    - 3 – Discontinuous veins infilled by amphiboles and biotite with minor pyroxene. The chlorite is replacing amphiboles. The veins can be either sub parallel or an acute angle to vein 2. No cross-cutting relationship visible.
- The quartz vein is altered by carbonate (dominantly along grain boundaries or near veins) with highest concentrations around veins.
- Disseminated trace pyrite grains are associated with amphiboles, or in higher accumulation in proximity to vein 1 and 3.

Paragenesis:

- amphibole = biotite -> quartz -> pyrite -> vein 1 (carbonate) -> vein 2 (hematite) -> chlorite

Mineralogy:

Alteration:

- Quartz (88%)
    - Bimodal distribution with coarser grains up to 500 micrometers exhibiting undulatory extinction. Finer grains tend to have less inclusions. The abundance of finer grained quartz tends to increase in vicinity to the veins.
- Carbonate (5%)
    - Within quartz vein: Medium to coarser grains exhibit twinning plane. Carbonate can be found within biotite grains or growing along edges of biotite/amphiboles.
    - Within vein 1: Massive carbonate infill within the vein.
- Amphibole (2%)
    - Within quartz vein: Grains are up to 200 micrometers as subhedral grains.
    - Within vein 3: Bimodal distribution ranging from coarser grains up to 500 micrometers and finer grained up to 150 micrometers. The amphiboles/biotite have been altered to chlorite.
- Pyroxene (2%)
    - Within vein 3: Subhedral grains up to 30 micrometers.
- Biotite (1%)
    - Within quartz vein: Finer grains tend to be around 100 micrometers and have sharp contacts with quartz grains and biotite grains.
    - Within vein 3: Medium grains up to 150 micrometers, associated with amphiboles.
- Chlorite (1%)
    - Within vein 3: Altering biotite grains up to 150 micrometers.
- Pyrite (1%)
    - Within vein 3 and 1: Anhedral grains up to 300 micrometers can be found associated with vein infill, or as disseminated anhedral grains within amphibole-carbonate.

ID: ER-2021-WP-8z-03A

Rock type: mylonite

Basic description:

- The rock is composed of quartz, amphibole, biotite, and plagioclase.
- The rock is associated with a series of veins:
    - 1 – boudinage vein infilled by quartz and amphibole. Locally has conjugate veins that are associated with thinner alteration halo but an increase in sulphides (pyrite dominated).
    - 2 – infilled by carbonate, amphiboles, clinozoisite with variable chlorite alteration. Cuts vein 1.
    - 3 - sub parallel veinlets to vein 2 are discontinuous. Cross cutting relationship not visible.
- The sulphides consist of dominantly pyrite with trace chalcopyrite. Most of the pyrite grains are found along vein 1 when near the intersection with vein 2, or in areas of patchy alteration. Vein 2 has trace disseminated pyrite found throughout the vein.

Paragenesis:

- host rock (titanite -> amphibole -> biotite -> plagioclase -> quartz) -> vein 1 -> pyrite -> vein 2 = vein 3 -> carbonate -> chlorite

Mineralogy:

Primary:

- Quartz (50%)
    - Within host rock (49%): Recrystallized quartz grains dominantly around 200 micrometers with micro inclusions.
    - Within vein 1 (1%): Medium grained crystals up to 100 micrometers in width.
- Amphibole (15%): Bimodal distribution with coarser grains up to 600 micrometers and commonly are sub-parallel to fabric and have inclusions of titanite and clinozoisite. Coarser amphiboles are commonly associated in proximity to fracturing or higher alteration intensity. Finer grains are up to 200 micrometers and commonly are sub-parallel to fabric but can also be variably oriented.
- Biotite (10%): Elongated grains up to 200 micrometers are variably oriented.
- Plagioclase (10%): Altered grains with the twinning planes being more deformation. The grains are inclusion-rich with weak sericite alteration.

Alteration:

- Carbonate (5%): Dominantly found along quartz-plagioclase grain boundaries.
- Titanite (5%): Subhedral to euhedral grains, dominantly less than 40 micrometers but locally can be up to 150 micrometers.
- Chlorite (4%)
    - Within host rock: Grains up to 300 micrometers as isolated patches. Commonly are inclusion rich.
    - Within veins: Massive alteration with medium to dark brown.
- Pyrite (1%)
    - Within host rock: Anhedral to subhedral grains up to 200 micrometers but commonly less than 50 micrometers. Highest concentrations are in proximity to alteration halos.
    - Within vein 1: Concentrated in conjugate veins to vein 1 associated with chlorite alteration.
    - Within vein 2: Anhedral to subhedral grains up to 200 micrometers. The grains are found as inclusions within quartz and unknown blue.
- Clinozoisite (1%)

    - Within host rock: Dominantly fine grained less 20 micrometers, with some grains being equant and some being elongated. Higher concentrations are with coarser amphibole-chlorite.
    - Within vein 2: Coarse grains up to 800 micrometers with inclusion of pyrite.
- Chalcopyrite (trace)
    - Within vein 2: Anhedral grains up to 50 micrometers associated with pyrite.

ID: ER-2021-WP-8z-3B

Rock type mylonite

Basic description:

- The host rock is composed of quartz, amphibole, biotite, and plagioclase.
- Lighter beige alteration within the rock is associated with higher intensity chlorite alteration.
- The host rock is associated with a series of veins:
    - 1 - Weakly boudinage quartz-carbonate vein.
    - 2 – Undulating vein infilled with amphibole. The alteration halo is highly variable in thickness ranging from 500 to 3,000 micrometers. Cuts vein 1 and 4.
    - 3 - sub parallel to vein 1 are discontinuous sections of quartz, and chlorite associated with higher concentrations of clinozoisite. Cross cutting relationship not visible.
    - 4 – Parallel vein with same infill, thickness, and orientation as vein 1.

Paragenesis:

- host rock (titanite -> amphibole -> biotite -> plagioclase -> quartz) -> vein 3 -> vein 1 -> vein 2 -> carbonate -> chlorite

Mineralogy:

Primary:

- Quartz (49%)
    - Within host rock (48%): Recrystallized quartz grains, commonly around 200 micrometers.
    - Within vein 1 (1%): Recrystallized grains commonly around 100 micrometers, and locally can be less 50 micrometers. Rare triple junction points. Contacts with carbonate and host rock are sharp.
- Amphibole (15%)
    - Within host rock (12%): Elongated grains have a weak fabric aligned with vein 1, some of the coarser grains are over 200 micrometers.
    - Within vein 2 (3%): Subhedral grains ranging from 50 to 200 micrometers containing micro inclusions.
- Plagioclase (8%): Weakly to moderately sericite altered grains up to 300 micrometers. Grains exhibit simple to polysynthetic twinning. Coarser grains tend to be more altered and have a higher abundance of micro inclusions.
- Biotite (5%): Subhedral grains around 50 micrometers, some are aligned to the orientation of vein 1 and some are randomly oriented.
- Orthoclase (2%): Within vein 1: Subhedral grains up to 100 micrometers with weak to moderate sericite alteration.

Alteration:

- Chlorite (15%): Found dominantly as a fine-grained massive alteration associated with veins. Also found as a minor phase altering biotite grains.
- Carbonate (4%)
    - Within host rock: Higher abundance associated with higher chlorite alterations.
    - Within vein 1: Anhedral grains up to 200 micrometers.
- Titanite (1%): Subhedral grains less than 20 micrometers, with higher concentration closer to alteration or in association with chlorite
- Pyrite (1%)
    - Within host rock: Anhedral grains up to 40 micrometers associated with coarser amphiboles-chlorite.

    - Within vein 1: Anhedral grains up to 100 micrometers. Stretched out parallel to vein orientation.
- Clinozoisite (1%)
    - Within host rock: Anhedral grains less than 20 micrometers. Anisotropic and blue under cross-polars.
- Sphalerite (trace): Anhedral grains with reddish staining up to 20 micrometers.

ID: ER-2021-WP-8z-06

Rock type: mylonite

Basic description:

- The host rock is dominated by recrystallized quartz, plagioclase, amphibole, and biotite grains.
- The rock is associated with various veins:
    - 1 - recrystallized quartz infilled vein with no visible alteration halo. Locally the vein is discontinuous.
    - 2 – boudinage vein infilled with amphibole. Cross cutting relationship with vein 1 is not notable. Cuts vein 3.
    - 3 – undulating vein infilled with very fine-grained black to dark green minerals. The vein is irregular and often splits into smaller veinlets.
- The sulphides are dominated by pyrite and can be either found as (1) disseminated less than 50 micrometers grain through the host rock or (2) as coarser grains up to 100 micrometers associated with coarser amphiboles or higher chlorite patches. The sulphides contain an irregular zonation around the grains.

Paragenesis:

- host rock (amphibole -> biotite -> plagioclase -> quartz) -> vein 1 (quartz) = vein 2 (amphibole) -> vein 3 (very fine-grained black infill)

Mineralogy:

Primary:

- Quartz (30%)
    - Within host rock (29%): Recrystallized fine-grained up to 100 micrometers, commonly less than 30 micrometers. Commonly exhibit triple junction points and minor micro inclusions.
    - Within vein 1 (1%): Quartz crystals can be up to 150 micrometers and have amphibole inclusions.
- Plagioclase (15%): Subhedral grains can be up to 150 micrometers and commonly display simple twinning. The grains have a weak to moderate sericite alteration.
- Amphibole (13%)
    - Within host rock (10%): Bimodal distribution with finer grains commonly being less than 50 micrometers and oriented parallel to either vein 1 or 2. The coarser grains can be up to 300 micrometers wide are commonly deformed, have inclusions of unknown blue mineral and commonly associated with coarser grained pyrite.
    - Within vein 2 (3%): Anhedral amphibole crystals can be up to 200 micrometers.
- Biotite (8%): Anhedral grain up to 50 micrometers are oriented parallel to either vein 1 or 2.

Alteration:

- Orthoclase alteration (4%): Medium to dark brown texture destructive alteration.
- Albite alteration (10%): Light to medium brown massive alteration associated with vein 2 and 3. Contains darker brown patches.
- Carbonate (3%): Minor carbonate alteration is associated with lower portion of the vein 2 alteration.
- Pyrite (1%): Within host rock: Bimodal distribution with finer grains being subhedral to anhedral commonly less than 30 micrometers are found along grain boundaries of quartz crystals. Coarser grains are typically over 60 micrometers and are dominantly associated with coarse grained amphibole crystals.

- Clinozoisite (trace): Within host rock: Anhedral to subhedral grains up to 20 micrometers and associated with coarse grained amphiboles.

ID: ER-2021-WP-8z-07

Rock type: Clinochlore vein with albite alteration halo

Basic description:

- Clinochlore vein with alteration halo composed of strongly albite altered volcanic rock. The alteration halo consists of very fine- to fine-grained quartz and plagioclase grains with patchy medium to dark brown alteration patches. The alteration halo contains muscovite and clinochlore rich sections. Have a higher abundance of titanite and patchy medium to dark brown alteration.

Paragenesis:

- zircon = titanite = sphalerite -> clinochlore -> muscovite = carbonate

Mineralogy:

Alteration:

- Quartz (40%)
    - Along contact of the vein: Quartz grains up to 2,000 micrometers exhibit undulatory extinction. Grains exhibit undulatory extinction and have finer grained clinochlore inclusions.
    - Alteration halo: Recrystallized with bimodal distribution with coarser grains being up to 200 micrometers and finer grained commonly around 30-50 micrometers and contain micro inclusions. The coarser grains tend to exhibit more undulatory extinction.
- Clinochlore (35%)
    - Within the vein: Subhedral grain ranging from 200 to 400 micrometers. The grains have minor micro inclusions of zircons and titanites.
    - Within alteration halo: Bimodal distribution, with finer grains less than 50 micrometers that are randomly oriented throughout the alteration halo. and the coarser grains are up to 200 micrometers.
- Plagioclase (7%)
    - Within the alteration halo: Subhedral grains up to 150 micrometers with moderate to strong sericite alteration. Some exhibit simple twinning.
- Titanite (4%)
    - Within the vein: Minor amounts of titanite are found within the clinochlore vein in proximity to the contact of the vein up to 100 micrometers.
    - Within alteration halo: Are dominantly found within the alteration halo up to 300 micrometers but are commonly around 100 micrometers. The concentrations of titanite generally increases towards the darker patches of the alteration.
- Muscovite (3%)
    - Along contact of the vein: Subhedral grains up to 40 micrometers wide oriented sub parallel to the contact of the vein.
    - Within alteration halo: Subhedral grains up to 30 micrometers. Associated with a higher abundance of clinochlore and titanites.
- Carbonate (2%)
    - Within the alteration halo: Dominantly found along grain boundaries of quartz-plagioclase grains as anhedral grains.
- Pyrite (trace)

    - Within the alteration halo: Anhedral to subhedral grains less than 30 micrometers associated within more altered sections of plagioclase or clinochlore.
- Chalcopyrite (trace)
    - Within the alteration halo: Anhedral grains up to 10 micrometers associated with more altered sections. Can be associated with pyrite.
- Sphalerite (trace): Found along contact of the vein as anhedral grains, that can be up to 100 micrometers.
- Zircon (trace): Subhedral grains up to 30 micrometers found within coarse grained clinochlore. The zircon exhibits radioactive halo.

ID: ER-2021-WP-8z-08

Rock type: Mylonite in contact with alteration halo from ER-2021-WP-8z-07

Basic description:

- The host rock is composed dominantly of plagioclase, quartz, amphibole, and biotite.
- The alteration consists of very fine-grained quartz, plagioclase, and clinochlore. The feldspars exhibit weak to moderate sericitization, and minor amounts of carbonate and chlorite alteration.
- The alteration halo is associated with boudinage discontinuous vein infilled clinochlore. The grains have inclusions of titanite and clinozoisite.
- The contact with albite alteration and the host rock is associated with clinochlore and muscovite. Sections of the contact contain boudinage quartz grains.

Paragenesis:

- plagioclase -> quartz -> titanite = clinozoisite -> clinochlore -> biotite = muscovite = carbonate

Mineralogy:

Primary:

- Quartz (41%)
    - Within host rock (21%): Grains up to 200 micrometers exhibit undulatory extinction.
    - Within the albite alteration (15%): Finer grained compared to host rock with grains dominantly up to 150 micrometers.
    - Along contact of alteration halo and host rock (5%): Anhedral grains up to 50 micrometers as discontinuous patches.
- Plagioclase (25%): Subhedral grains up to 200 micrometers exhibit weak to moderate sericite alteration and micro inclusions. The grains exhibit simple to polysynthetic twinning.
- Biotite (9%): Tend to be smaller than the brown alteration and have a bimodal distribution. Coarser grains range from 400 to 600 micrometers and are found along the contact or in proximity to the contact which have a fabric oriented to the contact. Along the contact they are associated with a higher abundance of titanite. Finer grains are less than 100 micrometers and are distributed throughout the alteration and within the host rock, with higher abundance in the host rock. In proximity to the contact within the alteration the amphiboles have a fabric oriented with the contact.

Alteration:

- Albite (10%): Massive alteration with medium brown coloration.
- Clinochlore (7%): Grains tend to be coarser up to 2,000 micrometers. They are found along the contact with the host rock and the albite alteration. The grains dominantly have a discontinuous fabric, and commonly associated with clinozoisite and titanite. Localized patches can be found within the albite alteration.
- Titanite (3%): Anhedral to subhedral grains up to 20 micrometers. Higher abundance found within the contact associated with clinochlore. Can be found within the alteration and the host rock.
- Muscovite (2%): Subhedral grains up to 200 micrometers are found along the contact of the albite alteration and the host rock.
- Clinozoisite (2%): Dominantly found as inclusions within brown amphiboles but can also be found within the plagioclase inclusions.
- Carbonate (1%): Dominantly found along grain boundaries of quartz-plagioclase grains.
- Sphalerite (trace): Anhedral grains up to 60 micrometers are dominantly found in areas of coarser quartz grains, carbonate, and clinochlore.

ID: ER-2021-WP-8z-14

Rock type: mylonite

Basic description:

- Host rock is composed of quartz, plagioclase, clinochlore, clinozoisite, and biotite.
- The host rock is associated with various veins:
    - 1 – Massive quartz vein with medium to dark brown alteration halo.
    - 2 – Boudinage vein infilled with clinochlore and quartz. The vein splits into multiple sub parallel veins over a short distance up to 400 micrometers. Cuts vein 1.
    - 3 – Undulating vein infilled with quartz, plagioclase, and carbonate with variable chlorite alteration. Cuts vein 2.
    - 4 - Boudinage veins infilled with quartz infill and similar alteration style as vein 3 but does not cut the quartz veining. The vein pinches out in proximity to vein 3.
    - 5 – Boudinage carbonate vein. Cross cutting relationship is not visible as the vein pinches out before the intersection with vein 2.

Paragenesis:

- host rock (titanite -> clinochlore = plagioclase -> quartz) -> vein 1 (quartz vein) -> vein 2 (amphibole) -> vein 4 (quartz) = vein 3 (quartz-plagioclase-carbonate) -> chlorite

Mineralogy:

Primary:

- Quartz (55%)
    - Within host rock (48%): Recrystallized quartz grains with typical size up to 200 micrometers, the grains are inclusion rich.
    - Within the quartz vein (7%): Bimodal distribution with coarser grained grains can be up to 600 micrometers in width, and exhibit undulatory extinction. Contains abundant micro inclusions. The finer grains range up to 300 micrometers are more concentrated in proximity to veins.
- Plagioclase (20%)
    - Within host rock (17%): The grains are up to 300 micrometers and exhibit simple and polysynthetic twinning. The grains have lots of inclusions and weak to moderate sericite alteration.
    - Within vein 3 (3%): The grains are up to 100 micrometers and exhibit polysynthetic twinning.
- Biotite (13%): The grains can be up to 300 micrometers and are elongated sub parallel to the vein 3 orientation in proximity to fracturing.

Alteration:

- Clinochlore (15%): Can be found as alteration of biotite, or subhedral grains up to 200 micrometers with inclusions of titanite, quartz and clinozoisite.
- Clinozoisite (3%): Highest concentrations are around massive quartz veining contact as fine-grained grains up to 60 micrometers.
- Carbonate (2%): Minor carbonate alteration found within fracturing or within quartz-plagioclase grain boundaries.
- Titanite (1%): Fine grained subhedral to euhedral grains up to 50 micrometers. Found throughout the chaotic unit but higher concentrations are in proximity to vein 3, which show weak folding texture.

ID: ER-2021-WP-8z-15

Rock type: Quartz vein cutting a mylonite

Basic description:

- The host rock is composed of fine-grained quartz, feldspar, clinochlore, biotite, and muscovite matrix.
- The host rock is associated with various veins:
    - 1 – undulating vein infilled with muscovite, clinochlore, quartz, titanite, and carbonate.
    - 2 – vein infilled with very coarse-grains of quartz. The contact with the host rock is sharp and locally contains titanite and/or carbonate.
    - 3 – vein infilled with recrystallized quartz grain. The vein is parallel to the fabric and vein 1 and.

Paragenesis:

- host rock (plagioclase -> biotite -> quartz) -> vein 1 (titanite -> muscovite -> clinochlore) -> vein 2 (quartz) = vein 3 (quartz)

Mineralogy:

Primary:

- Quartz (56%)
    - Within host rock (30%): Recrystallized grain up to 100 micrometers with minor micro inclusions.
    - Within vein 2 (20%): Coarse grains up to 8,000 micrometers with undulating extinction. The grain boundaries have finer grained quartz up to 100 micrometers and irregular boundaries.
    - Within vein 3 (6%): Recrystallized quartz with bimodal distribution, the coarser grains are up to 150 to 200 micrometers and finer grained are less than 50 micrometers.
- Biotite (25%): The grains can be up to 200 micrometers and make up the fabric of the rock.
- Plagioclase (10%): The grains are commonly around 150 to 200 micrometers with weak to moderate sericite inclusions and display simple twinning. Coarse grained plagioclase can be up to 400 micrometers with strong sericite alteration and abundant micro inclusions.

Alteration:

- Clinozoisite (3%)
    - Within host rock: Anhedral grain throughout the host rock up to 200 micrometers, but commonly less than 50 micrometers. The higher abundance is with more intense alteration or with relict plagioclase.
- Clinochlore (2%)
    - Within vein 1: Coarse grains up to 500 micrometers aligned to the orientation of the vein. Commonly associated with a higher abundance of titanites.
- Muscovite (2%)
    - Within vein 1: Anhedral to subhedral grains up to 400 micrometers, commonly less than 40 micrometers, oriented sub parallel to the contact of the vein.
- Carbonate (2%)
    - Within vein 3: Anhedral grains altering the quartz infill veins.
- Titanite (1%): Subhedral grains up to 200 micrometers with highest accumulation with vein 1 (clinochlore). Within the host rock the grains are finer grained up to 40 micrometers and are concentrated in proximity to the veining.
- Pyrrhotite (trace)
    - Within vein 1: Disseminated grains up to 100 micrometers associated with quartz.

ID: ER-2021-WP-8z-17A

Rock type: mylonite

Basic description:

- The host rock is composed of quartz, plagioclase, clinochlore, pyroxene, and biotite.
- Alteration patches have a moderate-darker brown appearance in thin section with no apparent associated vein. The patches can be either parallel or cutting the fabric.
- The host rock is associated with various veins:
    - 1 – weakly boudinage vein infilled with coarse-grained quartz. The vein has a strong albite alteration halo up to 200 micrometers in width.
    - 2 – boudinage vein infilled with quartz, clinochlore, and carbonate. Minor albite alteration halo up to 40 micrometers. Cuts vein 3.
    - 3 – boudinage vein infilled with quartz and weak patchy carbonate alteration.
    - 4 – Strongly undulating vein infilled with pyroxenes.

Paragenesis:

- vein 4 (pyroxene) = vein 3 (quartz) -> vein 2 (quartz-clinochlore) -> vein 1 (quartz)

Mineralogy:

Primary:

- Quartz (46%)
    - Within the host rock (42%): Very fine-grained with weak alteration up to 100 micrometers.
    - Within vein 1 (2%): Very coarse-grained crystals up to 1,500 micrometers. The grains show undulatory extinction and are altered with patchy hematite and carbonate.
    - Within vein 2 and 3 (2%): Recrystallized quartz up to 200 micrometers
- Plagioclase (19%)
    - Within the host rock (18%): Very fine-grained with weak alteration up to 100 micrometers.
    - Relict phenocrysts within matrix (1%): Subhedral to euhedral grain up to 600 micrometers exhibiting simple twin. The grains are moderately sericite altered with micro inclusions.
- Pyroxene (10%)
    - Within the host rock (7%): Subhedral to euhedral fine grained up to 70 micrometers. The grains are dominantly more equant than elongated.
    - Within vein 4 (3%): Subhedral to euhedral bimodal distribution of grains ranging from coarser grained 200 to 300 micrometers, and finer grained around 50 micrometers. The vein does not exhibit an alteration halo.
- Biotite (5%)
    - Subhedral grains up to 150 micrometers which make up the fabric with the rock along with amphiboles.

Alteration:

- Chlorite (15%)
    - Within the host rock: Anhedral grains up to 150 micrometers with random orientation.
    - Within vein 2: Anhedral grains up to 40 micrometers oriented sub-parallel to the vein.
- Clinozoisite (5%)
    - Within the host rock: Grains up to 50 micrometers are found through the host rock. Higher associated with stronger alteration patches.

- Pyrite (trace): Anhedral grain less than 50 micrometers, with slightly higher concentration around vein 2.

ID: ER-2021-WP-8z-17B

Rock type: mylonite

Basic description:

- The host rock is composed of quartz, plagioclase, pyroxene, amphibole, and biotite. There are alteration patches which have a moderate-darker brown appearance in thin sections with no apparent associated fracture. These patches can be parallel to or cutting the fabric.
- The host rock is associated with various veins:
    - 1 – Undulating vein infilled with carbonate and has patchy hematite alteration. Cuts fabric and all veins
    - 2 – irregular vein with breccia infill containing fragments of host rock, and parallel to fabric. The veins are associated with chlorite alteration halo.
    - 3 – Same characteristics as vein 2 but in a different location. Offsets vein 4.
- Discontinuous sections of recrystallized quartz infill vein.
- Sulphides are dominated by pyrite as trace disseminated grains. The grains have a higher abundance closer to the veins.

Paragenesis:

- vein 2 & 3 (breccia infill) -> vein 1 (carbonate-hematite)

Mineralogy:

Primary:

- Quartz (53%)
    - Within host rock (50%): Recrystallized grains up to 100 micrometers, contains micro inclusions.
    - Within discontinuous section of recrystallized quartz (3%): The grains can be up to 200 micrometers with micro inclusions.
- Biotite (15%): Make up the fabric of the rock with larger grains up to 200 micrometers, but commonly the grains are less than 100 micrometers.
- Plagioclase (4%): The grains are about 200 micrometers and have a weak to moderate sericite alteration.

Alteration:

- Albite alteration (20%): Dominantly as massive alteration medium brown along veins.
- Clinozoisite (6%): Disseminated throughout the unit with grains less than 50 micrometers, but locally up to 100 micrometers. The grains have a higher abundance with vicinity to alteration intensity.
- Chlorite (3%): Anhedral grains up to 20 micrometers.
- Carbonate (3%)
    - Within vein 1: Anhedral grains around the infill of the vein.
- Titanite (trace)
    - Within vein 1: Found along edges of the vein and anhedral to subhedral grains up to 80 micrometers.
- Pyrite (trace): Disseminated grains dominantly associated with vein 1 as anhedral to subhedral grains.

ID: ER-2021-WP-8z-18

Rock type: Laminated unit

Basic description:

- The host rock is composed of layers ranging from quartz-plagioclase dominant to muscovite-biotite dominant to biotite-clinozoisite-sulphide dominant layers. The fabric within the unit is strongly aligned. The muscovite-biotite layers are also associated with coarser and higher abundance of sphalerite and sulphides.
- Host rock is associated with various veins:
    - 1 – undulating and boudinage vein infilled with carbonate and has minor clinochlore with no alteration halo. Offset by muscovite-biotite dominant layers.
    - 2 – Boudinage vein infilled by clinozoisite grains. The vein is associated with local higher abundance of clinozoisite.
    - 3 – Undulating vein infilled with clinochlore with titanite inclusions. Sphalerite is found in proximity to the clinochlore grains. Offsets vein 2.
- Sulphides are dominated by pyrrhotite with minor chalcopyrite, pyrite, and sphalerite. They are dominantly associated with muscovite-biotite rich layer and veins. Within the muscovite-biotite rich layers the sulphides are elongated to the fabric. The sulphides have an irregular black coating around them.

Paragenesis:

- vein 1 (carbonate) -> muscovite-biotite rich layer -> vein 3 (clinochlore) -> vein 2 (carbonate)

Mineralogy:

Primary:

- Quartz (52%)
    - Within host rock (48%): Recrystallized quartz grains ranging from 50 to 100 micrometers with micro inclusions.
    - Parallel to the fabric (4%): Discontinuous coarser quartz rich layers have grains up to 200 micrometers. Locally associated with anhedral sphalerite.
- Biotite (17%): The grains range from 100-300 micrometers and aligned with the fabric of the rock, with coarser grains being associated with muscovite-biotite rich layers.
- Muscovite (10%): Bimodal distribution. The muscovite grains are subhedral up to 30 micrometers within the quartz-plagioclase rich layers, and subhedral up to 100 micrometers within the muscovite-biotite rich layers. Coarser muscovite grains tend to have a higher chlorite alteration and increase in clinozoisite and sulphides concentrations.
- Plagioclase (5%): Grains can be up to 100 micrometers and have weak to moderate sericite alteration.
- Clinozoisite (3%)
    - Within host rock (2%): Anhedral to subhedral grains up to 300 micrometers but commonly less than 100 micrometers with higher concentrations around the muscovite-biotite rich layers.
    - Withing vein 2 (1%): Subhedral to anhedral grains vary from 50 to 200 micrometers with sharp grain boundaries.

Alteration:

- Pyrite (4%): Anhedral grains up to 300 micrometers with higher abundance in muscovite-biotite rich layers. The grains are elongated to the fabric.
- Clinochlore (3%): Within vein 3: Anhedral grains up to 150 micrometers, with carbonate alteration. Locally associated with titanite and sphalerite.

- Sphalerite (3%): Anhedral grains associated with muscovite vein 3 or with higher concentrations of muscovite-biotite. The grains are up to 70 micrometers associated with a more quartz rich section of the infill.
- Carbonate (3%): Within vein 1: Anhedral to subhedral grains up to 300 micrometers, some of which show twinning planes.
- Titanite (trace): Anhedral grains up to 300 micrometers associated with vein 3. The grains are anhedral to subhedral up to 80 micrometers.
- Chalcopyrite (trace): Anhedral grains associated with pyrrhotite.
- Pyrrhotite (trace): Subhedral grains associated with pyrite.

ID: ER-2021-WP-8z-19

Rock type: mylonite

Basic description:

- The host rock is composed of quartz, plagioclase, muscovite, and biotite.
- The host rock is associated with various veins:
    - 1 – Boudinage vein infilled with carbonate and hematite altered. The rims of the vein have a darker massive coloration. The chlorite alteration halo is highly variable from 200 to over 3,000 micrometers. The vein has albite alteration in proximity to the vein which grades to potassic alteration distal to the vein.
    - 2 – Vein infilled with quartz.
- Discontinuous lenses of quartz. The grains contain inclusions of amphiboles and contain no alteration halo.
- Darker patches of alteration with no visible vein. They are offset by vein 1.

Paragenesis:

- vein 2 (quartz) -> Vein 1 (carbonate)

Mineralogy:

Primary:

- Quartz (35%)
    - Within host rock (30%): Recrystallized quartz grains are generally less than 50 micrometers but can be up to 100 micrometers. The grains contain micro inclusions.
    - Within vein 2 (2%): Anhedral grain up to 50 micrometers
    - Discontinuous quartz lenses (3%): Recrystallized coarser grains up to 150 micrometers.
- Plagioclase (18%): Can be found either as finer grains up to 50 micrometers or as coarser grains up to 200 micrometers. The coarser grains tend to be strongly sericite altered and associated with higher abundance of clinozoisite.
- Biotite (2%): Subhedral grains make up the fabric of the rock with grains up to 100 micrometers.

Alteration:

- Clinochlore (10%): Subhedral grains make up the fabric of the rock with grains up to 100 micrometers. Some of the coarser grains can be up to 300 micrometers and have micro inclusions.
- Clinozoisite (6%): Highest accumulations are with relict plagioclase and grains can be up to 30 micrometers.
- Carbonate (2%): Associated with vein 1 infill and altered by hematite.
- Hematite (1%): Massive alteration associated as alteration of vein 1.
- Titanite (1%): Associated with veins or with coarser amphiboles up to 30 micrometers.

ID: ER-2021-WP-8z-20

Rock type: mylonite

Basic description:

- The host rock is composed of quartz, plagioclase, biotite, clinozoisite, and clinochlore.
- The host rock is associated with various veins:
    - 1 - Boudinage vein infilled with clinochlore-carbonate-muscovite. The alteration halo is variable up to 300 micrometers. Offsets vein 2.
    - 2 – Boudinage vein infilled with clinochlore.
    - 3 – Undulating vein infilled with carbonate. Chlorite alteration increases towards quartz contact. Sulphides are associated with the vein. Cuts vein 4 (quartz)
    - 4 – Massive quartz vein.
- Patches of alteration parallel to foliation with no apparent vein with weak carbonate alteration. Offset by vein 3, 2 and 1.
- The patchy potassic alteration noticed in the rock is associated with loss of clinochlore and biotite and an increase in quartz, and feldspar.

Paragenesis:

- vein 1 (amphibole) -> vein 2 (amphibole-carbonate) -> vein 4 (quartz) -> vein 3 (carbonate)

Mineralogy:

Primary:

- Quartz (34%)
    - Within host rock (14%): Recrystallized quartz grains up to 100 micrometers containing micro inclusions.
    - Within vein 4 (20%): Very coarse-grained up to 3,000 micrometers. The grains have undulatory extinction with abundant micro inclusions. Along the grain boundaries the grains sizes get finer to about 100 micrometers.
- Plagioclase (28%): Grain sizes are typically less than 100 micrometers but can also be found as relict plagioclase grains up to 300 micrometers. The coarser grains have abundant micro inclusions of clinozoisite.
- Biotite (4%): The grains are up to 100 micrometers and make up the fabric of the rock.

Alteration:

- Clinochlore (20%)
    - Within host rock: The grain are dominantly less than 100 micrometers but can also be coarser up to 400 micrometers which are more deformed and have higher inclusion count.
    - Within vein 1: Anhedral grains ranging from 100 to 300 micrometers.
    - Within vein 2: Anhedral grains up to 400 micrometers. The grains are elongated to the fabric of the rock.
- Albite alteration (7%): Massive medium to dark brown alteration associated with veining.
- Carbonate (4%)
    - Within vein 1: Anhedral to subhedral grains up to 400 micrometers.
    - Within vein 3: Anhedral grains up to 50 micrometers.
- Clinozoisite (2%): Dominantly associated with relict plagioclase crystals or with higher abundance of alteration with grains less than 20 micrometers.
- Titanite (1%): Associated with coarse clinochlore as subhedral grains up to 100 micrometers, or along contact with the quartz vein and the host rock.

- Zircons (trace): Subhedral grains up to 10 micrometers found as inclusions within clinochlore. Contains radioactive halos around the grains.

ID: ER-2021-WP-8z-21

Rock type: mylonite

Basic description:

- The host rock is composed of quartz, plagioclase, biotite and clinochlore. There is patchy medium brown albite alteration throughout the host rock with higher accumulations of clinochlore and sulphides.
- The host rock is associated with various veins:
    - 1 – Vein infilled with coarse-grained quartz with abundant micro inclusions.
    - 2 – Boudinage and undulating vein infilled with clinochlore-clinozoisite and associated with titanites and altered by patchy carbonates.
    - 3 – Undulating vein infilled with quartz. The orientation of the vein is parallel to the vein 2 contact. Offset by vein 4.
    - 4 – Boudinage vein infilled by carbonate. Offset by vein 3 (quartz) and vein 1 (quartz) but are cut by vein 2 (clinochlore-clinozoisite)
    - 5 – Boudinage vein infilled by massive quartz-feldspar with hematite staining. Offset by vein 4 (carbonate)
    - 6 – Vein infilled with coarse clinozoisite. The vein is offset by vein 5 (quartz-feldspar) and vein 4 (carbonate).
- The sulphides have a higher concentration around coarse clinochlore.

Paragenesis:

- vein 1 (quartz) -> vein 3 (quartz) = vein 6 (clinozoisite) -> vein 5 (quartz-feldspar) -> vein 4 (carbonate) -> vein 2 (clinochlore- clinozoisite)

Mineralogy:

Primary:

- Quartz (44%)
    - Within host rock (42%): Recrystallized grains up to 150 micrometers, inclusion-rich
    - Within vein 1 (1%): Very coarse grains up to 3,000 micrometers. The grains have finer grains of quartz along grains boundaries up to 150 micrometers or along veins. The coarser grains have undulatory extinction and have abundant inclusions.
    - Within vein 3 (1%): Coarser grains up to 500 micrometers, but commonly up to 150 micrometers. The grains have carbonate, amphibole, and micro inclusions.
- Clinozoisite (10%)
    - Within host rock (2%): Anhedral to subhedral grains up to 50 micrometers through the unit with higher concentrations with clinochlore and biotite.
    - Within vein 2 (8%): Bimodal distribution of subhedral to euhedral grains ranging from 100 to 300 micrometers. The grains have micro inclusions.
- Biotite (6%): Subhedral grains up to 100 micrometers make up the fabric of the rock.

Alteration:

- Clinochlore (10%)
    - Within host rock: Bimodal distribution with finer grains less than 150 micrometers, and coarser grains up to 400 micrometers. The coarser grains have a chlorite alteration.
    - Within vein 1: Anhedral grains up to 300 micrometers.
    - Within vein 2: Coarse grains up to 300 micrometers randomly oriented. The grains have micro inclusions and are associated with titanite and clinozoisite.

- Albite alteration (16%): Dominantly found as massive alteration halo associated with the veining.
- Carbonate (7%)
    - Within vein 2: Anhedral grains up to 20 micrometers.
    - Within vein 3: Anhedral inclusion with the quartz.
    - Within Vein 4: Anhedral grains up to 30 micrometers.
- Clinozoisite (5%)
    - Within host rock: Anhedral grains up to 30 micrometers distributed throughout the rock. Higher concentrations are with stronger alteration patches.
    - Withing vein 2: Coarse grains up to 400 micrometers, but commonly less than 200 micrometers.
- Titanite (1%): Within vein 2: Subhedral to euhedral grains up to 150 micrometers. The grains have weak carbonate alteration and micro inclusions.
- Pyrite (1%): Anhedral grains throughout the rock with higher accumulation in stronger alteration patches or along veins
- Chalcopyrite (trace): Anhedral grains up to 40 micrometers associated with pyrite.

ID: ER-2021-WP-8z-22

Rock type: mylonite

Basic description:

- Strongly altered rock with most of the original fabric being overprinted. The host rock is composed of quartz, plagioclase, muscovite, biotite. The fabric of the rock is associated with clinochlore-biotite. Alteration halos are difficult to discern due to the abundant vein infills.
- The rock is associated with variable veins:
    - 1 – Undulating and boudinage vein infilled with clinozoisite. The grains are variably carbonate altered and have darker brown patches. The vein jogs within the section (labelled 8 on slide). Associated with disseminated pyrite. The vein offsets all the veins within the section.
    - 2 – Undulating vein infilled with very fine-grained minerals with dark brown alteration. The veins are irregular and split into multiple segments. Albite alteration halo is about 50 to 100 micrometers. The vein offsets vein 1 and 3
    - 3 – Boudinage vein infilled with recrystallized quartz. The grains range from 200 to less than 100 and have variable carbonate alteration. The vein is found in two locations which are offset by vein 1.
    - 4 - Same vein characteristic as vein 2 that is sub parallel to vein 2. The vein is cut by vein 1 (clinozoisite).
    - 5 – Boudinage vein infilled with quartz and anhedral clinochlore with no alteration halo. The vein cuts vein 6 (quartz).
    - 6 – Boudinage vein infilled with quartz grains. There is a jog in the vein in proximity to vein 1 (clinozoisite). The vein is offset by vein 5 (quartz-clinochlore)
- Discontinuous lenses of quartz infill with grains up to 150 micrometers but also finer grained less than 50 micrometers. The quartz grains have inclusions of clinochlore and micro inclusions.

Paragenesis:

- vein 3 (quartz) -> vein 2 (breccia infill) -> vein 1 (clinozoisite)
- vein 6 (quartz) -> vein 5 (quartz-clinochlore)

Mineralogy:

Primary:

- Quartz (25%)
    - Within host roc (20%)k: Recrystallized quartz grains are commonly less than 40 micrometers, and with coarser grains being up to 100 micrometers. The grains have variable alteration and micro inclusions. The coarser grains exhibit undulating extinction.
    - Within vein 3 (1%): The grains are highly veined and infilled with carbonate and clinozoisite. The coarser grains are up to 400 micrometers and finer grained less than 100 micrometers. The grains exhibit undulating extinction.
    - Within discontinuous quartz lenses (3%): Recrystallized quartz grains up to 150 micrometers with micro inclusions. Contain carbonate infill around grain boundaries, and inclusions of clinozoisite and clinochlore.
    - Within vein 6 (1%): The grains are up to 400 micrometers with finer grains less than 100 micrometers. The grains are veined and have micro inclusions. The coarser grains have undulating extinction.

- Plagioclase (23%): The grains are less than 100 micrometers, some of which exhibit simple twinning.
- Biotite (5%): The grains are less than 100 micrometers and make up the fabric of the rock. Chlorite alteration around the grains.

Alteration:

- Albite alteration (20%): Dominantly found as massive alteration around veins. Medium brown in color.
- Clinochlore (10%)
    - Within host rock: The grains are less than 100 micrometers and make up the fabric of the rock. In more clinochlore rich sections, the grains can be up to 300 micrometers. Coarser grains of clinochlore are usually associated with higher concentrations of sulphides.
    - Within vein 5: Anhedral grains less than 60 micrometers. The grains have a weak carbonate alteration.
- Carbonate (6%): Dominantly associated with vein infill; the grains are typically less than 150 micrometers.
- Muscovite (5%)
    - Within vein 2: Discontinuous sections of subhedral muscovite up to 50 micrometers, parallel to the vein
    - Within vein 3: Subhedral grains up to 70 micrometers elongated sub parallel to the orientation of veining.
- Clinozoisite (3%)
    - Within host rock: Subhedral grains up to 60 micrometers, associated with higher alteration and clinochlore-biotite layers.
    - Within vein 1: The grains are up to 150 micrometers. The grains are altered by carbonate and a dark alteration.
- Pyrite (1%)
    - Within vein 1: Disseminated grains up to 40 micrometers with the chlorite alteration halo of the vein.
    - Within vein 6: Anhedral grains up to 250 micrometers associated as inclusions with carbonate.
- Pyrrhotite (trace)
    - Within vein 3: Anhedral grains up to 60 micrometers found as inclusions in clinochlore.
- Sphalerite (trace): Associated with vein 4 with carbonate alteration. Anhedral grains up to 100 micrometers.

ID: ER-2021-WP-8z-25A

Rock type: Amphibole vein with albitized alteration halo

Basic description:

- The alteration halo consists of very fine- to fine-grained quartz and plagioclase crystals that make up the mass of the alteration. Patchy darker brown alteration throughout the rock.
- The host rock is associated with various veins:
    - 1 – Vein infilled with coarse-grained clinochlore. Carbonate alteration was noted along contact with quartz and amphibole grains.
    - 2 – Boudinage vein infilled with carbonates. The vein is parallel to vein 1 and cuts vein 1.
    - 3 – Vein infilled with clinozoisite that is parallel to vein 2 (carbonate infill). The vein cuts vein 1.
- Within the albite alteration halo there are undulating patches of medium to dark brown alteration with no apparent fracture.

Paragenesis:

- vein 1 (clinochlore) -> quartz infill = vein 2 (carbonates) = vein 3 (clinozoisite)

Mineralogy:

Primary:

- Quartz (29%)
    - Within host rock (28%): The quartz grains are less than 100 micrometers and have abundant micro inclusions.
    - Within vein 1 along the contact (1%): Coarse grained up to 700 micrometers. Exhibit undulatory extinction and contains inclusions of clinochlore. Carbonate alteration along grain boundary of quartz and clinochlore.
- Plagioclase (19%): The grains are commonly less than 100 micrometers, locally can be up to 300 micrometers with moderate to strong sericite alteration and micro inclusions.

Alteration:

- Clinochlore (25%)
    - Within host rock: The grains are typically less than 100 micrometers and are randomly oriented. Coarser clinochlore up to 200 micrometers are found through the host rock.
    - Within vein 1: Coarse grains up to 400 micrometers with micro inclusions. Contain titanite and quartz inclusions.
- Albite alteration (20%): Patches of texture destructive medium to dark brown alteration.
- Clinozoisite (4%)
    - Within host rock: Anhedral grains less than 100 micrometers through the host rock
    - Within vein 3: Anhedral grains up to 200 micrometers.
- Carbonate (3%)
    - Within host rock: Anhedral grains up to 100 micrometers as patchy alteration within the host rock or along grain boundaries of vein 1 (amphibole) and coarser quartz grains.
    - Within vein 2: Coarse grained up to 800 micrometers. Contains inclusions of pyroxene grains.
- Titanite (trace): Found within the host rock as anhedral grains up to 100 micrometers, or as an inclusion within vein 1.

ID: ER-2021-WP-8z-25B

Rock type: mylonite with albitized alteration

Basic description:

- The host rock is composed of quartz, plagioclase, clinochlore, biotite and clinozoisite.
- The host rock is associated with variable vein:
    - 1 – Boudinage vein infilled with discontinuous clinochlore and quartz-carbonate. The alteration halo is variable ranging from 100 to 1,000 micrometers.
    - 2 – Thin vein infill up to 50 micrometers infilled with quartz and has variable albite alteration. There are multiple sub parallel vein types with similar characteristics. Cut by vein 1.
    - 3 – Healed vein up to 10 micrometers infilled with micro crystalline quartz. The alteration halo is variable from 200-600 micrometers. Cross cutting relationship with vein 1 is not visible.
- Alteration halo is dependent on the angle of the vein to the fabric. The more parallel to the fabric the more variable the alteration halo.

Paragenesis:

- vein 2 (quartz) = vein 3 (quartz) -> vein 1 (quartz-carbonate)

Mineralogy:

Primary:

- Quartz (40%)
    - Within host rock (38%): The quartz grains are less than 100 micrometers and have micro inclusions.
    - Within vein 1 (2%): Anhedral grains up to 200 micrometers, exhibiting undulatory extinction and micro inclusions.
- Plagioclase (20%): Grains less than 100 micrometers and have weak to moderate sericite alteration. The coarser grains can be up to 300 micrometers and are associated with stronger alteration and higher micro inclusions.
- Biotite (4%): The grains are less than 100 micrometers and make up the fabric of the rock.

Alteration:

- Albite alteration (20%): Dominantly found as massive alteration around vein or as patchy alteration within host rock.
- Clinochlore (8%): The grains within albite alteration are less than 100 micrometers and randomly oriented. The grains within the host rock vary from 100 micrometers to over 300 micrometers and make up the fabric of the rock. Coarser amphiboles have more inclusions of host rock.
- Carbonate (5%): Patchy alteration within host rock as anhedral grains up to 30
- Unknown blue (2%): Anhedral grains up to 100 micrometers with higher associated to amphibole-biotite sections.
- Pyrrhotite (1%): Disseminated grains up to 40 micrometers associated with amphiboles or with chlorite alteration.
- Titanite (trace): Anhedral to subhedral grains up to 60 micrometers. The titanite grains are associated with a higher abundance of amphibole-biotite sections.

ID: ER-2021-WP-8z-29

Rock type: Laminated unit

Basic description:

- The host rock consists of either quartz-, muscovite-, biotite-, or clinozoisite-rich layers. The layers with higher abundance of biotite have a higher occurrence of sulphides, dominated by pyrrhotite with minor pyrite, chalcopyrite, and sphalerite. The clinozoisite tends to be associated with layers with coarse quartz grains.
- The host rock is associated with various veins:
    - 1 – Boudinage vein infilled with discontinuous carbonate grains. The biotite-rich layers tend to offset the vein.

Paragenesis:

- Laminated unit -> vein (carbonate)

Mineralogy:

Primary:

- Quartz (24%)
    - Within host rock (20%): Recrystallized grains up to 150 micrometers with micro inclusions
    - Clinozoisite-rich layers (4%): Bimodal distribution with grains up to 400 micrometers, and finer grained along grain boundaries or along veins dominantly less than 50 micrometers.
- Muscovite (20%): Within the quartz-plagioclase layer the grains are finer around 100 micrometers, and in the muscovite-biotite rich layer the grains get coarser to 400 micrometers. The grains have a strong fabric.
- Biotite (14%): Within muscovite-biotite rich layers the grains can be up to 400 micrometers and usually occupy the core of the layer. The grains have a strong fabric and offset the vein (carbonate)
- Plagioclase (14%): The grains are dominantly less than 150 micrometers, some of which exhibit simple twinning.

Alteration:

- Pyrrhotite (5%): Anhedral grains up to 60 micrometers. Within the muscovite-biotite rich layers the grains are coarser up to 300 micrometers and elongated parallel to fabric. Highest concentration is found within muscovite-biotite rich layers.
- Clinozoisite (5%)
    - Within host rock (2%): Anhedral grains up to 50 micrometers, with higher accumulations in the muscovite-biotite rich layers
    - Within vein 1 (3%): Subhedral grain with bimodal distribution. The coarser grains are up to 400 micrometers, and finer grains less than 200 micrometers. The grains have sharp contact with muscovite-quartz.
- Carbonate (4%): Carbonate is dominantly found within vein (carbonate), and in vicinity to clinozoisite-rich layers.
- Sphalerite (3%): Anhedral grains up to 40 micrometers. They have an elongation parallel to the fabric.
- Titanite (1%): Higher abundance in muscovite-biotite rich layers with grains less than 100 micrometers.
- Pyrite (trace): Anhedral grains up to 80 micrometers associated with pyrrhotite.
- Chalcopyrite (trace): Anhedral grains up to 60 micrometers associated with pyrrhotite.

ID: ER-2021-WP-8z-30

Rock type: mylonite

Basic description:

- Th host rock is composed of quartz, plagioclase, and biotite with minor titanite and clinochlore.
- Host rock is associated with various veins:
    - 1 – Vein infilled with coarse quartz grains. The contact with the host rock has no alteration halo.
    - 2 – Vein infilled with coarse quartz grains. The contact with the host rock contains carbonate, muscovite and clinochlore. The veins offset vein 1.

Paragenesis:

- fabric -> vein 1 (quartz) -> vein 2 (quartz)

Mineralogy:

Primary:

- Quartz (40%)
    - Within host rock (27%): The grains are up to 100 micrometers and have abundant micro inclusions.
    - Within vein 1 (3%): Very coarse grained over 2,000 micrometers. The grains have micro inclusions.
    - Within vein 2 (10%): Very coarser grained up to 2,000 micrometers and have finer grained quartz along the quartz-quartz grain boundaries. The grains exhibit undulatory extinction and have abundant micro inclusions.
- Plagioclase (20%): The grains are typically less than 100 micrometers, with coarser grains up to 300 micrometers associated with stronger alteration and higher abundance of micro inclusions.
- Biotite (11%): The grains are up to 100 micrometers and make up the fabric of the rock.

Alteration:

- Clinochlore (11%)
    - Within host rock: The grains are typically less than 100 micrometers, but coarser grains can be up to 300 micrometers. The grains make up the fabric of the rock.
    - Within vein 2 alteration halo: Coarse grain up to 400 micrometers with a moderate alignment of grains to the orientation of the vein. The amphiboles have inclusions of clinozoisite and are associated with titanites and carbonate alteration.
- Muscovite (5%)
    - Contact of vein 2: Anhedral grains up to 150 micrometers that are oriented sub parallel to the contact.
- Carbonate (4%): Anhedral grains up to 200 micrometers associated with vein 2.
- Albite alteration (4%): Dominantly found as massive alteration halo as medium brown color in vein 2.
- Titanite (3%)
    - Within host rock: Anhedral grains up to 60 micrometers.
    - Vein 2 contact alteration halo: Subhedral grains up to 150 micrometers associated with coarser muscovite or chlorite.
- Clinozoisite (2%): Anhedral grains up to 200 micrometers associated with coarse grained amphibole-chlorite.
- Pyrrhotite (trace): Anhedral grains up to 100 micrometers associated with carbonates or coarse chlorite along the edge of vein 2 alteration halo.

ID: ER-2021-WP-8z-31

Rock type: mylonite

Basic description:

- The host rock is dominated by quartz, plagioclase, and biotite with minor clinozoisite.
- The host rock is associated with various vein:
    - 1 - Massive quartz vein. Patchy carbonate alteration and titanites are found along the contact.
    - 2 – Thin vein infill of quartz less than 50 micrometers. Offset by vein 3.
    - 3 – Irregular vein infilled with brecciation and dark brown massive mineral. The vein splits into multiple. Cuts vein 1 (quartz).

Paragenesis:

- vein 1 (quartz) = vein 2 (quartz) -> vein 3 (breccia infill)

Mineralogy:

Primary:

- Quartz (25%)
    - Within host rock (14%): The grains up are generally less than 100 micrometers and have abundant micro inclusions. The coarser grained sections have grains up to 300 micrometers and exhibit undulatory extinction.
    - Within vein 1 (10%): Coarse grains up to 3,000 micrometers. The grain boundaries have finer grained quartz up to 150 micrometers. The grains have micro inclusions of titanites and amphiboles. When vein 3 cuts the quartz vein the grains are strongly brecciated
    - Within vein 2 (1%): Grains up to 200 micrometers
- Plagioclase (5%): The grains are generally less than 100 micrometers but can be up to 200 micrometers. There is a moderate to strong sericite alteration associated with them.
- Biotite (2%): The grains are up to 200 micrometers and are randomly oriented.

Alteration:

- Albite alteration (57%): Massive alteration associated with vein, dominantly vein 3 (breccia). The alteration is texture destructive and medium to dark brown.
- Clinochlore (5%): The grains are up to 200 micrometers and are randomly oriented.
- Clinozoisite (3%)
    - Within host rock: Anhedral grains up to 100 micrometers distributed throughout the host rock.
    - Along contact of vein 1: Coarse clinozoisite up to 400 micrometers associated with titanites. Clinozoisite can also be found as isolated lenses of infill up to 150 micrometers.
- Carbonate (2%): Associated along contact with vein 1 (quart)
- Titanite (1%)
    - Within host rock: Anhedral grains can be up to 100 micrometers. The finer grained titanites are associated with areas of stronger alteration or along veins up to 100 micrometers.
    - Along contact of vein 1: Coarser subhedral to euhedral titanites up to 400 micrometers

ID: ER-2021-WP-8z-32

Rock type: mylonite

Basic description:

- Massive quartz vein cutting the host rock. The host rock is strongly altered.
- The host rock is associated with various veins:
    - 1 – Boudinage and undulating vein infilled with clinozoisite. In proximity to the veining there is darker brown patches of alteration. Cuts vein 3 (quartz) and vein 4 (breccia).
    - 2 – Boudinage and undulating vein infilled with clinozoisite. The style of infill is very similar to vein 1 but at a different angle.
    - 3 – Massive quartz vein.
    - 4 – Irregular vein infilled with brecciation less than 10 micrometers in width. Cuts vein 3 (quartz).

Paragenesis:

- vein 3 (quartz) -> vein 4 (breccia) -> vein 1 (clinozoisite) = vein 2 (clinozoisite)

Mineralogy:

Primary:

- Quartz (20%)
    - Within host rock (8%): The grains are up to 100 micrometers and are abundant with micro inclusions.
    - Within vein 3 (12%): The coarse grains are up to 3,000 micrometers with abundant inclusions. The grains exhibit undulatory extinction and have finer grained quartz along grain boundaries.
- Plagioclase (11%): The grains are typically less than 100 micrometers with coarser grains up to 300 micrometers.
- Clinozoisite (8%)
    - Within host rock (4%): Anhedral to subhedral grains usually less than 100 micrometers and associated with stronger alteration.
    - Within vein 1 (2%): Coarse grains up to 200 micrometers randomly oriented within the vein. The grains have micro inclusions.
    - Within vein 2 (2%): Coarse grains up to 200 micrometers randomly oriented within the vein. The grains have micro inclusions.

Alteration:

- Albite alteration (53%): Dominantly as massive alteration halo around the veins of medium brown color.
- Carbonate (3%): Anhedral patchy alteration around veins.
- Clinochlore (3%): The grains are dominantly less than 200 micrometers with no fabric except in proximity to the contact with vein 3 (quartz).
- Titanite (1%): Coarser grained up to 100 micrometers titanites are associated with the contact with host rock and vein 4 (quartz), and finer grained less than 100 micrometers are associated with albite alteration.
- Sphalerite (1%): Anhedral infill around the grain boundaries of vein 3 (quartz).

ID: ER-2022-WP-8z-49

Rock type: Diorite

Basic description:

- Relict phenocrysts of plagioclase have abundant inclusions of clinozoisite, as well as chlorite and amphiboles.
- Coarse amphiboles have been altered by chlorite, associated with inclusions of Ilmenite.

Petrogenesis

- ilmenite -> amphiboles -> biotite -> plagioclase -> quartz -> clinozoisite

Mineralogy:

Primary:

- Plagioclase (45%): Relict phenocryst grains up to 150 micrometers. The grains exhibit simple and polysynthetic twinning and have abundant inclusions of clinozoisite, chlorite, amphiboles, sulphides and titanites.
- Quartz (25%): Subhedral grains up to 100 micrometers exhibiting undulatory extinction. The grains have irregular grains boundaries with micro inclusions. The quartz makes up the matrix of the host rock.
- Amphiboles (15%): Subhedral to anhedral grains up to 150 micrometers, commonly between 60-80 micrometers. The grains contain inclusions of sulphides and titanite. The grains exhibit alteration halos and locally simple twinning.
- Biotite (3%): Subhedral grains up to 100 micrometers being altered by chlorite. The grains contain inclusions of sulphides.

Alteration:

- Clinozoisite (5%): Anhedral to subhedral grains found as alteration within plagioclase. The grains are randomly oriented within the plagioclase.
- Chlorite (3%): Subhedral to anhedral grains up to 25 micrometers, commonly less than 15 micrometers. The grains can be either found as elongated blades with inclusions of titanite and micro inclusions or altering biotite grains.
- Ilmenite (2%): Anhedral grains up to 30 micrometers, typically less than 10 micrometers. The grains have been altered along the edges to titanite, and commonly contain micro inclusions within the core of the grain. Typically found along contacts with quartz and amphibole, chlorite, or plagioclase.
- Titanite (1%): Subhedral to euhedral grains up to 15 micrometers associated with chlorite and amphiboles. The grains have irregular grain boundaries and contain micro inclusions.
- Pyrite (1%): Anhedral to subhedral grains up to 20 micrometers, commonly less than 10 micrometers. The grains are typically inclusion-poor but inclusion-rich grains are also found. Dominantly found associated with amphiboles and chlorite as inclusions.
- Chalcopyrite (trace): Anhedral disseminated grains up to 3 micrometers in width. Dominantly found as inclusions within amphiboles but can also be found along quartz grains contacts.

ID: ER-2022-WP-8z-50

Rock type: Laminated unit

Basic description:

- The white layer in the center has a boudinage quartz vein altered by carbonate cutting the unit, and coarse clinozoisite inclusions. The rims of the vein have sub-parallel coarser biotite and clinozoisite grains along the contacts as well as increase titanite grains.
- The rest of the layering is due to variability and coarseness of biotite and clinozoisite. Darker layers are more biotite rich.
- Parallel quartz infill layer associated with quartz and carbonate with minor inclusions of clinozoisite.

Petrogenesis

- clinozoisite -> biotite -> quartz = plagioclase -> carbonate

Mineralogy:

Primary:

- Quartz (40%)
    - Within the host rock (35%): Anhedral to subhedral grains up to 5 micrometers exhibiting undulatory extinction. The grains contain micro inclusions.
    - Within the quartz layer (5%): Subhedral grains up to 15 micrometers exhibit undulatory extinction. Quartz is associated with carbonate alteration as well as inclusions of clinozoisite and biotite. The grains contain abundant micro inclusions.
- Plagioclase (22%): Make up the host rock along with quartz. The anhedral grains are up to 5 micrometers. Weak to moderate sericite alteration.
- Biotite (20%): Bimodal distribution that makes up the fabric of the rock along with elongated clinozoisite. Coarser grains are up to 50 micrometers, commonly less than 20 micrometers. The grains have inclusions of clinozoisite and are found either in biotite rich layers or along quartz vein contact. Finer grains are up to 5 micrometers. Contains inclusions of clinozoisite.

Alteration:

- Clinozoisite (15%)
    - Within the quartz layer (5%): Coarse grains up to 40 micrometers, commonly less than 25 micrometers found dominantly along the edges of the vein infill. Containing inclusions of biotite and micro inclusions.
    - Within the host rock (10%): Anhedral grains sub parallel to the fabric up to 10 micrometers.
- Carbonate (3%): Anhedral grains up to 20 micrometers found along fracture infill. The carbonate alteration also alters the host rock in proximity to the fracture.

ID: ER-2022-WP-8z-51

Rock type: Gabbro

Basic description:

- The thin section is dominated by coarse amphiboles within a matrix of fine-graine amphiboles with minor quartz, plagioclase, titanite, chlorite and sulphides. The coarse amphiboles make up the fabric of the grain.
- Chlorite and titanites are found along grain boundaries of coarse amphiboles and are elongated parallel to the coarse amphiboles.

Paragenesis:

- sulphides -> amphibole -> titanite -> quartz -> chlorite

Mineralogy:

Primary:

- Amphibole (80%): Bimodal distribution. Coarse grains are up to 80 micrometers, commonly less than 50 micrometers. The grains are elongated making up the fabric of the host rock. Finer grains are up to 10 micrometers found within the matrix of the host rock.
- Quartz (10%): Anhedral grains up to10 micrometers make up the matrix of the host rock along with clinozoisite, plagioclase and finer amphiboles.
- Plagioclase (2%): Anhedral grains up to10 micrometers make up the matrix of the host rock along with clinozoisite, quartz and finer amphiboles.

Alteration:

- Titanite (4%): Anhedral grains up to 15 micrometers are dominantly crystalizing along the edges of coarse amphiboles.
- Chlorite (3%): Subhedral grains up to 15 micrometers associated with amphiboles and aligned parallel to subparallel to the fabric of the host rock.
- Pyrite (1%): Subhedral to anhedral grains up to 5 micrometers and are inclusion free. Found as inclusions within coarse amphiboles.
- Chalcopyrite (trace): Anhedral grains up to 3 micrometers, either found as isolated grains or associated with pyrite or pyrrhotite, found as inclusions within coarse amphiboles.
- Pyrrhotite (trace): Anhedral grains up to 5 micrometers found as inclusions within coarse amphiboles.

ID: ER-2022-WP-8z-52

Rock type: Quartz vein

Basic description:

- Very coarse quartz grains with interstitial sulphides and silicates around the grain boundaries. The coarse quartz grains contain finer grained quartz along the grain boundaries and undulatory extinction.
- Between the coarse-grained quartz there is an infill of sulphides, chlorite and clinozoisite. The sulphides contain inclusions of quartz and chlorite.

Paragenesis:

- quartz -> clinozoisite -> chlorite -> sulphides

Mineralogy:

Primary:

- Quartz (81%): Coarse grains up to 50 micrometers exhibit undulatory extinction and recrystallization texture. The grains contain micro inclusions and have carbonate alteration.

Alteration:

- Clinozoisite (5%): Subhedral to anhedral grains up to 30 micrometers, commonly less than 15 micrometers. The grains are in associated with chlorite along the grain boundaries of
- Chlorite (5%): Subhedral grains up to 15 micrometers found along the grain contact. The grains wrap around the coarse-grained quartz.
- Carbonate (3%): Anhedral grains up to 10 micrometers found in associated with sulphides, and along grain boundaries of quartz.
- Pyrrhotite (3%): Anhedral grains up to 60 micrometers found along the quartz grain boundaries. The pyrrhotite contains abundant micro inclusions and is associated with higher abundance of chalcopyrite.
- Chalcopyrite (2%): Anhedral grains found in association with pyrite and pyrrhotite or along grain boundaries of silicates.
- Pyrite (1%): Subhedral to euhedral grains up to 20 micrometers are inclusion-poor. The grains are commonly associated with pyrrhotite and chalcopyrite.
- Sphalerite (trace): Found as inclusion within pyrrhotite grains.

ID: ER-2022-WP-8z-53

Rock type: Laminated unit

Basic description:

- Multiple quartz layers associated with the Laminated unit. The contacts with the quartz layers have a higher abundance of chlorite, and clinozoisite inclusions.
- The layers range from quartz-plagioclase dominant to clinochlore-rich layers to quartz-dominant layers.
- Quartz vein cutting the unit having coarser grained crystals, and sulphides along the contact with the Laminated unit.
- Sulphides are dominated by pyrrhotite with minor chalcopyrite and sphalerite. The grains have a black zonation around them (fine grained sulphides) and are found in higher abundance in proximity to the chlorite grains.

Paragenesis:

- clinozoisite = titanite -> chlorite -> quartz vein -> sulphides

Mineralogy:

Primary:

- Quartz (41%)
    - Within host rock: (15%) Anhedral grains less than 5 micrometers making up the
    - Within the quartz veins (26%): Coarse grains up to 50 micrometers with undulatory extinction and recrystallization texture. The grains are carbonate altered. Chlorite and clinozoisite grains are found along grain boundaries in proximity to the contact with host rock.
- Plagioclase (5%)**:** Anhedral grains up to 5 micrometers with weak sericite alteration

Alteration:

- Chlorite (34%): Subhedral grains up to 50 micrometers, commonly less than 30 micrometers that make up the fabric of the host rock. The grains are elongated parallel to the fabric and have higher abundance in proximity to the quartz veins. Contains inclusions of clinozoisite, sulphides and quartz.
- Clinozoisite (8%): Subhedral to anhedral grains up to 20 micrometers. The grains are found as inclusions within chlorite.
- Carbonate (4%): Anhedral grains up to 20 micrometers dominantly found within the quartz vein, and in proximity to the vein.
- Pyrrhotite (4%): Anhedral grains up to 60 micrometers found along grain boundaries and have abundant micro inclusions. Pyrrhotite is associated with chalcopyrite and contains inclusions of sphalerite.
- Chalcopyrite (2%): Anhedral grains up to 20 micrometers associated with pyrrhotite and less commonly sphalerite.
- Titanite (2%): Subhedral grains up to 2 micrometers elongate parallel to the fabric of the host rock. The grains are hosted within the quartz-clinozoisite matrix.
- Sphalerite (trace): Anhedral grains up to 15 micrometers found as either an inclusion within pyrrhotite or in associated with pyrrhotite and chalcopyrite. Some of the grains contain chalcopyrite disease.
- Ilmenite (trace): Anhedral grains being altered to titanite up to 10 micrometers, commonly less than 5 micrometers. The grains are hosted within coarse chlorite.

ID: ER-2022-WP-8z-54

Rock type: Laminated unit

Basic description:

- The host rock is composed of layers ranging from biotite-, muscovite-, or quartz-rich. The muscovite grains are coarser grained relative to the biotite. The quartz-rich layers tend to have an increased abundance of chlorite and coarser muscovite. Also, the pyrite grains are coarser relative to the phyllosilicate-rich layers and are more euhedral.

Paragenesis:

- clinozoisite -> muscovite = biotite -> quartz -> chlorite -> sulphides

Mineralogy:

Primary:

- Quartz (25%)
    - Within host rock (10%): Anhedral grains up to 5 micrometers make up the matrix of the host rock.
    - Within quartz-rich layer (15%): Subhedral grains up to 20 micrometers exhibit undulatory extinction. The grains have inclusions of chlorite, sulphides, muscovite, biotite, and chlorite.
- Muscovite (25%)
    - Within host rock (22%): Subhedral grains up to 40 micrometers, commonly less than 15 micrometers. Contains inclusions of clinozoisite.
    - Within quartz-rich layer (3%): Subhedral grains up to 80 micrometers aligned parallel to the contact.
- Biotite (25%)
    - Within host rock (24%): Subhedral grains up to 40 micrometers, commonly less than 15 micrometers. Contain inclusions of clinozoisite.
    - Within quartz-rich layer (1%): Subhedral grains up to 70 micrometers aligned parallel to the contact.
- Plagioclase (11%): Anhedral grains up to 5 micrometers making up the matrix of the host rock.

Alteration:

- Chlorite (5%): Within quartz-rich layers: Anhedral to subhedral grains up to 40 micrometers, commonly less than 20 micrometers are oriented parallel to the intrusions. Chlorite is altering biotite and muscovite when in proximity to the veins. Contains inclusions of clinozoisite, sulphides, but also grows around the sulphide grains.
- Pyrite (5%)
    - Within host rock (3%): Subhedral grains up to 20 micrometers associated with sections of coarser quartz grains.
    - Within quartz-rich layers (2%): Subhedral to euhedral grains up to 30 micrometers which are inclusion-poor. The grains are hosted in quart-rich fracture infill.
- Clinozoisite (4%): Subhedral to euhedral grains up to 30 micrometers, commonly less than 15 micrometers, exhibiting dissolution texture. Coarser and more euhedral grains are found in proximity to quartz veins. The finer grains and more anhedral are commonly elongated to the fabric of the host rock.
- Pyrrhotite (trace): Anhedral grains up to 20 micrometers, hosted within quartz-rich fracture infill.
- Chalcopyrite (trace): Anhedral grins up to 10 micrometers associated with quartz-rich fracture infill.

- Ilmenite (trace): Anhedral grains are found within the host rock, elongated parallel to the fabric of the host rock. The grains are associated with muscovite and biotite grains. The ilmenite grains have been altered to titanites.

ID: ER-2022-WP-8z-55

Rock type: Laminated unit

Basic description:

- Carbonate fracture infill with quartz grains along the contact. The carbonate contains abundant micro inclusions.
- The host rock is composed of quartz-plagioclase matrix with coarse muscovite, garnet, and finer grains of biotite and clinozoisite.

Paragenesis:

- garnet -> muscovite = plagioclase -> clinozoisite -> biotite -> quartz -> carbonate vein

Mineralogy:

Primary:

- Quartz (15%)
    - In host rock (10%): Anhedral grains less than 10 micrometers with micro inclusions.
    - In carbonate vein (2%): Anhedral grains over 150 micrometers exhibiting undulatory extinction and abundant micro inclusions. The grains have inclusion of clinozoisite. Carbonate grains are found along the edges of the grains.
    - In discontinuous lenses (3%): Anhedral grains up to 20 micrometers with no alteration halo. The grains have micro inclusions.
- Muscovite (15%): Coarse subhedral to euhedral grains up to 50 micrometers and are randomly oriented. The grains grow around garnets and contain inclusion of quartz-plagioclase.
- Biotite (12%): Subhedral grains up to 10 micrometers, commonly less than 5 micrometers. The grains make up the fabric of the host rock. The grains grow around clinozoisite.
- Garnet (5%): Subhedral to euhedral grains up to 30 micrometers and contain inclusions of quartz and plagioclase. Contact boundaries are sharp and irregular.
- Plagioclase (4%): Subhedral grains up to 20 micrometers with weak sericite alteration.

Alteration:

- Carbonate (30%): Subhedral grains over 150 micrometers. Contain inclusions of quartz, titanite, garnet, muscovite, biotite. Some of the carbonate has been altered to ankerite giving a yellowish hue in hand specimen.
- Clinozoisite (10%): Anhedral grains up to 10 micrometers, commonly less than 5 micrometers.
- Albite alteration (5%): Texture destructive medium to dark brown alteration. Patchy sections along the carbonate vein contact.
- Chlorite (4%): Subhedral grains are found along the contact of the carbonate vein and host rock. The chlorite grains contain inclusions of sulphides and titanites.
- Titanite (trace): Subhedral to anhedral grains up to 70 micrometers associated with chlorite along the contact with the carbonate vein and host rock.
- Pyrite (trace): Anhedral grain up to 2 micrometers in proximity to the carbonate vein and host rock contact, within the carbonate grains.

ID: ER-2022-WP-8z-56

Rock type: Clinochlore infilled vein with albite alteration

Basic description:

- Coarse amphibole vein infill with muscovite and titanite inclusions. The vein is also being infilled with quartz that is altered by carbonate.
- The vein has an albitized alteration halo (medium to dark brown in thin section). Clinozoisite is found within the alteration halo. The muscovite within the alteration halo is finer grains and more anhedral.

Paragenesis:

- muscovite -> plagioclase = quartz -> vein infill (titanite -> muscovite -> clinochlore -> quartz -> carbonate) -> albite alteration = carbonate alteration

Mineralogy:

Primary:

- Quartz (30%)
    - Within host rock (28%): Subhedral to anhedral grains up to 10 micrometers. The grains exhibit undulatory extinction and have abundant micro inclusions.
    - Within vein infill (2%): Anhedral grains up to 300 micrometers, commonly less than 150 micrometers. The grains exhibit undulatory extinction and have carbonate alteration. Localized recrystallization texture. Contains inclusions of host rock in proximity to the contact, titanite, muscovite and Clinochlore grains.
- Muscovite (8%)
    - Within host rock (7%): Bimodal distribution. Anhedral to subhedral grains up to 30 micrometers and are not oriented. The grains have irregular boundaries. Within the albite alteration halo the grains are more anhedral and finer grained up to 10 micrometers.
    - Within amphibole vein (1%): The grains are more elongated up to 50 micrometers, commonly less than 30 micrometers. The grains are found as inclusions within the Clinochlore grains and are not oriented.
- Plagioclase (5%): Anhedral grains up to 10 micrometers with strong sericite alteration.

Alteration:

- Clinochlore (30%)
    - Within amphibole vein: Subhedral grains infilling vein up to 60 micrometers, commonly less than 40 micrometers. The clinochlore is randomly oriented and contains inclusions of titanite, muscovite, quartz, and carbonate.
- Albite alteration (15%): Medium to dark brown texture destructive alteration. The alteration contains finer grains of muscovite, and quartz. The vein has been almost completely resealed, with remnant altered quartz.
- Carbonate (5%): Anhedral grains up to 100 micrometers, commonly less than 50 micrometers found within the vein infill altering the Clinochlore, quartz, and host rock in proximity to the contact. Contains inclusions of titanite, muscovite, quartz, and Clinochlore.
- Clinozoisite (4%): Anhedral grains up to 5 micrometers are found within the albite alteration. The grains are dominantly found within the quartz-plagioclase rich matrix, and less commonly within the albite alteration.
- Titanite (3%): Subhedral to euhedral grains up to 60 micrometers, commonly less than 20 micrometers found within the vein infill. The grains are found along grain boundaries of quartz or as inclusions within quartz, and clinochlore.

ID: ER-2022-WP-8z-57

Rock type: mylonite cut by quartz-carbonate vein

Basic description:

- The contact of quartz-carbonate vein has an increase abundance of oriented muscovite and chlorite grains, as well as ilmenite with outer zoned of titanite and pervasive albite alteration.
- Variable fractures that cut host rock with albite alteration halos. The fractures are boudinage and infilled with quartz-chlorite-carbonate and have irregular albite alteration halo.

Paragenesis:

- muscovite -> biotite -> ilmenite -> quartz= plagioclase -> vein infill (quartz -> chlorite -> carbonate -> albite)

Mineralogy:

Primary:

- Quartz (23%)
    - Within host rock (17%): Anhedral grains up to 10 micrometers, commonly less than 5 micrometers. The grains show undulatory extinction and have abundant micro inclusions.
    - Within vein infill (6%): Anhedral grains up to 50 micrometers with undulatory extinction and recrystallization texture along grain boundaries. The dissolution grains are commonly less than 10 micrometers. The grains have carbonate alteration and have inclusions of albite alteration, clinozoisite, and chlorite.
- Plagioclase (8%): Anhedral grains less than 5 micrometers with moderate sericite alteration.
- Biotite (5%): Subhedral grins up to 10 micrometers, commonly less than 5 micrometers randomly oriented.

Alteration:

- Carbonate (25%): Anhedral grains up to 60 micrometers, commonly less than 30 micrometers. Contain inclusion of quartz, titanite, chlorite, ilmenite.
- Albite (15%): Light to medium brown texture destructive alteration. The alteration has an increase abundance of clinozoisite grains, and inclusions of ilmenite, chlorite, carbonate, quartz.
- Chlorite (8%)
    - Along the contact of quartz and host rock: Subhedral grains up to 50 micrometers, commonly less than 30 micrometers. The grains are elongated sub-parallel to the contact with the host rock and show signs of deformation. The grains contain inclusions of titanite. The grains found within carbonate alteration are randomly oriented.
    - Within vein infill: Subhedral grains up to 30 micrometers elongated parallel to the fracture. The grain has a fold fabric and contain inclusions of titanite.
- Muscovite (7%): Near the contact with host rock and quartz-carbonate vein the grains become elongated up to 30 micrometers. The grains are associated with ilmenite, titanite and chlorite. Further away from the contact the grains are randomly oriented and more subhedral up to 20 micrometers, commonly less than 10 micrometers.
- Ilmenite (4%)
    - Along the contact within host rock: Anhedral grains up to 10 micrometers, commonly less than 5 micrometers. Within the host rock the grains are more equant, and within the alteration halo of the vein contact the grains are elongated parallel to the contact.

    - Within vein infill: Elongated grains up to 30 micrometers found along grain contact of carbonate and in proximity to chlorite alteration. Locally grains wrap around the contact of chlorite and albite alteration.
- Clinozoisite (5%): Anhedral grains up to 5 micrometers are found within the host rock, and in higher abundance in proximity to albite alteration.
- Pyrrhotite (trace): Subhedral grains found within carbonate matrix. The grains are found as disseminated clusters and exhibit alteration halo.
- Pyrite (trace): Anhedral grains up to 5 micrometers are found in proximity of the alteration halo.
- Chalcopyrite (trace): Anhedral grain less than 2 micrometers found in proximity to the alteration halo.

ID: ER-2022-WP-8z-58

Rock type: Laminated unit

Basic description:

- The chaotic unit being cut by a vein infilled with coarse chlorite and quartz. The vein is associated with albite alteration dominantly along the contacts with host rock and is dominantly aligned parallel to the contact.
- Sphalerite grains are found as a fracture infill or as inclusions within quartz vein associated with clinozoisite.

Paragenesis:

- muscovite -> biotite -> quartz = plagioclase -> quartz vein -> ilmenite -> chlorite -> carbonate

Mineralogy:

Primary:

- Quartz (37%)
    - Within host rock (29%): Anhedral grains less than 10 micrometers exhibiting undulatory extinction and micro inclusions.
    - Within vein (8%): Anhedral grains up to 150 micrometers with undulatory extinction and recrystallization texture with grains less than 10 micrometers along the grain boundaries. The quartz grains have abundant micro inclusions as well as inclusions of titanite, sphalerite, ilmenite, chlorite, and carbonate.
- Plagioclase (10%): Anhedral grains up to 10 micrometers with sericite alteration and locally simple twinning.
- Biotite (10%): Subhedral grains up to 15 micrometers, commonly less than 10 micrometers making up the fabric of the host rock.
- Muscovite (5%): Subhedral to anhedral grains up to 30 micrometers with irregular grain boundaries. Within the alteration halo of the vein the grains are typically finer grained less than 20 micrometers.

Alteration:

- Albite (15%): Light to medium brown texture destructive pervasive alteration. The darker patches are more Ca-rich sections.
- Chlorite (10%): Subhedral to anhedral grains up to 30 micrometers, commonly less than 20 micrometers, dominantly found along the quartz contact with host rock. Other places are found within albite alteration halo. The grains contain inclusions of titanite, quartz, ilmenite, muscovite.
- Clinozoisite (6%): Subhedral to anhedral grains less than 5 micrometers distributed throughout the host rock. Locally the grains are elongated parallel to the fabric. Higher concentrations are in proximity to the alteration halos or contact.
- Titanite (3%): Anhedral grains up to 5 micrometers with higher concentrations in proximity to the albite alteration or associated with chlorite.
- Carbonate (2%): Anhedral grains up to 40 micrometers dominantly found along the quartz contact with host rock. Contains inclusions of chlorite, quartz, titanite, ilmenite.
- Ilmenite (2%)
    - Within host rock (1%): Anhedral grains less than 5 micrometers distributed throughout the host rock.
    - Within quartz vein (1%): Anhedral grains up to 80 micrometers associated with the fracture infill cutting the quartz vein. The ilmenite is being cut by chlorite infill fracture.

- Sphalerite (trace): Anhedral grains up to 60 micrometers found along a fracture infilled with carbonate cutting the quartz vein.

ID: ER-2022-WP-8z-59

Rock type: mylonite

Basic description:

- Two instances of white clay infilled veins. The thicker vein with more extensive albite alteration is cutting the clinozoisite-quartz vein, and the thinner vein with lower degree of alteration halo is being terminated against the same clinozoisite-quartz vein.
- Sulphides patches within host rock is associated with medium to light brown albite alteration. Highest concentration of sulphides is found within the clinozoisite-quartz vein that is between the two white clay infill veins dominated by chalcopyrite-pyrrhotite-pyrite-sphalerite.

Paragenesis:

- titanite -> chlorite = vein (zeolite) = vein (quartz-clinozoisite) -> carbonate

Mineralogy:

Primary:

- Quartz (30%)
    - Within host rock (28%): Anhedral grains up to 10 micrometers with undulatory extinction and abundant micro inclusions.
    - Within clinozoisite-quartz vein infill (2%): Anhedral grains up to 20 micrometers with undulatory extinction and recrystallization texture. The grains contain inclusions of clinozoisite, titanite, and carbonate.
- Plagioclase (6%): Anhedral grains up to 10 micrometers with moderate sericite alteration.
- Biotite (15%): Anhedral grains up to 15 micrometers, commonly less than 10 micrometers non-oriented.

Alteration:

- Albite (15%): Medium brown texture destructive alteration found in proximity to veins. Spotty albite alteration is found throughout the host rock commonly associated with higher abundance of sulphide clusters.
- Potassic alteration (10%): Dark brown texture destructive alteration associated with vein infill.
- Clinozoisite (10%)
    - Within clinozoisite-quartz vein: Subhedral to euhedral grains up to 50 micrometers, commonly less than 20 micrometers. The grains are crystallizing around chlorite grains and have carbonate around the grains. Within the alteration halo clinozoisite is finer grained less than 5 micrometers, randomly oriented. The grains are found as inclusions within chlorite grains. Medium to dark brown texture destructive halo up to 50 micrometers.
- Chlorite (6%): Subhedral grains up to 50 micrometers are found associated with clinozoisite-quartz vein. The grains are found dominantly along the rims of the vein infill commonly aligned parallel to the contact with host rock. The grains have inclusions of titanite, quartz, and clinozoisite.
- Titanite (3%): Subhedral grains up to 15 micrometers, commonly less than 5 micrometers are associated with chlorite grains and are non-oriented.

- Ilmenite (3%): Anhedral grains up to 5 micrometers are found throughout the host rock, with higher abundance and grain size in proximity to the alteration halos. The ilmenite is being altered by titanites.
- Zeolite (3%): Within zeolite vein infill: Anhedral grains up to 30 micrometers. Contain inclusions of quartz and chlorite.
- Carbonate (1%): Anhedral grains up to 15 micrometers are found within clinozoisite-quartz vein infill. The grains are dominantly found along grain boundaries.
- Chalcopyrite (1%)
    - Within clinozoisite-quartz vein infill: Anhedral grains up to 25 micrometers with the highest abundance in contact with clinozoisite and chlorite grains.
    - Within alteration halos: Disseminated grains less than 3 micrometers within the alteration halos. Also found as patches within host rock associated with albite alteration.
- Pyrite (trace): Disseminated grains up to 10 micrometers, commonly less than 5 micrometers associated with alteration halos.
- Pyrrhotite (trace): Disseminated grains up to 5 micrometers, commonly less than 5 micrometers associated with alteration halos.
- Sphalerite (trace): Anhedral grains up to 5 micrometers associated with clinozoisite-quartz grains. Has a reddish hue in transmitted light.

ID: ER-2022-WP-8z-60

Rock type: Potassic altered breccia

Basic description:

- Brecciated section of potassic altered clasts with a very fine-grained matrix. The clasts consist of an altered quartz-feldspar mylonite host rock. The matrix consists of very fine-grained clasts of host rock with localized sections of clinozoisite and minor chlorite.

Paragenesis:

- feldspars -> quartz -> clinozoisite -> clinochlore

Mineralogy:

Primary:

- Feldspars (67%): Anhedral grains less than 10 micrometers with strong sericite alteration. The grains look very similar to the host rock and the clasts.
- Quartz (30%)
    - Within host rock (25%): Anhedral grains up to 5 micrometers
    - Within clasts (5%): Anhedral grains up to 5 micrometers. Locally contains sections of coarser grains up to 15 micrometers.

Alteration:

- Clinozoisite (3%): Found as localized sections with the matrix of the. The grains are anhedral up to 20 micrometers.
- Clinochlore (1%)
    - Within host rock: Anhedral grains up to 40 micrometers.
    - Within breccia: Anhedral grains up to 20 micrometers dominantly found along edges of clasts.

ID: ER-2022-WP-8z-61

Rock type: mylonite

Basic description:

- Host rock is composed of biotite, quartz, plagioclase, and trace disseminated ilmenite-titanite.
- Host rock is associated with various veins:
    - 1 – vein is infilled with coarse clinozoisite. Strong albite alteration halo.
    - 2 – vein with quartz-carbonate infill. The vein cuts 1 and orientation changes to be parallel to the vein 1.
    - 3 – The inside of the vein is missing and no longer visible. Remnant clinozoisite infill left on the edges with minor ilmenite inclusions. Contains weak albite alteration halo. Cuts vein 1 and 2.

Paragenesis:

- host rock -> vein 1 (clinozoisite) -> vein 2 (quartz-carbonate) -> vein 3

Mineralogy:

Primary:

- Quartz (20%)
    - Within host rock (19%): Anhedral grains up to 10 micrometers, commonly less than 5 micrometers. Small patches of coarser quartz up to 15 micrometers with weak undulatory extinction.
    - Within vein 2 (1%): Anhedral grains up to 20 micrometers.
- Plagioclase (15%): Anhedral grains up to 10 micrometers, commonly less than 5 micrometers. Inclusions of clinozoisite.
- Biotite (10%): Anhedral to subhedral grains up to 20 micrometers randomly oriented within the host rock. Biotite is not visible in the alteration halos.

Alteration:

- Albite alteration (30%): Light to medium brown alteration associated with veining.
- Orthoclase alteration (12%): Medium to dark brown alteration associated with veining.
- Chlorite (5%): Anhedral to subhedral grains up to 30 micrometers found within host rock and alteration patches. The chlorite grains are cut by vein 3. Contains inclusions of ilmenite, titanites, and quartz.
- Clinozoisite (3%)
    - Within host rock: Anhedral grains up to 10 micrometers.
    - Within vein 1: The grains have a bimodal grain size ranging from coarse grains 10-25 micrometers, and finer grains less than 5 micrometers. Weak carbonate alteration along the edges of the vein. The vein splits into smaller offshoots on an angle to the main vein.
    - Within vein 3: Anhedral grains up to 30 micrometers with inclusions of ilmenite-titanite.
- Ilmenite-Titanite (3%): Anhedral grains up to 20 micrometers with a zonation of titanite.
- Carbonate (2%)
    - Within vein 1: Anhedral grains up to 20 micrometers dominantly along edges of the vein.
    - Within vein 2: Anhedral grains up to 20 micrometers.
    - Within vein 3: Anhedral grains up to 30 micrometers.

ID: ER-2022-WP-8z-62

Rock type: Laminated unit

Basic description:

- The host rock is composed of layers that are either quartz-, muscovite- or biotite-rich. The muscovite-rich layers tend to have a stronger pervasive albite alteration. Coarse phenocrysts of plagioclase are found within muscovite-rich layers with the phyllosilicates wrapping around the plagioclase. The plagioclase has medium brown alteration and inclusions of clinozoisite.
- The rock is cut by quartz vein with recrystallization texture. Patchy medium brown alteration along the contact. Contains inclusions of strong altered host rock.

Paragenesis:

- host rock -> vein (quartz)

Mineralogy:

Primary:

- Quartz (30%)
    - Within quartz-rich layer (18%): Anhedral grain up to 40 micrometers with weak recrystallization texture. Contains inclusions of biotite.
    - Within biotite-rich layer (2%): Anhedral grains up to 10 micrometers.
    - Within muscovite-rich layer (2%): Anhedral grains up to 10 micrometers.
    - Within quartz vein (8%): Anhedral grains up to 400 micrometers with undulating extinction. Contains inclusion of muscovite, biotite and clinozoisite.
- Muscovite (25%): Within muscovite-rich layer: Anhedral grains up to 50 micrometers oriented parallel to the fabric. Contains inclusions of clinozoisite.
- Biotite (15%): Within biotite-rich layer: Subhedral grains up to 20 micrometers oriented parallel to the fabric.
- Plagioclase (10%)
    - Within biotite-rich layer (8%): Anhedral grains up to 10 micrometers with weak sericite alteration.
    - Within phenocryst layer (2%): Anhedral grain up to 100 micrometers with light to medium brown alteration. Contains inclusions of clinozoisite.

Alteration:

- Albite alteration (10%): Medium brown alteration is dominantly associated with muscovite-rich layers.
- Clinozoisite (10%)
    - Within biotite-rich and muscovite-rich layers: Anhedral grains up to 10 micrometers elongated parallel to the fabric.

ID: ER-2022-WP-8z-63

Rock type: mylonite

Basic description:

- The host rock consists of plagioclase, quartz, biotite and clinozoisite.
- The host rock is associated with various veins:
    - 1 – Quartz infilled with grains up to 60 micrometers, exhibits minor undulatory extinction. Cuts vein 2.
    - 2 – vein infilled with clinochlore, muscovite, and minor quartz, clinozoisite, and titanite.
    - 3 – infield with massive quartz and variable albite alteration halo. Cut by vein 2.

Paragenesis:

- vein 3 (quartz) -> vein 2 (clinochlore-muscovite) -> vein 1 (quartz)

Mineralogy:

Primary:

- Quartz (30%)
    - Within host rock (28%): Anhedral grains up to 10 micrometers, commonly less than 5 micrometers.
    - Within vein 3 (1%): Massive anhedral grains up to 5 micrometers
    - Within vein 1 (1%): Anhedral grains up to 60 micrometers
- Biotite (20%): Anhedral grains up to 10 micrometers.
- Plagioclase (15%): Subhedral grains up to 15 micrometers with weak sericite alteration. Contains inclusions of muscovite.
- Muscovite (9%): Anhedral grains up to 60 micrometers parallel to orientation of the vein. Altered by chlorite.

Alteration:

- Albite alteration (13%)
    - Within vein 3: Highly variable texture destructive medium brown alteration up to 200 micrometers.
    - Within vein 2: Texture destructive alteration up to 50 micrometers.
- Clinochlore (9%)
    - Within host rock: Anhedral grains up to 50 micrometers. Contain inclusions of clinozoisite.
    - Within vein 2: Anhedral grains up to 30 micrometers that are sub parallel to the vein.
- Clinozoisite (3%)
    - Within host rock: Anhedral grains up to 5 micrometers as inclusions within clinochlore.
    - Within vein 2: Anhedral grains up to 10 micrometers found along the edges of the vein.
- Titanite (3%)
    - Within vein 2: Anhedral grains up to 15 micrometers.
- Rutile (trace)
    - Within vein 1: Elongated grains up to 40 micrometers. Found as inclusions within quartz.

ID: ER-2022-WP-8z-64

Rock type: contact between feldspar porphyry and the volcanic rock

Basic description:

- The thin section is a contact between the feldspar porphyry and the volcanic rock with the alteration cutting through the contact. Higher abundance of clinochlore, amphiboles, and clinozoisite within the volcanic rock relative to the feldspar porphyry.
- The feldspar porphyry matrix consists of fine-grained quartz, plagioclase, and biotite with minor ilmenite-titanite. The plagioclase phenocrysts are strongly altered and contain inclusions of ilmenite-titanite. The biotite grains are aligned parallel to the contact and wrap around the plagioclase phenocrysts.
- The volcanic rock is dominated by amphiboles that are elongated sub parallel to the contact. Contains lenses of quartz infill
- The thin section is cut by various veins:
    - 1 – various zeolite infill veins cut through both the volcanic and the feldspar porphyry rocks, as well as through the contact. Cuts vein 2.
    - 2 – chlorite and quartz infill with thin orthoclase alteration.

Paragenesis:

- volcanic rock -> feldspar porphyry -> vein 2 (chlorite and quartz) -> vein 1 (zeolite)

Mineralogy:

Primary:

- Quartz (30%)
    - Within volcanic rock (10%): Anhedral grains up to 15 micrometers wide with recrystallization texture. Contain inclusions of amphiboles.
    - Within feldspar porphyry (20%): Anhedral grains up to 10 micrometers wide, commonly less than 5 micrometers wide.
- Amphiboles (30%): Within volcanic rock: Anhedral grains up to 30 micrometers wide, commonly less than 15 micrometers. The amphiboles are elongated sub parallel to the contact. Contains inclusions of ilmenite-titanite.
- Plagioclase (19%): Within felspar porphyry: Coarse subhedral phenocrysts up to 60 micrometers wide with strong sericite alteration. The grains exhibit simple or polysynthetic twinning, and minor oscillatory zonation. The grains contain inclusions of ilmenite-titanite. Anhedral grains up to 5 micrometers wide with sericite alteration.

Alteration:

- Orthoclase alteration (10%)
    - Within feldspar porphyry: Light to medium brown texture destructive alteration associated with veining.
    - With volcanic rock: Medium brown texture destructive alteration found within the matrix of the volcanic rock.
- Chlorite (3%)
    - Within volcanic rock: Anhedral grains up to 5 micrometers wide are commonly found in more altered sections.
    - Along contact: Anhedral grains up to 10 micrometers elongated parallel to the contact. Contains inclusions of clinozoisite.
    - Along vein 2: Anhedral grains up to10 micrometers elongated parallel to the vein. Dominantly found along edges of the vein.
- Clinozoisite (3%)

    - Along contact: Anhedral grains up to 5 micrometers wide as equant crystals.
    - Within feldspar porphyry: Anhedral grains up to 3 micrometers wide associated with altered sections.
- Ilmenite-titanite (3%)
    - Within volcanic rock: Anhedral grains up to 3 micrometers wide. Contain zonation of titanite around ilmenite grains.
    - Within feldspar porphyry: Anhedral grains up to 5 micrometers elongated parallel to the biotite grains. Higher accumulation and coarser grains are found within alteration halos.
    - Within vein 2: Anhedral grains up to 8 micrometers wide, elongated parallel to the vein.
- Zeolite (2%)
    - Within vein 1: Anhedral grains up to 10 micrometers
- Pyrite (trace)
    - Within volcanic rock: Anhedral grains up to 2 micrometers wide found along edges of amphiboles grains.
    - Within feldspar porphyry: Anhedral grains up to 3 micrometers wide that can be either as an inclusion within feldspar phenocrysts or in associated with biotite grains.

ID: ER-2021-W-F-02

Rock type: mylonite

Basic description:

- The rock is composed of very fine-grained quartz-plagioclase-amphiboles with weak to moderate albite alteration. The darker patches are associated with increased chlorite alteration.
- The rock is associated with various veins:
    - 1 – Boudinage vein infilled with coarse grained quartz and coarse grained subhedral to euhedral clinozoisite grains. The vein pinches out as it gets closer to vein 2. Near the contact with vein 3 the chlorite concentration increases, and clinozoisite crystals become more altered by chlorite.
    - 2 – Vein infilled with coarse grained quartz.
    - 3 - Boudinage vein infilled with zeolite. Part of the vein has been lost during thin section preparation. The alteration halo has variably oriented clinozoisite and chlorite grains and minor titanites with an outer albite alteration. Cuts vein 1 and 2.

Paragenesis:

- vein 1 (quartz-clinozoisite) -> vein 2 (quartz) -> vein 3 (zeolite)

Mineralogy:

Primary:

- Quartz (54%)
    - Within the host rock (52%): The grains are up to 100 micrometers and are inclusion-rich.
    - Within vein 1 (1%): Anhedral grains up to 400 micrometers with undulatory extinction and weak recrystallization texture. The grains have inclusions of clinozoisite and chlorite.
    - Within vein 2 (1%): Recrystallized grains up to 700 micrometers with undulatory extinction. The grains have inclusions of clinochlore, plagioclase phenocrysts and muscovite.
- Amphiboles (25%): Grains are up to 100 micrometers and are randomly oriented, and coarser grains can be up to 300 micrometers.
- Plagioclase (1%)
    - Within host rock (1%): anhedral grains up to 60 micrometers.
    - Within vein 2 (trace): Coarse grained inclusions up to 600 micrometers. The grains have moderate to strong sericite alteration and exhibit polysynthetic twinning.

Alteration:

- Chlorite (15%)
    - Within host rock: Grains can be up to 600 micrometers and have variable inclusions including clinozoisite, titanites, amphiboles and clinozoisite grains.
    - Within vein 3 halo: Anhedral grains up to 50 micrometers randomly oriented. Contains inclusions of titanite.
- Clinozoisite (6%)
    - Within host rock: Subhedral grains up to 50 micrometers with highest concentration around the vein or with coarse chlorite grains.
    - Within vein 1: Coarse grained up to 1,000 micrometers in width. The grains have sharp contact with the host rock. When in proximity to vein 2 (quartz) the chlorite concentration increases, and the clinozoisite becomes altered.
    - Within vein 3 halo: Randomly oriented grains up to 150 micrometers.
- Carbonate (2%): Massive alteration dominantly associated with vein 3.

- Titanite (trace): Subhedral grains up to 50 micrometers with highest concentration around the vein or with coarse chlorite grains.
- Pyrite (trace): Disseminated pyrite up to 150 micrometers associated with coarser chlorite grains.
- Chalcopyrite (trace): Disseminated grains up to 10 micrometers associated with silicate in proximity to pyrite.

ID: ER-2021-WP-F-03

Rock type: Sheared volcanics with massive pyrite veining

Basic description:

- The host rock is a sheared volcanics dominated by very fine-grained quartz, with the fabric of the unit defined by muscovite or biotite. Pyrite and pyrrhotite are found within the layering and around the quartz-rich sections.
- The contact with quartz inclusions and sheared host rock is dominated by sulphides (pyrite-pyrrhotite-chalcopyrite). The sulphides are concentrated around the contacts of the vein and are also coarser grained around the contact. The vein is composed of dominantly quartz with minor inclusions of pyrite and muscovite, biotite, or chlorite.
- Pyrite can either be found as anhedral to subhedral coarse grains with lots of inclusions, or as smaller subhedral to euhedral grain that are inclusion-poor. Sulphides have a black zonation around them consisting of very fine-grained sulphides.

Paragenesis:

- clinozoisite -> muscovite = biotite -> chlorite -> pyrite

Mineralogy:

Primary:

- Quartz (33%)
    - Within the host rock: Grains are up to 100 micrometers and have micrometer inclusions.
    - Within quartz-rich sections: Grains can be up to 300 micrometers and have inclusions of amphiboles.
- Muscovite (15%)
    - Within host rock: The amphiboles are commonly less than 100 micrometers and have a fabric to them. The coarser grains can be up to 300 micrometers.
    - Within quartz-rich sections: The amphiboles are coarser and more abundant with grains up to 500 micrometers.
- Biotite (3%)
    - Within host rock: Anhedral grains up to 200 micrometers
    - Within quartz-rich sections: Coarse grains up to 300 micrometers with fabric parallel to contact. The grains have been altered by chlorite.

Alteration:

- Pyrrhotite (14%): Dominant sulphides within the section. The grains are anhedral and inclusion-rich.
- Chlorite (10%): Dominantly found within the quartz-rich sections with grains up to 600 micrometers and in high abundance. Some of the chlorite grains have a blue hue to them in cross polars.

  Chlorite is altering the amphiboles.
- Chalcopyrite (4%): Anhedral grains associated dominantly with pyrrhotite.
- Pyrite (3%): Subhedral to euhedral grains. The euhedral grains are growing along the contact with the host rock associated with pyrrhotite. Two generations of pyrite consisting of finer grains that are inclusion-poor and subhedral to euhedral, and coarser grains that are more anhedral and contain abundant inclusions.
- Clinozoisite (5%)
    - Within host rock: Subhedral grains up to 50 micrometers with no fabric.
    - Within quartz-rich section: Coarser pyroxene grains up to 150 micrometers. Higher abundance is associated with higher amphibole-biotite-chlorite.

ID: ER-2021-WP-F-04

Rock type: Massive quartz in contact with sheared layer

Basic description:

- Massive quartz vein in contact with a strongly altered chlorite and clinozoisite rich host rock.
- The contact between massive quartz and clinozoisite-rich layer has an increased abundance of sulphides and decreased clinozoisite grain size.
- The quartz vein has crack and seal texture infilled with variable minerals ranging from quartz-chlorite-sulphides to amphiboles- chlorite-sulphides oriented sub-parallel to the orientation of the contact. The amphiboles are generally aligned to the orientation of the contact.
- Sulphides consist of pyrite and chalcopyrite. The pyrite can be either inclusion-rich or inclusion-poor.

Paragenesis:

- clinozoisite -> chlorite = quartz -> amphibole -> pyrite -> chalcopyrite

Mineralogy:

Primary:

- Quartz (60%)
    - Within quartz vein: Bimodal distribution with coarser grains up to 500 micrometers, and finer grains less than 100 micrometers. The grains have abundant micro inclusions, and exhibit undulatory extinction.
- Amphiboles (15%)
    - Within clinozoisite-rich layer: Anhedral to subhedral grains up to 500 micrometers. The grains wrap around the clinozoisite clasts.
    - Within crack and seal texture: Subhedral grains up to 800 micrometers with the grains oriented with the vein. The grains are inclusion-rich and associated with a higher abundance of sulphides.

Alteration:

- Clinozoisite (11%)
    - Within clinozoisite-rich layer: Subhedral to euhedral grains up to 600 micrometers. Closer to the contact the clinozoisite grains become finer less than 100 micrometers.
    - Within crack and seal texture: Anhedral grain up to 200 micrometers that have been altered.
- Chlorite (8%)
    - Within clinozoisite-rich layer: Altering amphiboles, with stronger abundance in proximity to the contact with quartz vein.
    - Within crack and seal texture: Subhedral grains up to 700 micrometers. The chlorite grains are found as inclusions within sulphides or altering amphiboles.
- Pyrite (4%): Subhedral to anhedral grains up to 800 micrometers and are inclusion-poor. Contain chalcopyrite as inclusion. Subhedral to euhedral grains up to 200 micrometers are dominantly inclusion-poor and can be associated with chalcopyrite.
- Chalcopyrite (1%): Anhedral grains up to 70 micrometers associated with pyrite.
- Titanite (1%): Subhedral grains up to 30 micrometers as inclusions within clinozoisite-rich layers.

ID: ER-2021-WP-F-07

Rock type: Massive pyrite layers with quartz within the Laminated unit

Basic description:

- The host rock is dominated by layers that are either muscovite-rich or biotite-rich. The biotite-rich layers have a higher component of quartz-plagioclase relative to the muscovite-rich layers.
- The contact with quartz veining is associated with a higher abundance of biotite or muscovite and locally can have elongated titanites. The pyrite has an irregular zonation around the grains composed of fine-grained pyrite.
- The sulphides are dominated by pyrite-pyrrhotite-chalcopyrite, with highest concentrations within the quartz vein in proximity to the contact. Chalcopyrite is dominantly found crystalizing along the grain boundaries of pyrite but can also be found as an inclusion within pyrite. Pyrrhotite commonly is found as isolated anhedral grains or growing along pyrite grain boundaries. Sulphides are dominantly inclusion-poor.

Paragenesis:

- clinozoisite -> muscovite = biotite -> chlorite -> pyrite -> pyrrhotite = chalcopyrite

Mineralogy:

Primary:

- Muscovite (41%)
    - Within host rock: The grains are dominantly less than 100 micrometers with strong fabric. The coarser grains can be up to 150 micrometers.
    - Near contact to quartz clasts: Grains can be up to 250 micrometers and have a weak fabric with the orientation of the contact. Found as inclusions within pyrite grains.
- Quartz (30%)
    - Within host rock: Very fine grained usually less than 50 micrometers.
    - Within quartz-rich sections: Grains are up to 200 micrometers and inclusion-rich. Common to have triple junction point.
- Plagioclase (5%): Very fine grains with grains less than 50 micrometers.

Alteration:

- Pyrite (8%)
    - Within host rock: Disseminated grains less than 50 micrometers.
    - Within quartz clasts: Subhedral to euhedral grains up to 700 micrometers and are inclusion-rich. Associated with pyrrhotite. Contains inclusions of pyrrhotite and chalcopyrite. Inclusion-poor grains can be up to 500 micrometers and contain chalcopyrite along grain boundaries.
- Chlorite (6%): Dominantly found as inclusions with fractured quartz inclusions or in proximity to the contact with host rock and quartz.
- Biotite (4%): Grains can be up to 100 micrometers and follow the contact with quartz and host rock.
- Clinozoisite (2%): Found in muscovite-biotite rich layers as anhedral grains less than 50 micrometers.
- Pyrrhotite (2%): Anhedral grains associated with quartz clasts. The pyrrhotite is inclusion-rich and is found along grain boundaries of pyrite.
- Chalcopyrite (trace): Found along grain boundaries of pyrite or as inclusions with inclusion-rich pyrite. Chalcopyrite contains pyrite as inclusions.
- Titanite (trace): Anhedral grains up to 20 micrometers are found in proximity to contact with the quartz-rich sections.

ID: ER-201-WP-F-08

Rock type: Altered volcanic rock along the contact with the quartz vein

Basic description:

- The sample was taken along the contact of a massive quartz vein and altered volcanic rocks.
- The host rock is dominated by coarse grained clinozoisite with minor biotite, quartz, plagioclase, chlorite, and sulphides. Along the contact with the contact with the quartz vein there is an increased amount of sulphides, and randomly oriented biotite grains. Within the quartz vein have parallel sections of the host rock that is altered and is dominated by muscovite and chlorite with minor clinozoisite and sulphides.
- Quartz vein has two different vein types (1) smoky quartz in proximity to the host rock and (2) milky quartz distal to the contact.
    - Smoky quartz has crystals up to 300 micrometers exhibiting undulatory extinction and recrystallization texture.
    - Milky quartz grains are similar in size but do not exhibit recrystallization texture and undulatory extinction.

Paragenesis:

- sulphides -> clinozoisite -> muscovite -> plagioclase -> chlorite

Mineralogy:

Primary:

- Clinozoisite (40%)
    - Within host rock: Bimodal distribution with coarse grains up to range from 300 to 600 micrometers, and finer grained from 50 to 200 micrometers. The finer grained are more euhedral and contain less inclusions compared to the coarser grain. The coarse-grained inclusions tend to accumulate in the core of the grain.
    - Within parallel layers of host rock to the contact: Subhedral to euhedral grains up to 400 micrometers. The grains have minor inclusions.
- Quartz (30%)
    - Within host rock: The grains are infilling the matrix with grains up to 150 micrometers. Contain micro inclusions and exhibit undulatory extinction.
    - Within smoky quartz vein: The recrystallized grains are up to 600 micrometers and exhibit undulatory extinction. The grains have micro inclusions and carbonate around grain boundaries.
    - Within milky quartz vein: The grains are up to 500 micrometers, with some grains around 100 micrometers. The grains contain inclusions of clinozoisite.
- Biotite (10%)
    - Within host rock: The grains are up to 200 micrometers growing around the clinozoisite grains. The grains are randomly aligned.
    - Within parallel layers of host rock to the contact: Anhedral grains up to 50 micrometers associated with coarse clinozoisite and sulphides. The grains wrap around the coarser quartz grains.
- Muscovite (3%)
    - Within parallel layers of host rock to the contact: Anhedral to subhedral grains up to 300 micrometers. The grains are aligned parallel to the contact of the quartz vein. Contains inclusions of clinozoisite.
- Plagioclase (2%)

    - Within host rock: Subhedral grains up to 700 micrometers exhibiting simple twins. The grains grow around the clinozoisite grains and have weak to moderate sericite alteration.

Alteration:

- Carbonate (5%): Anhedral grains associated with chlorite and intergrown around sulphides and clinozoisite grains.
- Chlorite (4%): Grains up to 400 micrometers and associated with titanite inclusions. The grains are altering clinozoisite grains and wrapping around the grains.
- Pyrite (4%)
    - Within host rock: Subhedral grains up to 100 micrometers, found as inclusions within clinozoisite grains or crystalizing prior to clinozoisite. The grain can either be inclusion-rich or inclusion-poor.
    - Within parallel layers of host rock to the contact: The grains are coarser up to 600 micrometers and associated with amphibole and clinozoisite grains. The grains are subhedral to euhedral and are inclusions rich.
- Titanite (2%): Subhedral grains are less than 50 micrometers and associated with coarse amphibole and chlorite as inclusions.

ID: ER-2021-WP-F-10

Rock type: Quartz vein within a Laminated unit

Basic description:

- Laminated unit consists of muscovite-clinozoisite dominant layers with minor chlorite, quartz, and sulphides. The Laminated unit has a quartz vein that is parallel to the fabric. In proximity to the quartz vein there is pervasive albite alteration that gets weaker away from the contact. Close to the contact the muscovite and clinozoisite are coarser, and clinozoisite is more euhedral. Sulphides are dominated by pyrite and minor pyrrhotite and chalcopyrite with a zonation composed of very fine-grained sulphides.
- The quartz vein is infilled with coarse grained quartz with recrystallization texture, and undulatory extinction. Patchy carbonate alteration around quartz grain boundaries. Parallel sections of the host rock are found within the quartz vein. The sections have an increased abundance of carbonate, chlorite, and albite alteration.

Paragenesis:

- clinozoisite -> titanite -> muscovite -> quartz -> chlorite -> carbonate -> sulphides

Mineralogy:

Primary:

- Quartz (38%)
    - Within host rock: Within the muscovite rich area, the grains are up to 60 micrometers and in low abundance, whereas in muscovite poor section the grains can be up to 300 micrometers. The grains are inclusion-rich.
    - Within crack and seal texture: The grains are up to 700 micrometers and inclusion-rich. Finer grains can be found in proximity to fracturing up to 200 micrometers.
- Muscovites (15%)
    - Within host rock: Anhedral to subhedral grains up to 200 micrometers. Strong fabric with clinozoisite and titanite inclusions.
    - Within crack and seal texture: Anhedral to subhedral grains up to 400 micrometers aligned to the orientation of the fracture.
- Plagioclase (10%): Anhedral grains up to 50 micrometers with sericite alteration.

Alteration:

- Albite alteration (10%): Pervasive texture destructive medium to dark brown alteration. Found in proximity to the quartz vein and within parallel section of the host rock in the quartz vein.
- Clinozoisite (10%)
    - Within host rock: Anhedral grains with elongation of the muscovite. Grains can be up to 300 micrometers and are dominantly inclusion-poor.
    - Within crack and seal texture: Anhedral grains up to 70 micrometers. The grains can be either inclusion-rich or inclusion-poor and both have irregular black coating around the grains.
- Chlorite (5%): Within crack and seal texture: Grains are up to 300 micrometers associated with muscovite and carbonate alteration. The grains are aligned to the elongation of the fracture. Grains grow around the muscovite grains.
- Sphalerite (3%): Within crack and seal texture: Anhedral grains infilling around the quartz grains. Contains inclusions of quartz, chlorite, muscovite, and anhedral inclusions of chalcopyrite.
- Chalcopyrite (2%): Anhedral grains up to 50 micrometers. Can occur either as isolated grains or in association with pyrite, pyrrhotite, or sphalerite. Found as chalcopyrite disease within sphalerite.

- Carbonate (2%): Anhedral to subhedral grains up to 200 micrometers, some exhibiting twinning planes. Carbonates wrap around quartz grains and chlorite.
- Pyrrhotite (1%): Within crack and seal texture: Anhedral to subhedral grains up to 200 micrometers. Associated with chlorite and carbonate alteration.

ID: ER-2021-WP-F-11

Rock type: Sulphide-rich layers within the Laminated unit

Basic description:

- The layers range from muscovite-rich to clinozoisite-rich to clinozoisite-biotite-rich to quartz-rich layers. The quartz-rich layers have a higher accumulation of chlorite along the contacts, and coarser sulphides along quartz grain boundaries.
- Sulphides consist of pyrite, pyrrhotite, and chalcopyrite grains. The sulfide grains have a black zonation around them which consist of very fine-grained sulphides. Pyrite is dominantly subhedral to euhedral and inclusion-poor and commonly found as an inclusion within inclusion-rich pyrrhotite. Chalcopyrite is inclusion-rich and contains inclusions of pyrrhotite and pyrite.

Paragenesis:

- clinozoisite -> biotite -> plagioclase -> quartz -> carbonates -> sulphides -> chlorite

Mineralogy:

Primary:

- Quartz (38%): Bimodal distribution of grains ranging from coarser 300 micrometers and finer grained less than 50 micrometers. The coarser grains are associated with lower abundance of biotite.
- Biotite (8%): The grains are up to 150 micrometers with a fabric wrapping around the clinozoisite grains. The biotite-poor area is finer grained up to 70 micrometers.
- Plagioclase (2%): The grains are up to 150 micrometers with weak to moderate sericite alteration.

Alteration:

- Pyrite (15%): Pyrite grains are subhedral to euhedral ranging in size from 100 to 300 micrometers. The pyrite grains are dominantly inclusion-poor. The grains can be found as inclusions within pyrrhotite or chalcopyrite.
- Pyrrhotite (13%): Anhedral grains associated with quartz-rich sections that are inclusion-rich.
- Clinozoisite (10%): Subhedral grains with bimodal distribution range from coarser grained up to 300 micrometers and finer grained less than 100 micrometers. The grains have irregular boundaries and are inclusion-rich. The grains have a higher abundance in biotite-rich zones.
- Chlorite (6%): Grains can be up to 300 micrometers and have a preferred orientation. Contains inclusions of pyrite.
- Carbonate (4%): Anhedral grains are found around grain boundaries of quartz.
- Chalcopyrite (2%): Anhedral grains associated with pyrite or pyrrhotite. The grains can be found as inclusions within pyrite or along grain boundaries of pyrite and pyrrhotite. Contains inclusions of pyrite.
- Sphalerite (2%): Anhedral grains up to 30 micrometers are found around the grain boundaries of quartz and sulphides. The grains have chalcopyrite disease.

ID: ER-2021-WP-F-13

Rock type: sheared contact between mylonite and feldspar porphyry

Basic description:

- The volcanic rock is composed of amphiboles, quartz, plagioclase with minor titanite and sulphides (pyrite and minor chalcopyrite). Minor phenocrysts of strongly altered plagioclase. Contains patchy albite alteration that are medium brown and also has darker brown patches of alteration. The darker patches of alteration as associated with a higher abundance of sulphides.
- The feldspar porphyry is composed of phenocrysts of altered feldspar within a matrix dominated by quartz, plagioclase, biotite with minor sulphides, clinozoisite, and chlorite. The small splay of the feldspar porphyry unit cuts volcanic rock.
- Contact between feldspar porphyry and the volcanic rocks. The contact has a higher abundance of coarse chlorite aligned parallel to the contact. Associated with chlorite are anhedral titanite inclusions.

Paragenesis:

- volcanic rock (titanite -> amphiboles -> sulphides) -> feldspar porphyry (feldspar -> clinozoisite = biotite = sulphides)

Mineralogy:

Primary:

- Amphibole (49%)
    - Within volcanic rock: Bimodal distribution with finer grained less than 150 micrometers and coarser grains up to 400 micrometers. The amphiboles have been replaced by unknown opaque that has a brown reaction rim.
    - Within contact: Grains up to 300 micrometers oriented with the fracture contact and mixed with chlorite.
- Quartz (17%)
    - Within volcanic rock: Grains up to 100 micrometers with minor micro inclusions.
    - Within feldspar porphyry: Recrystallized grains up to 200 micrometers exhibit undulatory extinction. Inclusions of amphiboles.
- Plagioclase (15%)
    - Within volcanic rock: Strongly sericite altered clasts up to 400 micrometers. The amphiboles wrap around the grains and in some cases cut through the grain. The grains have micro inclusions.
    - Within feldspar porphyry: Grains that exhibit simple and polysynthetic twinning are potentially mixed with feldspar clasts.
- Microcline (4%)
    - Within feldspar porphyry: Coarser grains up to 1,200 micrometers. The grains are moderately to strongly sericite altered and contain micro inclusions. Amphiboles are crystallizing around the clasts. Ilmenite-titanite is found around grains boundaries with brown alteration halo.

Alteration:

- Chlorite (10%): Along the contact: Coarse grains up to 500 micrometers oriented with the orientation of the contact. The grains have inclusions of ilmenite-titanite and are carbonate altered.
- Carbonate (3%): Along the contact: Anhedral grains up to 60 micrometers.
- Clinozoisite (3%)

    - Within volcanic rock: Anhedral grains up to 70 micrometers associated with amphibole-chlorite rich section.
    - Within feldspar porphyry: Anhedral grains up to 50 micrometers as inclusions within feldspar.
- Ilmenite-titanite (3%): Ilmenite core with a zonation of titanite around the ilmenite. Anhedral grains up to 70 micrometers are found as patches around edges of amphiboles.
- Pyrite (trace): Within volcanic rock: Subhedral grains up to 60 micrometers as inclusions with quartz grains. The pyrite has an irregular black coating around the grain.
- Chalcopyrite (trace): Within volcanic rock: Anhedral grains up to 40 micrometers associated with amphiboles or quartz inclusions.

ID: ER-2021-WP-F-17

Rock type: Quartz vein with sulphides along edges within the Laminated unit

Basic description:

- The Laminated unit has variable layers that range from clinozoisite-muscovite dominant to quartz-feldspar dominant to muscovite dominant. Boudinage quartz vein is parallel to the layers with massive sulphides along both contacts. The Laminated unit layers that are in proximity to the quartz vein have albite alteration. Closer to the contact with the quartz vein muscovite gets coarser and is more altered by chlorite.
- The quartz vein is dominated by very coarse quartz grains with undulatory extinction and minor recrystallization texture.
- Sulphides are dominated by pyrite with minor pyrrhotite and chalcopyrite. The pyrrhotite grains can be found either as a round inclusion or along grain boundaries. Chalcopyrite can be found as round inclusions within pyrite, along pyrite grain boundaries or around quartz grain boundaries. Both pyrrhotite and chalcopyrite are found near proximity to the quartz vein only. Sulphides contain an irregular zonation around the edges composed of very fine-grained sulphides.

Paragenesis:

- clinozoisite -> muscovite -> quartz -> chlorite -> sulphides -> carbonate

Mineralogy:

Primary:

- Muscovite (35%)
    - Within host rock: Grains are up to 100 micrometers, with weak fabric. The grains wrap around pyroxene grains.
    - Along the contact: The muscovite abundance increases in proximity to the contact. The muscovite grains are oriented along the contact. There are pyroxene and unknown blue as inclusions. Chlorite and carbonate alter the muscovite grains.
- Quartz (20%)
    - Within host rock: Recrystallized grains up to 10 micrometers, contains micro inclusions.
    - Within quartz vein: Coarser grains up to 4,000 micrometers exhibiting undulating extinction. Grains have chlorite and carbonate along grain boundaries and are abundant with micro inclusions.
- Plagioclase (9%): The grains are up to 200 micrometers and exhibit simple twinning. The grains have weak to moderate sericite alteration.

Alteration:

- Albite alteration (10%): Medium to dark brown texture destructive alteration found in proximity to the quartz vein.
- Pyrite (10%)
    - Within quartz vein: Subhedral grains along the contact of the host rock to quartz with grains up 600 micrometers. Contains inclusions of chlorite, chalcopyrite, and host rock. Grains are inclusion-rich and inclusions poor.
- Clinozoisite (13%): Subhedral grains up to 200 micrometers with inclusions. The grains can be found either within muscovite rich layers or in proximity to the contact. Found as inclusions within chlorite and pyrite grains.
- Biotite (2%): Anhedral grains up to 20 micrometers are found within proximity to the quartz vein.
- Chlorite (2%): Dominantly found along the contact with the quartz vein. The grains are up to 250 micrometers and can be found as inclusions within the sulphides.
- Carbonate (1%): Found dominantly within quartz vein or near proximity to the contact. Carbonate grains are along pyrite grain boundaries or crystallizing from along pyrite grains or associated with muscovite-rich contact.

- Chalcopyrite (trace)
    - Within quartz vein: Anhedral grains as inclusions within pyrite or along grain boundaries up to 80 micrometers. Chalcopyrite and pyrrhotite can be found in the same inclusion.
- Pyrrhotite (trace)
    - Within quartz vein: Anhedral grains as inclusions within pyrite or along grain boundaries up to 120 micrometers.
- Sphalerite (trace): Anhedral grains up to 150 micrometers along the contact with quartz vein. The grains are found as inclusions within pyrite.

ID: ER-2021-WP-F-18

Rock type: mylonite

Basic description:

- The host rock is composed of very fine-grained quartz, plagioclase, biotite with minor chlorite and sulphides (pyrite-pyrrhotite).
- The rock is associated with various veins:
    - 1 – Irregular patchy chlorite alteration. The alteration exploits the fabric within the rock and gives the appearance of a spiky alteration. The alteration is not associated with any visible fracture.
    - 2 - weakly boudinage vein infilled with recrystallized quartz. The alteration halo is wavy up to 300 micrometers.
    - 3 - Quartz infilled vein on an angle to vein 2. The vein diminishes within the alteration and cross cutting is uncertain.
    - 4 - recrystallized fine-grained quartz infill with coarse grained patchy chlorite. When the vein interacts with vein 6 the chlorite vein orientation does not change, also the chlorite grains are found along the edges of the contact. After the intersection with vein 6 (carbonate) the chlorite becomes more discontinuous.
    - 5 – Boudinage vein infilled with recrystallized quartz grains and coarse plagioclase. The vein has a carbonate overprint in proximity to vein 6 (carbonate infill). The vein is offset by vein 6.
    - 6 - carbonate infilled vein with minor inclusions of host rock within the vein. Small euhedral to subhedral titanite grains found within the center of the vein only when in proximity to vein 4 (chlorite). The thicker part of the vein is with the interaction with vein 4 (chlorite).
    - 7 - discontinuous sections infilled with quartz. The vein is not visible when in vicinity to either vein 5 (quartz) or vein 4 (chlorite-quartz infill).
    - 8 - hairline vein infilled with quartz with albite alteration halo with darker brown patches. No visible cross-cutting relationship noted.
    - 9 - Discontinuous section of chlorite-quartz. The alteration halo is variable and has inclusions of clinozoisite grains. Cut by vein 7.

Paragenesis:

- vein 5 (quartz) -> vein 4 (quartz) -> vein 6 (carbonate)

Mineralogy:

Primary:

- Quartz (44%)
    - Within host rock: Recrystallized grains up to 100 micrometers. Commonly have micro inclusions.
    - Within vein 2: Grains are up to 200 micrometers and have micro inclusions. The contact is sharp, and some grains exhibit undulatory extinction.
    - Within vein 3: Grains are up to 200 micrometers and have micro inclusions. The grains have local chlorite grains around the rims of the vein.
    - Within vein 4: Grains up to 60 micrometers.
    - Within vein 5: Grains up to 150 micrometers with micro inclusions. The grains have carbonate alteration around the grains when in proximity to vein 6.
    - Within vein 7: Grains up to 60 micrometers with micro inclusions. The grain boundaries are sharp. Some of the quartz grains have an odd yellow coloration in cross polars.

    - Within vein 8: Massive infill with no discernable grain sizes.
    - Within vein 9: Grains can be up to 100 micrometers and have micro inclusions. The grain boundaries are sharp.
- Amphibole (15%): The grains are typically around 150 micrometers and form the fabric of the rock. The grains have patchy carbonate alteration.
- Plagioclase (6%): Subhedral grains commonly below 150 micrometers with weak to moderate sericite alteration. The coarser grains can be up to 300 and exhibit polysynthetic twinning and moderate to strong sericite alteration. The grains have micro inclusions.

Alteration:

- Chlorite (25%)
    - Within vein 1: Massive alteration. The alteration exploits the fabric of the rock and produces a varying thickness of alteration. Within the alteration there are darker brown patches.
    - Within vein 4: Elongated grains up to 350 micrometers to the orientation of the vein, with grains up to 60 micrometers. When in contact with vein 6 the chlorite grains are found on either side of the vein.
    - Within vein 5: Elongated grains around the edges of the vein up to 100 micrometers.
    - Within vein 9: Grains can be up to 300 micrometers and have inclusions of titanite and amphiboles. The alteration halo has darker brown patches.
- Carbonate (3%)
    - Within vein 6: Subhedral grains up to 200 micrometers. The grains contain inclusions of titanite, chlorite, host rock and sulphides.
- Clinozoisite (4%): Anhedral grains up to 40 micrometers with higher concentrations in proximity to alteration patches.
- Biotite (1%): Anhedral to subhedral grains up to 100 micrometers and make up the fabric of the host rock with amphiboles.
- Pyrrhotite (1%): Disseminated grain associated with pyrite up to 40 micrometers.
- Titanite (1%)
    - Within vein 2: Anhedral grains up to 50 micrometers as inclusions within amphiboles.
    - Within vein 6: Anhedral grains up to 50 micrometers found as inclusions within carbonate matrix.
- Pyrite (trace)
    - Within host rock: Anhedral grains up to 60 micrometers. The grains have an irregular black alteration halo.
    - Within vein 2: Subhedral grains up to 70 micrometers associated with amphiboles.

ID: ER-2022-WP-F-44

Rock type: mylonite

Basic description:

- The host rock is dominated by quartz, plagioclase, clinozoisite with minor biotite, chlorite and titanite.
- Quartz vein cut the rock with minor recrystallization texture. The quartz grains contain inclusions of clinozoisite, chlorite, and carbonate. Along the contact of the vein there is a higher abundance of chlorite aligned to the orientation of the contact. Also, a higher abundance of sulphides is associated along the contact with the chlorite.
- The sulphides contain inclusions of quartz, chlorite, and carbonate grains. Two zones of sulphide distribution which include: (1) chalcopyrite-pyrite dominant with minor pyrrhotite. The zone occurs where the quartz vein pinches out to dominantly chlorite and minor quartz; and (2) pyrrhotite dominant with coarser grained pyrite and minor chalcopyrite. Contains zonation of sulphides consisting of very fine-grained sulphides.

Paragenesis:

- host rock -> quartz -> chlorite -> sulphides -> carbonate

Mineralogy:

Primary:

- Quartz (40%)
    - Within host rock: Very fine grains up to 5 micrometers with irregular grain boundaries
    - Within quartz vein: Anhedral to subhedral grains up to 40 micrometers, exhibiting undulatory extinction. The grains have irregular boundaries with finer grain quartz up to 10 micrometers found along the contacts. The grains contain abundant micro inclusions.
- Plagioclase (10%): Very fine grains up to 5 micrometers with sericite alteration.
- Biotite (5%): Anhedral grains found along fractures up to 40 micrometers, being altered to chlorite. Finer grains up to 10 micrometers can be found through the host rock as randomly oriented grains.

Alteration:

- Chlorite (20%): Dominantly found along contact with quartz and host rock up to 60 micrometers. The coarser grains are sub parallel to parallel to the contact. Finer grains up to 20 micrometers can be found within the host rock in proximity to the contact. The finer grains are randomly oriented.
- Clinozoisite (15%): Subhedral to euhedral grains up to 60 micrometers, commonly less than 20 micrometers. The grains have high relief and anomalous blue and yellow interference colors. The grains contain abundant micro inclusions, including titanite. The grains have irregular contact with host rock, found in higher concentrations where there is a texture destructive light to moderate brown alteration.
- Carbonate (3%): Dominantly found along contact with quartz vein and host rock. Euhedral to subhedral grains, up to 50 micrometers (commonly less than 30 micrometers), dominantly aligned parallel to subparallel to the contact.
- Pyrrhotite (3%): Massive texture dominantly concentrated along contact of quartz with host rock. Disseminated po found within proximity of contact within the host rock up to 20 micrometers. Contains inclusions of subhedral-euhedral pyrite grains and anhedral chalcopyrite. Chalcopyrite is dominantly found along contact or edges of grains opposed to inclusions. Pyrrhotite grains contain abundant micro inclusions.

- Pyrite (2%): Subhedral to euhedral grains up to 60 micrometers. The grains are dominantly inclusion free, with only edges of the grains having grain inclusions. Contains inclusions of anhedral chalcopyrite.
- Chalcopyrite (1%): Anhedral grains are associated with either pyrite or pyrrhotite. Can be found as inclusions within pyrite or pyrrhotite. Locally contain chalcopyrite rich zone characterized by minor pyrrhotite and finer grained (up to 30 micrometers) subhedral to euhedral pyrite grains.
- Titanite (1%): Anhedral inclusions within chlorite or clinozoisite up to 10 micrometers.

ID: ER-2022-WP-F-45

Rock type: mylonite

Basic description:

- The host rock is composed of quartz, plagioclase with minor muscovite, sulphides, clinozoisite and biotite.
- Host rock is associated with various veins:
    - 1 - subparallel to the fabric of the host rock. The vein is dominated by strong carbonate infill with anhedral quartz grains. Chlorite can be found along both hanging wall and footwall contact, with some grains found as inclusions within the vein infill. Albite alteration halo is texture destructive ranging from 40 to 70 micrometers.
    - 2 - infill has mostly been plucked out during the thin section process, with only remnant of infill found along the contact with host rock. Alteration is highly variable as it cuts fabric on an angle. The alteration halo is moderate brown and is texture destructive. The vein offsets vein 1.

Paragenesis:

- host rock -> vein 1 (quartz -> carbonate) -> vein 2 (zeolite)

Mineralogy:

Primary:

- Quartz (40%)
    - Within host rock: Subhedral to anhedral grains up to 10 micrometers exhibiting undulatory extinction. The grains have irregular grains boundary and contain micro inclusions.
    - Within vein 1: Anhedral grains up to 10 micrometers dominantly concentrated along the contact with the host rock. Can be found as inclusions within carbonate infill.
- Plagioclase (10%): Anhedral to subhedral grains up to 10 micrometers. Irregular grain boundaries with quartz.
- Biotite (5%): Subhedral grains up to 10 micrometers. The grains make up the fabric of the host rock. In proximity to alteration halo the biotite gets altered by chlorite.
- Muscovite (2%): Anhedral grains up to 30 micrometers exhibiting birds eye extinction commonly less than 10 micrometers. The grains are randomly oriented throughout the sample, and coarser grains are associated within proximity to alteration.

Alteration:

- Orthoclase/albite alteration (30%): Light to moderate brown alteration. Texture destructive.
- Zeolite (Laumontite; 4%): Vein 2: Low birefringence and very soft. Only remnants of the infill are left on the edges of the vein. Raman spectroscopy showed a good match to a laumontite (zeolite).
- Chlorite (3%)
    - Vein 1: Subhedral to euhedral grains up to 30 micrometers. The grains are found along the hanging wall and footwall contact, oriented parallel to sub parallel to the contact.
    - Alteration halo: Subhedral to euhedral grains up to 40 micrometers dominantly oriented parallel to fabric altering biotite.
- Carbonate (3%): Vein 1: Main infill of the vein. Anhedral to subhedral grains up to 70 micrometers. Contains inclusions of chlorite and quartz.
- Ilmenite-Titanite (2%): Alteration halo: Found as disseminated grains in associated with titanite and chlorite.
- Pyrite (1%)

    - Vein 1: Anhedral disseminated grains up to 3 micrometers as inclusions within carbonates.
    - Alteration halo of vein 3-A: Anhedral grains up to 10 micrometers, associated with light to moderate brown alteration.
- Chalcopyrite (trace): Disseminated rains up to 2 micrometers found as isolated sections in proximity to alteration halo and chlorite grains.

ID: ER-2022-WP-F-46

Rock type: mylonite

Basic description:

- Host rock is composed of quartz, plagioclase, biotite, titanite and sulphides. Disseminated ilmenite with zonation of titanite aligned parallel to the fabric. Ilmenite that is not within the alteration halo is not altering to titanite.
- Host rock is associated with various veins:
    - 1 – Vein infilled with zeolite with orthoclase alteration. The fracture splits into multiple discontinuous parallel fractures. Cuts vein 2.
    - 2 - Vein infilled with quartz with albite alteration. Associated with higher concentrations of inclusion-poor pyrite along the edges of the contact with minor chalcopyrite.

Paragenesis:

- host rock -> vein 2 (quartz) -> vein 1 (zeolite)

Mineralogy:

Primary:

- Quartz (28%)
    - Within host rock: Anhedral grains up to 10 micrometers with irregular contacts.
    - Within vein 2: Massive grains up to 5 micrometers
- Plagioclase (15%): Anhedral grains up to 10 micrometers with micro inclusions.
- Biotite (10%): Make up the fabric of the host rock with grains up to 5 micrometers.
- Amphiboles (10%): Anhedral grains elongated parallel to the fabric of the host rock up to 10 micrometers.
- Muscovite (2%): Anhedral grains up to 10 micrometers dominantly parallel to the fabric but can also be randomly oriented.

Alteration:

- Albite alteration (20%): Texture destructive alteration light to medium brown in color, associated with increased number of ilmenite alteration.
- Orthoclase alteration (10%): Texture destructive alteration medium to dark brown in color, associated with increased number of ilmenite alteration.
- Zeolite (2%): Within vein 1: Anhedral grains up to 30 micrometers, exhibiting low interference colors and containing abundant micro inclusions.
- Ilmenite-Titanite (3%): Irregular grains up to 15 micrometers. Within the host rock the grains are elongated parallel to the fabric. As the grains come to proximity to the alteration halo the ilmenite alteration increases and contain zonation of titanite around the edges of the grains.
- Pyrite (trace): Euhedral to subhedral grains up to 20 micrometers associated with quartz infilled vein. The grains are crystallizing within the host rock in proximity to the vein.
- Chalcopyrite (trace): Disseminated grains up to 2 micrometers are found within proximity to vein 2 and higher occurrence of pyrite.

ID: ER-2022-WP-F-47

Rock type: Feldspar porphyry

Basic description:

- Host rock is dominated by anhedral coarse-grained amphiboles. The amphiboles contain inclusions of ilmenite, pyrite, quartz, and plagioclase. Ilmenite-titanite are concentrated around the edges of the amphibole grains.
- Contains altered coarse-grained phenocrysts of plagioclase that are abundant in inclusions. The inclusions consist of clinozoisite, amphiboles, biotite, and quartz.
- Sulphides have black zonation around them composed of fine-grained parent sulphide.

Paragenesis:

- plagioclase -> clinozoisite -> amphiboles -> biotite = sulphides

Mineralogy:

Primary:

- Amphiboles (40%): Coarse subhedral to euhedral amphiboles up to 70 micrometers, but commonly range between 30-50 micrometers. The grains wrap around the plagioclase phenocrysts. Contains inclusions of sulphides and
- Quartz (26%): Anhedral grains up to 10 micrometers, commonly less than 5 micrometers. The grains exhibit irregular grains boundaries and some show undulatory extinction.
- Plagioclase (15%): Very coarse phenocrysts over 300 micrometers exhibiting simple and polysynthetic twinning. The grains are inclusion-rich (in some cases the inclusions are within the core of the grains and sometimes throughout the entire grains). Contains inclusions of clinozoisite, amphiboles, biotite, and quartz.
- Biotite (5%): Anhedral grains randomly oriented up to 15 micrometers.

Alteration:

- Ilmenite (7%): Elongated grains up to 20 micrometers associated with coarse amphibole grains. Includes inclusions of chalcopyrite.
- Clinozoisite (4%): Anhedral grains up to 10 micrometers, dominantly found as inclusions within plagioclase.
- Chalcopyrite (2%): Disseminated anhedral grains up to 10 micrometers but commonly less than 5 micrometers. Commonly associated within proximity to pyrite.
- Pyrite (1%): Anhedral grains up to 10 micrometers, but commonly less than 5 micrometers. Inclusion-poor grains.
- Titanite (trace): Alteration of ilmenite around the edges.
- Sphalerite (trace): Elongated grain up to 10 micrometers hosted within amphibole grains.

ID: ER-2022-WP-F-48

Rock type: Volcanic rock

Basic description:

- The host rock is dominated by coarse grained amphiboles within a matrix of finer grained amphiboles, sulphides, clinozoisite and ilmenite-titanite.
- The host rock is associated with:
    - 1 - Thin (less than 10 micrometers) boudinage fractures are cutting the host rock infilled with quartz. The fractures are randomly oriented and have no alteration halos associated with them.

Paragenesis:

- amphibole -> titanite -> quartz = sulphides

Mineralogy:

Primary:

- Amphibole (80%)
    - Coarse grained phenocrysts: Subhedral coarse grains are up to 200 micrometers, commonly less than 150 micrometers with micro inclusions and alteration rims. Being altered by chlorite. Contain inclusions of quartz, and sulphides.
    - Within matrix: Anhedral to subhedral finer grains are less than 10 micrometers in width. The grains are more typically associated with quartz, titanite and sulphides.
- Quartz (15%)
    - Within matrix: Anhedral grains up to 5 micrometers.
    - Within vein: Anhedral grains up to 10 micrometers.

Alteration:

- Titanite (3%): Anhedral grains up to 3 micrometers distributed throughout the host rock. Commonly not associated with coarser grained amphiboles
- Chlorite (3%): Subhedral grains up to 40 micrometers, dominantly found altering coarse amphiboles.
- Pyrite (2%): Anhedral to subhedral grains up to 10 micrometers, commonly less than 5 micrometers, distributed throughout the host rock. Commonly associated with coarser amphiboles. Grains are inclusion-poor but can contain inclusions of pyrrhotite or chalcopyrite.
- Pyrrhotite (1%): Anhedral grains up to 5 micrometers, commonly associated with pyrite and chalcopyrite.
- Chalcopyrite (trace): Disseminated anhedral grains up to 5 micrometers, commonly associated with either pyrite or pyrrhotite.

ID: ER-2022-WP-F-49

Rock type: Laminated unit

Basic description:

- The Laminated unit is composed of biotite-, muscovite-, or quartz-rich layers. Biotite-rich layers are also associated with subhedral to euhedral chlorite and subhedral to euhedral clinozoisite dominantly found along the core of the layer elongated parallel to the fabric. Muscovite-rich layers are dominated by quartz-feldspar-biotite. The biotite grains are finer grained than in the biotite-rich layer. Chlorite is elongated parallel to fabric.
- Sulphides are dominantly associated with biotite-rich layers but can also be associated with muscovite-rich layers. The sulphides are elongated parallel to the fabric.

Paragenesis:

- quartz = plagioclase -> clinozoisite -> biotite -> titanite -> chlorite = sulphides

Mineralogy:

Primary:

- Quartz (44%)
    - Within layers: Finer grains are up to 5 micrometers found dominantly within the muscovite-rich layers. The grains exhibit undulatory extinction and contain micro inclusions.
    - Within quartz-rich layers: Coarser grains are up to 15 micrometers with undulatory extinction. The grains contain inclusions of biotite.
- Biotite (35%)
    - Within biotite-rich layers: Coarser grains up to 15 micrometers, commonly less than 10 micrometers. The grains make up fabric of the host rock.
    - Within muscovite-rich layers: Finer grains are up to 5 micrometers.
- Plagioclase (4%): Anhedral grains up to 5 micrometers found within the biotite-rich layers associated with quartz.

Alteration:

- Chlorite (6%): Subhedral grains up to 30 micrometers, found within biotite-rich layers sub-parallel to fabric. Contains inclusions of biotite and quartz.
- Clinozoisite (4%): Subhedral to euhedral grains up to 20 micrometers in width. The grains have irregular grain boundaries and are randomly oriented in biotite-rich layer.
- Titanite (3%): Subhedral grains up to 20 micrometers associated with chlorite within the biotite-rich layers.
- Pyrite (2%): Anhedral to subhedral grains up to 20 micrometers found within the biotite-rich layers and are inclusion-poor. Associated with pyrrhotite and chalcopyrite and contains inclusions of chalcopyrite and pyrrhotite.
- Pyrrhotite (1%): Anhedral grains up to 10 micrometers associated with biotite-rich layers. The grains are associated with pyrite and chalcopyrite and contain inclusions of pyrite and chalcopyrite.
- Chalcopyrite (1%): Anhedral grains up to 5 micrometers, found as disseminated grains within the biotite-rich layers. The grains are dominantly found along the grain boundaries but can also be found as inclusions with the sulphides.

ID: ER-2022-WP-F-50

Rock type: mylonite

Basic description:

- The host rock is composed of quartz, plagioclase, biotite, clinozoisite and minor chlorite. The host rock has a fabric to it defined by aligned biotite and muscovite grains.
- The host rock is associated with various veins:
    - 1 – Vein infilled with zeolite. Part of the vein has been plucked out during the thin section process. The albite alteration halo is light to medium brown. Cuts vein 2.
    - 2 – vein infilled with chlorite and minor quartz and titanite inclusions.

Paragenesis:

- host rock -> vein 2 (chlorite) -> vein 1 (zeolite)

Mineralogy:

Primary:

- Quartz (20%)
    - Within host rock: Anhedral grains up to 10 micrometers, commonly less than 5 micrometers.
    - Within vein 2: Anhedral grain up to 20 micrometers with weak undulatory extinction. The grains contain micro inclusions.
- Plagioclase (10%): Anhedral grains up to 10 micrometers, commonly less than 5 micrometers with sericite alteration.
- Biotite (15%): Anhedral to subhedral grains up to 5 micrometers that make up the fabric of the host rock with muscovite. The concentration of biotite decreases the closer it is to the vein with white infill.
- Muscovite (10%): Anhedral to subhedral grains up to 10 micrometers making up the fabric of the host rock with biotite.

Alteration:

- Albite alteration halo (28%): Texture destructive alteration halo ranging from light to dark brown. The most common is light to medium brown. The darker patches are more calcic or titanium rich. Along the contact of host rock and zeolite infill vein the darker patches are Ti-rich.
- Clinozoisite (10%): Anhedral to subhedral grains up to 10 micrometers. Have a higher abundance within the alteration halo.
- Chlorite (4%): Subhedral grains up to 40 micrometers aligned to the fabric of the host rock. The grains are alteration biotite and muscovite.
- Carbonate (2%): Anhedral grains up to 15 micrometers are found within the host rock in proximity to the zeolite infill vein, or along the contact of vein and host rock.
- Zeolite (2%): White vein infill in hand specimen. The majority of the veins have been plucked out during the process of making thin section.
- Titanite (1%): Darker brown patches of the contact with the host rock and the vein are Ti-rich, according to Raman titanite.
- Pyrite (trace): Disseminated anhedral grains up to 10 micrometers found within host rock and alteration.

ID: ER-2022-WP-F-51

Rock type: mylonite

Basic description:

- The host rock is composed of quartz, plagioclase, biotite, chlorite, and sulphides.
- The vein is associated with various veins:
    - 1 – infilled with chlorite, quartz, and plagioclase. Carbonate alteration is dominantly found along the contact of the vein. The albite alteration halo is medium brown with small darker brown patches. Cuts vein 2.
    - 2 – infilled with massive quartz and irregular medium to dark brown alteration halo. The veins consist of a series of sub parallel veins with same alteration halos.
    - 3 – discontinuous sections of chlorite infilled vein with weak alteration halo. Cut by vein 2.

Paragenesis:

- host rock -> vein 3 (chlorite) -> vein 2 (massive quartz) -> vein 1 (chlorite-quartz-plagioclase)

Mineralogy:

Primary:

- Quartz (33%)
    - Within host rock: Anhedral grains up to 10 micrometers.
    - Within vein 1: Anhedral grains up to 50 micrometers.
    - Within vein 2: Massive quartz.
- Plagioclase (15%)
    - Within host rock: Anhedral grains up to 10 micrometers.
    - Within vein 1: Anhedral grains up to 50 micrometers with moderate sericite alteration.
- Biotite (15%): Anhedral grains up to 15 micrometers that are randomly oriented.

Alteration:

- Albite alteration (15%): Texture destructive medium to dark brown alteration. Associated with various veining.
- Chlorite (10%)
    - Within host rock: Anhedral grains up to 150 micrometers. Contain inclusions of titanite and clinozoisite.
    - Within vein 1: Anhedral grain up to 100 micrometers. Contains inclusions of sulphides and quartz.
    - Within vein 3: Anhedral grains up to 30 micrometers oriented parallel to the vein.
- Clinozoisite (6%)
    - Within host rock: Anhedral grains up to 10 micrometers.
- Ilmenite-Titanite (3%)
    - Within vein 1: Irregular grains up to 50 micrometers, dominantly found along the contacts. Elongated parallel to the contact. Contains zonation of titanite around the ilmenite grains.
    - Within host rock: Irregular grains up to 20 micrometers containing titanite around the edges of the vein.
- Pyrite (2%): Disseminated anhedral to subhedral pyrite grains up to 10 micrometers. Distributed through the host rock.
- Titanite (1%): Anhedral grains up to 10 micrometers. Dominantly found as inclusions within chlorite.

ID: ER-2022-WP-F-52

Rock type: mylonite

Basic description:

- The host rock is dominated by quartz, plagioclase, biotite, clinozoisite, and minor chlorite.

Paragenesis:

- host rock -> vein (titanite -> zeolite -> muscovite -> chlorite)

Mineralogy:

Primary:

- Quartz (30%)
  - Within host rock: Anhedral grains up to 5 micrometers.
  - Within vein: Anhedral grains up to 10 micrometers with undulating extinction. The grains are found along the contact.
- Plagioclase (15%): Anhedral grains up to 5 micrometers with weak sericite alteration.
- Biotite (15%): Subhedral to anhedral grains up to 10 micrometers

Alteration:

- Orthoclase alteration (10%): Texture destructive alteration that is medium to dark brown in color.
- Albite alteration (9%): Texture destructive alteration that is light to medium brown in color.
- Clinozoisite (6%)
  - Within host rock: Anhedral grains up to 10 micrometers.
- Chlorite (5%)
  - Within host rock: Anhedral grains up to 20 micrometers
  - Within alteration halo: Anhedral grains up to 40 micrometers.
  - Within vein: Anhedral grains up to 40 micrometers, dominantly oriented parallel to the contact. The grains contain inclusions of titanite.
- Muscovite (4%)
  - Within host rock: Anhedral grains up to 15 micrometers. Contains inclusions of biotite.
  - Within vein: Subhedral grains up to 50 micrometers with inclusions of titanite.
- Zeolite (3%)
  - Within vein: Anhedral grains elongated sub-parallel to the orientation of the vein. The mineral is found along the core of the fracture. Contains inclusions of muscovite.
- Titanite (2%): Anhedral to subhedral grains up to 20 micrometers. Found as inclusion within zeolite and chlorite.

ID: ER-2022-WP-F-53

Rock type: mylonite

Basic description:

- Highly deformed quartz vein hosted within volcanic rock. The quartz vein is altered by light to medium brown texture destructive alteration with patches of dark brown.

Paragenesis:

- amphibole -> chlorite -> quartz -> quartz vein

Mineralogy:

Primary:

- Amphibole (60%)
    - Within host rock: Bimodal distribution with coarser grains up to 50 micrometers, and finer grained up to 10 micrometers.
- Quartz (20%)
    - Within host rock: Anhedral grains up to 5 micrometers.
    - Within quartz vein: Anhedral grains up to 60 micrometers with strong recrystallization texture. Contains inclusions of clinozoisite, titanite and host rock.

Alteration:

- Albite alteration (8%): Light to medium dark texture destructive alteration. Contains patches of dark brown alteration.
- Chlorite (3%)
    - Within host rock: Subhedral elongated grains up to 20 micrometers. Wrap around amphibole grains.
- Clinozoisite (3%)
    - Within host rock: Subhedral grains up to 20 micrometers. Contains inclusions of amphibole.
    - Within quartz vein: Anhedral grains up to 10 micrometers as inclusions within quartz vein.
- Titanite (1%)
    - Within host rock: Anhedral grains up to 5 micrometers can be either found as inclusion within amphiboles or along grain boundaries of coarser amphiboles.
    - Within quartz vein: Anhedral to subhedral grains up to 30 micrometers.

ID: ER-2022-WP-F-54

Rock type: quartz vein cutting the Laminated unit

Basic description:

- The Laminated unit is composed of either quartz-, muscovite- or clinozoisite-rich layers.
- The host rock is associated with various veins:
    - 1 – Vein infilled with quartz. The vein is infilled with coarse quartz with recrystallization texture. The contact contains chlorite and clinozoisite.

Paragenesis:

- host rock -> vein (quartz)

Mineralogy:

Primary:

- Quartz (54%)
    - Within host rock: Anhedral grains up to 5 micrometers.
    - Within quartz vein: Anhedral grains up to 200 micrometers with undulatory extinction. The grains exhibit recrystallization texture. Contain micro inclusions.
- Muscovite (15%)
    - Within host rock: Anhedral grains up to 40 micrometers that make up the fabric of the rock. When associated with albite alteration the grains are coarser up to 60 micrometers.
- Clinozoisite (10%)
    - Within host rock: Anhedral grains up to 20 micrometers elongated to the fabric.
- Plagioclase (5%)
    - Within host rock: Anhedral grains up to 5 micrometers with weak sericite alteration.
- Biotite (3%)
    - Within host rock: Anhedral grains up to 10 micrometers elongated parallel to the fabric.

Alteration:

- Albite alteration (5%)
    - Within host rock: Light to medium brown texture destructive alteration.
- Chlorite (4%)
    - Within host rock: Anhedral grains up to 40 micrometers, or as an alteration of muscovite.
    - Within quartz vein: Anhedral grains up to 30 micrometers were found along quartz grain boundaries.
- Clinozoisite (2%)
    - Along quartz contact: Folded texture, anhedral grains up to 5 micrometers.
- Ilmenite-titanite (2%)
    - Within host rock: Anhedral grains up to 20 micrometers. Contains zonation of titanite.
- Pyrrhotite (1%)
    - Within host rock: Anhedral grains up to 15 micrometers with higher accumulation in the quartz-rich layers.
- Pyrite (1%)
    - Within host rock: Anhedral grains up to 15 micrometers that are inclusion-poor. Have a higher accumulation in the quartz-rich layers.
- Chalcopyrite (trace)
    - Within host rock: Anhedral grains up to 5 micrometers.

ID: ER-2022-WP-N-23

Rock type: Laminated unit

Basic description:

- Alternating layers of muscovite-rich, biotite-rich, and quartz-plagioclase-rich layers. All layers have an associated clinozoisite elongated parallel to the fabric. Trace relict feldspar phenocrysts are found within the layers. The fabric wraps around the phenocrysts that are strongly altered. Disseminated pyrite grains are found throughout the layers.
- Parallel to the layers is a quartz vein with minor recrystallization texture. The contacts of the vein have an increased amount of chlorite and muscovite parallel to the contact. Minor carbonate alteration is found along quartz grain boundaries.

Paragenesis:

- plagioclase phenocrysts -> clinozoisite = pyrite -> biotite = musc -> quartz = plagioclase -> carbonate

Mineralogy:

Primary:

- Quartz (25%)
    - Within layers: Anhedral grains less than 5 micrometers
    - Within quartz vein: Subhedral grains up to 50 micrometers, commonly around 30-40. Contains recrystallization texture and contains carbonate along grain boundaries.
- Plagioclase (20%)
    - Within layers: Anhedral grains less than 5 micrometers
    - Phenocrysts: The clasts are up to 100 micrometers and are strongly altered. Contain inclusions of muscovite and clinozoisite. Pervasive medium to dark brown alteration. The fabric wraps around the clasts.

Alteration:

- Muscovite (20%)
    - With quartz vein: Up to 40 micrometers that is parallel to the contact. The grains wrap around plagioclase phenocryst.
    - Within layers: Up to 10 micrometers and contain inclusions of clinozoisite.
- Biotite (20%)
    - Within layers: Subhedral grains up to 10 micrometers, commonly less than 5 micrometers.
- Clinozoisite (10%)
    - Within layers: Subhedral grains up to 20 micrometers, commonly less than 10 micrometers. The grains are elongated parallel to fabric. In proximity to the quartz vein the grain size increases to 30 micrometers.
- Carbonate (1%)
    - Within quartz vein: Anhedral grains up to 20 micrometers found along quartz grain boundaries, or parallel to the contact.
- Chlorite (1%)
    - Within layers: Anhedral grains up to 10 micrometers.
    - Withing quartz vein: Anhedral grains up to 30 micrometers that are parallel to the contact of the vein.
- Pyrite (1%)
    - Within the layers: Disseminated anhedral grains up to 3 micrometers.
    - Within quartz vein: Subhedral grain up to 10 micrometers.

ID: ER-2022-WP-N-24

Rock type: Laminated unit

Basic description:

- Alternating layers of biotite-, muscovite-, or quartz-rich layers. The layers have an elongated clinozoisite parallel to the fabric.
- Sulphides are dominated by pyrite with a higher abundance in the biotite- or muscovite-rich layers.
- Contains quartz-rich lenses with coarser quartz grains. The lenses are elongated parallel to the fabric.

Paragenesis:

- clinozoisite -> muscovite = biotite -> chlorite -> quartz = plagioclase

Mineralogy:

Primary:

- Muscovite (28%): Anhedral grains can be up to 20 micrometers, commonly less than 5 micrometers with weak chlorite alteration. The grains are parallel to the fabric.
- Biotite (20%): Anhedral grain up to 15 micrometers, commonly less than 5 micrometers aligned parallel to the fabric.
- Quartz (20%)
    - Within host rock: Anhedral grains less than 5 micrometers.
    - Within fracture infill: Anhedral grains up to 15 micrometers.
- Plagioclase (17%): Anhedral grains less than 5 micrometers with weak sericite alteration.

Alteration:

- Clinozoisite (10%): Subhedral grains up to 15 micrometers, commonly less 10 micrometers that are elongated parallel to the fabric.
- Chlorite (3%): Subhedral grains up to 10 micrometers that are elongated parallel to the fabric. The grains are altering muscovite and biotite.
- Pyrite (1%): Anhedral grains less than 5 micrometers are inclusion-poor. The grains increase in abundance in biotite- or muscovite-rich layers.
- Pyrrhotite (trace): Anhedral grains less than 10 micrometers.
- Chalcopyrite (trace): Anhedral grains less than 5 micrometers, associated with pyrrhotite and pyrite.

ID: ER-2022-WP-N-25

Rock type: Laminated unit

Basic description:

- Altering layer of muscovite- to biotite- to quartz-rich layers. The muscovite-rich layers have minor chlorite, and light to medium brown alteration. The biotite-rich layers have finer relative to the muscovite grains and have chlorite alteration. The quartz-rich layers have minor muscovite, biotite, clinozoisite and titanite. The clinozoisite and titanite are elongated parallel to the fabric.
- Layers contain remanent phenocrysts of altered plagioclase. The clasts contain inclusion of chlorite and clinozoisite, and the fabric wraps around the grains.
- Host rock is associated with veins:
    - 1 – Infilled with chlorite, clinozoisite and quartz. The clinozoisite are subhedral to euhedral. Cuts fabric.

Paragenesis:

- host rock -> vein 1 (clinozoisite -> quartz -> chlorite)

Mineralogy:

Primary:

- Quartz (17%)
    - Within host rock: Anhedral grains less than 5 micrometers.
    - Within vein: Anhedral grains up to 20 micrometers show minor undulating extinction and have inclusions of titanite.
- Plagioclase (10%)
    - Within host rock: Anhedral grains less than 5 micrometers with weak sericite alteration.
    - Phenocrysts: Anhedral grains that are strongly altered. Contain inclusions of clinozoisite and chlorite. The fabric wraps around the grains.
- Muscovite (25%): Anhedral grains up to 10 micrometers with minor chlorite alteration. In muscovite-rich layers the grains increase in size up to 30 micrometers.
- Biotite (15%): Anhedral grains commonly less than 5 micrometers with minor chlorite alteration. The grains are oriented parallel to the fabric.

Alteration:

- Clinozoisite (15%)
    - Within layers: Anhedral grains up to 10 micrometers that are elongated parallel to the fabric.
    - Within vein: Subhedral grains up to 30 micrometers, commonly less than 20 micrometers.
- Albite alteration (10%): Medium to dark brown texture destructive alteration.
- Chlorite (3%)
    - Within vein: Anhedral grains up to 20 micrometers. Contains inclusions of clinozoisite and quartz.
    - With layers: Anhedral grains up to 10 micrometers.
- Carbonate (3%)
    - Within layers: Anhedral grains up to 20 micrometers associated with albite altered sections.
    - Within vein: Anhedral grains up to 30 micrometers are found along contacts of the vein.
- Titanite (1%)
    - Within vein: Anhedral grains up to 10 micrometers, found as inclusion within chlorite.

- Ilmenite-Titanite (1%): Anhedral up to 10 micrometers elongated parallel to the fabric. Exhibits zonation of titanite around the grains.

ID: ER-2022-WP-N-26

Rock type: Laminated unit with quartz-layers

Basic description:

- The thin section is a series of alternating layers that are either muscovite-, biotite-, or quartz-rich layers. Clinozoisite is elongated parallel to the fabric, but it is found in higher concentrations within the biotite-rich layers. Disseminated pyrite is found throughout all the layers, but it has higher concentrations in the muscovite-rich layers and is also coarser grained.
- Quartz layers have an increase amount of chlorite and biotite along the contact, as well as sulphides (pyrite and sphalerite). The pyrite grains are clast rich.

Paragenesis:

- sulphides (sphalerite -> pyrite) -> clinozoisite -> muscovite = biotite -> quartz = plagioclase

Mineralogy:

Primary:

- Quartz (30%)
    - Within host rock: Anhedral grains less than 5 micrometers.
    - Within quartz layers: Anhedral grains up to 100 micrometers with recrystallization texture and micro inclusions. There is carbonate, sphalerite, and pyrite found along grain boundaries.
- Plagioclase (17%): Anhedral grains less than 5 micrometers.
- Muscovite (25%)
    - Within layers: Anhedral grains up to 20 micrometers, oriented parallel to the fabric
    - Within quartz veins: Anhedral grains up to 30 micrometers. Contain inclusions of pyrite and have chlorite alteration.
- Biotite (10%): Subhedral grains less than 10 micrometers with minor chlorite alteration.

Alteration:

- Clinozoisite (10%)
    - Within layers: Anhedral grains up to 30, commonly less than 20 micrometers.
- Pyrite (4%)
    - Within quartz veins: Subhedral grains up to 30 micrometers that are inclusion-rich and contain inclusions of muscovite and sphalerite.
    - Within layers: Disseminated subhedral grains less than 10 micrometers, commonly less than 5 micrometers.
- Chlorite (3%): Anhedral grains up to 30 micrometers that contain inclusions of clinozoisite.
- Sphalerite (1%): Found along contact with quartz and host rock as anhedral grains up to 30 micrometers.
- Chalcopyrite (trace): Found along contact with quartz and host rock less than 5 micrometers, associated with pyrite.

ID: ER-2022-WP-N-27

Rock type: Laminated unit cut by a vein

Basic description:

- The Laminated unit with layers ranging from quartz-, muscovite- and biotite-rich. Contains relict phenocrysts of plagioclase that have inclusions of biotite, muscovite, and chlorite. The fabric wraps around the phenocrysts.
- The rock is cut by veining:
    - 1 – vein infilled with zeolite. The alteration halo is variable depending what layer is being associated with. If interacts with a phyllosilicate-rich layer the halo is thicker, and if quartz-rich the halo is thinner. Cuts the Laminated unit.

Paragenesis:

- sulphides -> clinozoisite -> muscovite = biotite -> chlorite -> quartz = plagioclase

Mineralogy:

Primary:

- Quartz (25%)
    - Within host rock: Anhedral grains less than 5 micrometers.
    - Within vein: Anhedral grains up to 15 micrometers that are inclusions rich.
- Plagioclase (20%): Anhedral grains less than 5 micrometers, plagioclase phenocrysts with simple twin.
- Muscovite (15%)
    - Within layers: Anhedral grains up to 15 micrometers elongated parallel to the fabric.
    - Within alteration halo: Anhedral grains up to 40 micrometers. Contains inclusions of clinozoisite and pyrrhotite.
- Biotite (15%)
    - Within layers: Anhedral grains up to 10 micrometers, elongated parallel to the fabric.
    - Within alteration halo: Anhedral grains up to 30 micrometers.

Alteration:

- Orthoclase alteration (5%): Pervasive medium to dark brown alteration associated with veining.
- Carbonate (4%): Anhedral grains less than 10 micrometers, associated with areas of plagioclase phenocrysts or layers of coarser quartz or less commonly coarser bio or music, or as pervasive alteration within host rock.
- Clinozoisite (6%): Anhedral grains up to 15 micrometers, higher abundance in proximity to the alteration halo. The grains are elongated parallel to the fabric.
- Chlorite (4%): Anhedral grains up to 20 micrometers. Chlorite is noted altering muscovite and biotite. Higher concentration in proximity to veining.
- Zeolite (3%): Within vein: Anhedral grains up to 15 micrometers, fracture undulates but width is roughly 20 micrometers. Associated with medium to dark brown texture destructive alteration halo, darker patches tend to have coarser muscovite, biotite, chlorite, and sulphides.
- Pyrrhotite (3%): Disseminated subhedral grains up to 5 micrometers with higher abundance within alteration halos or with coarser muscovite.
- Chalcopyrite (trace): Disseminated anhedral grains less than 5 micrometers that are found within layers.

ID: ER-2022-WP-N-28

Rock type: mylonite

Basic description:

- The host rock has strong pervasive albite alteration throughout the entire thin section. The thin section is hosted within feldspar porphyry.
- Host rock contains coarse phenocrysts of plagioclase that are strongly altered and contain inclusions of clinozoisite, muscovite and chlorite.
- Host rock is associated with below veins:
    - 1 – infill has been dominantly removed during thin section process. The relict minerals are composed of minor zeolite and clinozoisite. Dark brown alteration halo in proximity to the vein. Cuts vein 2.
    - 2 – discontinuous vein infilled with chlorite, quartz, associated with albite alteration halo.

Petrogenesis

- vein 2 (chlorite-quartz) -> vein 1 (clinozoisite)

Mineralogy:

Primary:

- Quartz (15%)
    - Within host rock: Anhedral grains up to 5 micrometers.
    - Within vein 2: Anhedral grains up to 10 micrometers.
- Plagioclase (11%)
    - Within host rock: Anhedral grains up to 5 micrometers.
    - Relict phenocrysts within host rock: Subhedral grains up to 160 micrometers with strong alteration. Contains inclusions of clinozoisite and quartz

Alteration:

- Albite alteration (40%): Texture destructive light to medium brown alteration.
- Orthoclase alteration (15%)
    - Alteration halo of vein 1: Dark brown texture destructive alteration halo.
- Clinozoisite (10%)
    - Within host rock: Anhedral grains up to 5 micrometers.
    - Within vein 1: Anhedral grains up to 10 micrometers are found along edges of the vein.
- Chlorite (2%)
    - Within host rock: Anhedral grains up to 20 micrometers.
- Zeolite (4%)
    - Within vein 1: Anhedral grains up to 50 micrometers
- Pyrite (3%)
    - Within host rock: Anhedral grains up to 15 micrometers that are inclusion-poor.

ID: ER-2021-WP-P-14

Rock type: mylonite

Basic description:

- The host rock is composed of chlorite, clinozoisite, quartz and plagioclase.
- Sulphides consist of pyrite, pyrrhotite, and chalcopyrite. Pyrite and pyrrhotite can both be either inclusion-rich or inclusion-poor. Sphalerite is commonly associated with either pyrrhotite or pyrite.

Paragenesis:

- clinozoisite -> amphibole -> quartz -> sulphides -> chlorite

Mineralogy:

Primary:

- Amphibole (30%): Bimodal distribution with coarser grains over 1,000 micrometers and finer grains commonly less than 200 micrometers. The grains have fabric associated with them and have inclusions of clinozoisite, and sulphides.
- Quartz (22%): Bimodal distribution of 100 micrometers with micro inclusions. In more quartz-rich areas the grains can be up to 200 micrometers and show undulatory extinction.
- Plagioclase (4%): Subhedral grains up to 100 micrometers, some exhibiting simple twinning.

Alteration:

- Chlorite (15%): Grains can be up to 200 micrometers and have a bluish hue in cross polars. Chlorite is altering the amphiboles. Inclusions of sulphides, sphalerite, and clinozoisite.
- Pyrite (14%): Bimodal distribution of coarse grains over 600 micrometers and finer grains less than 100 micrometers. Contains inclusions of chlorite, sphalerite, and host rock. Contains grains that are inclusion-rich and grains that are inclusion-poor. Inclusion-rich tend to be coarser and more anhedral.
- Sphalerite (8%): Disseminated grains around grain boundaries of silicates. The grains get coarser in higher accumulations of sulphides. Contains inclusions of pyrrhotite-pyrite-chalcopyrite and host rock.
- Clinozoisite (4%): Bimodal distribution of clinozoisite. The finer grains are commonly less than 100 micrometers and coarser grains up to 400 micrometers.
- Pyrrhotite (3%): Anhedral grains associated with pyrite-chalcopyrite. The grains are inclusion-rich.
- Chalcopyrite (1%): Anhedral grains are associated along grain boundaries of silicates and associated with pyrite and pyrrhotite.

ID: ER-2022-WP-P-33

Rock type: Granite (lower granite from Peek-a-Boo zone)

Basic description:

- Coarse-grained clinozoisite and muscovite grains within sericite altered plagioclase and quartz matrix.
- Chlorite is found altering clinozoisite and biotite grains, and more commonly associated with titanite grains.
- No fabric associated with the host rock.

Paragenesis:

- biotite -> muscovite -> clinozoisite -> plagioclase -> quartz -> titanite -> chlorite -> carbonate

Mineralogy:

Primary:

- Plagioclase (40%): Subhedral grains up to 60 micrometers with moderate to strong sericite alteration. The grains contain inclusions of biotite, muscovite, clinozoisite. The grains exhibit simple and polysynthetic twinning.
- Quartz (30%): Subhedral grains up to 20 micrometers with undulatory extinction and micro inclusions. The grains contain inclusions of clinozoisite, titanite and muscovite.
- Muscovite (8%): Elongated grains up to 40 micrometers, commonly 20-30 micrometers. The grains are found as inclusion in plagioclase, clinozoisite. Grains have been altered by chlorite.
- Biotite (1%): Subhedral grains up to 20 micrometers non-oriented. The grains have been altered by chlorite.

Alteration:

- Clinozoisite (15%): Subhedral to anhedral grains up to 70 micrometers with irregular grain contacts. The grains contain inclusions of biotite, titanite, plagioclase.
- Chlorite (3%): Subhedral grains up to 30 micrometers are found along grain boundaries of quartz-plagioclase. The grains contain inclusion of titanites and are altering biotite and muscovite grains.
- Carbonate (2%): Anhedral grains up to 20 micrometers are found in associated with muscovite and clinozoisite grains or as inclusion in plagioclase.
- Titanite (1%): Subhedral to anhedral grains up to 10 micrometers, commonly less than 5 micrometers associated with chlorite or clinozoisite grains but can also be found along grain boundaries of plagioclase grains.
- Pyrite (trace): Disseminated grains less than 3 micrometers are found as inclusions within altered plagioclase or clinozoisite.
- Chalcopyrite (trace): Disseminated grains are less than 1 micrometer are found as inclusions within altered plagioclase associated with pyrite.

ID: ER-2022-WP-P-34

Rock type: Granite (Upper granite from Peek-a-Boo)

Basic description:

- The matrix of the rock is made up of sericite altered plagioclase and quartz grains.
- The fabric is composed of muscovite, biotite, clinozoisite, and chlorite. The grains exhibit wavy deformation fabric.

Paragenesis:

- sulphides -> clinozoisite -> muscovite = biotite -> magnetite -> plagioclase -> quartz -> titanite -> chlorite

Mineralogy:

Primary:

- Plagioclase (40%): Subhedral to euhedral grains up to 80 micrometers with moderate to strong sericite alteration. The grains have muscovite, biotite and clinozoisite wrapping around the grains. The grains exhibit simple and polysynthetic twinning. Sericite alteration can be either patchy throughout the grains or found along the core of the grain.
- Quartz (27%): Anhedral grains up to 30 micrometers, commonly less than 20 micrometers exhibiting undulatory extinction and micro inclusions. They have inclusions of biotite, muscovite and clinozoisite.
- Biotite (15%): Subhedral grains up to 20 micrometers with inclusions of titanites. The grains are elongated parallel to the fabric, and in cases wrap around plagioclase grains. The grains have been altered by chlorite.
- Muscovite (10%): Subhedral grains up to 50 micrometers with inclusions of titanite. The grains make up the fabric of the host rock and wrap around plagioclase grains. The grains have been altered by chlorite.

Alteration:

- Clinozoisite (7%): Anhedral grains up to 30 micrometers elongated parallel to the fabric. The grains have irregular grain boundaries and contain inclusions of titanite. Biotite grains crystallize along the edges of the grains.
- Chlorite (1%): Subhedral grains up to 20 micrometers altering chlorite and muscovite grains. Contains inclusions of titanites.
- Titanite (trace): Subhedral grains less than 5 micrometers associated with muscovite, biotite, and chlorite grains.
- Magnetite (trace): Subhedral to euhedral grain less than 3 micrometers are found around the core of altered plagioclase grains.

ID: ER-2022-WP-P-35

Rock type: Laminated unit

Basic description:

- Layered unit. The layers are varying proportions of muscovite, biotite, clinozoisite, or quartz. The layers tend to be either biotite- or muscovite-rich with darker layers being biotite-rich. Pyrite grains are associated with clinozoisite- or quartz-rich layering. The clinozoisite and pyrite are elongated parallel to the fabric. Some of the darker layers have a texture destructive alteration associated with the layers.

Paragenesis:

- pyrite -> clinozoisite -> biotite = muscovite -> plagioclase = quartz

Mineralogy:

Primary:

- Quartz (15%): Anhedral grains up to 5 micrometers with micro inclusions. Quartz grains close to the fracture infill are coarser up to 10 micrometers exhibiting undulatory extinction.
- Plagioclase (10%): Anhedral grains up to 5 micrometers making up the matrix of the host rock.
- Muscovite (25%): Anhedral to subhedral grains up to 30 micrometers, but commonly less than 20 micrometers. The grains are part of the fabric.
- Biotite (25%): Anhedral to subhedral grains up to 20 micrometers. The grains are part of the fabric.

Alteration:

- Clinozoisite (15%): Anhedral to subhedral grains with dissolution texture and aligned parallel to the fabric.
- Chlorite (3%): Anhedral grains up to 10 micrometers randomly oriented.
- Carbonate (trace): Anhedral grains up to 10 micrometers associated with section of coarser quartz grains. Found along grain boundaries.
- Sphalerite (trace): Anhedral grains up to 5 micrometers associated with pyrite grains. Sphalerite is only found in proximity to the fracture infill.
- Pyrite (7%): Anhedral grains up to 15 micrometers aligned parallel to the fabric. Found as inclusions within quartz-plagioclase and clinozoisite.

ID: ER-2022-WP-P-36

Rock type: Laminated unit

Basic description:

- The host rock is composed of layers that are either quartz-, clinozoisite-, or biotite and quartz-rich. The clinozoisite is elongated parallel to the fabric.
- The layers wrap around a clast inclusion that is dominated by coarse grained clinozoisite. Around the clast there is an alteration halo dominated by quartz and plagioclase with medium brown pervasive alteration.

Paragenesis:

- clinozoisite -> muscovite = biotite -> chlorite

Mineralogy:

Primary:

- Quartz (35%)
    - Within biotite-rich layers: Anhedral grains up to 10 micrometers.
    - Within quartz-rich layers: Anhedral grains up to 40 micrometers. Contains inclusions of biotite and clinozoisite.
    - Quartz vein parallel to fabric: Anhedral grains up 100 micrometers with minor recrystallization texture. Contains inclusion of coarse grained clinozoisite. Contains dark brown alteration halo on either side of the vein.
    - Within clast inclusion: Anhedral grains up to 60 micrometers with recrystallization texture. Contains inclusions of clinozoisite.
- Biotite (25%)
    - Quartz-rich layers: Anhedral grains up to 20 micrometers.
    - Biotite-rich layers: Anhedral grains up to 50 micrometers elongated parallel to the fabric. The grains contain inclusions of clinozoisite.
- Muscovite (5%)
    - Quartz-rich layers: Anhedral grains up to 30 micrometers.
    - Within clast inclusion: Subhedral grains up to 30 micrometers oriented parallel to the clast along the contacts.

Alteration:

- Clinozoisite (20%)
    - Biotite-rich layers: Anhedral to subhedral grains up to 20 micrometers.
    - Within quartz-rich layers: Anhedral grains up to 20 micrometers elongated parallel to the fabric.
    - Within quartz vein parallel to fabric: Euhedral grain up to 70 micrometers.
    - Within clast inclusion: Subhedral to euhedral grains up to 150 micrometers, commonly less than 50 micrometers. Also contains finer grained clinozoisite less than 10 micrometers.
- Orthoclase alteration (10%): Medium to dark brown texture destructive alteration.
- Chlorite (5%)
    - Within layers: Anhedral grains up to 30 micrometers elongated parallel to the fabric.
- Titanite (trace)
    - Within clast inclusion: Subhedral grains up to 10 micrometers are found along the edges of the clast contact.

ID: ER-2022-WP-P-37

Rock type: Volcanic rock

Basic description:

- Host rock is dominated by amphiboles with ilmenite-titanite, quartz and plagioclase and minor pyrite. Coarse amphiboles make up the fabric of the host rock wrapping around coarse clasts of plagioclase. Amphiboles also contain elongated ilmenite-titanite grains.
- Host rock is associated with veins:
    - 1 - Clinozoisite-titanite-carbonate infilled vein with weak carbonate alteration is cutting through the host rock. Weak carbonate alteration is found around the edges.

Paragenesis:

- host rock -> vein (ilmenite -> titanite -> clinozoisite -> carbonate)

Mineralogy:

Primary:

- Amphibole (70%): Subhedral to anhedral grains making up the fabric of the host rock. The grains contain inclusions of ilmenite and quartz and wrap around the grains of plagioclase.
- Quartz (10%): Subhedral grains up to 10 micrometers with undulatory extinction and micro inclusions. The coarser grains are found as small clusters between amphiboles.
- Plagioclase (8%): Coarse grains have strong sericitization. The grains contain inclusions of ilmenite and exhibit simple twinning.

Alteration:

- Ilmenite-Titanite (5%): Elongated grains up to 30 micrometers, commonly less than 20 micrometers being altered by titanite around the edges. The grains are elongated parallel to the fabric of the host rock and are found as inclusions within amphiboles.
- Titanite (2%)
    - Within vein: Anhedral grains up to 10 micrometers found within vein infill, randomly oriented.
- Clinozoisite (2%)
    - Within vein: Euhedral to subhedral grains up to 10 micrometers randomly oriented found within vein infill.
- Carbonate (1%)
    - Within vein: Anhedral grains up to 10 micrometers.
- Chalcopyrite (1%): Disseminated anhedral grains less than 3 micrometers found within amphibole grains.
- Pyrite (1%): Disseminated anhedral inclusions-poor grains up to 10 micrometers, commonly less than 3 micrometers. The grains are found as inclusions within amphibole grains.

ID: ER-2022-WP-P-38

Rock type: Laminated unit

Basic description:

- The host rock consists of alternating biotite-, quartz-, or clinozoisite-rich layers.
- The layers wrap around a coarse lens dominated by clinozoisite with minor quartz.

Petrogenesis

- clinozoisite -> biotite -> quartz -> plagioclase -> pyrite = chlorite

Mineralogy:

Primary:

- Quartz (30%)
    - Within quartz-rich layers: Anhedral grains up to 5 micrometers wide
    - Within quartz layers: Anhedral grains up to 50 micrometers with undulatory extinction and recrystallization texture. Contains inclusions of clinozoisite.
    - Within clinozoisite-rich lenses: Anhedral grains up to 20 micrometers with micro inclusions.
- Clinozoisite (30%)
    - Within clinozoisite-rich layers: Anhedral grains up to 20 micrometers.
    - Within clinozoisite lenses: Anhedral grains up to 60 micrometers.
- Biotite (20%)
    - Within biotite-rich layers: Anhedral grains up to 30 micrometers elongated parallel to the fabric.
    - Within quartz-rich layers: Anhedral grains up to 5 micrometers elongated parallel to the fabric.

Alteration:

- Albite alteration (15%): Light to medium brown texture destructive alteration with higher accumulation along the clinozoisite lenses.
- Chlorite (5%): Anhedral grains up to 10 micrometers with higher concentrations around the clinozoisite-rich lenses.
- Pyrite (trace)
    - Within clinozoisite lenses: Anhedral grains up to 10 micrometers wide that are inclusion-poor, found along grain boundaries of quartz and clinozoisite.

ID: ER-2022-WP-P-39

Rock type: mylonite

Basic description:

- The host rock is associated with quartz, plagioclase, biotite, and clinozoisite.
- The rock is associated with various veins:
    - 1 – Boudinage vein infilled with quartz and has hematite staining. The vein pinches as swells. Cuts off 2.
    - 2 – Vein infilled with clinozoisite, carbonate, pyrite, and quartz with hematite staining. Pyrite is elongated parallel to the vein.
- Contains patches of strong albite alteration that have no associated fracture. The area is associated with strong albite and carbonate alteration and coarse titanite, muscovite, clinozoisite, pyrite, chlorite, and ilmenite.

Paragenesis:

- host rock -> vein 2 (clinozoisite) -> vein 1 (quartz)

Mineralogy:

Primary:

- Quartz (28%)
    - Within host rock: Anhedral grains up to 5 micrometers
    - Albite alteration zone: Anhedral grains up to 60 micrometers.
- Plagioclase (15%): Anhedral grains up to 5 micrometers with weak sericite alteration.
- Biotite (15%): Anhedral grains up to 10 micrometers.
- Orthoclase (2%)
    - Albite alteration zone: Phenocrysts of plagioclase up to 200 micrometers with albite alteration and microcline twinning.

Alteration:

- Clinozoisite (15%)
    - Within host rock: Anhedral grains up to 20 micrometers that are elongated parallel to the biotite.
    - Within vein 2: Anhedral grains up to 20 micrometers.
    - Albite alteration zone: Anhedral grain up to 30 micrometers.
- Ilmenite-Titanite (10%)
    - Within host rock: Anhedral grains up to 15 micrometers with inner ilmenite and outer titanite rims. The grains have an irregular shape.
    - Within alteration halos: Anhedral grains up to 60 micrometers with inner ilmenite and outer titanite rims. The grains have a higher concentration with chlorite-rich areas.
- Carbonate (7%)
    - Within vein 2: Anhedral grains up to 30 micrometers.
    - Albite alteration zone: Anhedral grains up to 60 micrometers.
- Pyrite (4%)
    - Within host rock: Anhedral grain up to 5 micrometers.
    - Albite alteration zone: Subhedral grains up to 50 micrometers are inclusion-poor. Contains inclusions of clinozoisite.
    - Within vein 2: Anhedral grain up to 20 micrometers elongated parallel to the vein.
- Muscovite (2%): Albite alteration zone: Subhedral grains up to 40 micrometers.
- Titanite (2%): Albite alteration zone: Subhedral to euhedral grains up to 100 micrometers. Dominantly associated with carbonates.

ID: ER-2022-WP-P-40

Rock type: mylonite

Basic description:

- Host rock is composed of quartz, plagioclase, clinozoisite and muscovite.
- The rock is associated with various veins:
    - 1 – The vein is composed of multiple veins with same orientation that are infilled with clinozoisite. The veins split into smaller veinlets that can either terminate or merge back with the vein. The veins do not have any alteration halo.
    - 2 - Boudinage veins infilled with clinozoisite. Alteration halo of texture destructive medium brown alteration. Contains a higher abundance of chlorite. The vein is cut by 1, but also cuts 1 at different areas.

Paragenesis:

- plagioclase -> clinozoisite -> muscovite -> quartz

Mineralogy:

Primary:

- Quartz (36%): Anhedral grains up to 5 micrometers.
- Plagioclase (30%): Subhedral grains up to 150 micrometers exhibit simple or polysynthetic twinning. Contains inclusions of clinozoisite and muscovite.
- Muscovite (15%): Subhedral grains up to 30 micrometers, commonly less than 20 micrometers randomly oriented throughout the rock.

Alteration:

- Clinozoisite (10%)
    - Within host rock: Subhedral grains up to 100 micrometers that contain inclusions of muscovite.
    - Within vein 1: Anhedral grains up to 20 micrometers.
    - Within vein 2: Anhedral grains up to 20 micrometers.
- Chlorite (3%)
    - Within vein 2: Anhedral grains up to 200 micrometers containing inclusions of clinozoisite, titanite, and quartz.
- Pyrite (3%)
    - Within host rock: Anhedral grains up to 10 micrometers.
    - Within alteration hao: Subhedral to euhedral grain up to 60 micrometers, commonly less than 20 micrometers that are inclusion-poor.
- Biotite (2%): Anhedral grains up to 40 micrometers are found in localized areas with higher chlorite concentrations. Biotite is being altered by chlorite.
- Titanite (1%): Anhedral to subhedral grains up to 30 micrometers randomly oriented throughout the grains.
- Sphalerite (trace)
    - Within alteration halo: Anhedral grains up to 30 micrometers associated with coarser pyrite grains.

Appendix C: SEM-EDS

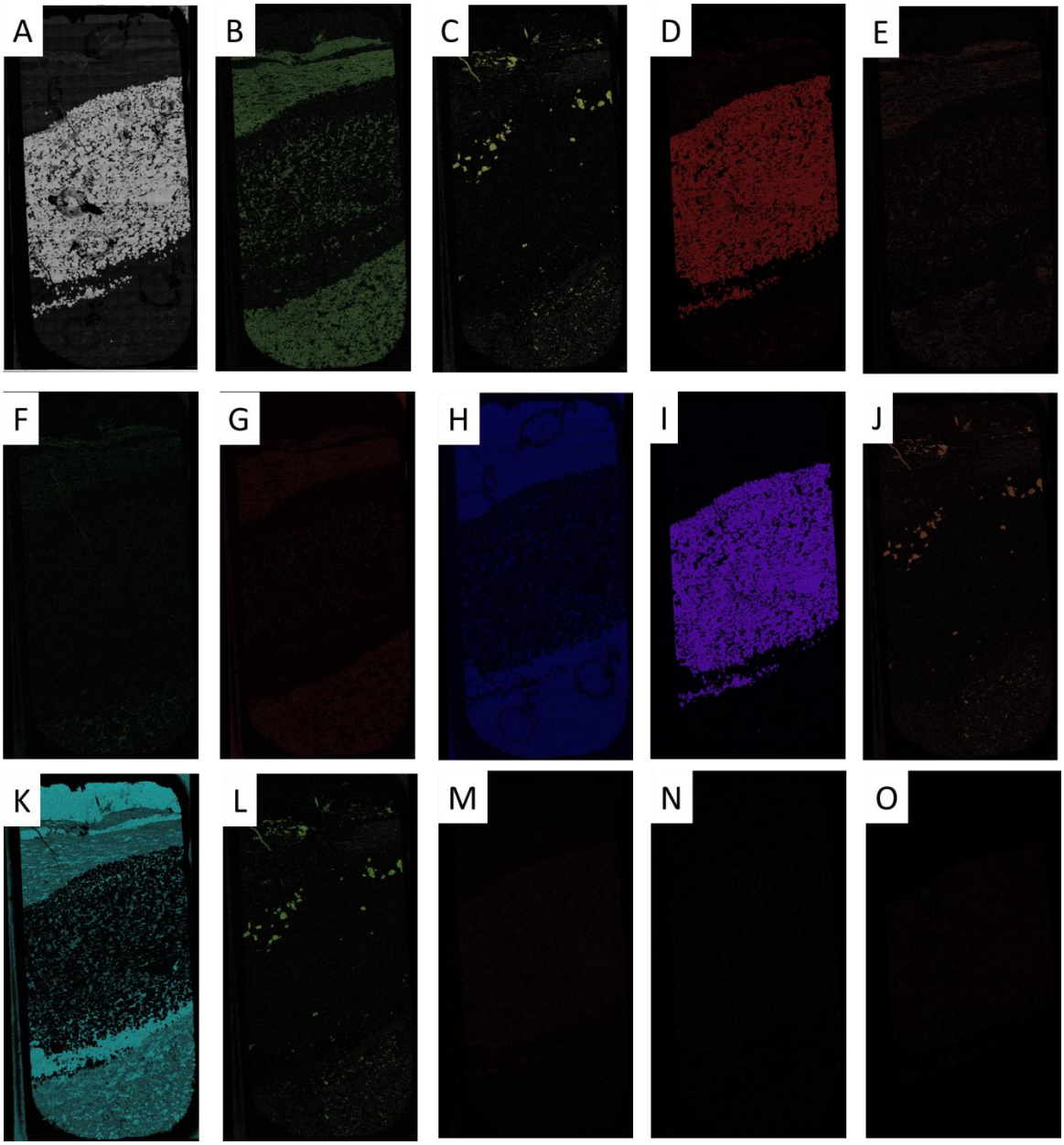

Figure C.1: SEM elemental maps of the ER-WP-2021-8z-01 thin section. SEM image of the section (a), aluminum (b), calcium (c), iron (d), potassium (e), magnesium (f), sodium (g), oxygen (h), sulfur (i), antimony (j), silicon (k), tellurium (l), titanium (m), copper (n), and zinc (o).

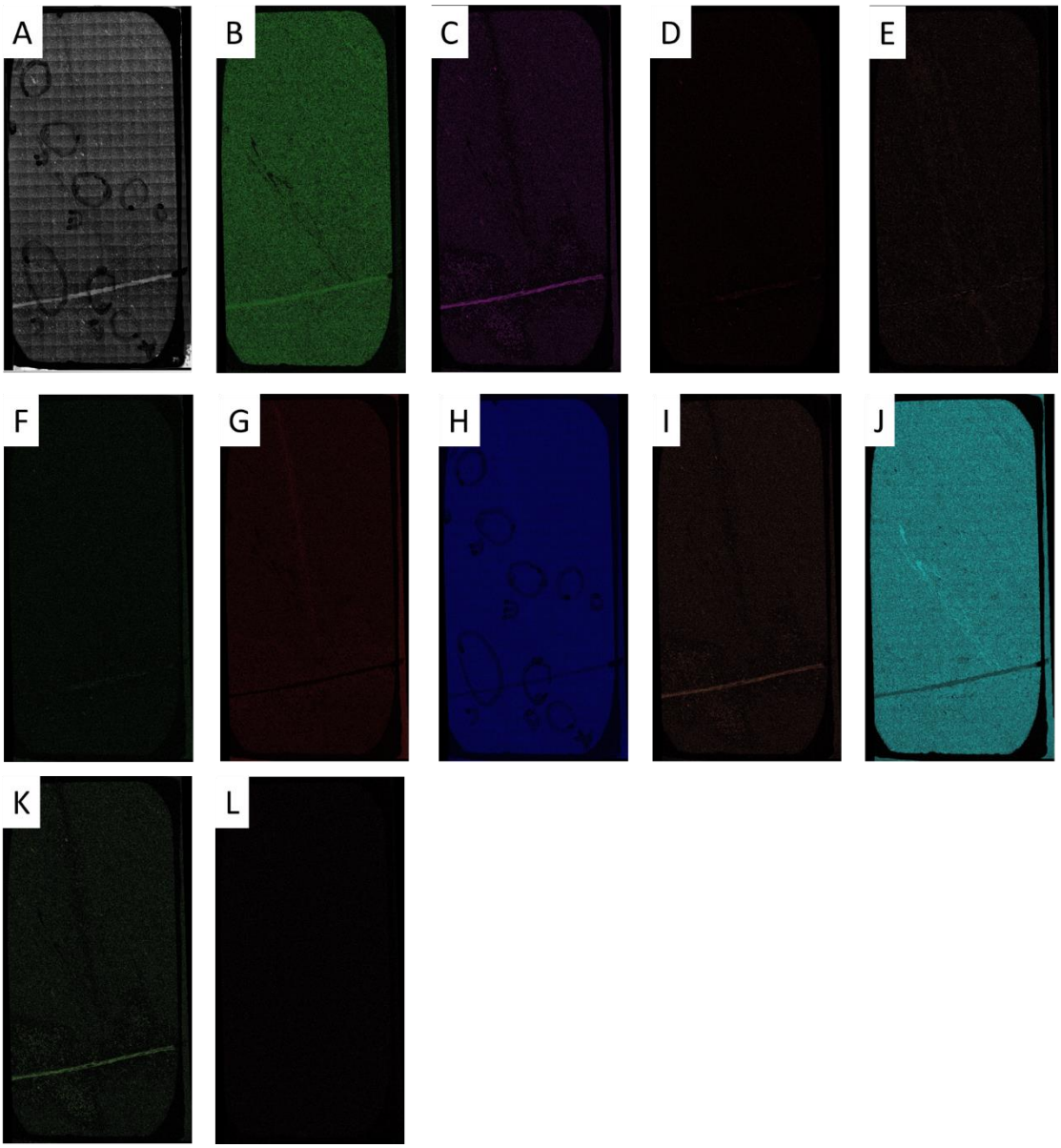

Figure C.2: SEM elemental maps of the ER-WP-2021-8z-19 thin section. SEM image of the section (a), aluminum (b), calcium (c), iron (d), potassium (e), magnesium (f), sodium (g), oxygen (h), antimony (i), silicon (j), tellurium (k), and titanium (l).

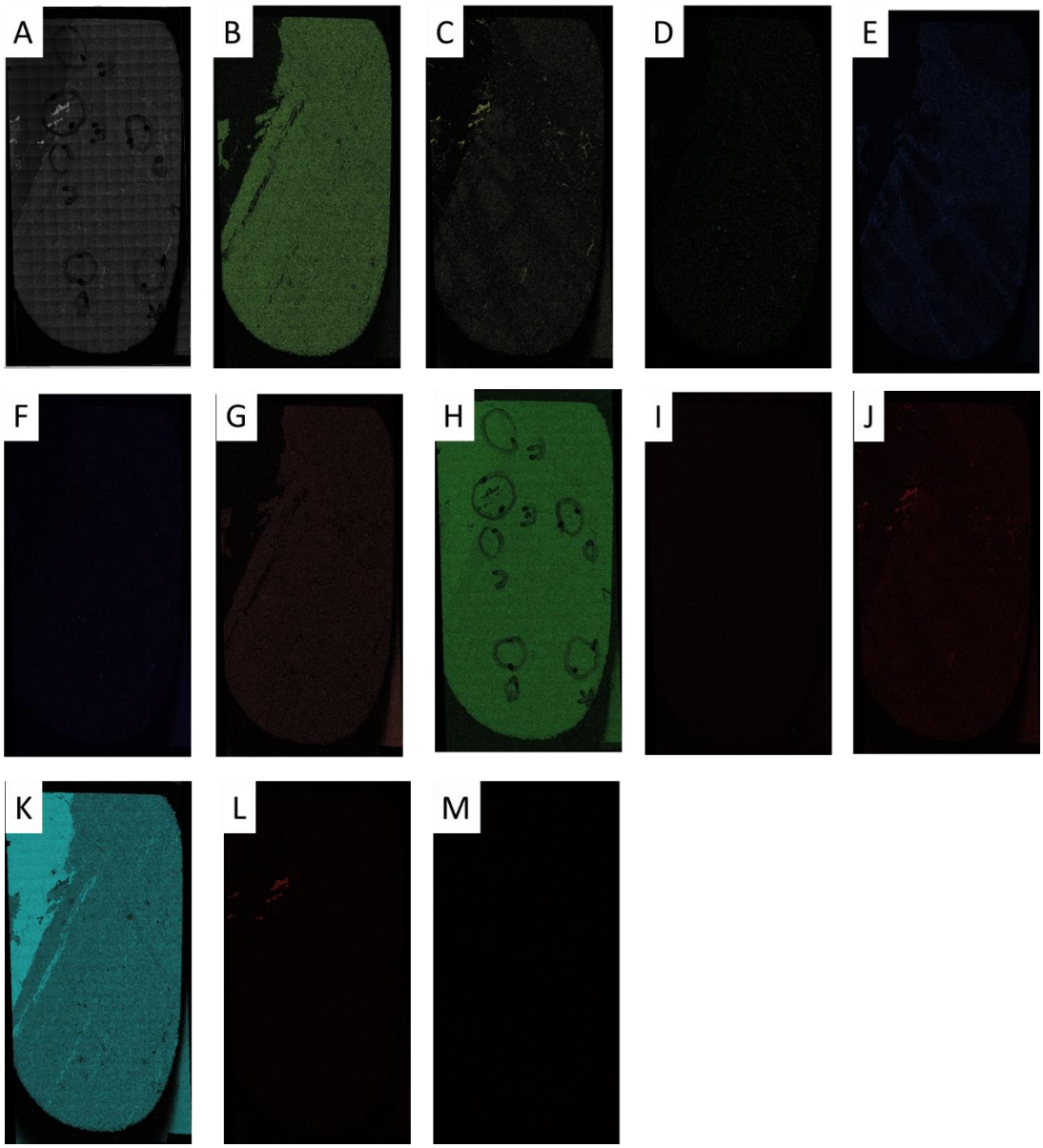

Figure C.3: SEM elemental maps of the ER-WP-2021-8z-31 thin section. SEM image of the section (a), aluminum (b), calcium (c), iron (d), potassium (e), magnesium (f), sodium (g), oxygen (h), sulfur (i), antimony (j), silicon (k), titanium (l), and zinc (m).

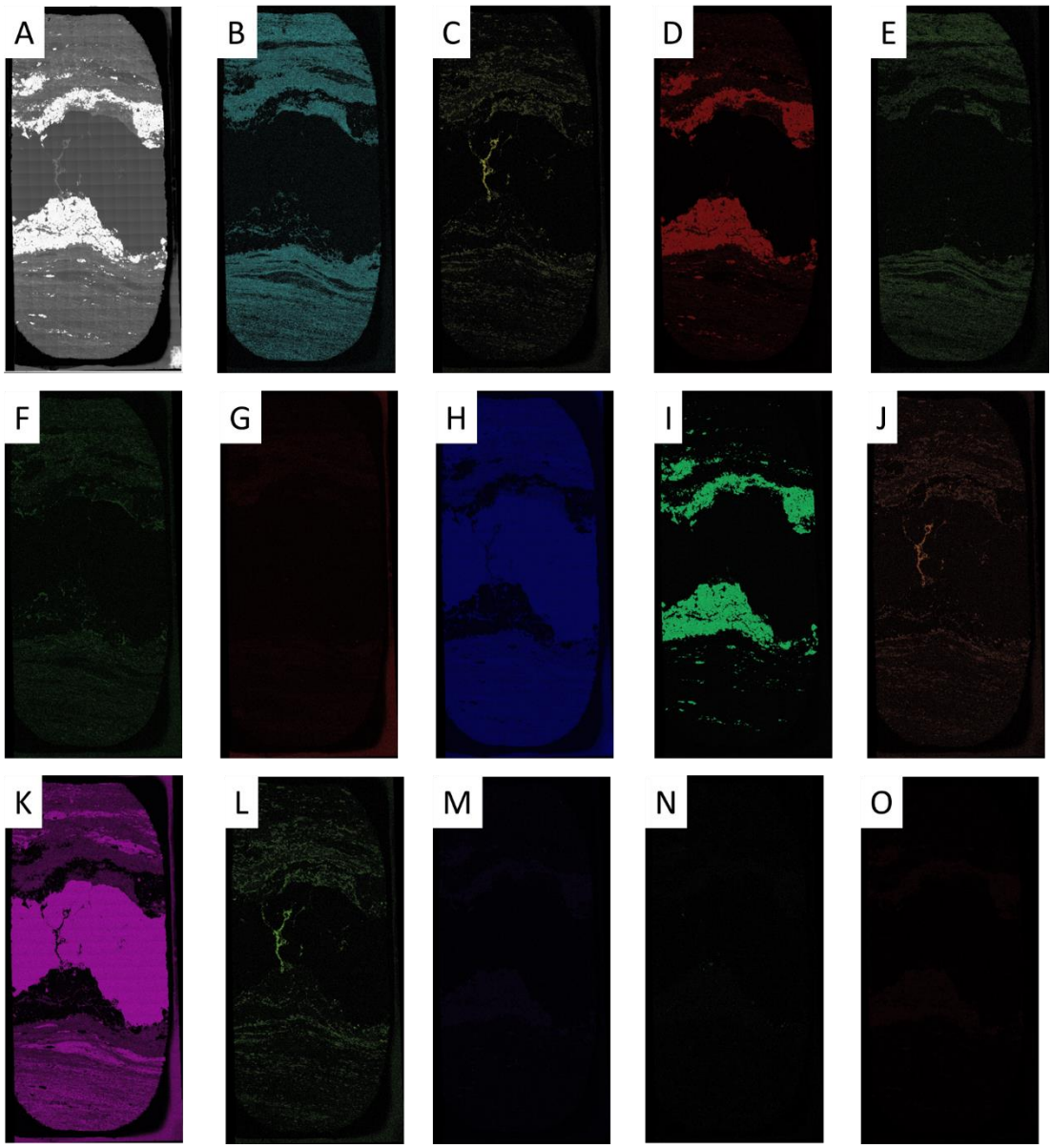

Figure C.4: SEM elemental maps of the ER-WP-2021-F-17 thin section. SEM image of the section (a), aluminum (b), calcium (c), iron (d), potassium (e), magnesium (f), sodium (g), oxygen (h), sulfur (i), antimony (j), silicon (k), tellurium (l), titanium (m), copper (n), and zinc (o).